UNIVERSITAT POLITÈCNICA de VALÈNCIA

INSTITUT DE DISSENY I FABRICACIÓ (IDF)

654

Synthesis and characterization of Indium Phosphide Quantum Dots for photoelectrochemical applications

By

IMEN HARABI

PhD thesis

Supervised by: Prof Dr. Bernabé Marí Soucase

Dr. Hanae Toura

Departamento de Física Aplicada-IDF Universitat Politécnica de Valencia (Spain)

February 2023

Studying physics, delving deeply into its fundamentals and those broad ideas on which it is based and, especially, independent scientific work brings enormous mental satisfaction.

Leonid Mandelstam

Table of contents

Acknowledgements

I thank first our **Almighty God**, the most Beneficent and the most Merciful, who has endowed us with the marvelous faculty of reasoning, for giving me the courage during all these long years of study and the will to complete the present work. His continuous grace and mercy were with me throughout my life.

I would like to express my deepest gratitude to Professor **Dr. Bernabé Marí Soucase** to have made me share his knowledge, for his advice, his support, and his help as well as for the great confidence and the kindness that he showed me throughout this work.

My gratitude also goes towards **Mr. Professor Miguel Alfonso Mollar** who gave me learned a lot experimentally and extend my sincere thanks to the UPV Electron Microscopy Service and to **Mr Ángel Sans Tresserras** for their help to learn how to work with characterization techniques.

I would like to dedicate this thesis to my sincere and generous father **Amor** and my loving mother **Zoubeida**, who encouraged and helped me at every stage of my life and longed to see this achievement come true.

Deepest thanks to my brothers and sisters **Rafik**, **Rached**, **Rafika**, **Rachida**, for their moral support and encouraging me throughout my course.

I am grateful to my brother **Rafik** for supporting me during this period of research. I would not have achieved the goals without him.

I would like to thank all my friends, especially **Dr. Safa**, **Dr Hana**, **Dr Hanen**, **Dr. Yousaf**, **Dr. Faisal**, and **Dr Shafi** who supported me.

At the end, special thanks to my friends **Asma**, **Hichem**, as I always felt so loved and appreciated by them and thank to them for their encouragement.

Imen Harabi

December 2022

Abstract (English)

Today, there are modern technological and engineering challenges that would advantage from the contributions of the nanoscience community and nanotechnology. At this scale, the physical and chemical properties of the systems are highly dependent on respect for the environment (energy saving, pollution minimization, global warming etc…). In this term, nanoparticles based on II-VI semiconductors "Quantum Dots" have been by far the most studied. Among several material, InP Quantum Dots has brought huge interest because of the low toxicity features. This promising element is the subject of this thesis. Hence, to obtain monodisperse particles in solution, the hot injection route has several advantages that make it a useful technique, such as controlling the size of the nanoparticles.

This work deals with the synthesis of InP Quantum Dot by hot injection method as the basis for photoelectrochemical application.

We started our work by optimizing the synthesis of InP QDs by the hot injection method while studying the synthesis parameters on the morphological, structural, and specially the photoluminescence properties of InP Quantum Dots.

Initially, the optimization of the Quantum Dots conditions was based on the enhancement the optical properties in particular the photoluminescence. When we passivated the InP QDs by ZnS shell, ZnS/ZnS double shell we succeed to decrease the surface defects resulting on the enhancement of the InP QDs photoluminescence. Also, the surface morphology of these QDs has a more regular spherical form and is well dispersed. On the other hand, the optical properties of the InP QDs doped with Vanadium was shown no improvement in the photoluminescence while there’s a decrease on the size of the nanoparticle.

The second aim of this thesis revolves around InP QDs deposited on metallic titanium dioxide nanotubes TiO_2 by spin coating method with a view to comparing the photoelectrochemical efficiency of core InP QDs, core/shell InP/ZnS QDs, and core/shell/shell InP/ZnS/ZnS QDs. This study shows an increase in the photocurrent almost 4 and 6 times higher than TiO_2/InP QDs. Hence, this measurement aims to observe the dynamic behavior of the material and to assess whether the charges recombine rapidly into the TiO_2 NTAs Nanotubes from the quantum dots. So, a good efficiency in the photocurrent response was obtained following the growth core/shell/shell system due to the successful passivation of non-radiative recombination sites such as surface trap states.

This result was supported by a simulation study of the different parameters characterizes the solar cell based TiO_2/InP, TiO_2/InP/ZnS and TiO_2/InP/ZnS/ZnS with software SCAPS-1D. According to this theoretical work, a good performance of the cell has obtained in the adding of ZnS layer. The simulation results show that the InP was able to successfully utilize the full spectrum of light when coated with ZnS layer on top.

Key words: Indium phosphide; Vanadium; core/shell InP/ZnS; core /shell/shell InP/ZnS/ZnS Quantum Dots; hot injection process; photoluminescence; fluorescence; TiO2 NTAs; Photoelectrochemical, simulation SCAPS1-D.

Resumen (Castellano)

Hoy en día, existen desafíos tecnológicos y de ingeniería que se beneficiarían de las contribuciones de la nanociencia y la nanotecnología. A esta escala, las propiedades físicas y químicas de los sistemas han de cumplir con el respeto al medio ambiente (ahorro de energía, minimización de la contaminación, calentamiento global, etc.). Para estos fines, las nanopartículas basadas en puntos cuánticos de semiconductores II-VI "Quantum Dots" han sido las más estudiadas. Entre varios materiales, los puntos cuánticos de InP (InP-QDs) han despertado un gran interés debido a las características de baja toxicidad. Este prometedor elemento es el tema central de esta tesis.

Para obtener partículas monodispersas en solución, la ruta de inyección en caliente presenta varias ventajas que la convierten en una técnica útil para controlar el tamaño de las nanopartículas. Este trabajo trata de la síntesis de puntos cuánticos de InP por el método de inyección en caliente para aplicaciones fotoelectroquímicas.

Comenzamos nuestro trabajo optimizando la síntesis de InP QDs por el método de inyección en caliente mientras estudiamos los parámetros de la síntesis sobre las propiedades morfológicas, estructurales y especialmente las propiedades de fotoluminiscencia de los puntos cuánticos de InP. Inicialmente, la optimización de las condiciones de los puntos cuánticos se basó en la mejora de las propiedades ópticas, en particular la fotoluminiscencia. Cuando pasivamos los InP QDs con una envolvente de ZnS, la doble envolvente ZnS/ZnS, logra disminuir los defectos superficiales y esto resulta en la mejora de la fotoluminiscencia de los InP QDs. Además, la morfología superficial de estos QDs tiene una forma esférica más regular y homogénea. Por otro lado, las propiedades ópticas de los InP QDs dopados con vanadio no mostraron ninguna mejora en la fotoluminiscencia, mientras que si se observó una disminución en el tamaño de las nanopartículas.

El segundo objetivo de esta tesis gira en torno a los QDs de InP depositados en nanotubos metálicos de dióxido de titanio (TiO2) por el método de recubrimiento por centrifugado con el fin de comparar la eficiencia fotoelectroquímica de los QDs de InP (núcleo), los QD de InP/ZnS de núcleo/corteza y los QD de InP/ZnS/ZnS de núcleo/corteza/corteza. Este estudio muestra un aumento en la fotocorriente casi 4 y 6 veces mayor que TiO2 / InP QDs. Esta medición tiene como objetivo observar el comportamiento dinámico del material y evaluar si las cargas se recombinan rápidamente en los nanotubos de TiO2 a partir de los puntos cuánticos. Se obtuvo una buena eficiencia en la respuesta de fotocorriente después del sistema de crecimiento del sistema núcleo/corteza/corteza debido a la pasivación de sitios de recombinación no radiativos, como los estados de trampas superficiales. Este resultado fue confirmado los estudios de simulación de los diferentes parámetros que caracterizan la célula solar basada en TiO2/InP, TiO2/InP/ZnS y TiO2/InP/ZnS/ZnS con el software SCAPS-1D. Según los cálculos numéricos, se ha obtenido un buen rendimiento de la mencionada célula con la adición de capa de ZnS. Los resultados de la simulación muestran que el InP fue capaz de utilizar todo el espectro de luz cuando se recubrió con la capa de ZnS en la parte superior.

Palabras clave: Fosfuro de indio; Vanadio; núcleo/corteza InP/ZnS; núcleo/corteza/corteza InP/ZnS/ZnS; Puntos cuánticos; Síntesis por inyección en caliente; fotoluminiscencia; Nanotubos de TiO2; Fotoelectroquímica; Simulación SCAPS1-D.

Resum (València)

Avui dia, hi ha desafiaments tecnològics i d'enginyeria que es beneficiarien de les contribucions de la nanociència i la nanotecnologia. En aquesta escala, les propietats físiques i químiques dels sistemes han de complir amb el respecte al medi ambient (estalvi d'energia, minimització de la contaminació, escalfament global, etc.). Per a aquestes finalitats, les nanopartícules basades en punts quàntics de semiconductors II-VI "Quantum Dots" han estat les més estudiades. Entre diversos materials, els punts quàntics d'InP (InP-QDs) han despertat un gran interès a causa de les característiques de baixa toxicitat. Aquest prometedor element és el tema central d'aquesta tesi.

Per obtenir partícules monodisperses en solució, la ruta d' injecció en calent presenta diversos avantatges que la converteixen en una tècnica útil per controlar la mida de les nanopartícules. Aquest treball tracta de la síntesi de punts quàntics d'InP pel mètode d'injecció en calent per a aplicacions fotoelectroquímiques. Comencem el nostre treball optimitzant la síntesi d'InP QDs pel mètode d'injecció en calent mentre estudiem els paràmetres de la síntesi sobre les propietats morfològiques, estructurals i especialment les propietats de fotoluminiscència dels punts quàntics d'InP. Inicialment, l' optimització de les condicions dels punts quàntics es va basar en la millora de les propietats òptiques, en particular la fotoluminiscència. Quan passivem els InP QDs amb una envolupant de ZnS, la doble envolupant ZnS/ZnS, aconsegueix disminuir els defectes superficials i això resulta en la millora de la fotoluminiscència dels InP QDs. A més, la morfologia superficial d' aquests QDs té una forma esfèrica més regular i homogènia. D'altra banda, les propietats òptiques dels InP QDs dopats amb vanadi no van mostrar cap millora en la fotoluminiscència, mentre que si es va observar una disminució en la mida de les nanopartícules.

El segon objectiu d'aquesta tesi gira al voltant dels QDs d'InP dipositats en nanotubs metàl·lics de diòxid de titani (TiO2) pel mètode de recobriment per centrifugat per tal de comparar l'eficiència fotoelectroquímica dels QDs d'InP (nucli), els QD d'InP/ZnS de nucli/cortesa i els QD d'InP/ZnS/ZnS de nucli/cortesa/cortesa. Aquest estudi mostra un augment en la fotocorrent gairebé 4 i 6 vegades més gran que TiO2 / InP QDs. Aquest mesurament té com a objectiu observar el comportament dinàmic del material i avaluar si les càrregues es recombinen ràpidament en els nanotubs de TiO2 a partir dels punts quàntics. Es va obtenir una bona eficiència en la resposta de fotocorrent després del sistema de creixement del sistema nucli/cortesa/cortesa a causa de la passivació de llocs de recombinació no radiatius, com els estats de trampes superficials. Aquest resultat va ser confirmat els estudis de simulació dels diferents paràmetres que caracteritzen la cèl·lula solar basada en TiO2/InP, TiO2/InP/ZnS i TiO2/InP/ZnS/ZnS amb el programari SCAPS-1D. Segons els càlculs numèrics, s' ha obtingut un bon rendiment de l' esmentada cèl·lula amb l' addició de capa de ZnS. Els resultats de la simulació mostren que l'InP va ser capaç d'utilitzar tot l'espectre de llum quan es va recobrir amb la capa de ZnS a la part superior.

Paraules clau: Fosfur d'indi; Vanadi; nucli/cortesa InP/ZnS; nucli/cortesa/cortesa InP/ZnS/ZnS; Punts quàntics; Síntesi per injecció en calent; Fotoluminiscència; Nanotubs de TiO2; Fotoelectroquímica; Simulació SCAPS1-D

Acronyms

Symbol	Explanation
QDs	Quantum dots
NCs	Nanocrystals
XRD	X-ray diffraction
TEM	Transmission electron microscopy
SEM	Scanning electron microscopy
EDS	Energy dispersive spectroscopy
PL	Photoluminescence
InP	Indium Phosphide
Cd	Cadmium
TiO_2	Titanium Oxide
ZnS	Zinc sulfide
$Zn\ (St)_2$	Zinc stearate
OLA	Oleylamine
P(TMS)3	Tris(triméthylsilyl)phosphine
$DMA)_3P$	Tris (dimethylamino) phosphine
DDT	1 dodecanthiol
InP:V	InP doped with Vanadium
N_2	Inert gaz
QE	Quantum Efficiency
GaAs	Gallium arsenide
GaP	Gallium phosphide

GaN	Gallium
ZB	Zinc blende
W	Wurtzite
BC	Conduction Band
BV	Valence Band
Eg	gap energy
Br	Bohr radius
m_e^*	Effective masses of the electron of the exciton
m_h^*	Effective masses of the hole of the exciton
ħ	Planck's constant
m_e	mass of the electron in vacuum
ε_r	The static dielectric permittivity,
e	Elementary charge
FWHM	Full Width at Half Maximum
QY	Quantum Yield
CFC	Face-centered cubic
R_3P	alkylphosphines
R_3PO	alkylphosphine oxide
NH_4F	ammonium fluorid

List of Figures

Chapter 1:

Chapter 2:

Chapter 3:

Chapter 4:

List of Tables

Chapter 1:

Chapter 3:

Chapter 4:

Preamble

Introduction

Today, energy has become the heart of all the activities which are used by man to feed himself, to move, to heat himself, to build himself. Among, these energy, solar energy is one of the energies that should be developed. Moreover that, the increasing needs for environmental protection have strongly stimulated research in the field of photovoltaics application in recent years.

This energy is indispensable and has many advantages because it is abundant, inexhaustible, and clean. The direct exploitation of solar energy by means of collectors reveals two very distinct technologies: thermal solar energy which produces calories and photovoltaic solar energy which produces electricity. The latter allows us to convert solar radiation directly into electricity using optoelectronic components called photovoltaic cells. These components are generally based on semiconductors.

Indeed, semiconductor materials have been booming in recent years innovative solutions to the world's technological and energy needs. It promises to revolutionize many areas, and it has a significant impact on our lives owing to its unique properties. In this regard, particular attention is paid to the fact that many researchers focus on semiconductor, which have been newly extended and adapted in several science areas (such as electronics, mechanics, chemistry, optics, biology, etc.) [1]

On the other hand, the electronic features of semiconductors can be altered through micro and nano manufacturing processes. In this context, the interest for the nanometric scale comes from the fact that the particles of nanometric dimensions have new properties, which cannot be obtained with the solid material.

So, the semiconductor nanoparticles are nanosized crystals composed of pure semiconductor materials (column IV elements: Si, Ge), binary type I-VII (CuCl, CuBr, AgBr…) , II-VI (CdS, ZnSe, PbS...), III-V (InP, GaP,GaAs…), or ternary type I-III-VI (CuInSe2, CuInS2...).[2] Moreover, Semiconductor nanoparticles are made up of several hundred to several thousand atoms, depending on their size.[3] They can be dispersed in solution by being in colloidal form. Then, a layer of organic molecules and ligan has covered the nanoparticles. These molecules ensure the colloidal stability of the nanoparticles in solution. In addition, they have a major influence on the physicochemical surface properties of the nanoparticles. Controlling the ligand layer of nanoparticles thus makes it possible to control and modulate their properties.[4]

Over the past twenty years, nanocrystals of semiconducting compounds, which include Quantum Dots, have emerged as the most important fluorescent probes due to their unique optical properties. Moreover, their optical properties can be modulated in different ways, for example, by the addition of a shell, or doping with different metals, thus facilitating their use for different applications requiring a specific absorption or emission wavelength precise.[5,6]

The most popular Quantum Dots are cadmium-based Quantum Dots (CdSe and CdTe). However, since 2012, cadmium (Cd) is classified as a definite carcinogen. [7] For that, the use of Cd, has been regulated by the European directive RoHS 2002/95/EC, which has prompted industries and research laboratories to find alternatives to minimize the toxicity of QDs. One of the solutions to minimize the toxicity of nanoparticles QDs is to replace the Cd core with a less toxic element. Currently, the most studied and promising element is indium phosphide (InP).

Indium Phosphide Quantum Dots has been especially explored by researchers thanks to their intriguing characteristics such as high optoelectronic properties with a narrow bulk bandgap 1.35eV an exciton Bohr radius of 11.3nm, a lattice distance constant 5.9Å and nontoxic materials.[11] These characteristics have offered various promising applications owing to the large exciton Bohr radius and bandgap compared to cadmium and lead.[5] In addition, this material is among the element most friendly to our environment.

It is important to note that the presented thesis focuses on InP QDs because it is considered as an excellent material related to several research works existing in the literature which have proved that a direct gap material is better suited for optoelectronic applications. Moreover, there is a clear reduction in toxicity compared to CdSe-based QDs, while maintaining the same optical properties.[10]. Thus, there is a considerable potential linked to the InP material for building high-performance optoelectronic devices and developing next generation displays [11].

On the other side, the use of semiconductor nanoparticles is growing rapidly. Indeed, the photoelectrochemical applications currently in use are mostly composed of large-gap semiconductors such as Titanium Oxide TiO_2.[12,13] Indeed, the light-sensitive properties of TiO_2, especially in its anatase form, are of great interest for many applications. [14,15] It is considered particularly interesting for the improvement of photocatalytic and photoelectrochemical and photovoltaic properties.

The present thesis is devoted to the synthesize nanoparticles based on InP Quantum Dots, enhancing the optical properties of these core QDs by doping with Vanadium and growing the ZnS based shell. The second part of this work is to synthesize films based on titanium dioxide

nanotubes, coupled by Quantum Dots for photoelectrochemical measurements, and illustrate the simulation results between the Quantum Dots and TiO_2.

The outline of this manuscript will be as follows:

- The first chapter is devoted to the synthesis of the knowledge useful for the understanding of this work, and those concerning the properties of Quantum Dots, InP, ZnS semiconductor, the doping element "the Vanadium" and titanium dioxide.

- In chapter II, we present the different methods of synthesis of the studied materials as well as the physicochemical methods of their characterization such as: XRD, SEM, TEM, UV-visible spectroscopy. Also, the numerical simulation is presenting in this part.

- Chapter III consists in studying the results obtained on the different materials prepared: Quantum Dots of InP, InP:V, InP/ZnS and InP/ZnS/ZnS.

- Chapter IV focuses on the results obtained on the nanostructured films based on TiO_2 nanotubes coupled with InP, ZnS Quantum Dots and the simulation results.

  This chapter focuses on:

  - Photo-electrochemical tests on TiO_2/InP, TiO_2/InP/ZnS, TiO_2/InP/ZnS/ZnS, nanostructured films, where we display the effect of the shell growth ZnS.

- Simulation study of different characteristic parameters of the InP/ZnS based Quantum Dots photovoltaic cell, to see the effect of shell ZnS Quantum Dots on the J-V characteristics, Quantum Efficiency (QE).

This work will end with a general conclusion that brings together the main results obtained.

References

[1] C. Burda, X. Chen, R. Narayanan, and M. A. El-sayed, *Chemistry and Properties of Nanocrystals of Different Shapes*. 2005.

[2] R. Koole, E. Groeneveld, and D. Vanmaekelbergh, *Size Effects on Semiconductor Nanoparticles*. .

[3] F. Schulz *et al.*, "Ligand Layer Engineering To Control Stability and Interfacial Properties of Nanoparticles," 2016, doi: 10.1021/acs.langmuir.6b01704.

[4] C. A. S. No, "Agents Classified by the IARC Monographs , Volumes 1 – 132," 2012.

[5] P. Reiss, M. Carrie, C. Lincheneau, L. Vaure, and S. Tamang, "Synthesis of Semiconductor Nanocrystals , Focusing on Nontoxic and Earth-Abundant Materials," 2016, doi: 10.1021/acs.chemrev.6b00116.

[6] M. Ando, M. Horie, Y. Akazawa-ogawa, Y. Hagihara, N. Murase, and Y. Shigeri, "Cytotoxicity of CdSe-based quantum dots incorporated in glass nanoparticles evaluated using human keratinocyte HaCaT cells," *Biosci. Biotechnol. Biochem.*, vol. 8451, pp. 1–4, 2016, doi: 10.1080/09168451.2015.1069702.

[7] K. D. Wegner, F. Dussert, D. Truffier-boutry, and A. Benayad, "Influence of the Core / Shell Structure of Indium Phosphide Based Quantum Dots on Their Photostability and Cytotoxicity," vol. 7, no. June, pp. 1–12, 2019, doi: 10.3389/fchem.2019.00466.

[8] V. Brunetti *et al.*, "quantum dots : in vitro and in vivo toxicity assessment," pp. 307–317, 2013, doi: 10.1039/c2nr33024e.

[9] F. Boxberg and J. Tulkki, "Quantum Dots : Phenomenology , Photonic and Electronic Properties , Modeling and Technology," pp. 107–118.

[10] A. L. Efros and L. E. Brus, "Nanocrystal Quantum Dots : From Discovery to Modern Development," 2021, doi: 10.1021/acsnano.1c01399.

[11] P. M. Petroff, A. Lorke, and A. Imamoglu, "E PITAXIALLY S ELF -A SSEMBLED Q UANTUM D OTS," vol. 46, no. 2001, 2020, doi: 10.1063/1.1381102.

[12] A. Al-ahmadi, – *A VARIETY OF NEW APPLICATIONS Edited by Ameenah Al-Ahmadi*. .

[13] Q. Zhou, J. Zhou, M. Zeng, G. Wang, Y. Chen, and S. Lin, "Photoelectrochemical Performance of Quantum dot-Sensitized TiO 2 Nanotube Arrays : a Study of Surface Modification by Atomic Layer Deposition Coating," 2017, doi: 10.1186/s11671-017-2036-6.

[14] M. Ni, M. K. H. L. Ã, D. Y. C. Leung, and K. Sumathy, "A Review and Recent Developments in Photocatalytic Water-Splitting Using TiO2 for Hydrogen Production A review and recent developments in photocatalytic water-splitting using TiO 2 for hydrogen production," no. April, 2007, doi: 10.1016/j.rser.2005.01.009.

[15] L. B. Hoch *et al.*, "Carrier dynamics and the role of surface defects : Designing a photocatalyst for gas-phase CO 2 reduction," pp. 8011–8020, 2016, doi: 10.1073/pnas.1609374113.

CHAPTER I

General information and theoretical framework

1 General information on semiconductor nanocrystals

1.1 Quantum Dots

Quantum dots (QDs) are crystalline particles of semiconductor or metal with a spherical shape and a nanometer size, with dimension that does not surpass the range of a few tens of nanometers, which implies that in such structures, excitons will be confined to the three dimensions. This corresponds to a few hundred or even ten thousand atoms are called "artificial atoms" because they allow to find the same density of state as an atom.[16]

Figure 1-1 shows a simplified image of a QD.[17] They are composed of a crystalline core covered with a layer of organic molecules. The ligands are generally surfactants containing a polar head bound to the surface of the NCs and a non-polar tail, for example one or more alkyl chains. This layer is necessary to stabilize the individual NCs as colloidal particles and to avoid their coalescence. The core itself may be covered with one or more shells of other semiconductor materials. These shells protect the photoactive core and improve its photophysical properties.

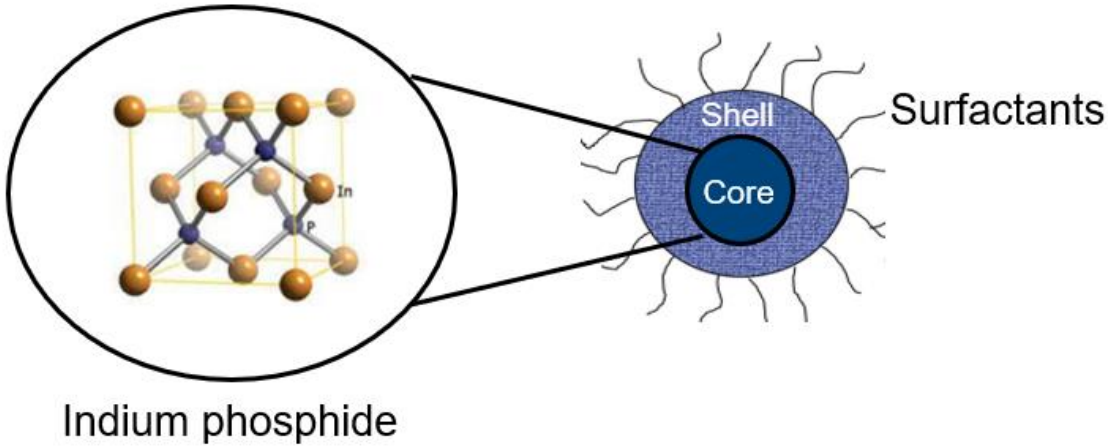

Figure 1-1: Schematic representation of a core/shell semiconductor nanocrystal.[20]

The QDs are therefore generally in the form of colloidal suspensions and can be synthesized via different methods, either directly in an aqueous medium or in organic medium and then transferred to an aqueous medium, if necessary, particularly for applications in a biological medium. [18,19]

Quantum Dots is a very promising tool in many fields, whether in electronics, optics, or medicine. Indeed, the solution processed optoelectronic materials dramatically offer lowered manufacturing price, the ease of synthesis, the high-quality properties, flexible substrate integrability, etc. Therefore, their nature, properties, and the synthesis of QDs are developed in the following paragraph. Moreover, Quantum dots have many applications such as solar cells, biological fluorescence labeling, LED devices, lasers, etc. and it is bound technologies such as nanobiotechnology.

The properties of what were then called "small crystalline particles", the term "Quantum Dot" (QDs) have undergone very rapid development since the first syntheses in 1982 via the research work of A. Ekimov's, and in solution by Louis E. Brus of Bell Laboratories in 1983, in 1986 by Mark Reed [17] and A. Henglein [20]. Since 1990s, QDs structures with reasonable optical properties were developed by epitaxy.[12,13]

Then, the first organometallic syntheses, developed in the Bawendi's group, made it possible to reach nanometric sizes with better control of their dispersion (typically 10% standard deviation in size) [21]. Moreover, that Louis E. Brus noticed differences in the behavior of nanoscale CdS particles compared to the bulk material [22]. Hence, since their discovery, several research works have concentrated on the use of QDs in fields as varied as the manufacture of transistors for electronics, solar cells, LEDs, and other laser diodes.

1.2 Semiconductor material

Generally, there are three types of material: insulators, conductors, and in particular semiconductors. (Figure 1-2)

Electric conduction results from the movement of electrons inside each band under the effect of an electric field. Electrical conduction is therefore determined from two specific energy bands. One is called the valence band which corresponds to low energy and the other is the conduction band which corresponds to high energy.

Concerning the insulators, the valence band is completely occupied by the electrons which prevents charge mobility, and the conduction band is completely empty. Consequently, there is a significant energy barrier that makes electron movement between the two bands impossible. However, in a semiconductor, the energy barrier is intermediate between conductors and insulators. Finally, for the conductors, the conduction and valence bands overlap, hence there is no band gap.[18]

Since the 1980s, technological advances have been made in semiconductor nanocrystals. These nanomaterials have interesting physical and chemical properties to the usual luminescent materials.[20,21]

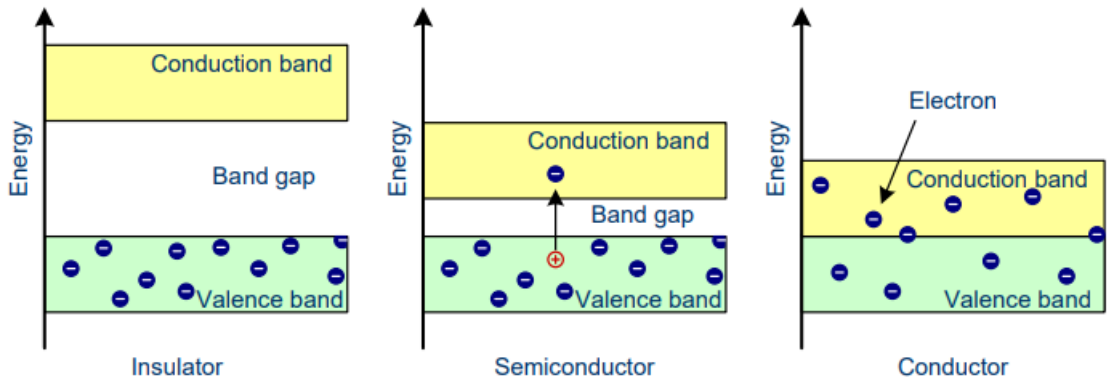

Figure 1-2: Energy barrier of metals, semiconductors, and insulators. [27]

In this section, we will outline the physical properties of semiconductors of the III-V. Type III-V semiconductors are binary products composed of an element from column IIIA and an element from column VA of the periodic classification of the Mendeleyev Table, which are organized together to form two face-centered cubic sub-arrays offset from each other by a quarter of the cube's diagonal (a/4).There are several examples of these binary materials, such as gallium arsenide (GaAs), indium phosphide (InP) or gallium phosphide (GaP), and gallium (GaN).These semiconductor materials have applications as optical photoelectric sensors, lasers, solar cells, and modulators.

1.3 Structural properties of semiconductor

II-VI semiconductor Nanocrystals NCs exhibit the phenomenon of polymorphism, means they can crystallize in two distinct structures, zinc blende (ZB) and wurtzite (W) (figure 1-3).

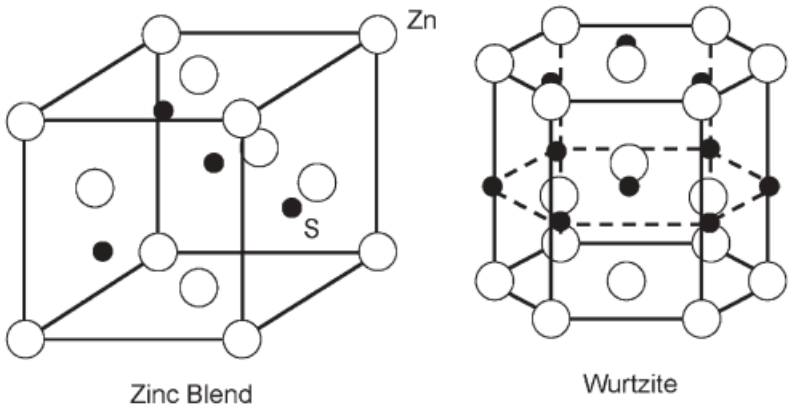

Figure 1-3: Elementary crystal lattices of the zinc blende (left) and wurtzite (right) of ZnS.

The Indium phosphide material is an example of a binary compound of type III-V. It crystallizes in the cubic zinc-blende structure. Figure 1-3 shows the elementary mesh (a) of the zinc blende structure, with the different positions of the indium and phosphorus atoms; indium atoms occupy the different cfc (face-centered cubic) positions of the cubic lattice,

while the phosphorus atoms occupy the four tetrahedral sites. The bonds between atoms III and V are strongly covalent; however, there is a weak ionic character in these bonds. In the case of indium phosphide, phosphorus has five peripheral electrons and indium has three. In the crystal, each indium atom is surrounded by four phosphorus atoms, and each phosphorus atom is surrounded by four indium atoms. There is therefore exchange of electrons so that each atom has four peripheral electrons. This distribution is at the origin of the partially ionic and partially covalent character of partly covalent character of the III-V bonds.

Most III-V semiconductors have a band pattern with a direct transition; this is called a direct gap. This gap that separates the last occupied states of the valence band and the first free states of the conduction band. Figure 1-4 shows the band diagram of the InP semiconductor. In general, direct-gap materials are best suited for optoelectronic. [34]

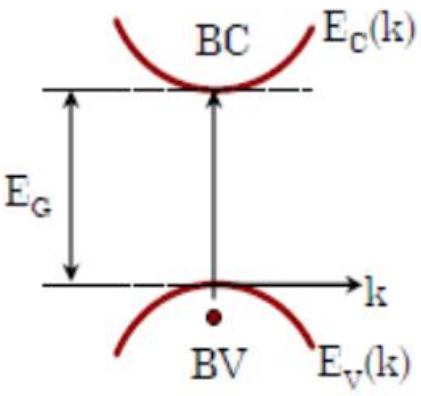

Figure 1-4: Electronic band structure of indium phosphide. [29]

The following table 1-1 shows some examples of the bandgap along with the interatomic distance.

Table 1-1: Example of gap and interatomic distance values.

	InP	Gap	InAs	InSb	GaAs
Eg(eV)	1.35	2.26	0.36	0.18	1.42
a_0 (Å)	5.87	5.45	6.06	6.48	5.65

Except for GaP, which is an indirect gap semiconductor, all the semiconductors presented in this table are direct transition. The InSb semiconductor has the highest lattice parameter while having the lowest band gap energy. This material provides better confinement of charge carriers.

2 Properties of Quantum Dots

2.1 Effect of the size and quantum confinement properties

The main interest of nanomaterials lies in the fact that new properties will emerge, and that these properties will vary according to the size and shape. For semiconductor-based nanoparticles, these variations can be demonstrated by a size effect called quantum confinement. In a bulk semiconductor, an electron can be excited from the valence band into the conduction band under ultraviolet light excitation by an energy input at least equal to that of the gap of the material, the wavelength of which varies according to their size. Therefore, it would be possible to obtain the full color range of the visible spectrum by varying only this parameter. Figure 1-5 is a photograph of solutions of different sizes of ultraviolet illuminated colloidal nanocrystals. [22] The red shift of the fluorescence of the larger core nanocrystals shows the effect of quantum confinement. Today it is feasible to achieve fluorescence quantum yields of such objects of more than of more than 80 % at room temperature.[23]

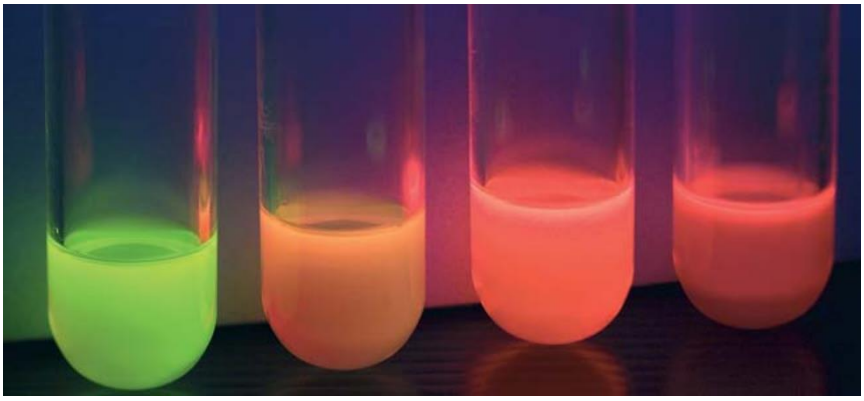

Figure 1-5: Semiconductor nanocrystals subjected to radiation ultraviolet rays.

Therefore, the unique properties of QDs stem from their small size (typically less than ten nanometers), which results in semiconductor elements with a high (nanometers) a scalable band gap and discrete band gap and discrete electron energy levels (Figure1-6).

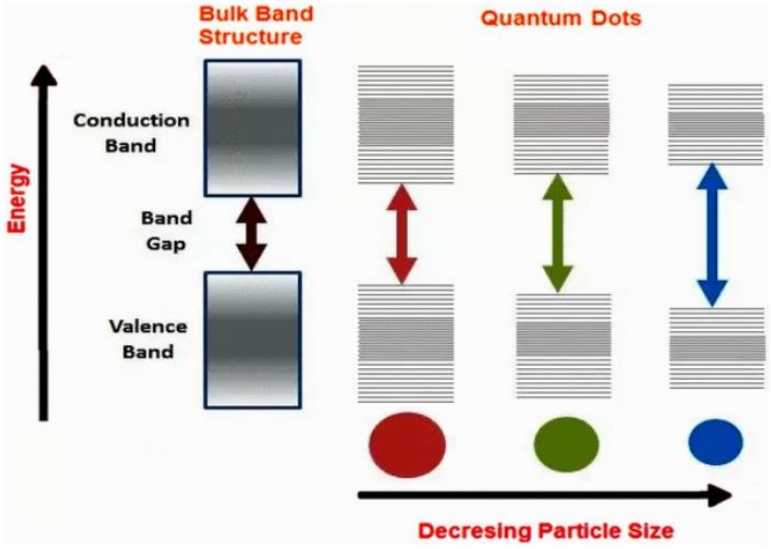

Figure 1-6: Electronic structure of a macroscopic semiconductor and Evolution of the gap according to the size of the QD.[32]

When a Quantum Dot is excited by photons with an energy bigger than or equal to the gap energy (Eg), an electron-hole pair is created. This nanoparticle can then emit a fluorescence

photon whose wavelength depends on the energy of the gap. Indeed, wavelength depends on the recombination energy between the fundamental levels of the electron and the hole.

Following a sufficient supply of energy (Eg), an exciton is formed and will allow for example, electrical conduction. The physical distance between the electron and the hole, called the Bohr radius, will have a discrete value, and which will determine the energy of the gap to be crossed to obtain this exciton. A specific Bohr radius of the semiconductor material is defined by the equation:

$$r_B = \frac{4\pi\varepsilon_0\,\varepsilon_r\hbar^2}{e^2 m_e}\left(\frac{1}{m_e^*}+\frac{1}{m_h^*}\right) \quad (1.1)$$

Where:

m_e^* = Effective masses of the electron of the exciton,

m_h^* = Effective masses of the hole of the exciton,

ħ = Planck's constant (ħ = $1.0546.10^{-34}$J.s),

m_e = The mass of the electron in vacuum (m_e = $9.110.10^{-34}$ kg),

ε_r = The static dielectric permittivity,

ε_0 = 8.854.10-12 F/m

e = Elementary charge (e=$1.602.10^{-19}$ C),

The m_e^* *and* m_h^*, rays of Bohr and ε_r depend on the material under consideration.

Three different confinement regimes can then be encountered depending on the size of the semiconductor nanoparticle. They depend on the size of the Bohr radius of the semiconductor material.

1) When the size of the semiconductor is very large compared to the Bohr radius $r >> r_B$, the electronic confinement regime is weak. Neither the electron nor the hole of the exciton obtained after irradiation are confined.

2) When $r \approx r_B$, the confinement regime is intermediate. Only the electron of the electron-hole is then confined within the nanocrystal.

3) When $r << r_B$, the confinement regime is strong. This time the hole and the electron are confined by the size of the nanoparticles.

In the case of Quantum Dots, the Bohr radius of the exciton is larger than the particle itself. It corresponds to quantum confinement. Thus, the energy diagram of a molecule consists of discrete energy levels, whereas that of a bulk material consists of energy continuum bands. Therefore, the Quantum dots is small and more the Bohr radius will be spatially constrained, the more energy the exciton will have, hence more the gap will be higher. So, one of the main characteristics of Quantum Dots is the increase in bandgap energy as their size decreases. (See Figure 1-6).

Assuming spherical Quantum Dots, the value of the gap energy Eg (in eV) of a Quantum Dots is offered by the formula (1.2) [24]:

$$E(r) = Eg(massif) + \frac{h^2}{8r^2}\left[\frac{1}{m_e^*} + \frac{1}{m_h^*}\right] - \frac{1.8\, e^2}{4\pi\, \xi_0 \xi_r\, \mathrm{r}} \quad (1.2)$$

Were:

Eg = The band gap,

$1/r^2$ (r in nm) = quantum confinement,

m_e^* = Effective masses of the electron of the exciton,

m_h^*= Effective masses of the hole of the exciton,

ħ = Planck's constant (ħ = $1.0546.10^{-34}$J.s),

ε_r= The static dielectric permittivity,

ε_0 = 8.854.10-12 F/m.

For the semiconductor nanoparticles used during this thesis (InP cores and InP/ZnS core/shell) a strong quantum confinement is observed. The InP core within nanoparticles have a size of between 2 and 7 nm, well below the Bohr radius of the material r_B = 9.9 nm. (See Table 1.2).

Table 1- 2: Parameters of some II-VI and III-V semiconductors.[34]

Materials	Structure	Type	Eg(eV) (300K)	m_e^*	m_h^*	ξ_r	r_B
ZnO	würtzite	II-VI	3.3	0.26	0.6	8.2	2.4
ZnSe	Zinc blende	II-VI	2.7	0.157	0.75	8.7	3.6
ZnS	**zinc blende**	**II-VI**	**3.6**	**0.28**	**0.61**	**8.9**	**2.5**
CdS	würtzite	II-VI	2.52	0.2	0.7	8.8	3.0
CdSe	würtzite	II-VI	1.76	0.12	0.45	9.5	5.3
CdTe	zinc blende	II-VI	1.45	0.1	0.4	7.2	4.8
GaAs	zinc blende	III-V	1.42	0.063	0.5	12.9	12.2
InP	**zinc blende**	**III-V**	**1.34**	**0.075**	**0.64**	**12.56**	**9.9**
InAs	zinc blende	III-V	0.35	0.027	0.41	14.9	31.2

On other side, when one of the 3 dimensions becomes very small than the De Broglie wavelength, we obtain quantum confinement in this direction. This implies a discretization of the energy levels and thus modifies the density of state, which quantifies the electronic states available for a given energy. This function of the energy therefore depends on the dimensionality of the system. As shown in figure1-7 the dimensionality of the density of states of the entities described, from the macroscopic crystal to the quantum dot. [25]

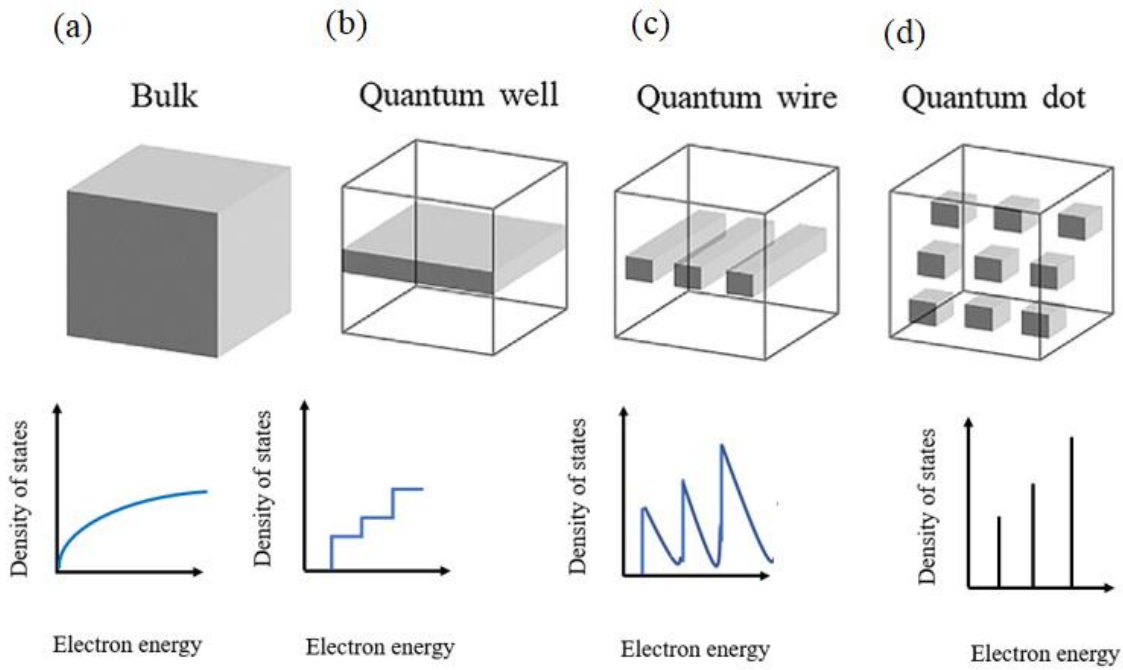

Figure 1-7: Representation of different systems for which the dimensionality of the density of states of states is progressively reduced.[40]; (a) a bulk material, (b) a Quantum Well, (c) a Quantum Wire and (d) a Quantum Dots.

In a bulk semiconductor, the carriers can move in all three directions in space. It has an energy band structure with dispersion in all three directions. The density of states around the gap then has a parabolic shape. A Quantum Well consists of a nanometric layer of a

semiconductor of low bandgap energy embedded in a semiconductor of higher bandgap energy. In this case, the electrons undergo a quantum confinement effect along one direction of the order of their de Broglie wavelength. The dispersion relation in this direction becomes discrete, without changing the dispersion relation in the other two directions. A reduction in the dimensionality of the potential shape allows the description of Quantum Wire systems, which have their density of states reduced to systems of Quantum Wires and takes on a shape known as "staircase", and Quantum Dots, which have their density of states reduced to zero dimensionality and the density of state takes the form of Dirac peaks. It is then close to that observed in atoms.[26] However, this analogy has its limits, as Quantum Dots are nanostructures composed of a few thousand atoms, and they are also coupled with their crystalline environment, inducing different properties as we will see later. This quantum confinement effect modifies the electronic properties of the structure. Thus, Quantum Dots contribute to the improvement of the current properties of devices in optoelectronics and photonics and open the way to new and very promising new applications.

2.2 Optical properties of Quantum Dots

The phenomenon of Exciton confinement in Quantum Dots in three dimensions will lead to some effective interesting properties, mainly photo physical. QDs are semiconductors whose physics-chemical properties are directly dependent on their shape and size of the nanoparticle.

2.2.1 Emission wavelength

The emission wavelength of QDs is directly related to their size. Indeed, if we refer to the simplified model of a particle in a QDs in the three-dimensional case, means for infinite potential barriers, without considering the deformation tensor and the Quantum Dots environment, we obtain the equation below giving the energy trend as a function of the dimensions of the nanostructure:

$$E_{nx,ny,nz} = [\frac{\hbar^2\pi^2}{2m}(\frac{n_x}{l_x})^2 + (\frac{n_y}{l_y})^2 + (\frac{n_z}{l_z})^2] \quad (I.3)$$

Were:

ħ = Planck's constant (ħ = $1.0546.10^{-34}$J.s),

m= Mass of the particle,

n_i= A positive non-zero integer

l_i= The size of the dimension following.

The energy is therefore inversely proportional to the square of the dimensions. The smaller the Dots are, the greater their energy and therefore the smaller the emission wavelength. The height of the Quantum Dots being often much smaller than their diameter (lens-shaped Quantum Dots), it is this dimension that determines their confinement energy and therefore their emission wavelength.

2.2.2 Absorbance and photoluminescence

As mentioned earlier, the photophysical properties of Quantum Dots depend on their dimensions and more precisely on the quantum confinement.[27] The optical properties of Quantum Dots enclosed the measurement of absorbance and photoluminescence.

The wavelength of a photon can be expressed as a function of its energy according to the relation:

$$\lambda = \hbar c / E_{photon} \quad (I.4)$$

Were:

ħ = Planck's constant (ħ = $1.0546.10^{-34}$J.s),

C= Speed of light in vacuum (c= 299 792 458 m/s),

E_{photon}= This is the energy of the photon

This relationship shows us that the more energetic a photon is, the shorter its wavelength will be.

An absorbed photon will therefore have a wavelength (equation I.5):

$$\lambda_{abs} = \hbar c/Eg \ (I.5)$$

This implies that a decrease in the size of the Quantum Dots leads to a shift in the absorption threshold due to the increase in Eg because of the quantum confinement phenomenon. [28]

A well-defined absorption maximum appears at the energy threshold, which accords to the first excitonic peak, means the optical transition from the first excitonic state (figure 1-8). The position of this peak depends on Eg and therefore on the size of the QDs, but a continuum of absorption for wavelengths below that of this first excitonic peak is observable regardless of the size or nature of the QD. Absorption bands can sometimes appear in this region of the spectrum [9].

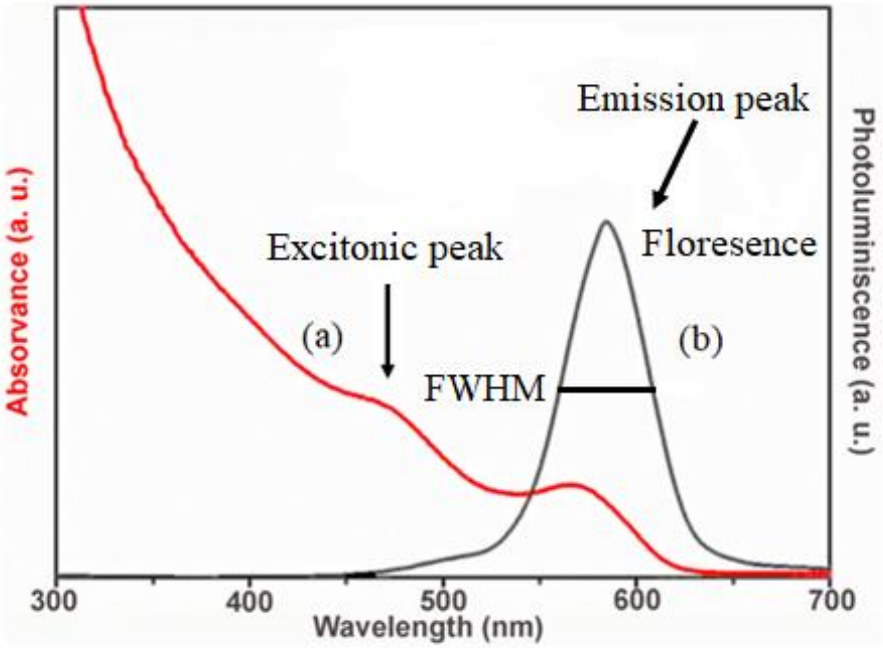

Figure 1-8: Typical absorption (a) and photoluminescence (b) spectra of quantum dots. The first excitonic peak is indicated by an arrow; also, the emission peak.[39]

The position of the excitonic peak is related by the gap and the diameter of the Quantum Dot. The shape and width of this peak are affected by the size distribution of the nanoparticles. The Full Width at Half Maximum (FWHM) of this peak corresponds to the polydispersity of the QDs in solution, a decisive parameter to control during the synthesis (Figure 1-8). For example, for a monodisperse population, the width at half height of the fluorescence spectra is of about 20 to 30 nm. If the QDs are more polydisperse in size, the half-value width of the spectrum can reach 50-60 nm. Furthermore, the peak energy is equal to the band gap energy and the peak intensity is a function of the passivation of the QD surface. Surface defects can also widen the peak [29]

2.2.3 Photoluminescence

Upon light excitation, the QD absorbs a photon leading to the formation of an exciton (electron-hole pair). Through radiative electron-hole recombination, the electron can return to its ground state (valence band) generating fluorescence. The spectrum of photoluminescence (PL) spectrum shows a fine, symmetrical line that moves with the diameter of the QDs (Figure 1-8). In theory, fluorescence corresponds to the emission of a photon of energy equal to the gap Eg. In fact, the PL line is shifted by a few nm towards longer wavelengths. This shift, called the shift originates from the particular structure of the energy levels of QDs. [30,31]

2.2.4 fluorescence

The development of semiconductor nanocrystal syntheses is particularly motivated by their fluorescence properties. These are very interesting compared to those of organic fluorophores. When the exciton is formed after the absorption of a photon, the system can return to its initial state by radiative recombination of the electron and hole. By performing a fluorescence spectrum, a narrow symmetrical line appears corresponding to an energy equal to that of the band gap. (Figure 1-8). However, a Stokes shift is classically observed. If the energy absorbed by excitation of a photon is greater than the band gap, then there is a loss of energy (heat or phonons) from the excited electron between the time of its excitation and relaxation.[32,33] One way of quantifying these phenomena is the quantum yield (QY),which can only be obtained for nanoparticles with a well passivated surface. Therefore, it is obtained from the ratio of the number of photons absorbed to the number of photons emitted.

3 Applications of Quantum Dots

Quantum Dots is considered as a pioneering and ground-breaking science. It is a widely studied system, both theoretically [34,35], and experimentally [36]. This latter is extensively seen as a unified technology having a deep impact in the everyday life and can be used across diverse fields of science [37,38]

In this regard, particular attention is paid to the fact that many researchers focus on nanoscience's and nanotechnologies, which have been newly extended and adapted in several science areas (such as electronics, mechanics, chemistry, optics, biology, etc.)

Quantum Dots have many significant advantages combining solution processing with the spectral tenability offered by the effect of quantum size effect. In fact, solution-processed optoelectronic materials offer reduced fabrication cost and facilitate large-area fabrication. As an example, televisions based on a quantum box filter are classic LED televisions. TVs based on a quantum box filter, which are conventional LED TVs. Also, the international company Amazon uses the Quantum Dots filter on its Kindle tablet. In addition, that, Quantum Dots have many applications such as solar cells applications, light emitting diodes, in the design of lasers, sensors, photodetectors and transistors. [39,40]

Moreover, A very promising application of Quantum Dots is their use in the biomedical field and more particularly for biomedical imaging. In this domain, organic fluorophores are mainly and historically the most used. They exhibit low toxicity and rapid elimination. However, their properties optics are not optimal. Indeed, these systems have an emission wavelength fixed, low fluorescence intensities when observed as a single particle and they photobleached very quickly.[28]

4 The choice of the material and Different pathways of InP synthesis

4.1 The Choice of indium phosphide Quantum Dots

In this work, the key question that can be here asked is "how to reconcile the best Quantum Dot in order to have good conductivity and try to avoid the drawbacks of this QD and efficiently produce the energy"[41]. On the other hand, the challenge arises in trying to pick out relevant materials for energy conversion [42,43].

Indium phosphide is an inorganic compound with the formula InP, it is a binary semiconductor of type III V, made up of indium and the phosphor. Like most III-V semiconductors, indium phosphide has a blende-type structure, means two face-centered cubic meshes (CFC) of each of the two components nested and shifted by one vector (1/4;1/4;1/4), or from another point of view, a CFC mesh is one of the constituents in which four of the eight tetrahedral sites are occupied by the other constituents.

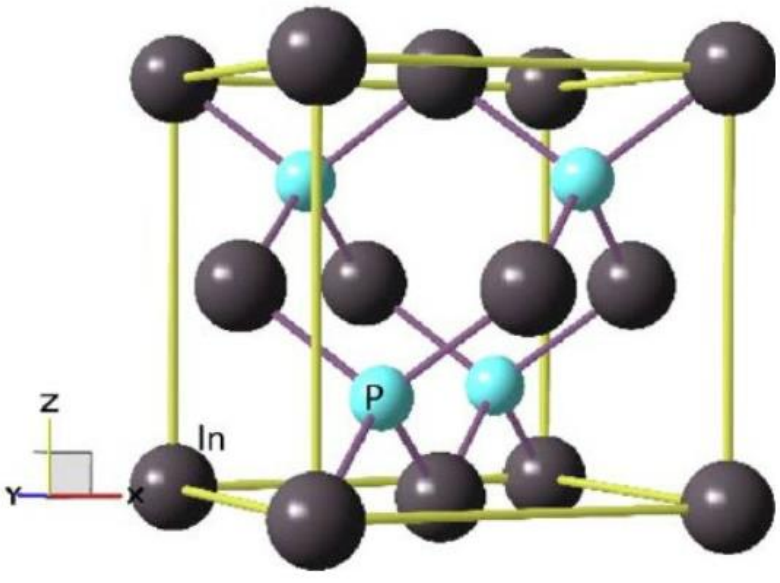

Figure 1-9: Crystal structure of InP.[59]

There are several reasons why we decided to work on InP. The first is the toxicity of

NCx semiconductors II-VI, means based on cadmium, lead and mercury. Indeed, these materials, despite their greater maturity in terms of synthesis compared to InP (notably CdSe), have significant intrinsic toxicities.

In addition, comparative studies between InP/ZnS and CdSe/ZnS show that the former are more stable.[44–46]Indeed, the InP/ZnS are less degraded and the elements are not released into the biological environment.[42,47] In vivo, the study also shows that InP/ZnS affect the biochemical system less than CdSe/ZnS, which can lead to destruction of membranes, genes and the disruption of several biochemical phenomena necessary for life.[10] Other studies show the very low intrinsic toxicity of InP.[10,48]

InP has a direct band gap energy at 300 K of 1.35 eV which corresponds to 925 nm in wavelength and a lattice distance constant 5.9 Å, which favours the recombination of charge carriers, [49] its quantum confinement effects are greater than those of semiconductors of the II-VI series (CdS, CdSe).

The crystal structure of this Nanocrystal semiconductor is predominantly made of zinc blende, although growth in wurtzite is possible. Its Bohr radius is about 12 nm.[50] Bare InP generally have a Quantum Yield (QY) of less than 1% mainly due to defects and surface traps. These nanocrystals are also very sensitive to oxidation in the presence of water and oxygen.[51] To increase their optical properties and stability, it is common to grow a shell of another semiconductor. In this way, it is possible to obtain highly luminescent objects up to 70-85% QY.[52]

In addition to its lower toxicity compared to II-VI materials, the wide range of wavelengths achievable by InP makes it a material of choice for optoelectronic or biomedical applications.

Like all luminescent semiconductor, we can modulate the emission wavelength of the InP according to its size. Given its wide band gap and large Bohr radius, it is theoretically

possible to Nanocrystal emitting in the whole spectrum from visible to near IR. This wider electromagnetic spectrum compared to CdSe makes it possible to envisage applications in the biomedical applications that are not possible with CdSe NCx. In recent years, the growing interest in the synthesis of InP nanocrystals has led to the publication of reviews on the subject.[28] Therefore, the wide variety of compounds that can be made, make them excellent candidates for the improvement of future optoelectronic components. [53]

So, it is important to note that the presented investigation focuses on InP because it is considered as an excellent material related to several research works existing in the literature which have proved that a direct gap material is better suited for optoelectronic applications [51]. Thus, there is a considerable potential linked to the InP material for building high-performance optoelectronic devices and developing next generation displays [54].

4.2 Methods to synthesis nanocrystals (NCs)

In the last 25 years, the synthesis of nanoparticles has brought huge interest with outstanding features such as ease in the synthesis and the high-quality properties obtained. These characteristics have offered various promising applications. [55,56]

Indeed, two approaches exist for the synthesis of NCs: the physical process, and colloidal solution chemistry techniques.

Physical synthesis can be done for example by lithographic techniques or epitaxial.[57,58]. The advantage of these is that they allow the production of considerable quantity of NCs. Conversely, colloidal liquid phase synthesis is advantageous for obtaining monodisperse NCs with good control, although the quantities produced are generally much smaller than a gram. This is the type of technique that we will develop in this thesis.

Thus, the synthesis of NC semiconductors is classified into two types: on the one hand, precipitation in the aqueous phase, in the presence of stabilizers, on the other hand,

preparation of Nc in non-aqueous phase. The non-aqueous phase has two important features: the temporal separation of the nucleation and the growth.

4.2.1 Synthesis in aqueous media

This method is carried out in an aqueous solution containing the appropriate reagents and stabilizers such as surfactants or polymers.[84] It ensures the formation of nanocrystals. Surfactants bind to the surface of the nanoparticles by steric hindrance or electrostatic.

The advantages of this method are the simplicity of their experimental conditions and the use of standard reagents. However, it has certain limitations[59]: the nanoparticles obtained are generally weakly crystalline due to the low reaction temperature, the synthesis yield is often low and the size dispersion of the synthesized NCs is mostly higher than 15%.

4.2.2 Synthesis in non-aqueous media

The introduction of high temperature preparation methods in 1993 has been a very important advance for the synthesis of CdS, CdSe and CdTe NCs that are much more monodisperse than those made in the aqueous phase.[21] The change is the use of neutral organometallic precursors in an organic solvent under high temperature.

Among the neutral organometallic precursors used in the literature in the late 1980s were trioctylphosphine selenide and dimethyl cadmium. During these works, the synthesize of CdSe clusters and NCs at different sizes was done by organometallic precursors in reverse micelles at room temperature according to the research group of Steigerwald et al. [86]

4.2.3 Coordinating solvent synthesis

The first syntheses in non-aqueous media were carried out in coordinating solvent. The choice of solvent in this case is very importance because it acts as a surface ligand, it conditions the "solubility" of NCs and the stability of the colloidal dispersion. During this synthesis, the ubiquitous solvent molecules growth forming a steric barrier for the reagents. This experience results in particles that exhibit very good crystallinity in the wurtzite structure.[60]

Generally, the coordinating solvents used are a mixture of alkylphosphines R_3P and alkylphosphine oxide R_3PO (where R is an alkyl chain containing 4 or 8 carbon atoms).[61]

Two approaches to coordinating solvents were used in succession: the first was based on organometallic precursors, and the second was based on inorganic precursors.

4.2.3.1 Organometallic synthesis

The first organometallic synthesis recorded typically led to NCs with a size dispersion of 8-10% for CdSe and 10-15% for CdS and CdTe.[62] This experience is based on using organometallic, chalcogen precursors in a coordinating solvent under high temperature.

Hence, the introduction of cosurfactants such as hexadecylamine HDA has affected of the size dispersion of the NCs.[54] The surface passivation has been greatly improved due to the reduced steric hindrance of these surfactants, increasing the Quantum Yield (QY) to values of 10-25%.[54,63]

The increase in the quantity of Se at lower temperatures (240°C) promotes order and surface reconstruction, leading to the reproducible formation of quasi-monodisperse CdSe NCs with QY up to 85%.[63,64]

A wide variety of coordinating precursor/solvent pairs, allowing the mutual interactions to obtain the optimal synthesis parameters for each type of NCs, makes this method very versatile.

4.2.3.2 Inorganic synthesis

Synthesis from inorganic precursors has been developed more recently by Peng et al.[65]

The Cd phosphonate complex is sufficiently reactive with respect to trioctylphosphine selenide and tellurium and leads to monodisperse NCs of 2.5 -5 nm in diameter. As in the case of organometallic synthesis [89], the size distribution can be improved by using a mixture of solvent trioctylphosphine oxide (TOPO)/HDA.[92] Hence, the nanoparticles synthesized using carboxylic acids for cadmium complexation. The shape of these nanoparticles can be controlled by the amount of the concentration of monomers, which in any case must be higher for anisotropic growth than for spherical particles.

4.2.4 Synthesis in non-coordinating solvent

Coordinating solvents such as TOPO and HDA are solid at room temperature, harmful and expensive, which is why they have recently been replaced by non-coordinating solvents which do not have these disadvantages. [66] These new solvents are typically long-chain alkanes or alkenes such as 1-octadecene ODE. Unlike coordinating solvents, non-coordinating solvents cannot play the role of ligand in the prepared of NCs. The control of the size of the NCs is done by changing the amount of ligand (means phosphines, carboxylic or phosphonic acids) introduced into the medium.[67] This type of synthesis allows monodisperse NCs and has already been adapted to several types of semiconductors: ZnS, ZnSe [68], ZnxCd1-xS [69], InAs, InP [70,71] or even PbSe [92].

With the development of non-coordinating solvent synthesis, selenium dissolved in ODE (Se/ODE) based syntheses have been developed for CdSe, thus avoiding the use of air-sensitive trialkylphosphine selenides.[72] However, Jasienak et al. observed that Se/ODE leads to a twofold lower number of nuclei than TOP-Se, indicating that selenium is more

accessible with TOP-Se than with than with Se/ODE. [73] CdSe NCs have been newly obtained using olive oil as a coordinating solvent, thus reducing cost of reagents. [73]

To simplify the synthesis protocol and to obtain a synthesis that can be easily transposable on a larger scale, many teams have sought to free themselves from the sought to avoid the limiting step for the purpose of extrapolation: the rapid injection of the precursors.[74]

4.3 Formation mechanism

Colloidal syntheses are aimed at obtaining dispersions composed of objects with equivalent properties and a suitable size in order to obtain a monodisperse population, means with a variation in size of less than 5%.[75]

LaMer et al. initiated this research and proposed the concept of burst nucleation at 1940s. [76] During this experience, the shape and the size distribution of these nanoparticles can be controlled throughout the growth process. Otherwise, nuclei would form during growth, the history of each particle would be different, and control of size dispersion would become very difficult. Thus, the synthesis of colloids requires a separation in time of nucleation and nucleus growth. [76] LaMer et al. use the homogeneous nucleation process for this separation. In this process, the nuclei appear in a homogeneous solution without any seeds for heterogeneous nucleation. There is then an important potential barrier for nucleation, as the system changes spontaneously from the homogeneous to the heterogeneous phase.

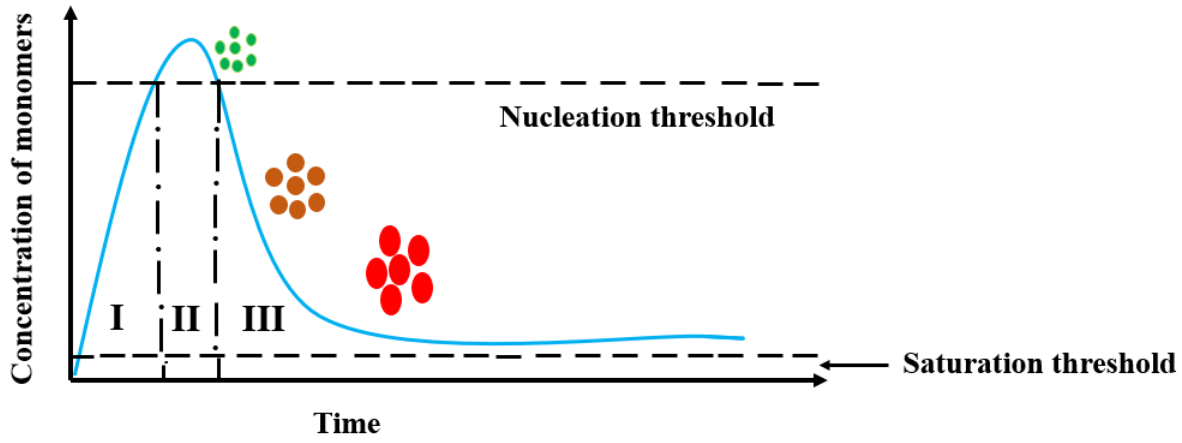

Figure 1-10: LaMer model representing the evolution of monomer concentration as a function of the time.[94]

The LaMer diagram, Figure 1-10, shows the evolution of the supersaturation of the solution as a function of time and is very useful to visualize how the potential barrier can induce instantaneous nucleation. This model can be broken down into three stages noted I, II and III.

When the precursors are injected into the reaction medium, a significant conversion of the precursors into monomers (reactive species) occurs. The concentration of monomers then increases sharply until the medium is supersaturated. This increase in concentration continues to lead to the nucleation threshold (stage I). There is then spontaneous formation of nuclei, which corresponds to the appearance of a crystalline phase within a liquid supersaturated with monomers. The formation of the nuclei causes a decrease in the concentration of monomers, which falls below the nucleation threshold (stage II). Nucleation stops in favour of the growth phase (stage III).

In his model, LaMer also introduces the concept of a nucleation explosion which this explosion occurs if the nucleation and growth stages are not separated. This explosion occurs if the nucleation stage is very short because all the nuclei are formed very quickly and then a slow and "homogeneous" growth of the NCx. This separation in time between the nucleation phase and the growth phase makes it possible to obtain more monodisperse NCx.

The growth stage is governed by a thermodynamic equilibrium between the monomers present in solution and the NCx formed. If the concentration of monomers remains slightly above the supersaturation threshold and if we consider the growth of NCx growth limited by diffusion phenomena, then the size dispersion of the sample decreases during the growth phase.[77,78]

Another phenomenon takes place during the formation of NCx and results in the increase in the sample size dispersion. This is the Ostwald ripening which corresponds to the inter-diffusion of monomers from the smallest particles to the largest. Thus, the size of the smallest particles decreases until they are completely consumed and the size of the largest increases.

To obtain a sample with good properties it is properties, it is preferable to avoid this phenomenon which makes the size dispersion of NCx.

4.4 Different ways to synthesis InP

4.4.1 Synthesis InP in coordinating solvents

A coordinating solvent acts as both a solvent and a ligand to stabilize the NCx in solution.

The synthesis of NCx of CdE (E = Se, S, Te) in a mixture of trioctylphosphine and trioctylphosphine oxide (TOP/TOPO) is based on the work of Murray et al.[8], Micic et al. developed a new type of synthesis of InP Quantum Dots in these same high-boiling solvents (about 400 °C).[79] The syntheses of InP QDs are carried out almost exclusively in Schlenk glassware under an inert atmosphere because of the sensitivity of the material to water and oxygen. In 1994, they proposed a high-temperature synthesis (260-300 °C) in a TOP/TOPO mixture.[79] The indium precursor, a chlorooxalatoindium, is mixed with P(TMS)3 in TOP/TOPO mixture at room temperature (RT) and then heated to 270°C for 3 to 7 days.

The Quantum Dots are characterized by absorbance, fluorescence, X-ray diffraction (XRD) and high-resolution TEM spectroscopy (Figure 1-11).

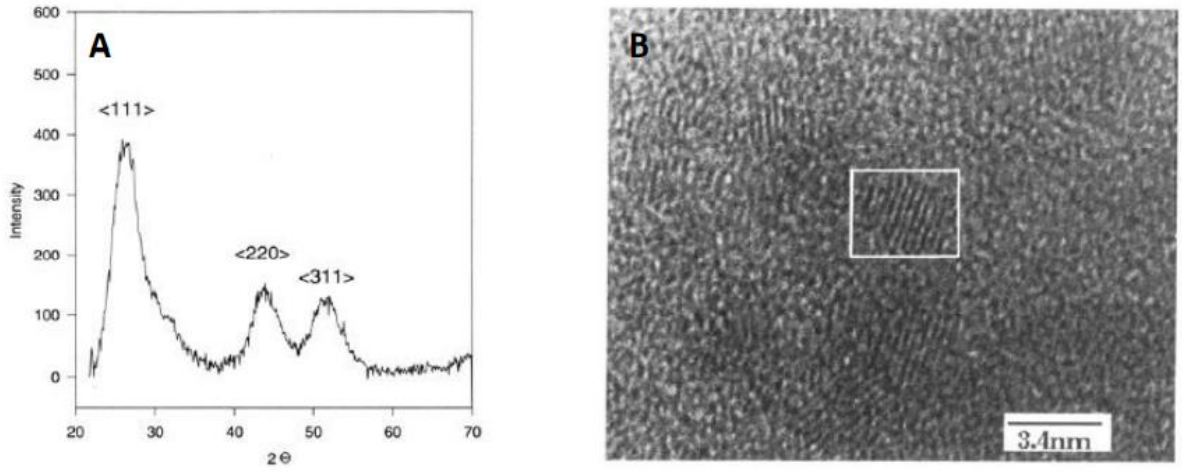

Figure 1-11: (A) X-ray diffractogram and (B) high resolution TEM image of InP NCx synthesized in a TOP/TOPO mixture.[98]

The absorbance spectra of the objects obtained show a first electronic transition with a broad shoulder around 530 nm. The Quantum Dots have a diameter of about 2.5 nm and have a zinc blende structure. However, no fluorescence is observed, only the surface states are visible. Subsequently, the same group improved this first synthesis by increasing the size of the accessible Quantum Dots particles by varying the precursor concentration and decomposition temperature.

In 1998, they showed that their Quantum Dots are partially oxidized on the surface. Guzelian et al. shown that an oxide layer forms on the surface of InP by X-ray photoelectron spectroscopy (XPS). [79,80]

In 2001, Micic et al. compared the inter-particle interactions between Quantum Dots film and a colloidal solution.[81] They observe that the excitonic peak is shifted to longer wavelengths and is larger in film than in solution.

After the synthesis of Micic et al., in 1994, other groups are interested in the synthesis of InP NCx. Alivisatos group proposed a synthesis in TOPO alone at high temperature.[80] the

precursors used are indium chloride (InCl3) and P(TMS)3 and the reaction lasts more than a week. The NCx obtained have a size ranging from 2 nm to 5 nm with a very good crystallinity and the characterizations carried out are very complete. After synthesis, the NCx are selectively precipitated which allows for sample size selection. In addition, the NCx undergo post-synthesis ligand exchange to solubilize them in different a polar solvent. They show that surface oxidation of NCx exposed to air causes an increase in fluorescence intensity, which they explain by a partial passivation of the surface of the partial passivation of the surface of the nanoparticles by the oxides.

The TOP/TOPO mixture was the most widely used coordinating solvent for the synthesis of InP Quantum Dots.

The synthesis of InP in coordinating solvent is the first path for the synthesis of InP with controlled size and optical properties. However, time constraints (several days) and post-synthesis size selectivity treatments have pushed towards the development of synthesis in non-coordinating solvents.

4.5 Synthesis InP in non-coordinating solvents with $P(TMS)_3$

Non-coordinating solvents do not act as ligands, unlike coordinating solvents. In this case, it is usually necessary to add ligand molecules to stabilize the nanoparticles in solution during and after the synthesis. Non-coordinating solvent synthesis has allowed a real breakthrough in InP synthesis by reducing reaction times and improving dispersion in solution. Non-coordinating solvents do not interact with the reagents that form the NCx. These solvents do not interact with the NCx and thus avoid blocking growth. The first non-coordinating solvent synthesis was developed by Peng's group in 2002 and allows the production of InP NCx in a few hours.[71] This involves injection at high temperature (300 °C) of $P(TMS)_3$ on a mixture

containing octadec-1-ene (ODE, Teb = 315 °C), indium acetate (In $(OAc)_3$) and a long alkyl chain. A preliminary acetate/long alkyl carboxylate exchange is carried out, by eliminating the acetic acid formed under vacuum at 120°C. Within a few minutes, NCx up to 3 nm in diameter are synthesized (maximum excitonic peak at 560 nm). The NCx show a well-defined absorbance spectrum but a very weak fluorescence. The narrow widths at the midpoints of the peaks show a reduced size dispersion confirmed by the TEM images with a dispersion of 4.7%.

Subsequently, several variants of the Peng team's synthesis were developed. In 2007, the same group described the use of an amine/carboxylic acid mixture in ODE with a reduced reaction temperature (<190 °C) and a reaction time of minutes. In $(OAc)_3$ and $P(TMS)_3$ react in the solvent/ligand mixture to NCx of InP with an absorbance maximum at the first excitonic peak of up to 700 nm. This synthesis shows good control of the NCx size and the role of the amine as an activator of indium carboxylates is suggested. ODE is the main non-coordinating solvent used for the synthesis of InP but some alternatives have been presented such as the use of esters. Xu et al. propose methyl myristate or dibutyl sebacate as a low-coordinating, high-boiling solvent.[82] For this synthesis, trimethylindium (InMe3) and $P(TMS)_3$ are introduced at high temperature into an ester/ligand mixture. The nature of the ligands used is studied and their role as their role as activators of $P(TMS)_3$ by hydrolysis is proposed. Although the NCx obtained are small (about 2.5 nm), the size dispersion is narrow. Other studies have also been carried out on the synthesis of InP using $P(TMS)_3$ by modifying the reaction conditions. In 2005, Strouse's team proposed a synthesis of InP in the microwave based on the synthesis of Peng's group.[83] In particular, the use of microwaves makes it possible to obtain a homogeneous temperature throughout the solution even at 300 °C. This synthesis is very fast and allows to obtain NCx with a very low size distribution (about 6%) and with an increase in fluorescence of up to 15% of the naked NCx. This strong increase will

be explained later by in situ stripping of the InP NCx.[84] Unfortunately, despite obtaining InP nanoparticles of very good quality, this method is difficult to perform because of the high cost of using an ionic liquid as a solvent.

$P(TMS)_3$, although still the most studied precursor, is toxic and highly pyrophoric in contact with air, which makes it a dangerous precursor to use.

4.6 Synthesis InP with P(NMe2)3

Tris(dimethylamino)phosphine $P(NMe_2)_3$ or more generally tris(dialkylamino)phosphine is a phosphorus precursor first used in 2004 for the synthesis of InP. This precursor has both the advantage of being inexpensive and of having limited toxicity compared to other phosphorus precursors. In addition, it is not pyrophoric in contact with air, unlike most of the precursors presented above. The first use of this precursor was inspired by the syntheses carried out by the Alivisatos and Nozik groups in a TOP/TOPO solvent mixture at 345°C. The NCx obtained with $P(NMe_2)_3$ show a wide size distribution (6.4 ± 3.2 nm) and poor crystallinity.

In 2008, Murase's group proposed two solvothermal studies using this precursor.[85] The first involves between InCl3 and $P(NMe_2)_3$ in a mixture of toluene and DDA which acts as a ligand to stabilize the Quantum Dots. With this route of synthesis, the reaction temperature is lowered and the synthesis, the reaction temperature is lowered to 180 °C but the reaction takes 24 hours. To obtain a correct size distribution (10%), a size-selective precipitation is performed after the synthesis. In 2013, the same group proposed a slightly different synthesis of InP Quantum Dots with a more complete characterization.[86]

The reaction consists of reacting InCl3 with ($P(NMe_2)_3$) in the presence of ZnCl2 in oleylamine (OLA), a strongly coordinating solvent, at 220 °C for 30 minutes. The amount of zinc and phosphorus is studied as well as the reaction temperature. Yang's team observed that the response was rapid in the first few minutes and then quickly stagnated. They also propose

the hypothesis that OLA, which seems to have an important role as a protic solvent, could release a proton that hydrolyse ($P(NMe_2)_3$) and thus form PH3. The latter would then react with the InOLA complex to form InP Quantum Dots.

Indeed, as this phosphorus precursor is inexpensive and much less hazardous than $P(TMS)_3$, a number of works on applications for LEDs have been carried out.[65,87]

Even more recently, Tessier et al. expand on the study carried out by Song et al.by using tris(diethylamino)phosphine instead of $P(NMe_2)_3$.[87] They study the influence of indium and zinc halides on the chemical yield (CY) of the reaction. They show that that a high Chemical Yield CY (up to 80% for $InCl_3$ and $ZnCl_2$) can be achieved for different wavelengths (570 nm for $InCl_3$ and $ZnCl_2$) by changing the indium zinc halide (InI3, $InBr_3$, $InCl_3$ and ZnI_2, $ZnBr_2$, $ZnCl_2$). The lighter the halide, the larger the size of the Quantum Dots formed. In these two studies, $ZnCl_2$ is added during the synthesis of InP Quantum Dots which allows a refinement of the excitonic peak.

The methods for colloidal synthesis of InP QDs described in the literature use organic agents such as literature use organic agents such as TOPO (trioctylphosphine oxide) or TOP (trioctylphosphine) to capture these nanoparticles and thus control their agglomeration. However, these nanoparticles still tend to aggregate under the effect of annealing at high temperatures, which often leads to irreversible precipitation phenomena. In addition, the reaction times of these colloidal syntheses are quite long. [88]

In order to overcome all these obstacles, an injection method for colloidal synthesis of InP QDs is presented in several research works.[89–91] This method is simple and fast, is carried out at room temperature and does not require annealing at high annealing.[71]

5 Controlling the shape of nanocrystals

We have seen previously that control of the size of the synthesized Quantum Dots was possible by controlling the formation mechanism. However, control of their shape is also possible. This control is very important since, like the size of the nanoparticles, their morphology greatly influences their physical properties.[92] The first NCx synthesized in 1993 by Murray et al. were spherical.[93] This morphology is the most thermodynamically favored since it minimizes the surface/volume ratio of NCx. To induce morphological anisotropy, it is important to promote kinetic growth by playing on the ligands and the quantity of monomers in solution. Indeed, the ligands will have an increased affinity for certain facets of the NC. Thus, by controlling the nature of the ligands, it is possible to direct the growth in one direction or another.[94] Nanowire [95], Nanodisc [96] or Nanoplatelet(NPL) [97] structures have been obtained.

6 The limits of use InP

As we have seen previously, InP is a very good candidate for replacing CdSe.[37,85] Unfortunately, the surface of InP nanocrystals often contains imperfections and defects such as reactive dangling bonds or vacant sites in the crystal lattice. These imperfections constitute electron traps, reduce the optical performance of the QDs and notably alter the fluorescence Quantum Yield (QY) and the photoluminescence. In addition, if the core of the Quantum Dots is not passivated, de-excitation via non-radiative paths may become more likely than radiative recombination and, as a result, the fluorescence quantum yield decreases considerably.[98] Hence, to achieve a more effective surface passivation we can use ligands, core/shell system and doping with another material.

The organic ligands that surrounding the NCs cannot prevent species such as water or oxygen from reaching the NC surface. However, they are labile compounds, and their stability depends on the strength of the bond to the surface atoms of the nanocrystals and their stability in the solvent itself. Another way to achieve a more effective surface passivation, an inorganic shell of another semiconductor (usually with a bigger band gap) is introduced onto the core to correct the surface defects. Hence, the photostability and QY of photoluminescence PL can be greatly enhanced by growing a shell of another larger gap semiconductor material around the NCs by heteroepitaxy, leading to a so-called core/shell system. For that, many research groups are currently working on improving the photophysical properties of QDs by introducing one or more shells on the surface of the photoactive surface of the photoactive core. [98–103]

Moreover, the optical (photoluminescence, absorption) and electrical properties can be improved in the case of InP QDs with doping by various elements in the electrical fields. Indeed, Vanadium has attracted considerable interest as a doping element. Till now, there are diverse studies on Vanadium [104,105] such as an appropriate material with good characters to improve cell performance [106,107]. Various benefits are related to the use of Vanadium. Indeed, this latter possesses a better corrosion resistance resulting from alkali compounds. On the other side, it can especially promote enhancing particle growing and amend both the value of the bandgap and UV–Vis spectrophotometry [107], which is earned to produce electrons and holes under visible light irradiation. Thus, it is taken into account as the main element used in doping [107].

7 Doping

Semiconductors exhibit several interesting properties that allow it to be the basis for electronic devices. There is certain type that contain certain impurities or atoms of more than one kind. these impurities are added into a semiconductor to increase the electric conductivity.

Indeed, in doped semiconductors, intruding atoms are introduced into the lattice. These atoms, having one valence electron than the atoms of the concentration of charge carriers (electrons or holes) by donating electrons to the conduction band or accepting holes in the valence band. For example, in silicon, introducing phosphorus atoms (column V) means introducing an excess of electrons, while boron atoms (column III) mean removing electrons and therefore introducing an excess of holes.

An important parameter to determine and control when doping semiconductors is the energy of the Fermi level, which corresponds to the maximum energy of the electrons at zero temperature.

The Fermi level in an intrinsic semiconductor is between the conduction band and the valence band.:

$$E_F = \frac{E_C + E_V}{2} + \frac{K_B T}{2} \, Ln \left(\frac{N_V}{N_C}\right) \quad \text{I.6}$$

By introducing dopants, the position of the Fermi level is changed. In the case of n-type doping, the Fermi level approaches the conduction band and in the case of p-type doping it approaches the valence band.[108]

In the case of dopants or high temperature, most dopants are ionized, and the position of the Fermi level is given by:

$$E_F = E_C - K_B T \, Ln \left(\frac{N_C}{N_D}\right) \text{ for an n-type doping} \quad \text{I.7}$$

$$E_F = E_V + K_B T \, Ln \left(\frac{N_V}{N_A}\right) \text{ for an p-type doping} \quad \text{I.8}$$

where N_A and N_D are the acceptor and donor dopant concentrations respectively.

Therefore, the doping of a material consists of adding small amounts of impurities to modify its properties and stability zones of the phases. Indeed, Vanadium is a "relatively" abundant element on earth with the chemical symbol V and atomic number 23. Its molar mass is 50.9 g/mol and its electronic configuration is [Ar] $3d^3 4s^2$. It is found in several oxidation states ranging from 0 to +V. It is mainly known for its uses as an additive in steel (DIY tools or surgical equipment) or in titanium-based alloys, as well as for its resistance to corrosion by acids (hydrochloric and hydrofluoric in particular). It is currently being studied to store electrical energy in a new type of battery called a flow battery, which would be faster to batteries, which can be recharged more quickly. Vanadium is also being studied for applications in neutron reactor fuel cladding due to its relatively low neutron capture efficiency.

On other hand, the III-V semiconductor with a direct gap, such as InAs, GaAs and InP are key constituents of optoelectronic components. Indeed, this later is further enhanced by the possibility of the doping element. Hence Vanadium as a dopant in II I-V materials has attracted considerable interest since it became apparent that the introduction of vanadium into GaAs could make the latter semi-insulating

Various studies have been carried out on GaAs, GaP and InP doped with vanadium.[109] Especially the study of vanadium doped InP only began in 1983.[110] Indeed, the study conducted by B. Lambert et al. have shown that the samples are of type n. In addition, they

illustrated that the Photoluminescence and Photoluminescence Excitation spectra was explained as internal transitions into $V^{2+}(3d^3)$.[110] George Bremond

et al. have demonstrated that they studied the p type InP doped with Vanadium and the luminescence excitation results showed that the position of donor level of vanadium and the valence band. About the Photoluminescence Excitation spectra, there was an excitation due to band-to-band transition over the band gap energy.[149] Miloud Boutaleb et al. studied the structural, electronic and magnetic properties of (B,In)1−xVxP by FP-LAPW process.[150] The In1−xVxP appears to be good candidates for spintronic application.

Vanadium is considered one of the best materials enhancement electrical properties.[111] However, no research is focused on enhancing the morphological features of InP Quantum Dots doped with Vanadium.

Hence, we propose to study the features of InP QDs doping with Vanadium, with a view to improve the optical properties especially the photoluminescence. This paragraph will be discussed in more detail in chapter III.

8 Shell/core structures

The surface condition of Quantum dots plays a significant role in both their optical properties and their chemical stability. For several years, efforts have been invested in avoiding defects in the core surface of the Quantum Dots to improve their photostability as well as their luminescence yields.[112]

Hence, to avoid undesirable surface state induced effects on the performance of semiconductor, an experimental science has known as "passivation" has developed. The latter has focused on implementing interface and surface treatments with the following objectives:

- Improving their optical properties, allowing optimal operation of the devices [113]

- Improving their electrical properties, allowing optimal operation of the devices.[114]

- Stabilizing their optical and electronic properties over time to eliminate any disturbance (air oxidation, contamination, etc.) on the functional characteristics of the device.[51]

Therefore, one strategy for dealing with these defects is to cover the nanoparticles with a shell of another semiconductor. The addition of one or more shells modifies the distribution of the quantum confinement of the charge carriers in the different materials of the core/shell system depending on the alignment of the semiconductor band structure.

Hence, the heterostructures are classified into three main families represented in the Figure 1-12. [115]

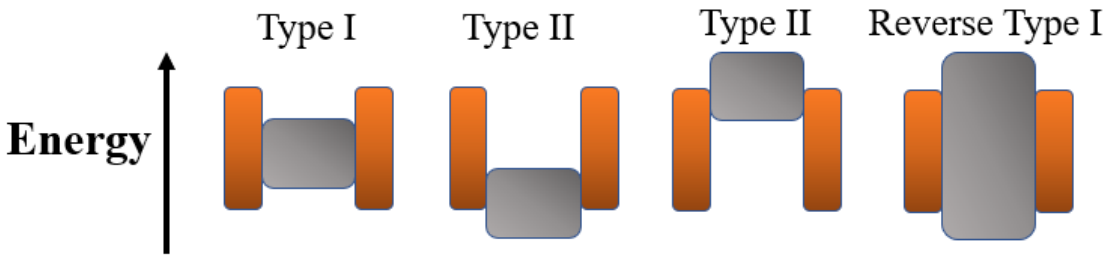

Figure 1-12: The structure types of core/shell Quantum Dots: type I, type II and inverted type.[138]

In the type I systems, a shell of another semiconductor with a larger band gap than the core is introduced. The valence band of the shell is lower in energy than that of the core and its conduction band is higher. Thus, both electrons and holes are both confined to the core. By consequently, this increase in confinement allows the optical properties of the material to be improved.

Type II: Two similar core-shell structures of this type exist. In the first, the potential values (in eV) of the valence and conduction bands of the core are lower than those of the shell.

In the second structure, on the other hand, the energies of the valence and conduction bands of the core are higher than those of the shell. The two charges of the exciton charges are this time separated. Depending on the type II heterostructure envisaged, one of the charges is located within the shell layer while the other charge remains localized within the core. (This type of structure is illustrated for example by CdTe/CdSe or ZnTe/CdTe).

Finally, a last type of configuration exists. In this time the semiconductor shell has a smaller gap than the core of the QDs. The conduction band of the the shell has a lower potential value than that of the core. Conversely, the valence band of the shell has a higher potential value than the core. The exciton electrons and holes are only located within the semiconducting shell during irradiation. (CdS/CdSe core-shell QDs belong to this category, for example).

The choice of a material for the shell considers two criteria: the difference in mesh parameters between the core and shell materials and the respective positioning of the gaps in the two materials. Indeed, the growth of a shell on a semiconductor is done by epitaxial growth. It is a growth of one crystal with respect to another where both materials have several common symmetry elements in their crystal lattices and close lattice parameters. If the difference in mesh parameters between the two materials is too great, it causes dislocations and defects due to the excessive stress of the shell structure on the core structure. However, even with these constraints it is possible to grow materials with a large mismatch of mesh parameters between them. [115]. For example, CdSe/CdS NCx have a core-shell lattice mismatch of 4 % between the core and the shell and CdSe/ZnSe NCx of 6.3%.[116] Similarly, heterostructures with two shells allow a buffer shell to be deposited with a mesh parameter between that of the core and that of the outer shell to reduce the stresses as in the CdSe/CdS/ZnS system.[32]

In our work, the introduction of a shell on the surface of InP QDs is intended to improve their optical properties. The choice of material must therefore satisfy the conditions for type alignment. In the light of these characteristics, ZnS was chosen as the material to form a shell on the surface of the nanoparticles. This process, in addition to improving the optical properties of the QD and to protect the core inside, makes it possible to slow down dissolution of the heart over time. Thus preventing the release of toxic ions.[117] In addition, there are several researchers work about the double-shell systems; and that will become the focus of our thesis in the chapter III.

9 Titanium dioxide TiO2

9.1 General introduction of TiO2

Discovered in 1971 by William Gregor in Great Britain, TiO_2 was first marketed in 1923 as a white pigment for paints. It is a unique material due to its remarkable properties, such as a large band gap (3.2 eV). In addition, titanium dioxide has very good semiconducting properties and low toxicity and photostability. Therefore, numerous studies have highlighted the use of this material for various applications.

It crystallizes mainly in the following three forms: anatase, rutile and brookite. Only rutile and anatase are used in TiO_2 application. The rutile phase is the most stable form of TiO_2. [9] Obtaining the anatase and rutile phases depends on the synthesis method. Indeed, anatase is not thermodynamically stable. In the bulk oxide, the band gap energy is 3.2 eV for anatase and 3.0 eV for rutile, with the valence band edge of anatase being 0.2 eV higher than that of rutile. The electronic properties of the anatase phase are of great interest for photovoltaic applications. Finally, brookite is the rarest form of the mineral. As its synthesis is difficult, it is rarely studied [9].

Recently, it has harvested a big interest in particular one-dimensional morphologies of TiO_2 such as nanotubes. Therefore, these nanotubes have brought huge interest with outstanding features due to their tubular structure. Moreover, it not only increases the specific surface of the material but also greatly improves its photoelectrochemical performance [118], making it a serious candidate as an electrode material for as an electrode material for photovoltaic cells. Indeed, a highly ordered structure of vertically aligned nanotubes offers longer electron scattering lengths and smaller electron transport time constants than an unorganized nanoparticle film. [119] Hence, Zwilling et al. were the first to demonstrate the formation of an aligned tubular structure during the anodic oxidation of an oxide film on metallic titanium or Ti-Al-V alloys in the presence of fluoride ions.[120] Subsequently, Grimes et al. characterized in detail layers or films of vertically aligned nanotubes obtained by anodization in HF. [121]

On other way, there are several synthesis routes leading to the formation of TiO_2 nanotubes, including the hydrothermal route, the template approach, anodization, or electrospinning. However, only the anodizing process will be detailed in this manuscript as this is the technique that was chosen for the TiO_2 nanotube syntheses carried out during this thesis. According to the literature, anodizing is the most widely explored technique.[122,123] This material has several advantages, such as lowered manufacturing price, rapidity and ease of application and ease of implementation. In addition, the anodized layer has a strong adhesion to the substrate and the morphology of the nanotubes is easily controllable (by varying the anodization parameters).[124]

Titanium dioxide has been of growing interest for the last twenty years because of its semiconducting properties. It is becoming very interest for light-harvesting technologies for various applications such as photovoltaic devices [152], photocatalysis [153], hydrogen production [13], gas detectors [154], etc.

9.2 TiO2 as promising substrate for InP QDs: photoelectrochemical measurement

In general, all semiconductors sensitive to visible light are subject to corrosion and oxidation when in contact with an electrolyte. It is therefore difficult to find a semiconductor whose physical properties (optical, electrical, ...) are both compatible with exposure to sunlight and contact with an electrolyte. Thus, only a few semiconductors, such as tin dioxide SnO2, zinc oxide ZnO or titanium dioxide TiO_2, are stable in contact with certain electrolytes.[125]

From these points, TiO_2 has been considered an excellent material to be studied. Moreover, its properties, such as non-toxicity for the environment and its relatively low cost, make it a material of choice. [126]

In this thesis, we studied the photoelectrochemical properties of TiO_2-based films in the presence of InP QDs because the good positioning of the conduction and valence bands of InP QDs with respect to TiO_2 makes it easy to inject the photogenerated electrons towards the latter as seen in figure 1-13.

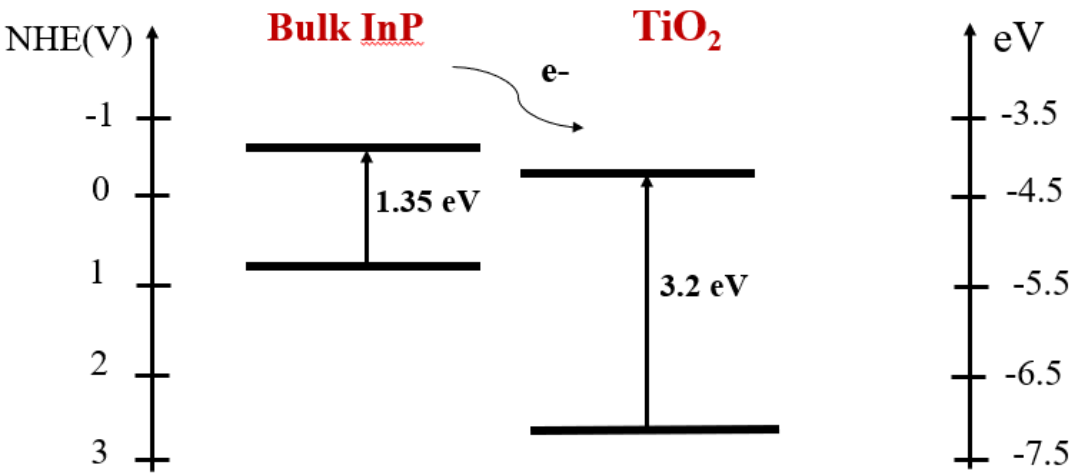

Figure 1-13: A schematic of band positions of bulk InP/TiO_2.[153]

In this regard we can cite the work of A. Zaban et al. [127].The method used for the formation of TiO_2 nanoparticles was sol-gel techniques and about the InP QDs was prepared via a chloroindium oxalate complex and $P(SiMe_3)_3$.[79] Indeed, according to this research work, TiO_2/InP QD for photoelectrochemical measurement are much more attractive due to the excellent ability of InP QDS in strong-base electrolyte (I-/I3-or hydroquinone/quinone acetonitrile solution) and the strong adsorption of InP QDs onto TiO_2 electrode film. Following this approach, photoelectrochemical solar cells have been developed by several researchers. Houman Bahmani Jalali et al. [128] prepared a photoelectrode composite based on InP/ZnO QDs onto ITO/TiO_2. The combination of the materials improved the photocurrent in and reduced the recombination rate by transferring charge carriers in the presence of Shell/Core. In their work, the core InP QDs synthetized by hot injection method, the growing of ZnO done by the thermal decomposition of zinc acetylacetonate and TiO_2 film prepared by a sol–gel dip-coating method. Investigations also extended to Cu shell doping approach. The research group of Hongyang Zhao et al. [129] illustrated that a copper doping with core /shell

InP/ZnSe improves the optoelectronic features. Hence, InP/ZnSe:Cu/ TiO_2/FTO improves the photocurrent density and long-term durability. Currently in the biomedical application, Onuralp Karatum et al. [126] synthetized InP/ZnS QDs by hot injection method. They used a commercially TiO_2 and a CSF solution to photocurrent measurement. Two type of devices bio interface presented in this research work: ITO/QD/ZnO and ITO/TiO_2/QD. A significant improvement in photocurrent was observed, thanks to InP/ZnS QDs than core InP QDs.

The type of heterojunctions that we will focus on in this study consists of associate a TiO_2 substrate with a UV-absorbing semiconductor (InP QDs, InP/ZnS QDs and InP/ZnS/ZnS QDs) and capable of transferring its excitation to TiO_2 and enhancing the photocurrent measurement.

Conclusion

In this first chapter, we have seen that the field of semiconductor nanocrystals has been extensively studied over the last thirty years. During this chapter, we have recalled some basic properties of Quantum Dots as well as their application.

Moreover that, we made an in-depth bibliographical study of Indium phosphide. We described its properties and structures and then detailed the history of InP Quantum Dots while evoking the principle and the mechanism of growth of these particles. In addition, we have shown the drawbacks limiting the use of InP QDs, while presenting possible strategies that would improve its performance.

In this chapter, we have also seen one of the methods used to improve the photocurrent efficiency of Quantum Dots by another semiconductor.

In the last part, we have highlighted the strategy of coupling TiO_2 NTs with Quantum Dots by spin coating method. We intend to enhance of these semiconductor nanocomposites the photoelectrochemical.

References

[1] S. Mahajan, M. Rani, R. Dubey, J. Mahajan, H. Ece, International Journal of Latest Research in Science and Technology, Int. J. Latest Res. Sci. Technol. 2 (2013) 518–521.

[2] C. Burda, X. Chen, R. Narayanan, M.A. El-sayed, Chemistry and Properties of Nanocrystals of Different Shapes, 2005.

[3] R. Koole, E. Groeneveld, D. Vanmaekelbergh, Size Effects on Semiconductor Nanoparticles, n.d. https://doi.org/10.1007/978-3-662-44823-6.

[4] F. Schulz, G.T. Dahl, S. Besztejan, M.A. Schroer, F. Lehmku, G. Gru, T. Vossmeyer, H. Lange, Ligand Layer Engineering To Control Stability and Interfacial Properties of Nanoparticles, (2016). https://doi.org/10.1021/acs.langmuir.6b01704.

[5] O. Yarema, M. Yarema, D. Bozyigit, W.M.M. Lin, V. Wood, Independent Composition and Size Control for Highly Luminescent Indium-Rich Silver Indium Selenide, (2015) 11134–11142. https://doi.org/10.1021/acsnano.5b04636.

[6] K.D. Wegner, F. Dussert, D. Truffier-boutry, A. Benayad, Influence of the Core / Shell Structure of Indium Phosphide Based Quantum Dots on Their Photostability and Cytotoxicity, 7 (2019) 1–12. https://doi.org/10.3389/fchem.2019.00466.

[7] C.A.S. No, Agents Classified by the IARC Monographs , Volumes 1 – 132, (2012).

[8] J.O. Uif, T. Rvbouvn, D. Sfhjnf, 1BTU QSFTFOU BOE GVUVSF PG JOEJVN QIPTQIJEF RVBOUVN EPUT, 15 (2022) 4468–4489.

[9] P. Ramasamy, K. Ko, J. Kang, J. Lee, Two-Step " Seed-Mediated " Synthetic Approach to Colloidal Indium Phosphide Quantum Dots with High-Purity Photo- and Electroluminescence, (2018). https://doi.org/10.1021/acs.chemmater.8b02049.

[10] V. Brunetti, H. Chibli, R. Fiammengo, A. Galeone, M.A. Malvindi, G. Vecchio, R. Cingolani, L. Nadeau, P. Paolo, quantum dots : in vitro and in vivo toxicity assessment, (2013) 307–317. https://doi.org/10.1039/c2nr33024e.

[11] D.A.G. Ramirez, J.S.A. Cerón, M.L.G. Herrera, J.P.L. Arias, M.P. González, Effect of the indium myristate precursor concentration on the structural , optical , chemical surface , and electronic properties of InP quantum dots passivated with ZnS, J. Mater. Sci. Mater. Electron. 30 (2019) 4885–4894. https://doi.org/10.1007/s10854-019-00783-6.

[12] Q. Zhou, J. Zhou, M. Zeng, G. Wang, Y. Chen, S. Lin, Photoelectrochemical Performance of Quantum dot-Sensitized TiO 2 Nanotube Arrays : a Study of Surface Modification by Atomic Layer Deposition Coating, (2017). https://doi.org/10.1186/s11671-017-2036-6.

[13] M. Ni, M.K.H.L. Ã, D.Y.C. Leung, K. Sumathy, A Review and Recent Developments in Photocatalytic Water-Splitting Using TiO2 for Hydrogen Production A review and recent developments in photocatalytic water-splitting using TiO 2 for hydrogen production, (2007). https://doi.org/10.1016/j.rser.2005.01.009.

[14] L.B. Hoch, P. Szymanski, K. Kaur, L. He, K. Liao, Q. Qiao, L.M. Reyes, Carrier dynamics and the role of surface defects : Designing a photocatalyst for gas-phase CO 2 reduction, (2016) 8011–8020. https://doi.org/10.1073/pnas.1609374113.

[15] Black Anatase TiO 2 Nanotubes with Tunable Orientation for High Performance Supercapacitors, (2019). https://doi.org/10.1021/acs.jpcc.9b05070.

[16] N. Cross, D.J. Woodsworth, Investigating the Electronic Properties of a Carbon, (2008).

[17] A.E. Commission, P. Reiss, A.E. Commission, J. Villain, Dans un laboratoire de nanosciences, (2011).

[18] U. Resch-genger, M. Grabolle, S. Cavaliere-jaricot, R. Nitschke, T. Nann, Quantum dots versus organic dyes as fluorescent labels, 5 (2008) 763–775. https://doi.org/10.1038/NMETH.1248.

[19] P. Reiss, M. Carrie, C. Lincheneau, L. Vaure, S. Tamang, Synthesis of Semiconductor Nanocrystals , Focusing on Nontoxic and Earth-Abundant Materials, (2016). https://doi.org/10.1021/acs.chemrev.6b00116.

[20] R. Saran, R.J. Curry, technologies, Nat. Publ. Gr. 10 (2016). https://doi.org/10.1038/nphoton.2015.280.

[21] M.A. Reed, R.J. Aggarwal, R.J. Matyi, T.M. Moore, A.E. Wetsel, Physical review, 60 (1988).

[22] C. Cea, Les nanocristaux semi-conducteurs fluorescents font leur gamme, (2005).

[23] M.T. Clarke, F.N. Viscomi, T.W. Chamberlain, N. Hondow, A.M. Adawi, J. Sturge, S.C. Erwin, J.G. Bouillard, S. Tamang, G.J. Stasiuk, colloidal quantum dots through thermal diffusion, Commun. Chem. (n.d.). https://doi.org/10.1038/s42004-019-0138-z.

[24] F.O.R.T.W. Orth, T. Exas, Q. Aprimer, QuantumDots: APrimer, (n.d.).

[25] Y. Wan, J. Norman, J. Bowers, Quantum dot microcavity lasers on silicon substrates, 1st ed., Elsevier Inc., 2019. https://doi.org/10.1016/bs.semsem.2019.05.002.

[26] Z.I. Alferov, The history and future of semiconductor heterostructures, (1998) 1–14.

[27] V. Biju, T. Itoh, A. Anas, Semiconductor quantum dots and metal nanoparticles : syntheses , optical properties , and biological applications, (2008) 2469–2495. https://doi.org/10.1007/s00216-008-2185-7.

[28] A. Physics, Optical Properties of Semiconductor Nanocrystals Cambridge Studies in Modern Optics, n.d.

[29] N. Fernández-delgado, M. Herrera, A.H. Tavabi, M. Luysberg, R.E. Dunin-borkowski, Applied Surface Science Structural and chemical characterization of CdSe-ZnS core-shell quantum dots, Appl. Surf. Sci. 457 (2018) 93–97. https://doi.org/10.1016/j.apsusc.2018.06.149.

[30] Q. Zhao, P.A. Graf, W.B. Jones, A. Franceschetti, J. Li, L. Wang, K. Kim, Shape Dependence of Band-Edge Exciton Fine Structure in CdSe Nanocrystals, (2007).

[31] I. Review, " 5 = 5;„ +, 75 (1995) 3728–3731.

[32] A.L. Rogach, No Title, n.d.

[33] M. Rosen, M. Kuno, M. Nirmal, D.J. Norris, M. Bawendi, Band-edge exciton in quantum dots of semiconductors with a degenerate valence band: Dark and bright exciton states, 54 (1996) 4843–4856.

[34] O. Stier, M. Grundmann, D. Bimberg, Electronic and optical properties of strained quantum dots modeled by 8-band k – p theory, 59 (1999) 5688–5701.

[35] A. Franceschetti, A. Zunger, Pseudopotential calculations of electron and hole addition spectra of InAs , InP , and Si quantum dots, 62 (2000) 2614–2623.

[36] E. Alkhazraji, A.M. Ragheb, M.A. Esmail, Q. Tareq, H. Fathallah, Electro-absorption and Electro-optic Characterization of L-Band InAs / InP Quantum-dash Waveguide, (2020). https://doi.org/10.1109/JPHOT.2020.2988584.

[37] M.D. Tessier, D. Dupont, K. De Nolf, J. De Roo, Z. Hens, Economic and Size-Tunable Synthesis of InP/ZnE (E = S, Se) Colloidal Quantum Dots., Chem. Mater. 27 (2015) 4893–4898. https://doi.org/10.1021/acs.chemmater.5b02138.

[38] A.M. Nightingale, J.C. DeMello, Improving the ensemble optical properties of InP quantum dots by indium precursor modification, J. Mater. Chem. C. 4 (2016) 8454–8458. https://doi.org/10.1039/C6TC02910H.

[39] D. V Talapin, J. Lee, M. V Kovalenko, E. V Shevchenko, Prospects of Colloidal Nanocrystals for Electronic and Optoelectronic Applications, (2010) 389–458.

[40] V.A. Online, L. Lai, L. Protesescu, M. V Kovalenko, M.A. Loi, Sensitized solar cells with colloidal PbS–CdS core–shell quantum dots †, (2014) 736–742. https://doi.org/10.1039/c3cp54145b.

[41] B. Chen, D. Li, F. Wang, InP Quantum Dots : Synthesis and Lighting Applications, 2002454 (2020) 1–20. https://doi.org/10.1002/smll.202002454.

[42] M.A. Ellis, G. Grandinetti, K.M. Fichter, Synthesis of Cd-free InP/ZnS Quantum Dots Suitable for Biomedical Applications, J. Vis. Exp. (2016). https://doi.org/10.3791/53684.

[43] T.-R. Kuo, S.-T. Hung, Y.-T. Lin, T.-L. Chou, M.-C. Kuo, Y.-P. Kuo, C.-C. Chen, Green Synthesis of InP/ZnS Core/Shell Quantum Dots for Application in Heavy-Metal-Free Light-Emitting Diodes, Nanoscale Res. Lett. 12 (2017) 537. https://doi.org/10.1186/s11671-017-2307-2.

[44] L.C. Lines, W. Jiang, Z. Yang, G. Lin, Cytotoxicity of InP / ZnS Quantum Dots With Different Surface Functional Groups Toward Two, 9 (2018) 1–12. https://doi.org/10.3389/fphar.2018.00763.

[45] H. Sengul, COMPARATIVE ASSESSMENT OF PHASE TRANSFER BEHAVIOUR OF INP / ZNS , Environmental Science Nano Comparative assessment of the phase transfer dots and CdSe / ZnS quantum dots under varying, (2019). https://doi.org/10.1039/C8EN01073K.

[46] V. Brunetti, I. Italiano, V. Brunetti, H. Chibli, R. Fiammengo, A. Galeone, M.A. Malvindi, G. Vecchio, R. Cingolani, J.L. Nadeau, P.P. Pompa, InP/ZnS as a safer alternative to CdSe/ZnS core/shell quantum dots: In vitro and in vivo toxicity assessment, (2012). https://doi.org/10.1039/c2nr33024e.

[47] B.J.M. Klostranec, W.C.W. Chan, Quantum Dots in Biological and Biomedical

Research : Recent Progress and Present Challenges, (n.d.). https://doi.org/10.1002/adma.200500786.

[48] H. Chibli, L. Carlini, S. Park, M. Dimitrijevic, J.L. Nadeau, Nanoscale Cytotoxicity of InP / ZnS quantum dots related to reactive oxygen species generation, (2011) 2552–2559. https://doi.org/10.1039/c1nr10131e.

[49] S. Tamang, C. Lincheneau, Y. Hermans, S. Jeong, P. Reiss, Chemistry of InP Nanocrystal Syntheses, Chem. Mater. 28 (2016) 2491–2506. https://doi.org/10.1021/acs.chemmater.5b05044.

[50] M. Green, S olution routes to III – V semiconductor quantum dots q, 6 (2002) 355–363.

[51] J. Jasinski, V.J. Leppert, S. Lam, G.A. Gibson, K. Nauka, C.C. Yang, Z. Zhou, Rapid oxidation of InP nanoparticles in air, 141 (2007) 624–627. https://doi.org/10.1016/j.ssc.2006.12.033.

[52] L. Li, P. Reiss, One-pot Synthesis of Highly Luminescent InP / ZnS Nanocrystals without, (2008) 11588–11589.

[53] G.O. Eren, S. Sadeghi, H. Bahmani Jalali, M. Ritter, M. Han, I. Baylam, R. Melikov, A. Onal, F. Oz, M. Sahin, C.W. Ow-Yang, A. Sennaroglu, R.T. Lechner, S. Nizamoglu, Cadmium-Free and Efficient Type-II InP/ZnO/ZnS Quantum Dots and Their Application for LEDs, ACS Appl. Mater. Interfaces. 13 (2021) 32022–32030. https://doi.org/10.1021/acsami.1c08118.

[54] D. V Talapin, A.L. Rogach, A. Kornowski, M. Haase, H. Weller, Highly Luminescent Monodisperse CdSe and CdSe / ZnS Nanocrystals Synthesized in a Hexadecylamine − Trioctylphosphine Oxide − Trioctylphospine Mixture, (2001).

[55] N. York, Visible Light Induced Hydrogen Production from in Situ Generated Colloidal Rhodium-Coated Cadmium Sulfide in Surfactant Vesicles Clarkson College of Technology Isolation from Pistacia Resins of a Bicyclic Triterpenoid Representing an Apparent Trapped, (2000) 2475–2476.

[56] A. Henglein, Small-Particle Research : Physicochemical Properties of Extremely Small Colloidal Metal and Semiconductor Particles, (1989).

[57] G.M. Wallraff, W.D. Hinsberg, Lithographic Imaging Techniques for the Formation of Nanoscopic Features, (1999).

[58] P.M. Petroff, A. Lorke, A. Imamoglu, E PITAXIALLY S ELF -A SSEMBLED Q UANTUM D OTS, 46 (2020). https://doi.org/10.1063/1.1381102.

[59] B.D. Ingert, M. Pileni, Limitations in Producing Nanocrystals Using Reverse Micelles as Nanoreactors **, 5 (2001) 136–139.

[60] A.P. Alivisatos, Perspectives on the Physical Chemistry of Semiconductor Nanocrystals, 3654 (1996) 13226–13239.

[61] C.B. Murray, D.J. Norris, M.G. Bawendi, Synthesis and Characterization of Nearly Monodisperse CdE (E = S , Se , Te) Semiconductor Nanocrystallites, (1993) 8706–8715.

[62] M. Bayer, E.H. Sargent, Semiconductor quantum dots: Technological progress and future challenges, 8541 (2021). https://doi.org/10.1126/science.aaz8541.

[63] L. Qu, X. Peng, Control of Photoluminescence Properties of CdSe Nanocrystals in Growth, 124 (2018) 2016–2018.

[64] S.G. Hickey, S.F. Wuister, D. Vanmaekelbergh, Single-Step Synthesis to Control the Photoluminescence Quantum Yield and Size Dispersion of CdSe Nanocrystals, (2003) 489–496.

[65] S. Lee, K. Lee, J. Jo, B. Park, Y. Kwon, S. Jang, H. Yang, emitting diode based on InP quantum dot color converters, 4 (2014) 1297–1302. https://doi.org/10.1364/OME.4.001297.

[66] L. Qu, Z.A. Peng, X. Peng, Alternative Routes toward High Quality CdSe Nanocrystals, (2001) 1–5.

[67] C.R. Bullen, P. Mulvaney, Nucleation and Growth Kinetics of CdSe Nanocrystals in Octadecene, (2004).

[68] P. Reiss, G. Quemard, S. Carayon, J. Bleuse, F. Chandezon, A. Pron, Luminescent ZnSe nanocrystals of high color purity, 84 (2004) 10–13. https://doi.org/10.1016/j.matchemphys.2003.11.002.

[69] X. Zhong, Y. Feng, W. Knoll, M. Han, Alloyed Zn x Cd 1 - x S Nanocrystals with Highly Narrow Luminescence Spectral Width, (2003) 13559–13563.

[70] D.W. Lucey, D.J. Macrae, M. Furis, Y. Sahoo, A.N. Cartwright, P.N. Prasad, Monodispersed InP Quantum Dots Prepared by Colloidal Chemistry in a Noncoordinating Solvent, (2005) 3754–3762.

[71] D. Battaglia, X. Peng, Formation of High Quality InP and InAs Nanocrystals in a Noncoordinating Solvent, (2002) 1–4.

[72] J. Jasieniak, C. Bullen, J. Van Embden, P. Mulvaney, Phosphine-Free Synthesis of CdSe Nanocrystals, (2005) 20665–20668.

[73] S. Sapra, A.L. Rogach, J. Feldmann, Phosphine-free synthesis of monodisperse CdSe nanocrystals in olive oil, (2006) 3391–3395. https://doi.org/10.1039/b607022a.

[74] G.G. Yordanov, G.D. Gicheva, B.H. Bochev, C.D. Dushkin, E. Adachi, The effects of temperature and carboxylic acid ligand on the growth of nanocrystalline CdSe in a hot paraffin matrix, 273 (2006) 10–15. https://doi.org/10.1016/j.colsurfa.2005.07.036.

[75] J. Park, J. Joo, S.G. Kwon, Y. Jang, T. Hyeon, Synthesis of Monodisperse Spherical Nanocrystals Angewandte, (2007) 4630–4660. https://doi.org/10.1002/anie.200603148.

[76] R.H. Dinegar, JOURNAL OF THE, 72 (1950).

[77] F. Wang, V.N. Richards, S.P. Shields, W.E. Buhro, Kinetics and Mechanisms of Aggregative Nanocrystal Growth, (2014). https://doi.org/10.1021/cm402139r.

[78] X. Peng, J. Wickham, A.P. Alivisatos, Kinetics of II-VI and III-V Colloidal Semiconductor Nanocrystal Growth : " Focusing " of Size Distributions, 7863 (1998) 5343–5344.

[79] O.I. Micic, C.J. Curtis, K.M. Jones, J.R. Sprague, A.J. Nozik, Synthesis and Characterization of InP Quantum Dots, (1994) 4966–4969.

[80] A.A. Guzelian, J.E.B. Katari, A. V Kadavanich, U. Banin, K. Hamad, E. Juban, A.P.

Alivisatos, R.H. Wolters, C.C. Arnold, J.R. Heath, Synthesis of Size-Selected , Surface-Passivated InP Nanocrystals, (1996) 7212–7219.

[81] O.I. Mic, Synthesis of extremely small InP quantum dots and electronic coupling in their disordered solid films, 4022 (2005). https://doi.org/10.1063/1.1379990.

[82] S. Xu, S. Kumar, T. Nann, Rapid Synthesis of High-Quality InP Nanocrystals, (2006) 1054–1055.

[83] J.A. Gerbec, D. Magana, A. Washington, G.F. Strouse, Microwave-Enhanced Reaction Rates for Nanoparticle Synthesis, (2005) 15791–15800.

[84] D.D. Lovingood, G.F. Strouse, Microwave Induced In-Situ Active Ion Etching of Growing InP Nanocrystals, (2008) 4–7.

[85] C. Li, M. Ando, N.M. Ã, Facile Preparation of Highly Luminescent InP Nanocrystals by a Solvothermal Route, 37 (2008) 856–857. https://doi.org/10.1246/cl.2008.856.

[86] W.S.H. Lee, J. Chul, Amine-derived synthetic approach to color-tunable InP / ZnS quantum dots with high fluorescent qualities, (2013). https://doi.org/10.1007/s11051-013-1750-y.

[87] W. Song, S. Lee, H. Yang, Fabrication of warm , high CRI white LED using non-cadmium quantum dots, 3 (2013) 1468–1473. https://doi.org/10.1364/OME.3.001468.

[88] O.I. Micié, J.R. Sprague, C.J. Curtis, K.M. Jones, J.L. Machol, A.J. Nozik, H. Giessen, B. Fluegel, G. Mohs, N. Peyghambarian, Synthesis and Characterization of InP , GaP , and GalnPi Quantum Dots, (1995) 7754–7759.

[89] O.B. Achorn, D. Franke, M.G. Bawendi, Seedless Continuous Injection Synthesis of Indium Phosphide Quantum Dots as a Route to Large Size and Low Size Dispersity, Chem. Mater. 32 (2020) 6532–6539. https://doi.org/10.1021/acs.chemmater.0c01906.

[90] S. Mahajan, M. Rani, R.B. Dubey, J. Mahajan, SYNTHESIS OF CdSe CRYSTAL USING HOT INJECTION METHOD, Int. J. Latest Res. Sci. Technol. 2 (2013) 518–521.

[91] J. Ministro, A study on the synthesis and the optical properties of InP-based quantum dots, University Gent, n.d.

[92] S.B. Brichkin, Synthesis and properties of colloidal indium phosphide quantum dots, Colloid J. 77 (2015) 393–403. https://doi.org/10.1134/S1061933X15040043.

[93] E.S. Cde, J. Te, A.C. Soc, Murray, C.B., Norris, D.J. & Bawendi, M.G. Synthesis and characterization of nearly monodisperse CdE (E = S, Se, Te) semiconductor nanocrystallites. J. Am. Chem. Soc. 115, 8706 − 871..., (2021). https://doi.org/10.1021/ja00072a025.

[94] X. Peng, L. Manna, W. Yang, J. Wickham, Shape control of CdSe nanocrystals, 404 (2000) 59–61.

[95] L. Manna, E.C. Scher, A.P. Alivisatos, R. V August, Synthesis of Soluble and Processable Rod- , Arrow- , Teardrop- , and Tetrapod-Shaped CdSe Nanocrystals, (2000) 12700–12706.

[96] V.F. Puntes, D. Zanchet, C.K. Erdonmez, A.P. Alivisatos, Synthesis of hcp-Co Nanodisks, (2002) 12874–12880.

[97] S. Ithurria, B. Dubertret, Quasi 2D Colloidal CdSe Platelets with Thicknesses Controlled at the Atomic Level, (2008) 16504–16505.

[98] H. Qian, L. Li, J. Ren, One-step and rapid synthesis of high quality alloyed quantum dots (CdSe – CdS) in aqueous phase by microwave irradiation with controllable temperature, 40 (2005) 1726–1736. https://doi.org/10.1016/j.materresbull.2005.05.022.

[99] P. Ramasamy, B. Kim, M.-S. Lee, J.-S. Lee, Beneficial effects of water in the colloidal synthesis of InP/ZnS core–shell quantum dots for optoelectronic applications, Nanoscale. 8 (2016) 17159–17168. https://doi.org/10.1039/C6NR04713K.

[100] W.A.C. Hen, W.E.W. Ang, L.E.I.S. Un, S.H.C. Hen, Q.U.N.Y. An, T.A.G. Uo, X.I.Z. Hou, C. Haoxing, Y.O.Z. Hang, Synthesis and characterization of InP / ZnSe / ZnS quantum dots for photo-emissive color conversion, 12 (2022) 1717–1730.

[101] A.J. Zavaraki, Q. Liu, H. Ågren, Nano-Structures & Nano-Objects Solar cell sensitized with ‘“ green ”’ InP-ZnS quantum dots : Effect of ZnS shell deposition, Nano-Structures & Nano-Objects. 22 (2020) 100461. https://doi.org/10.1016/j.nanoso.2020.100461.

[102] S.T. Quenching, Suppressed Thermal Quenching, (2021).

[103] N. Mordvinova, A. Vinokurov, T. Kuznetsova, O.I. Lebedev, S. Dorofeev, Highly luminescent core-shell InP/ZnX (X = S, Se) quantum dots prepared: Via a phosphine synthetic route, Dalt. Trans. 46 (2017) 1297–1303. https://doi.org/10.1039/c6dt03956a.

[104] M. Jiang, Y. Li, S. Li, H. Zhou, X. Cao, S. Bao, Y. Gao, H. Luo, P. Jin, Room Temperature Optical Constants and Band Gap Evolution of Phase Pure M 1 -VO 2 Thin Films Deposited at Different Oxygen Partial Pressures by Reactive Magnetron Sputtering, J. Nanomater. 2014 (2014) 1–6. https://doi.org/10.1155/2014/183954.

[105] A. Bouzidi, N. Benramdane, A. Nakrela, C. Mathieu, B. Khelifa, R. Desfeux, A. Da Costa, First synthesis of vanadium oxide thin films by spray pyrolysis technique, Mater. Sci. Eng. B. 95 (2002) 141–147. https://doi.org/10.1016/S0921-5107(02)00224-6.

[106] B. Lambert, B. Deveaud, Y. Toudic, G. Pelous, J.C. Paris, G. Grandpierre, Properties of vanadium in InP, Solid State Commun. 47 (1983) 337–340. https://doi.org/10.1016/0038-1098(83)90914-6.

[107] C. Lamsal, N.M. Ravindra, Optical properties of vanadium oxides-an analysis, J. Mater. Sci. 48 (2013) 6341–6351. https://doi.org/10.1007/s10853-013-7433-3.

[108] D. Collection, Modeling Radiation Effects on a Triple Junction Solar Cell using Silvaco ATLAS NAVAL POSTGRADUATE, (2012).

[109] P. Cedex, SPECTROSCOPIC INVESTIGATION OF VANADIUM IN lnP B. CLERJAUD, D. COTE and C. NAUD, 83 (1987) 194–197.

[110] J.C. Paris, PROPERTIES OF V A N A D I U M IN InP I +, 47 (1983) 337–340.

[111] M.A. Shafi, H. Ullah, S. Ullah, L. Khan, S. Bibi, B.M. Soucase, Numerical Simulation of Lead-Free Sn-Based Perovskite Solar Cell by Using SCAPS-1D †, (2022) 1–5.

[112] J.A. Dias, S.H. Santagneli, S.J.L. Ribeiro, Y. Messaddeq, Perovskite Quantum Dot Solar Cells : An Overview of the Current Advances and Future Perspectives, 2100205 (2021) 1–28. https://doi.org/10.1002/solr.202100205.

[113] W. Zhang, S. Ding, W. Zhuang, D. Wu, P. Liu, X. Qu, H. Liu, H. Yang, Z. Wu, K. Wang, X.W. Sun, InP / ZnS / ZnS Core / Shell Blue Quantum Dots for Efficient Light-Emitting Diodes, (n.d.). https://doi.org/10.1002/adfm.202005303.

[114] H.I. Ikeri, A.I. Onyia, P.U. Asogwa, Investigation Of Optical Characteristics Of Semiconductor Quantum Dots For Multi Junction Solar Cells Applications ., 8 (2019) 3531–3535.

[115] A.M. Smith, S. Nie, Semiconductor Nanocrystals : Structure , Properties , and Band Gap Engineering, (2010).

[116] P. Reiss, S. Carayon, J. Bleuse, A. Pron, Low polydispersity core / shell nanocrystals of CdSe / ZnSe and CdSe / ZnSe / ZnS type : preparation and optical studies, 139 (2003) 649–652. https://doi.org/10.1016/S0379-6779(03)00335-7.

[117] M. Ando, M. Horie, Y. Akazawa-ogawa, Y. Hagihara, N. Murase, Y. Shigeri, Cytotoxicity of CdSe-based quantum dots incorporated in glass nanoparticles evaluated using human keratinocyte HaCaT cells, Biosci. Biotechnol. Biochem. 8451 (2016) 1–4. https://doi.org/10.1080/09168451.2015.1069702.

[118] A. Ghicov, P. Schmuki, Self-ordering electrochemistry : a review on growth and functionality of TiO 2 nanotubes and other self-aligned MO x structures, (2009) 2791–2808. https://doi.org/10.1039/b822726h.

[119] H.E. Prakasam, K. Shankar, M. Paulose, O.K. Varghese, C.A. Grimes, ARTICLES A New Benchmark for TiO 2 Nanotube Array Growth by Anodization, (2007) 7235–7241.

[120] V. Zwilling, M. Aucouturier, E. Darque-ceretti, Anodic oxidation of titanium and TA6V alloy in chromic media . An electrochemical approach, 45 (1999) 921–929.

[121] S. Kobayashi, K. Hanabusa, Preparation of TiO 2 Hollow-Fibers Using Supramolecular Assemblies Seiji Shinkai Porous , nanostructured materials have attracted considerable attention because of their potential ap- materials is quite difficult . Nanostructured inorganic cationic charge moieties with the expectation that the, (2000) 1523–1525.

[122] J.M. Macak, H. Tsuchiya, A. Ghicov, K. Yasuda, R. Hahn, S. Bauer, P. Schmuki, TiO 2 nanotubes : Self-organized electrochemical formation , properties and applications, 11 (2007) 3–18. https://doi.org/10.1016/j.cossms.2007.08.004.

[123] C. Ruan, M. Paulose, O.K. Varghese, G.K. Mor, C.A. Grimes, Fabrication of Highly Ordered TiO 2 Nanotube Arrays Using an Organic Electrolyte, (2005) 15754–15759.

[124] K. Lee, A. Mazare, P. Schmuki, One-Dimensional Titanium Dioxide Nanomaterials : Nanotubes, (2014).

[125] V. Shrotriya, G. Li, Y. Yao, C. Chu, Y. Yang, Transition metal oxides as the buffer layer for polymer photovoltaic cells Transition metal oxides as the buffer layer for polymer photovoltaic cells, (2006) 1–4. https://doi.org/10.1063/1.2174093.

[126] O. Karatum, M.M. Aria, G.O. Eren, E. Yildiz, E.D. Glowacki, Nanoengineering InP Quantum Dot-Based Photoactive Biointerfaces for Optical Control of Neurons, 15 (2021) 1–14. https://doi.org/10.3389/fnins.2021.652608.

[127] A. Zaban, O.I. Mic, B.A. Gregg, A.J. Nozik, Photosensitization of Nanoporous TiO 2 Electrodes with InP Quantum Dots, 7463 (1998) 3153–3156.

[128] H.B. Jalali, M.M. Aria, U.M. Dikbas, S. Sadeghi, E ff ective Neural Photostimulation Using Indium-Based Type-II Quantum Dots, (2018). https://doi.org/10.1021/acsnano.8b02976.

[129] H. Zhao, X. Li, M. Cai, C. Liu, Y. You, R. Wang, A.I. Channa, F. Lin, D. Huo, G. Xu, X. Tong, Z.M. Wang, Role of Copper Doping in Heavy Metal-Free InP / ZnSe Core / Shell Quantum Dots for Highly Efficient and Stable Photoelectrochemical Cell, 2101230 (2021) 1–10. https://doi.org/10.1002/aenm.202101230.

[130] M.T. Clarke, F.N. Viscomi, T.W. Chamberlain, N. Hondow, A.M. Adawi, J. Sturge, S.C. Erwin, J.-S.G. Bouillard, S. Tamang, G.J. Stasiuk, Synthesis of super bright indium phosphide colloidal quantum dots through thermal diffusion, Commun. Chem. 2 (2019) 36. https://doi.org/10.1038/s42004-019-0138-z.

[131] T.K. Nideep, M. Ramya, M.M. Varier, M. Kailasnath, A Study of Nonlinear Optical Property of Cadmium Based Quantum Dots with Comparable Particle Size, Springer Singapore, n.d. https://doi.org/10.1007/978-981-15-9259-1.

[132] S. Kobayashi, N. Hamasaki, M. Suzuki, M. Kimura, H. Shirai, K. Hanabusa, Preparation of Helical Transition-Metal Oxide Tubes Using Organogelators as Structure-Directing Agents, 1 (2002) 6550–6551.

[133] Z. Miao, D. Xu, J. Ouyang, G. Guo, X. Zhao, Electrochemically Induced Sol − Gel Preparation of Single-Crystalline TiO 2 Nanowires, (2002).

[134] Enhancement of photocatalytic and photoelectrochemical properties of TiO2 nanotubes sensitized by SILAR - Deposited PbS nanoparticles _ Elsevier Enhanced Reader.pdf, (n.d.).

[135] J.M. Macak, S.P. Albu, P. Schmuki, Towards ideal hexagonal self-ordering of TiO 2 nanotubes pss, 183 (2007) 181–183. https://doi.org/10.1002/pssr.200701148.

[136] P. V Kamat, Quantum Dot Solar Cells . The Next Big Thing in Photovoltaics, (2013).

[137] M. Antoniadou, D.I. Kondarides, D.D. Dionysiou, P. Lianos, Quantum Dot Sensitized Titania Applicable as Photoanode in Photoactivated Fuel Cells, (2012).

[138] M.P. Genovese, I. V Lightcap, P. V Kamat, Sun-Believable Solar Paint . A Transformative One-Step Approach for Designing Nanocrystalline Solar Cells, (2012) 865–872.

[139] S. Park, T. Ikegami, K. Ebihara, Effects of substrate temperature on the properties of Ga-doped ZnO by pulsed laser deposition, 513 (2006) 90–94. https://doi.org/10.1016/j.tsf.2006.01.051.

[140] J. Verschraegen, M. Burgelman, Numerical modeling of intra-band tunneling for heterojunction solar cells in SCAPS, 515 (2007) 6276–6279. https://doi.org/10.1016/j.tsf.2006.12.049.

[141] P.E. Imoisili, T. Jen, Numerical Analysis and Performance improvement of Nanostructured Cu 2 O / TiO 2 pn heterojunction Solar Cells using SCAPS, (n.d.).

[142] M. Al-hattab, L. Moudou, M. Khenfouch, O. Bajjou, Numerical simulation of a new heterostructure CIGS / GaSe solar cell system using SCAPS-1D software, Sol. Energy. 227 (2021) 13–22. https://doi.org/10.1016/j.solener.2021.08.084.

[143] M.M.T. Al, Z.S. Yasin, Optoelectronics Simulation of CIGS - Based Solar Cells Using

a Cd - Free Nontoxic - ZrS x Se 2 − x as a Novel Buffer Layer, Brazilian J. Phys. (2022) 1–10. https://doi.org/10.1007/s13538-022-01146-z.

[144] U. Mandadapu, S.V. Vedanayakam, K. Thyagarajan, Numerical Simulation of Ch 3 Nh 3 PbI 3-X Cl x Perovskite solar cell using SCAPS-1D, (2017) 40–45.

[145] P. Ieee, P. Specialists, C. Washington, A. Niemegeers, M. Burgelman, MODELLING OF ac-CHARACTERISTICS SOLAR CELLS, (1996) 901–904.

[146] M. Burgelman, P. Nollet, S. Degrave, Modelling polycrystalline semiconductor solar cells, 362 (2000) 527–532.

[147] M. Mostefaoui, H. Mazari, S. Khelifi, A. Bouraiou, R. Dabou, Simulation of High Efficiency CIGS solar cells with SCAPS-1D software, Energy Procedia. 74 (2015) 736–744. https://doi.org/10.1016/j.egypro.2015.07.809.

[148] U. Holzwarth, N. Gibson, The Scherrer equation versus the "Debye-Scherrer equation," Nat. Nanotechnol. 6 (2011) 534–534. https://doi.org/10.1038/nnano.2011.145.

[149] O. Ehlert, A. Tiwari, T. Nann, Quantum confinement of the thermodynamic functions for the formation of electrons and holes in CdSe nanocrystals, J. Appl. Phys. 100 (2006) 1–6. https://doi.org/10.1063/1.2356607.

[150] M. Singh, M. Goyal, K. Devlal, Size and shape effects on the band gap of semiconductor compound nanomaterials, J. Taibah Univ. Sci. 12 (2018) 470–475. https://doi.org/10.1080/16583655.2018.1473946.

[151] M. Asemi, A. Suddar, M. Ghanaatshoar, Increasing the specific surface area of Cr-doped - nanoparticles by controlling the drying time for DSSC applications, J. Mater. Sci. Mater. Electron. 28 (2017) 15233–15238. https://doi.org/10.1007/s10854-017-7401-9.

[152] C. Ippen, T. Greco, A. Wedel, InP/ZnSe/ZnS: A Novel Multishell System for InP Quantum Dots for Improved Luminescence Efficiency and Its application in a Light-Emitting Device, J. Inf. Disp. 13 (2012) 91–95. https://doi.org/10.1080/15980316.2012.683537.

[153] E. Ryu, S. Kim, E. Jang, S. Jun, H. Jang, B. Kim, S. Kim, Communications, 21 (2009) 2425–2427.

[154] O.I. Mic, Synthesis of extremely small InP quantum dots and electronic coupling in their disordered solid films, 4022 (2005). https://doi.org/10.1063/1.1379990.

[155] S.J. Yang, J.H. Oh, S. Kim, H. Yang, Y.R. Do, Realization of InP / ZnS quantum dots for green , amber and red down-converted LEDs and their, (2015) 3582–3591. https://doi.org/10.1039/c5tc00028a.

[156] S. Xu, J. Ziegler, T. Nann, Rapid synthesis of highly luminescent InP and InP / ZnS nanocrystals †, (2008) 2653–2656. https://doi.org/10.1039/b803263g.

[157] K. Yong, H. Ding, I. Roy, W. Law, E.J. Bergey, A. Maitra, P.N. Prasad, Imaging Pancreatic Cancer Using Bioconjugated InP Quantum Dots, 3 (n.d.).

[158] S. Fung, B. Yang, C.K. Ng, M.K. Fung, C.C. Ling, A.B. Djuriˇ, Annealing study of titanium oxide nanotube arrays, 130 (2011) 1227–1231. https://doi.org/10.1016/j.matchemphys.2011.08.063.

[159] T.S. Bhat, A.D. Sheikh, N.L. Tarwal, S.D. Korade, C.K. Hong, J.H. Kim, ZnS passivated PbSe sensitized TiO 2 nanorod arrays to suppress photocorrosion in photoelectrochemical solar cells, Mater. Today Commun. 16 (2018) 186–193. https://doi.org/10.1016/j.mtcomm.2018.06.008.

[160] N. Simulation, P. For, Modeling Thin-film PV Devices, 153 (2004) 143–153. https://doi.org/10.1002/pip.524.

[161] S.K. M, S.P. Madhusudanan, A.R. Rajamani, M. Siaj, S.K. Batabyal, Barium Substitution in Kesterite Cu 2 ZnSnS 4 : Cu 2 Zn 1 − x Ba x SnS 4 Quinary Alloy Thin Films for E ffi cient Solar Energy Harvesting, (2020) 4–11. https://doi.org/10.1021/acs.cgd.0c00150.

[162] M. Jamil, A. Ali, K. Mahmood, M.I. Arshad, S. Tahir, M. Ajaz un Nabi, S. Ikram, N. Amin, S. Hussain, Numerical simulation of perovskite/Cu2Zn(Sn1-x Gex)S4 interface to enhance the efficiency by valence band offset engineering, J. Alloys Compd. 821 (2020) 153221. https://doi.org/10.1016/j.jallcom.2019.153221.

[163] Y. Raoui, H. Ez-Zahraouy, N. Tahiri, O. El Bounagui, S. Ahmad, S. Kazim, Performance analysis of MAPbI3 based perovskite solar cells employing diverse charge selective contacts: Simulation study, Sol. Energy. 193 (2019) 948–955. https://doi.org/10.1016/j.solener.2019.10.009.

[164] Chenming C. Hu, Modern Semiconductor Devices for Integrated Circuits, in: 2010.

[165] F. Baig, Y.H. Khattak, S. Ullah, B.M. Soucase, S. Beg, H. Ullah, Numerical analysis a guide to improve the efficiency of experimentally designed solar cell, Appl. Phys. A. 124 (2018) 471. https://doi.org/10.1007/s00339-018-1877-x.

[166] R. Toufanian, A. Piryatinski, A.H. Mahler, R. Iyer, J.A. Hollingsworth, A.M. Dennis, Bandgap Engineering of Indium Phosphide-Based Core/Shell Heterostructures Through Shell Composition and Thickness, Front. Chem. 6 (2018). https://doi.org/10.3389/fchem.2018.00567.

[167] V. Raj, F. Rougieux, L. Fu, H.H. Tan, C. Jagadish, Design of Ultrathin InP Solar Cell Using Carrier Selective Contacts, IEEE J. Photovoltaics. 10 (2020) 1657–1666. https://doi.org/10.1109/JPHOTOV.2019.2961615.

CHAPTER II

Synthesis methods and characterization techniques

This chapter presents the experimental methods and the different techniques of characterizations used throughout this work.

1 Experimental work

1.1 Synthesis of QDs

1.2 Organometallic synthesis: hot injection or heat-up

To obtain monodisperse particles in solution, it is essential to separate the nucleation and growth phases. In organometallic synthesis, two methods are commonly used to synthesize monodisperse nanoparticles. The first method, called "heat- up", consists in heating the reaction medium containing all the precursors in a controlled manner (fixed temperature ramp). The clusters form more and more rapidly as the temperature increases. Once the medium is saturated with clusters, the nucleation phase begins to form nuclei. The reaction time becomes a critical parameter during the homogeneous growth of the sprouts and to avoid the Ostwald ripening. It is important to know the reactivity of the precursors, the affinity of the ligands to the precursors as well as the heating rate to better separate the nucleation and growth phases. The particle size distribution is often larger in the case of heat-up but remains the most widely used method for synthesizing quantum dots on a large scale.

The second method, called hot injection method, consists of injecting one or more precursors into the hot solvent as shown schematically in Figure 2-1 to promote rapid nucleation. The Injection allows the controlled formation of nuclei of homogeneous size. In this case, hot injection requires highly reactive precursors to activate nucleation. This process is particularly suitable for growing nanoparticles Quantum Dots of good quality, while maintaining quality, good control over their composition, which be our route to syntheses the Quantum Dots. This method is a useful technique that enabled us to remove a glove box and open the door to the Schlenk line technique.

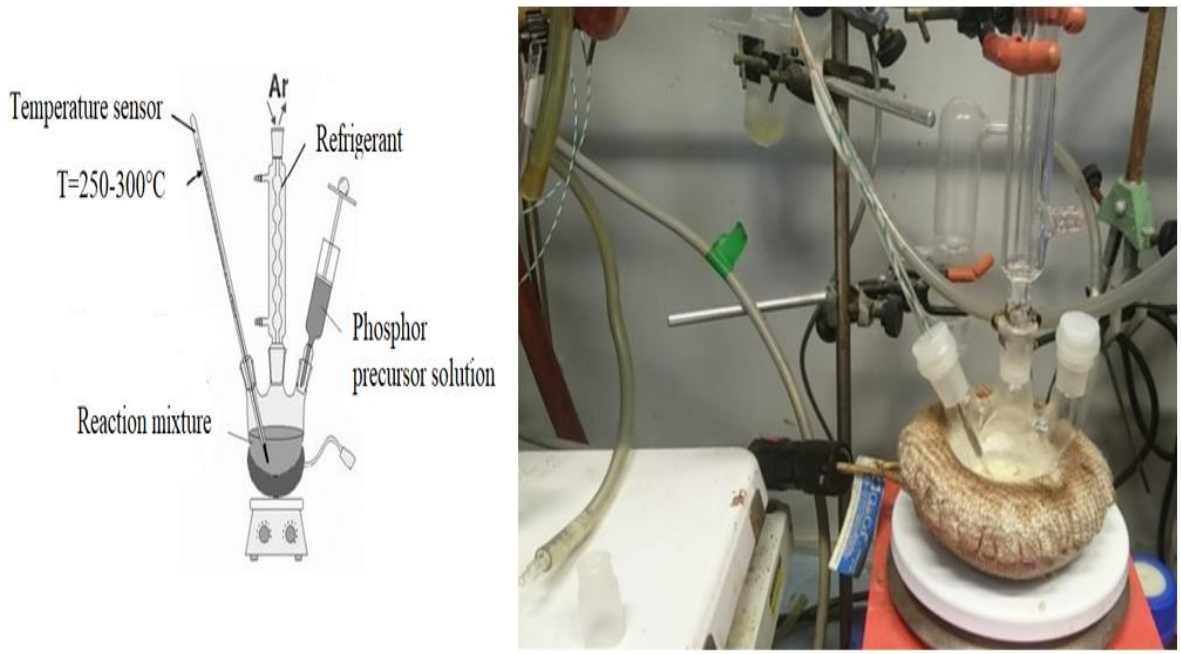

Figure 2-1: Schematic and photo of the hot injection reaction used for the synthesis of Core InP Quantum Dots.

1.3 Hot injection synthesis of InP QDs

The synthesis of InP QDs particles was carried out under mild conditions using Tris (dimethylamino) phosphine ($(DMA)_3P$) precursor. The QDs synthesized in this manuscript are very sensitive to air and water. Thus, the experiments described were carried out in Schlenk glass ware topped with a double vacuum/argon.

The products used are: $InCl_3$ (99.999%), $InBr_3$ (99.999%), $ZnCl_2$ (≥98%), tris(diethylamino)-phosphine ($(DMA)_3P$) (97%), zinc stearate ($Zn(St)_2$) (technical grade, 65%) were purchased from Sigma-Aldrich and 1 dodecanthiol (≥98%, Aldrich). Oleylamine (OLA) (>90%) was purchased from Acros Organics.

The synthesis of InP QDs is based on the work of Matthew A. Ellis et al.[130] The reaction began by mixed 0.4 g of ($InBr_3$)/($InCl_3$) and 0.25 g of ($ZnCl_2$) in (30 mL) Oleylamine (OLA) solution. For 1h the reaction was stirred and degassed by evacuating under vacuum and a

complete dissolution is achieved by constant agitation of the solution at room temperature 25°C. Then, the indium solutions were heated under vacuum to 120 $C°$ for 20 min. Afterward, the solution under inert gas (N_2) is heated at 220 $C°$ for 15 min, and Tris (dimethylamino) phosphine ($(DMA)_3P$) volume of 0.5 mL is rapidly remitted in the blend for 10 min. The solution gradually changes color from colorless to yellow, then to orange and finally to red/orange (see Figure 2-2). The reaction cooled down to room temperature.

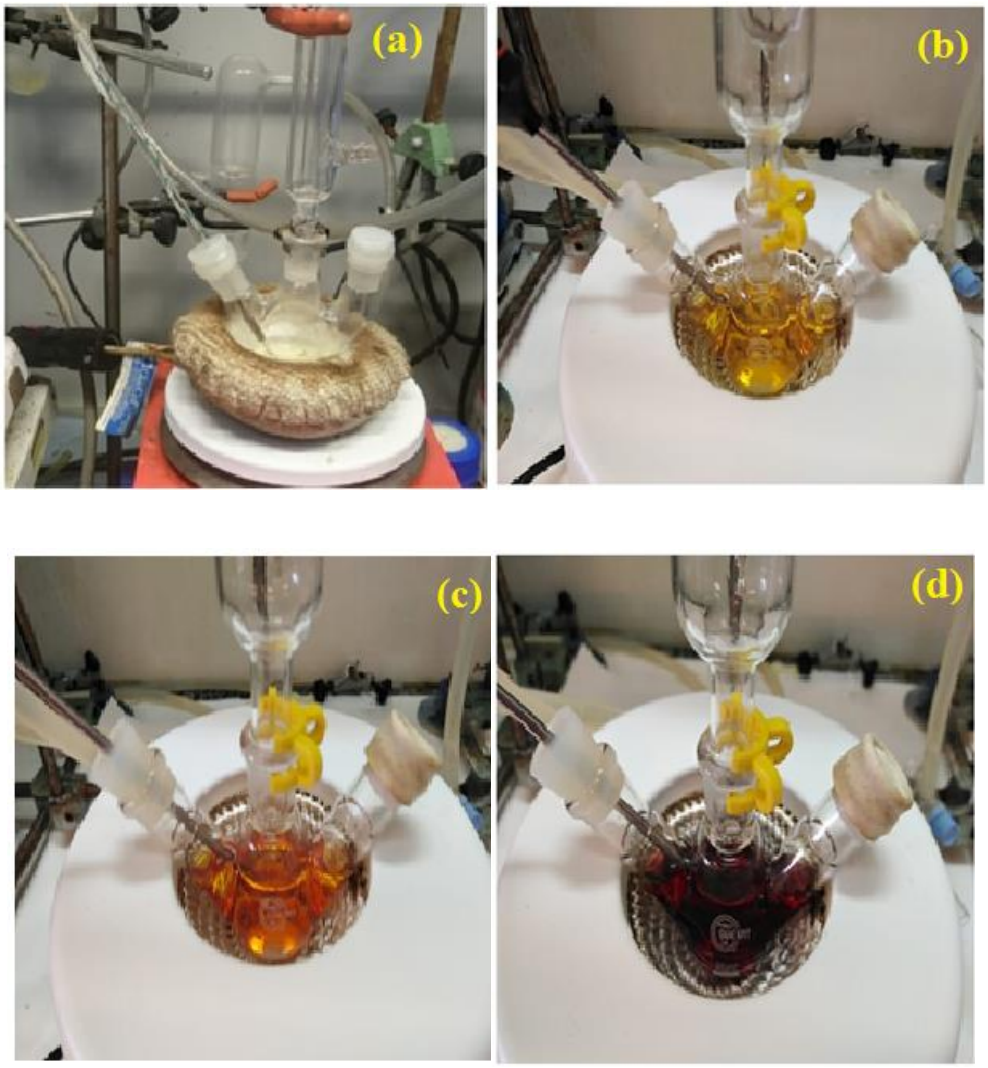

Figure 2-2: Synthesis process using hot-injection technique of InP QDs: a) The mixture is a white suspension for 1 h under vacuum. After increasing the temperature to 220°C under inert gas (e.g., N2), the solution changes color. It is (b) yellow for 15 min, (c) ora (c) orange when

we are injecting Tris (dimethylamino) phosphine ((DMA)3P) to this suspension solution and (d) red/orange after 10 min at 220°C.

1.4 Hot injection synthesis of InP QDs doped with Vanadium

We have carried out the synthesize Vanadium doped InP QDs with various concentrations varying from 5% to 10% by the hot-injection technique along with the same protocol in already depicted in the section 1.1 (hot injection synthesis of InP QDs).

Figure 2-3: InP Quantum Dots doped with Vanadium.

1.5 Hot injection synthesis of core/shell InP/ZnS QDs and core/shell/shell InP/ZnS/ZnS QDS

In this part, firstly we synthesized InP/ZnS core/shell QDs using a slightly modified version of the conditional method developed by Matthew A et al. [112] and Euidock Ryu et al. [131]. Hence, the formation of a Zinc shell around the core Indium phosphide QDs and the

formation of a Zinc shell around the shell/core InP/ZnS/ZnS by hot injection method was detailed. Indeed, after the optimized InP QDs synthesis, the reaction is placed at RT. Then,0.2 g of zinc stearate Zn $(St)_2$ was slowly added into the InP QDs solution, and stir evacuated under vacuum maintaining for 20 min RT. Under gaz, we raised the temperature to 230°C and allowed the reaction to proceed for 2h/3h. After that, we injected 1.79 g of DDT, and an anneal kept it for 1 hour. The reaction was complete, and the solution was brought down to room temperature.

On the other side, for the preparation of the InP/ZnS/ZnS, the same shelling process happened to synthesize InP/ZnS was added to the InP/ZnS blend (See Figure 2-4).

Figure 2-4: Highly luminescent core/shell InP/ZnS Quantum Dots and b) core /shell/shell InP/ZnS/ZnS Quantum Dots.

1.6 Purification and Storage

After synthesis, the Quantum Dots solution with required sizes was obtained after the complete removal of Ethanol by centrifugation at 4000 rpm for 10 min (Figure 2-5). The product was dispersed in dichloromethane and stored under an inert atmosphere in the dark at least one month at 4 °C

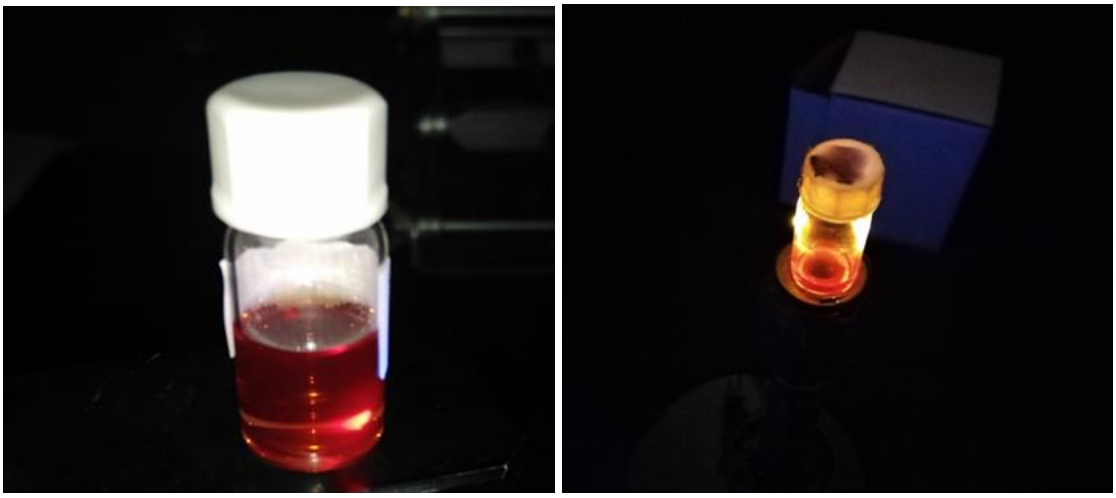

Figure 2-5: Photo of InP QDs solutions synthesized by hot injection process under UV illumination.

1.7 Synthesis of titanium dioxide nanotubes by anodization method

Among the different methods of manufacturing nanotubes [132,133],electrochemical anodization offers good adhesion and electrical conductivity as the oxide layer grows directly from the titanium metal substrate. [122,123]

The choice of the precursor is crucial as it influences the properties of the synthesized deposit in terms of its chemical structure (metal content stoichiometry, chain cross-linking, defects, layer contamination) and consequently its functional properties. Furthermore, the nanotubes allow a better transport and a better separation of the photogenerated charges, and consequently to improve the photoelectrochemical efficiency.

Indeed, anodizing consists of growing an oxide layer on the surface of a metal, by electrochemistry. In practice, two electrodes are connected to a generator, and immersed in an electrolyte[134]. When a sufficiently high voltage is applied between these two electrodes oxidation of the metal at the anode occurs and may lead to dissolution of the metal in the

electrolyte, or to the formation of a surface oxide layer. In the case of titanium anodizing oxidation leads to the formation of a TiO2 layer. (See Figure 2-6).

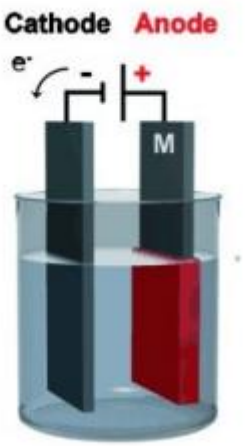

Figure 2-6: Anodization process.[10]

In our work, the electrochemical experiments are carried out at room temperature in using a direct current generator in a two-electrode cell where titanium is the working electrode using a solution containing ethylene glycol-fluorine (2 vol %), ultrapure water and ammonium fluoride ([NH_4F] =0.07 M). Also, the platinum is the counter electrode (sheet of platinum, S=1cm2). Prior to anodizing, the titanium sheet is mechanically polished with different abrasive papers, rinsed with acetone for 10 min and deionized water in a bath ultrasound and dried in the air. The Anodization is carried out at 60V for 2 hours under 30°C. Then, the sample is immediately sonicated in a distilled water to remove the initial TiO_2 NATs layer that has formed. It has been reported that the order and the adhesion of the nanotubes are improved when their growth is carried out on an electrode having already undergone the first anodization.[135] Hence, to obtain a clean and more consistent TiO_2 NATs layer, the second anodization of TiO_2 NTAs was maintained under the same synthesis conditions for the first anodization. The samples were then washed with ethanol and dried in the air. The TiO_2 NTAs

obtained were found to be amorphous, thus it was sintered for 3 hours at 400°C at a rate of 5°C/min) to produce TiO_2 NTAs with a crystalline anatase phase.

Finally, to the many advantages offered by this synthetic route, the resulting nanotubes are clamped to the metallic titanium substrate, forming an ohmic contact to collect the photogenerated electrons.

1.8 Deposition of the nanostructured films of TiO2/InP, TiO2/InP/ZnS and TiO2/InP/ZnS/ZnS by spin coating method.

Several methods have been used to deposit suspended nanoparticles on the nanostructured surface of TiO_2.[136–138]. In this work, the TiO_2-InP, TiO_2-InP/ZnS and TiO_2-InP/ZnS/ZnS nanostructures were prepared by spin coating method.

Regarding the choice of this deposition technique, we sought to adopt a simple strategy allowing to obtain reproducible porous films adapted to our application.

Indeed, this technique consists of spreading a few drops poured in the center of a substrate held on a support by a suction device. Thanks to the centrifugal force due to the rotation of a "spinner" (Figure 2.7), the deposited solution tends to cover the entire surface of the substrate uniformly, and the excess liquid is pushed out of the substrate.

Therefore, the InP/ZnS core/shell QD and InP/ZnS/ZnS core/shell/shell QD were deposited via a spin-coated process into the substrates TiO_2NTAs (1500 rpm for 30 s) which we used the same amount (2mmol) for each layer during the deposition. Then, the QD films were annealed at 100◦C for 30 min.

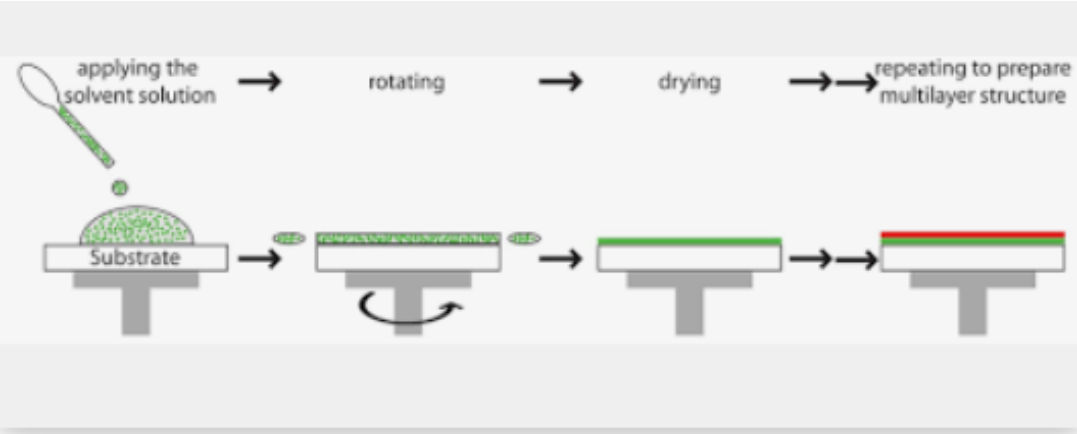

Figure 2-7: Schematic representation of the spin-coating method. [15]

1.9 Photoelectrochemical activity

The photo electrochemical measurements were carried out under illumination and in the dark on the TiO_2/InP, TiO_2/InP/ZnS, and TiO_2/InP/ZnS/ZnS samples using a standard three-electrode PEC cell. Where, the working electrode was TiO_2 NTAs (before and after surface modification by InP QDs, InP/ZnS QDs, and InP/ZnS/ZnS QDs. The surface area of the working electrode, which was exposed to the light, about 0.25 cm^2. The reference electrode was a saturated calomel electrode (CE), and the counter electrode was a platinum (Pt) wire as shown in Figure 2.8. These electrodes emerged in a 5 ml volume quartz cell, which contains an electrolyte solution of Na2S (0.5M) at pH=7.

The light source was Xenon lamp (PLSSXE300/300UV) equipped with a UV cut-off filter ($\lambda >$ 420 nm). The data was achieved through a potentiostat/galvanostat Autolab PGSTAT302N (Metrohm, Netherlands). The photocurrent was measured following the variation of photocurrent density as a function of time J = f(t) and cutting the illumination into fixed time intervals of time (20 s).

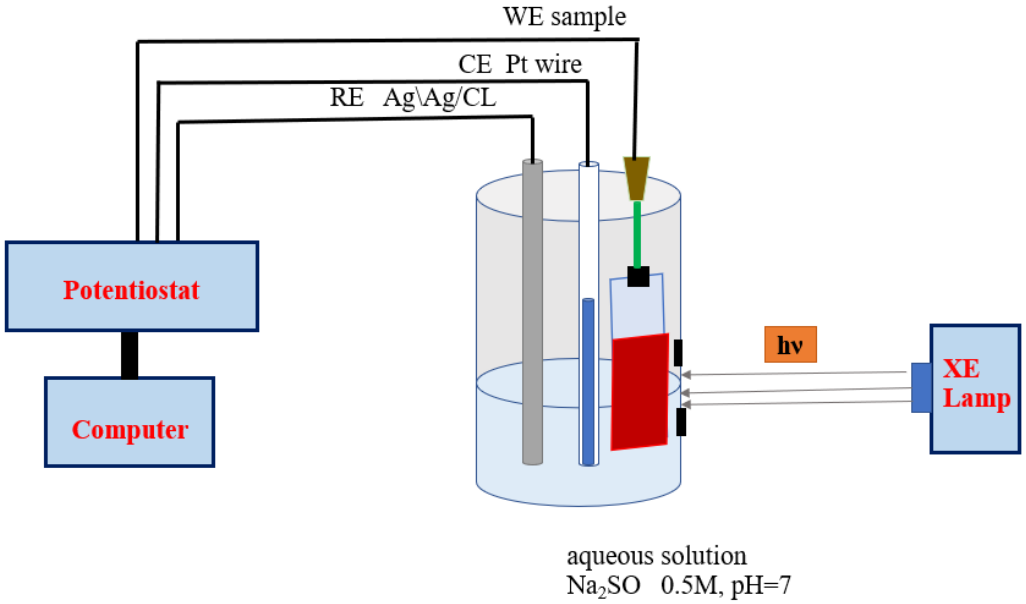

Figure 2-8: Photocurrent response of TiO2/InP, TiO2/InP/ZnS and TiO2/InP/ZnS/ZnS QDs under applied potential of -0.1976 V dark and under illumination.

2 Analysis technique

Several techniques for the characterization of quantum dots have been used since their appearance. In this section, we limit ourselves to presenting the main methods used in this thesis.

2.1 X-Ray Diffraction (XRD)

X-Ray Diffraction technique allows the identification of the nature of the crystalline properties of the solid or powder materials by comparing the diffraction peaks obtained with different databases from the literature. The principle is to irradiate a crystal sample with X-rays and measure the intensity of the diffracted rays at a position 2θ relative to the incident beam.

The study of elaborated crystalline materials was mainly carried out by X-Ray Diffraction followed by a Rietveld refinement. The principle is to bombard the sample with X-Rays and to observe the interferences of the radiation reflected by the planes of the Bragg grating at different angles. It should be noted that the atoms of a crystal belong to families of reticular planes denoted parallels (hkl). The distance between each set of parallel planes is called distance inter-reticular dhkl. The incident plane wave of wave vector k0 forms an angle θ with the planes, called Bragg angle Figure 2.9. The diffraction condition is given by Bragg's law:[139]

$$2d_{hkl}\sin\theta = n\lambda \quad (2.1)$$

With

- Half deviation (Bragg angle) the corresponding diffraction angle, the angle between a plane wave of a plane family hkl.
- h,k,l: Miller indices of the planes.
- λ: wavelength of the radiation used.
- n: the diffraction order.

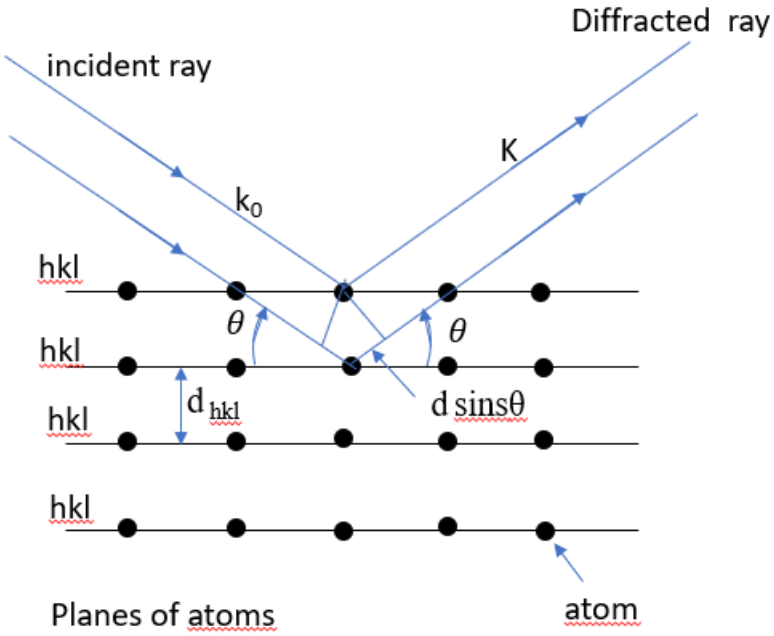

Figure 2-9: Schematic representation of the diffraction process.

The structural refinement of the diffractogram obtained was carried out using a Rigaku PDXL Software (Integrated x-ray powder diffraction software) and phase identification is carried out by comparison with the JCPDS (Joint Committee on Powder Diffraction Standards) standard files.

Otherwise, X-Ray Diffraction enables to identify the grain size using the Debye–Scherrer formula:

$$D = \frac{0.9\lambda}{B\cos\theta_B} \quad (2.2)$$

Where,θ_B is referred to the maximum of Bragg diffraction peak, λ denotes the x-ray wavelength and the full width at half maximum (FWHM) of diffracted peaks is named by B.

In this work, we used X-Ray Diffraction (XRD) (model Rigaku Ultima IV diffractometer) in the Bragg-Brentano configuration at 2(θ) angles from 20°to 60°with CuKα radiation (λ=1.5418 Å) by the drop-casting method as shown in Figure 2.10.

Figure 2-10: Image of the X-ray diffraction.

2.2 Transmission Electron Microscopy (TEM)

The history of electron microscopy began with the research work of Louis de Broglie, who had the intuition to associate a wave with electrons (massive, charged particles) to use them as a light beam in a microscope. Through this research, Ernst Ruska (Nobel Prize 1986) produced the first electromagnetic lenses, and later (1933) the first electron microscopy.

Transmission electron microscopy (TEM) is a technique based on the principle of the interaction of electrons with the matter. It consists of projecting a high-energy electron beam onto a sufficiently thin sample. A beam of high-energy electrons onto a sufficiently thin sample. All the electron beams transmitted and scattered elastically through the sample, is used to form the image or diffraction pattern.

The main interest of this technique is to allow access to information of a morphological, crystallographic, and chemical nature. This constitutes a direct investigation of the microstructure down to the nanometer scale. The electron microscopy study is based on the combination of information from direct space with that from Fourier space, in other words, the diffraction of electrons by the material. In this way, different results can be collected relating to the size, dispersion, shape, crystallinity, and crystal planes of the structure.

All the observations carried out in the framework of this thesis were made at the Electron Microscopy Service (SME) at the polytechnic university of Valencia. The microscopy used is the JEM-100CX2 model TEM see in Figure 2-11 which operates at 200 kV. The methods for preparing samples for microscopy are diverse and varied. It depends closely on the nature of the sample to be studied as well as the desired analysis. In our research work, after purification of the QDs, a drop of QDs diluted in dichloromethane is placed and dried on a copper grid directly on the carbon membrane. The diameter of the QD was determined from the TEM images using the software ImageJ.

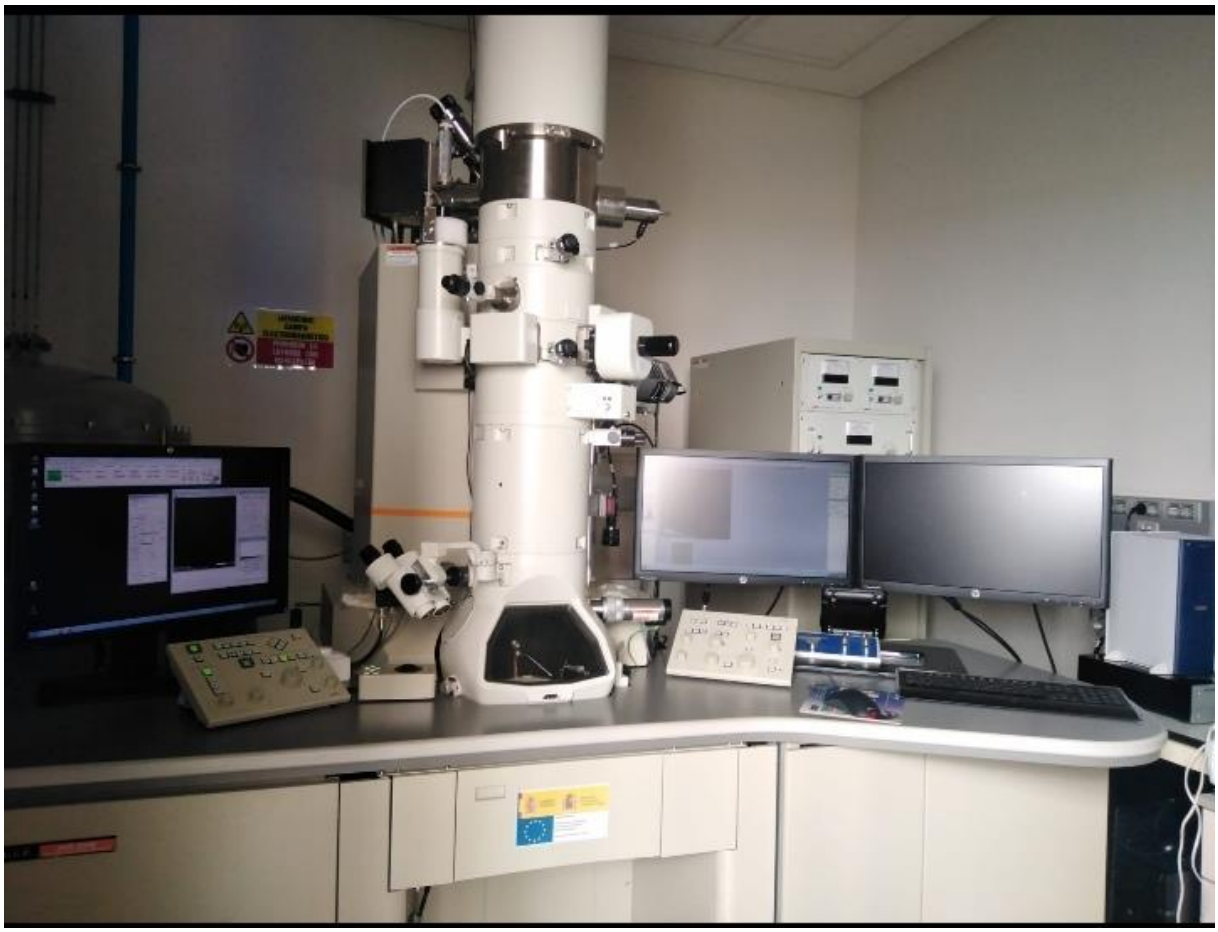

Figure 2-11: image of Transmission Electron Microscopy (TEM).

2.3 Scanning Electron Microscope

Scanning Electron Microscope (SEM) is currently the most widely used technique for microscale topography. It has the great advantage of being able to give a true topographic picture of the surface. The study of an image allows to identify the shape and dimensions of the particles and gives a morphological and structural description of the surface.

Therefore, the principle of SEM uses a very fine electron beam which scans the surface of the sample point by point like a probe. The interaction of the beam with the object creates different particle emissions which are analyzed with the help of detectors: Secondary electrons, backscattered electrons, scattered electrons, transmitted electrons, emitted X-rays are captured synchronously with the scanning of the beam on the sample. The material

analyzed must be conductive to avoid charging phenomena due to electrons. For poorly conductive materials, metallization can be carried out, for example, using carbon or gold.

The interaction between the electron beam and the surface of the solid lead an ionization of the outermost atoms. The electrons emitted by the target and having a low energy below (0.02 - 5 kV), are detected by a detector coupled to a video console whose scan is synchronized with the intensity of each of the electrons emitted by the target is determined by a detector coupled to a video console. The intensity of each of these signals modulates the brightness of the television screen, giving black and white images.

In this work, the images were obtained on a SEM-Zeiss ULTRA 55 microscopes (See Figure 2-12). This is a SEM equipped with a field emission gun. SEM equipped with a 30 kV field emission gun allowing a resolution on the nm scale. Moreover, the samples are fixed using a graphite adhesive and electrical conductor on a brass sample holder, then carbonized under vacuum by vaporization of a carbon wire. The layer of conductive carbon thus obtained some angstrom thick, is necessary to reduce the effect of loads that would compete with and alter the topographic contrast.

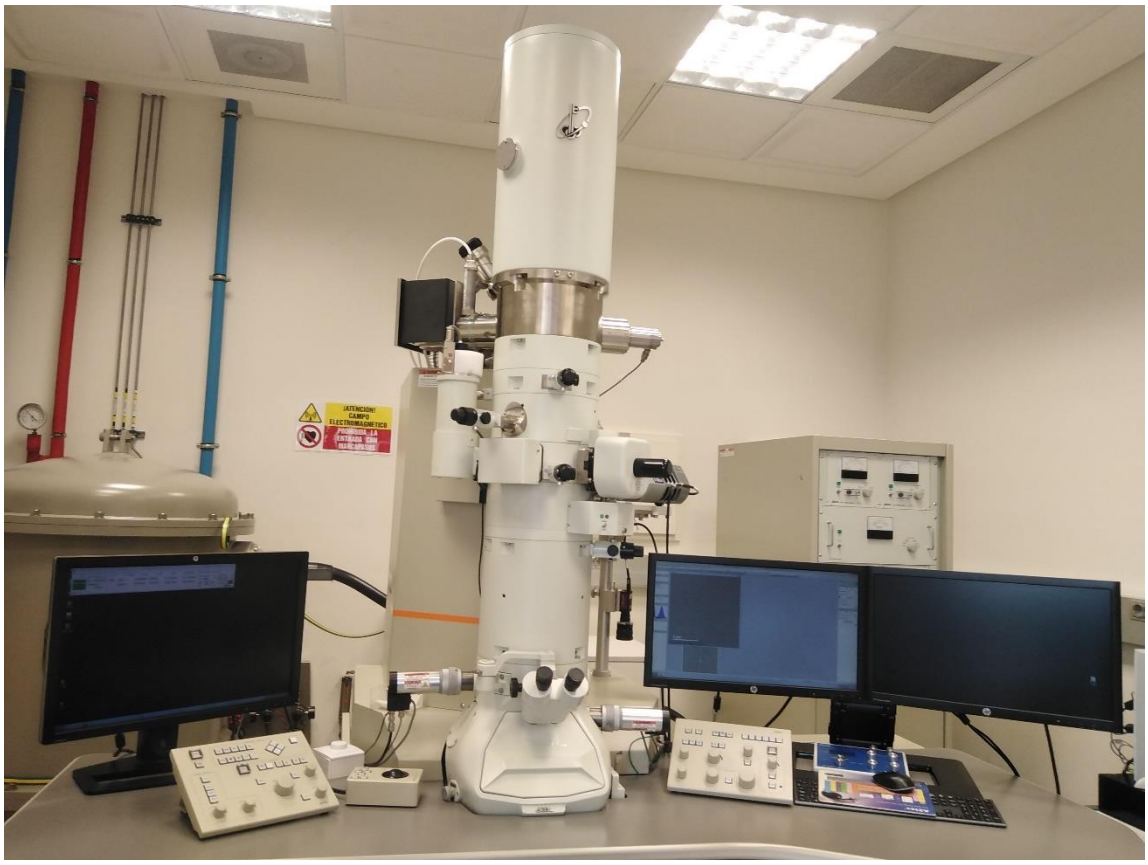

Figure 2- 12:image of scanning electron microscopy (SEM).

2.4 Energy-dispersive Spectroscopy (EDS)

It is a simple technique that allows a rapid quantitative analysis of the different elements present in solids. It is directly coupled to scanning electron microscopy and is performed via an EDS (Energy Dispersive Spectroscopy).

2.5 Photo-electrochemistry analysis

Electrochemical detection is a very popular detection method, and this category has developed rapid development despite a late start. It provides access to the transport of charges and particles between an electrode and a solution as show in figure 2-13. This technique uses a so-called:

- Potentiostat:

The potentiostat is a voltage-following amplifier that controls and measures the voltage between the working electrode and a reference electrode in solution. For a given voltage, it also measures the current flowing through the solution between the working electrode and a counter electrode. We are dealing with a three-electrode circuit which is commonly used in electrochemistry.

- The working electrode "WE"

This is the electrode who's potential and current are measured. It represents the study surface whose characteristics we want to know or deposit on. In our work, we are trying to deposit Quantum Dots on TiO_2 NTAs layer. Only one side of the sample is in contact with the solution.

- The reference electrode "RE"

The reference electrode is the second key component of any electrochemical cell. This electrode has a specific and constant potential, which makes it possible to impose a precisely defined potential on the working electrode. This is important, as the potentiostat can only control the difference in potential imposed between two electrodes. The reference electrode is used to measure the voltage of the working electrode. A reference electrode should have constant electrochemical properties if no current flows through it.

- The counter electrode "CE"

The counter electrode is a conductor that closes the circuit of the cell and allows the flow of electric current. The counter electrode is a conductor that closes the circuit of the cell and allows the flow of electric current through the solution into the working electrode. It is usually made of inert metals such as platinum and graphite.

The cell is made of an inert material, usually glass, Plexiglas, or Teflon in which the cell we used was made.

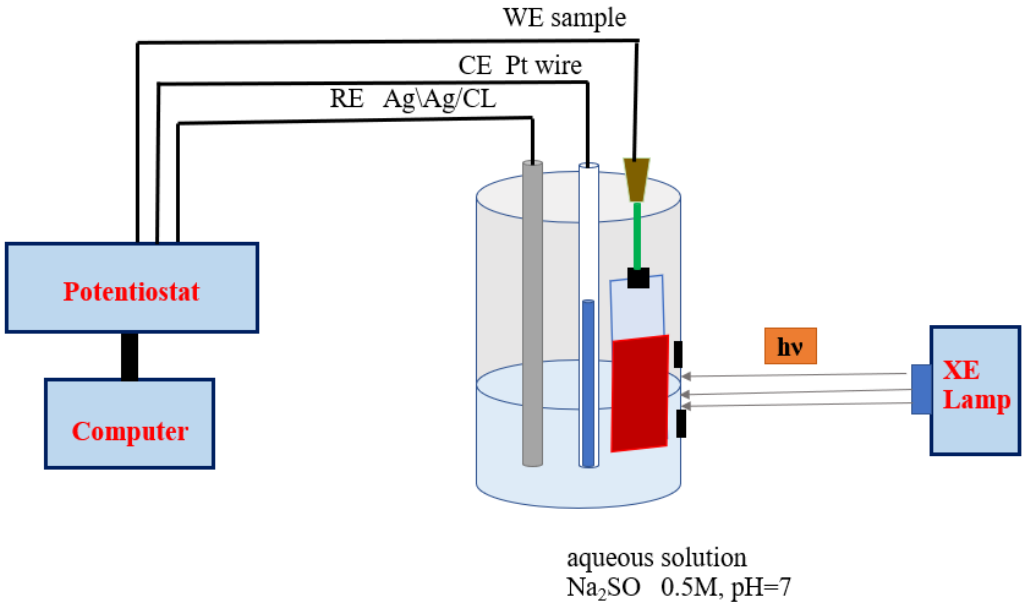

Figure 2-13: Photocurrent response of TiO2/InP, TiO2/InP/ZnS and TiO2/InP/ZnS/ZnS QDs under applied potential of -0.1976 V dark and under illumination.

2.6 UV spectroscopy

Optical spectroscopy is a non-destructive characterization technique. It provides information about the material (energy levels, etc.) from its interaction with incident radiation, usually ultraviolet (UV), visible or infrared (IR). Depending on the sensitivity of the equipment and the nature of the sample, different types of information will be obtained.

In our case, we used a double-beam spectrophotometer Ocean Optics HR4000 model U-Vis spectroscopy from 400 nm to 800 nm at room temperature, whose operating principle showed in Figure 2-14 It is used for measuring the optical properties of the Core InP and InP/ZnS

Core /Shell and InP/ZnS/ZnS Core/Shell/Shell suspended in Dichloromethane. The UV-visible measurements were made in solution using an optical path 5 ml quartz cuvette. For each analysis, the cuvette must be cleaned thoroughly to avoid the effects of contaminants on the sample undergoing analysis.

The UV-Visible-NIR spectrophotometer consists of four main parts: two light sources, the first is a xenon lamp for the UV-Visible range and the second is a halogen lamp for the infrared range, a monochromator (consisting mainly of a dispersive system, an entrance slit, and an exit slit), a sample compartment (the sample holder, the reference, and accessories) and a detector

The beam from the source is sent to a monochromator. At the output of the monochromator, the beam is sent to two mirrors. Each beam passes through either the sample or the reference. The two beams are then sent to a photomultiplier.

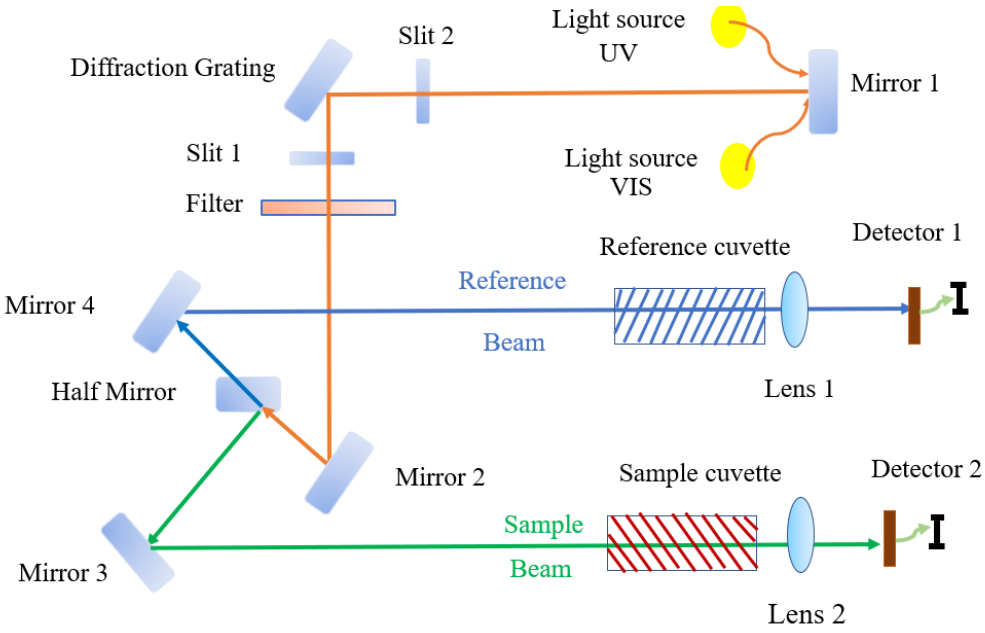

Figure 2-14: Schematic representation of a double beam spectrophotometer.

UV-visible spectroscopy allows us to measure the transmittance (T =I/I0) or absorbance (A=log(1/T)), where I0 is the incident light intensity, and I is the intensity measured after passing through the solution.

Spectroscopy also allows the deduction of the molar absorption coefficient (note ε) which is the ratio between the absorbance of a colored solution and the length of the optical path traversed by monochromatic radiation in each medium. Beer-Lamber's law allows this coefficient to be calculated using the following relationship [14]:

$$\varepsilon = \frac{A}{c*d}. \quad (2.3)$$

It is also possible to record solid absorption spectra by working in diffuse reflection using an optically transparent integrating sphere, rather than in transmission. This technique is very useful for measuring the band gap of a semiconductor.

In transmission mode, the principle of the measurement is based on the comparison of the light transmitted by the sample with that of a reference, usually the solvent.

In diffuse reflection mode, the instrument measures the light scattered by the sample and the light scattered by a reference, usually Teflon (white). The instrument measures the apparent absorbance equal to

$$\log(\frac{R0}{R}) \text{ , } \log(R0/R) \quad (2.4)$$

where R_0 is the reflectance of the reference and R is the reflectance of the sample.

2.6.1 Determination of the gap value

To determine the gap values of a semiconductor material, several approaches are possible, depending on whether it is in the form of a solution or a layer. In one case the absorption

spectrum of the sample is recorded in transmission mode, in the other in diffuse reflection mode.

2.6.2 Transmission mode (direct method)

Photon absorption due to the excitation of electrons from the valence band of the semiconductor to be studied towards its conduction band, with energy equal to or greater than the width of the band gap, leads to the appearance of an intense broad band from the UV band gap, leads to the appearance of a broad, intense band from the UV in the absorption spectrum.

The intersection of the slope of the descending part of the band with the x-axis determines the value of the long-wave gap. To express it in eV it can be converted as shown below:

$$\mathrm{E(eV)} = \frac{1240}{\lambda}\,\mathrm{(nm)}\ (2.5)$$

2.6.3 Photoluminescence

Photoluminescence (PL) is the most used spectroscopic technique for characterizing the optical properties of semiconductor materials. It's a non-destructive technique, and it is the preferred technique for characterizing samples as soon as they leave the growth chamber without any preparation to confirm the quality of the materials obtained. It consists in creating charge carriers in the semiconductor with the help of an intense and continuous excitation source, usually a laser whose photons have an energy above the bandgap of the semiconductor, and then collecting and analyzing the light emitted when the carriers recombine of the carriers.

In the case of semiconductor nanostructures (see in Figure 2-15), photons absorbed in the barrier generate electron-hole pairs that rapidly relax to lower energy levels before recombining radiatively. The PL signal depends on the lifetimes of the different relaxation processes.

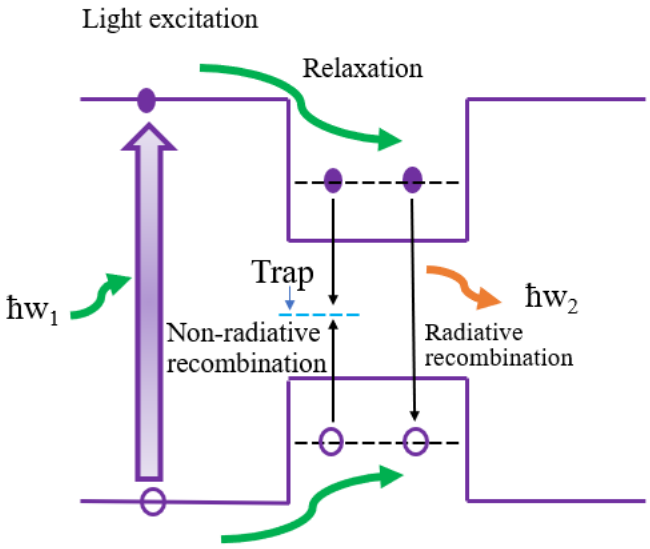

Figure 2-15: schema illustrating the principle of photoluminescence.

If we take the case of the Quantum Dots, which has a density of state corresponding to Dirac distributions, its emission peak at low temperature is very thin. If we consider the entire surface probed by the laser beam. We obtain a broad enough photoluminescence spectrum (a few meV) which results from the totality of the emissions from the Quantum Dots QDs. The width at half maximum (FWHM) then provides information on the inhomogeneous dispersion of the QDs.

These islands can have a variety of shapes: cubic, pyramidal, truncated pyramidal, truncated pyramid, and spherical. But the samples studied contain QDs that are very large compared to their height; in this way, they can be grouped into families. Each family is composed of QDs with the distribution of widths can be well modelled by a Gaussian.

Figure 2-16 clearly shows the optical response of a series of QDs that is perfectly homogeneous, resulting in a fine PL spectrum and a second series having a variety of size of QDs, resulting in a broad spectrum of PL.

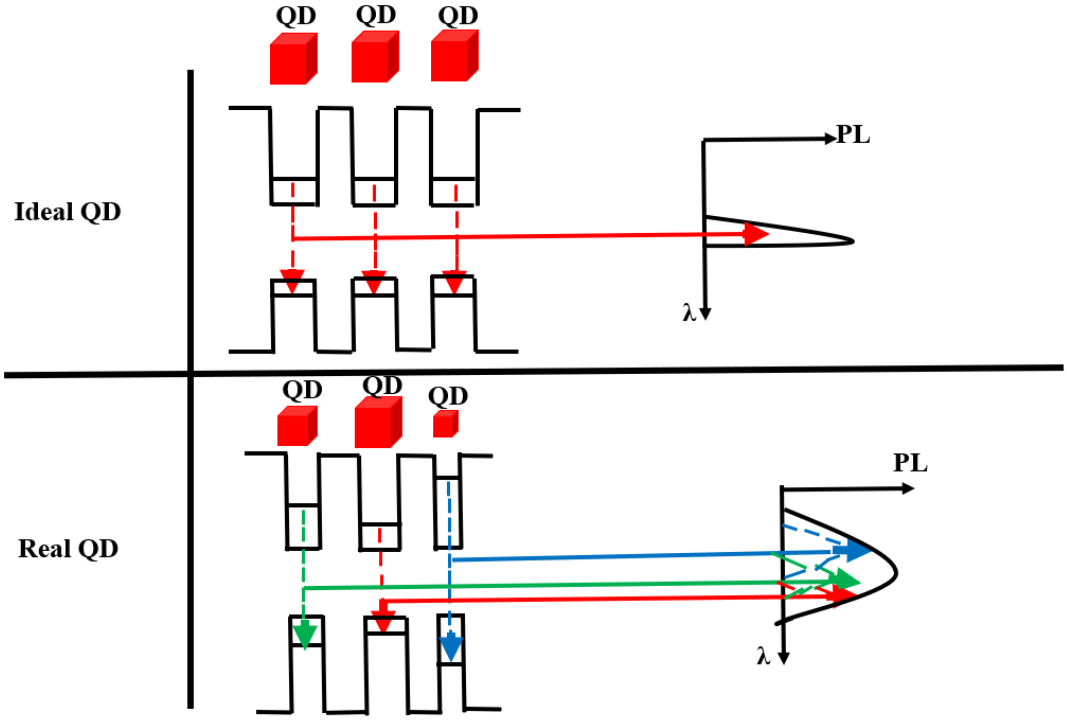

Figure 2-16: Illustration of the emission spectrum of ideal and isotropic quantum boxes and inhomogeneous. For the energy band structure, only the ground state transition is presented. The state transition is shown. The gap between two energy levels decreases as the size of the Quantum Dots increases.

The photoluminescence properties of Quantum dots were carried out using a luminescence spectrometer type Jobin Yvon-Horiba spectrometer, He-Cd laser. The excitation length was set at (λ = 325 nm), and the measurements were determined in the range 350-800 nm.

2.6.4 Spectroscopy of fluorescence

The fluorescence spectrum provides a more accurate view of the size dispersion of a sample and gives information on the quality of the sample. In fact, after the absorption of the photon, the formation of the exciton takes place. When the electron returns to its ground state, a photon is emitted, and fluorescence is then generated by a phenomenon called radiative recombination, corresponding to the reappearance of the electron and the hole. In addition, the fluorescence lifetime in the excited state is defined as the average time spent in the excited state before returning to the ground state.

In this thesis the fluorescence spectra were performed with a spectrofluorometer a Photon Technology International (PTI) (LSP-220B) fluorometer equipped with a 75 W Xe lamp. The lifetime is was measured at 1270 nm using a Hamamatsu NIR emission detector (peltier cooled at -62.8 ºC operating at 800 V, coupled to a grating monochromator). The excitation source is an Nd: YAG laser operating at 355 nm.

The temperature was set at 25°C. The following procedure for sample preparation was adopted. The excitation wavelength of QD's samples at λ=450 nm. For this purpose, a dilution of the QD's stock solution is made with dichloromethane.

2.7 Numerical Analysis

Simulation is a tool used by the researcher to study the results of an action on an element without carrying out the experiment on the real element. Recently, the numerical simulation of thin film cells has grown enormously. It is commonly used for solar cell optimisation. The most commonly used software for numerical simulation are: AMPS-1D, PC-1D, ASA, SCAPS-1D, SILVACO.

The SCAPS-1D simulator developed by Marc Burgelman is a program designed to run under the Windows operating system.[140] It allows the modelling of the physical and electrical performance of several electronic component .[141]

This avoids the need to manufacture several prototype cells with different parameters; time saving and low cost technique.[142] It solves the differential equations that govern the operation of electronic devices by numerical methods (finite element, least square etc).[143,144]

2.7.1 Presentation of SCAPS-1D

SCAPS-1D (Solar Cell Capacitance Simulator in one Dimension) is an electronic device simulation software owned by the GENT University of Belgium, [18] Department of Electronics, and Information Systems (ELIS). It has a database with the extension "def", whose various parameters (width, doping, etc.) can be modified.

The 1D SCAPS simulation is based on the numerical solution of the three fundamentals charge transport equations in semiconductors, which are respectively the Poisson equation and the continuity equation for electrons and holes. SCAPS 1-D was introduced into the literature with the articles. [145,146] Applications of simulation using SCAPS can be found in the consulted in the references. [111,144,147]

2.7.2 Basic concepts

To simulate and control all parameters of a photovoltaic device by means of SCAPS software, we must go through three main windows:

- Execution window (action panel).
- Device design and problem definition window (Definition panel)

- Results window.

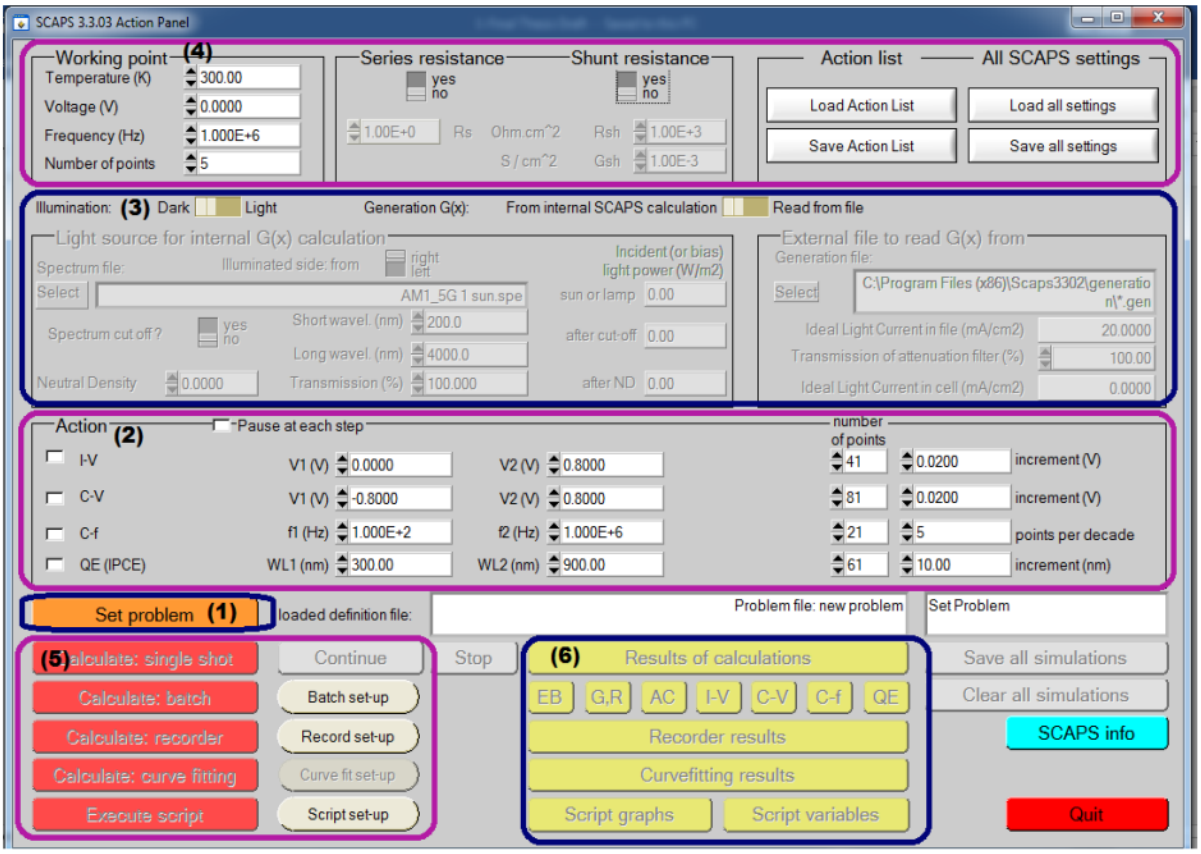

Figure 2-17: SCAPS software action panel window: “Start-up”.

SCAPS opens with the 'Action Panel' window. The other two windows, Device Design and Results, can be accessed at any time the other two windows, the Device Design window, and the Results window, as shown in the figure 2-17.

The panel consists of six Blocks, as follows:

1) Define the problem, as well as the geometry, materials and all the properties of the solar cell under study.
2) Indicate the circumstances under which the simulation is performed (specify the point of Operation).
3) Specify the measure (characteristic) to be simulated.
4) Start calculation(s).

5) Display simulation curves.

6) Results of calculations.

2.7.3Definition of the problem

Click on the SET PROBLEM button in the action panel and choose LOAD in the bottom right-hand corner of the panel that opens next Select and open (for example NUMOS CIGS Baseline.def.) This is an example file of a CIGS-based solar cell. Afterwards, it is possible to modify all the properties of the cell by clicking on 'SET PROBLEM' in the action panel.

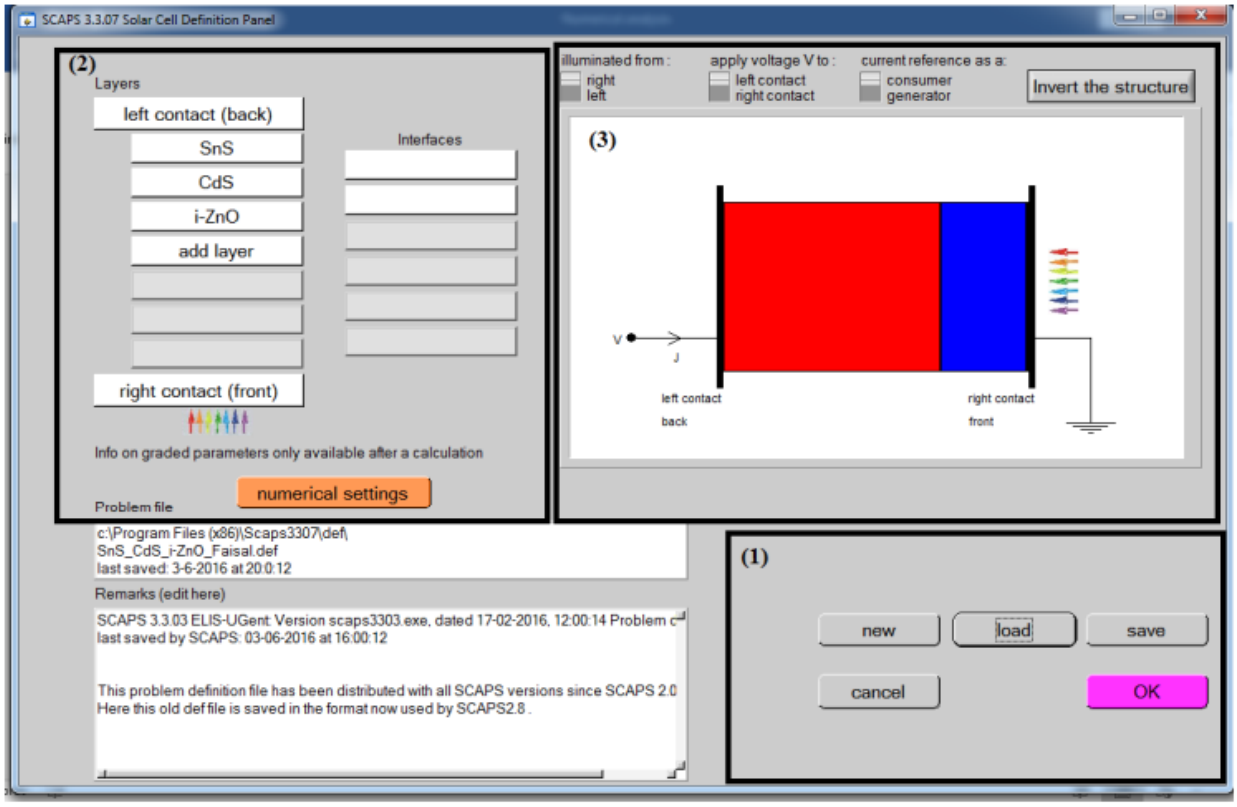

Figure 2-18: Defining the problem.

2.7.4Adding layers to structure

To modify the properties of layers, contacts and interfaces, a simple click be on “Add Layer” which be named “Layer properties panel” as illustrated in the figure 2-19.

In the Layer properties panel, one can indicate the basic physical parameters to be simulated. One can also adjust the initial and final values of the argument, as well as the number of steps.

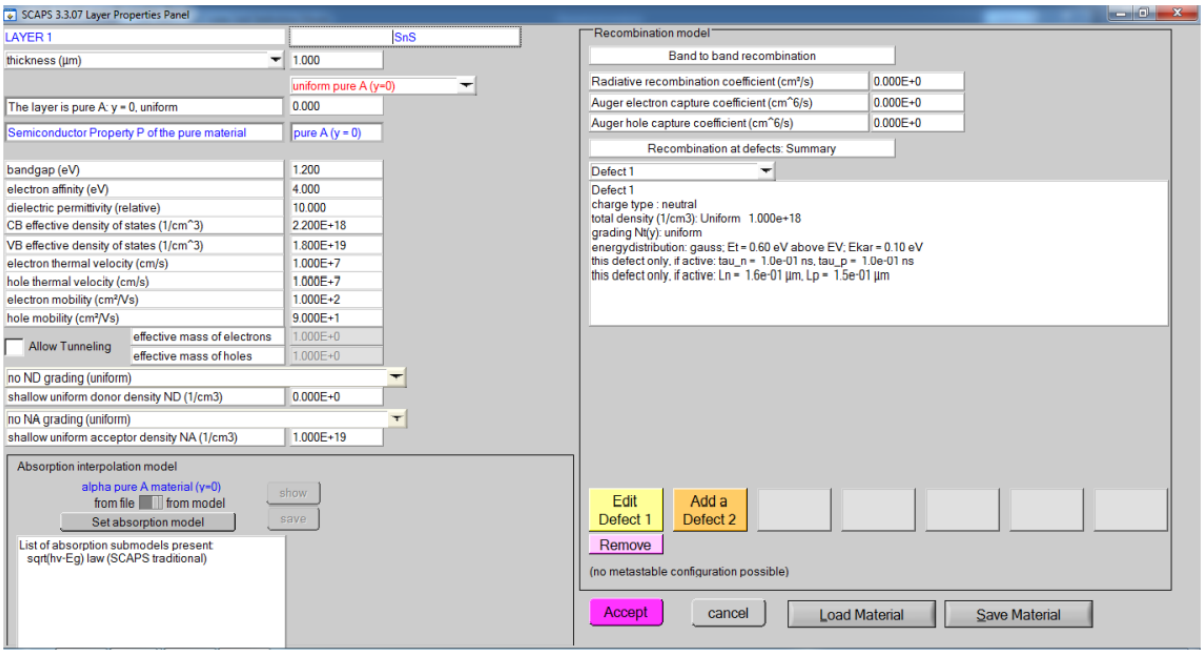

Figure 2-19: Layer properties panel

Whatever the structure of a solar cell, an optimization of its parameters is necessary to predict its best performance before moving on to the technological phase. Therefore, $SCAPS-1D$ optimized the parameters such as cell thickness, doping levels and profiles, contact configuration and optical confinement.

The optimal values of the parameters depend, of course, on the structure of the solar cell, the quality of the substrate material (lifetime, mobility), the quality of the ohmic contacts, the surface recombination rate (front and back side), etc.

Conclusion

In this chapter, we presented the hot injection method, which is used to synthesize the core InP QDs, core InP QDs doped with Vanadium, core /shell InP/ZnS QDs and core/shell/shell InP/ZnS/ZnS QDs. Also, we have described the preparation of titanium dioxide nanostructure deposited on metallic titanium plates by the anodization process. In addition, we have also chosen the spin coating method to prepare TiO2/InP, TiO2/InP/ZnS and TiO2/InP/ZnS/ZnS nanostructures due to its ease of processing and its low operating cost and its reproducibility. Finally, we described the different characterization techniques and SCAPS-1D software used in this study to characterize all the materials previously prepared.

References

[1] S. Mahajan, M. Rani, R. Dubey, J. Mahajan, H. Ece, International Journal of Latest Research in Science and Technology, Int. J. Latest Res. Sci. Technol. 2 (2013) 518–521.

[2] C. Burda, X. Chen, R. Narayanan, M.A. El-sayed, Chemistry and Properties of Nanocrystals of Different Shapes, 2005.

[3] R. Koole, E. Groeneveld, D. Vanmaekelbergh, Size Effects on Semiconductor Nanoparticles, n.d. https://doi.org/10.1007/978-3-662-44823-6.

[4] F. Schulz, G.T. Dahl, S. Besztejan, M.A. Schroer, F. Lehmku, G. Gru, T. Vossmeyer, H. Lange, Ligand Layer Engineering To Control Stability and Interfacial Properties of Nanoparticles, (2016). https://doi.org/10.1021/acs.langmuir.6b01704.

[5] O. Yarema, M. Yarema, D. Bozyigit, W.M.M. Lin, V. Wood, Independent Composition and Size Control for Highly Luminescent Indium-Rich Silver Indium Selenide, (2015) 11134–11142. https://doi.org/10.1021/acsnano.5b04636.

[6] K.D. Wegner, F. Dussert, D. Truffier-boutry, A. Benayad, Influence of the Core / Shell Structure of Indium Phosphide Based Quantum Dots on Their Photostability and Cytotoxicity, 7 (2019) 1–12. https://doi.org/10.3389/fchem.2019.00466.

[7] C.A.S. No, Agents Classified by the IARC Monographs , Volumes 1 – 132, (2012).

[8] J.O. Uif, T. Rvbouvn, D. Sfhjnf, 1BTU QSFTFOU BOE GVUVSF PG JOEJVN QIPTQIJEF RVBOUVN EPUT, 15 (2022) 4468–4489.

[9] P. Ramasamy, K. Ko, J. Kang, J. Lee, Two-Step " Seed-Mediated " Synthetic Approach to Colloidal Indium Phosphide Quantum Dots with High-Purity Photo- and Electroluminescence, (2018). https://doi.org/10.1021/acs.chemmater.8b02049.

[10] V. Brunetti, H. Chibli, R. Fiammengo, A. Galeone, M.A. Malvindi, G. Vecchio, R. Cingolani, L. Nadeau, P. Paolo, quantum dots : in vitro and in vivo toxicity assessment, (2013) 307–317. https://doi.org/10.1039/c2nr33024e.

[11] D.A.G. Ramirez, J.S.A. Cerón, M.L.G. Herrera, J.P.L. Arias, M.P. González, Effect of the indium myristate precursor concentration on the structural , optical , chemical surface , and electronic properties of InP quantum dots passivated with ZnS, J. Mater. Sci. Mater. Electron. 30 (2019) 4885–4894. https://doi.org/10.1007/s10854-019-00783-6.

[12] Q. Zhou, J. Zhou, M. Zeng, G. Wang, Y. Chen, S. Lin, Photoelectrochemical Performance of Quantum dot-Sensitized TiO 2 Nanotube Arrays : a Study of Surface Modification by Atomic Layer Deposition Coating, (2017). https://doi.org/10.1186/s11671-017-2036-6.

[13] M. Ni, M.K.H.L. Ã, D.Y.C. Leung, K. Sumathy, A Review and Recent Developments in Photocatalytic Water-Splitting Using TiO2 for Hydrogen Production A review and recent developments in photocatalytic water-splitting using TiO 2 for hydrogen production, (2007). https://doi.org/10.1016/j.rser.2005.01.009.

[14] L.B. Hoch, P. Szymanski, K. Kaur, L. He, K. Liao, Q. Qiao, L.M. Reyes, Carrier dynamics and the role of surface defects : Designing a photocatalyst for gas-phase CO 2 reduction, (2016) 8011–8020. https://doi.org/10.1073/pnas.1609374113.

[15] Black Anatase TiO 2 Nanotubes with Tunable Orientation for High Performance Supercapacitors, (2019). https://doi.org/10.1021/acs.jpcc.9b05070.

[16] N. Cross, D.J. Woodsworth, Investigating the Electronic Properties of a Carbon, (2008).

[17] A.E. Commission, P. Reiss, A.E. Commission, J. Villain, Dans un laboratoire de nanosciences, (2011).

[18] U. Resch-genger, M. Grabolle, S. Cavaliere-jaricot, R. Nitschke, T. Nann, Quantum dots versus organic dyes as fluorescent labels, 5 (2008) 763–775. https://doi.org/10.1038/NMETH.1248.

[19] P. Reiss, M. Carrie, C. Lincheneau, L. Vaure, S. Tamang, Synthesis of Semiconductor Nanocrystals , Focusing on Nontoxic and Earth-Abundant Materials, (2016). https://doi.org/10.1021/acs.chemrev.6b00116.

[20] R. Saran, R.J. Curry, technologies, Nat. Publ. Gr. 10 (2016). https://doi.org/10.1038/nphoton.2015.280.

[21] M.A. Reed, R.J. Aggarwal, R.J. Matyi, T.M. Moore, A.E. Wetsel, Physical review, 60 (1988).

[22] C. Cea, Les nanocristaux semi-conducteurs fluorescents font leur gamme, (2005).

[23] M.T. Clarke, F.N. Viscomi, T.W. Chamberlain, N. Hondow, A.M. Adawi, J. Sturge, S.C. Erwin, J.G. Bouillard, S. Tamang, G.J. Stasiuk, colloidal quantum dots through thermal diffusion, Commun. Chem. (n.d.). https://doi.org/10.1038/s42004-019-0138-z.

[24] F.O.R.T.W. Orth, T. Exas, Q. Aprimer, QuantumDots: APrimer, (n.d.).

[25] Y. Wan, J. Norman, J. Bowers, Quantum dot microcavity lasers on silicon substrates, 1st ed., Elsevier Inc., 2019. https://doi.org/10.1016/bs.semsem.2019.05.002.

[26] Z.I. Alferov, The history and future of semiconductor heterostructures, (1998) 1–14.

[27] V. Biju, T. Itoh, A. Anas, Semiconductor quantum dots and metal nanoparticles : syntheses , optical properties , and biological applications, (2008) 2469–2495. https://doi.org/10.1007/s00216-008-2185-7.

[28] A. Physics, Optical Properties of Semiconductor Nanocrystals Cambridge Studies in Modern Optics, n.d.

[29] N. Fernández-delgado, M. Herrera, A.H. Tavabi, M. Luysberg, R.E. Dunin-borkowski, Applied Surface Science Structural and chemical characterization of CdSe-ZnS core-shell quantum dots, Appl. Surf. Sci. 457 (2018) 93–97. https://doi.org/10.1016/j.apsusc.2018.06.149.

[30] Q. Zhao, P.A. Graf, W.B. Jones, A. Franceschetti, J. Li, L. Wang, K. Kim, Shape Dependence of Band-Edge Exciton Fine Structure in CdSe Nanocrystals, (2007).

[31] I. Review, " 5 = 5;„ +, 75 (1995) 3728–3731.

[32] A.L. Rogach, No Title, n.d.

[33] M. Rosen, M. Kuno, M. Nirmal, D.J. Norris, M. Bawendi, Band-edge exciton in quantum dots of semiconductors with a degenerate valence band: Dark and bright exciton states, 54 (1996) 4843–4856.

[34] O. Stier, M. Grundmann, D. Bimberg, Electronic and optical properties of strained quantum dots modeled by 8-band k – p theory, 59 (1999) 5688–5701.

[35] A. Franceschetti, A. Zunger, Pseudopotential calculations of electron and hole addition spectra of InAs , InP , and Si quantum dots, 62 (2000) 2614–2623.

[36] E. Alkhazraji, A.M. Ragheb, M.A. Esmail, Q. Tareq, H. Fathallah, Electro-absorption and Electro-optic Characterization of L-Band InAs / InP Quantum-dash Waveguide, (2020). https://doi.org/10.1109/JPHOT.2020.2988584.

[37] M.D. Tessier, D. Dupont, K. De Nolf, J. De Roo, Z. Hens, Economic and Size-Tunable Synthesis of InP/ZnE (E = S, Se) Colloidal Quantum Dots., Chem. Mater. 27 (2015) 4893–4898. https://doi.org/10.1021/acs.chemmater.5b02138.

[38] A.M. Nightingale, J.C. DeMello, Improving the ensemble optical properties of InP quantum dots by indium precursor modification, J. Mater. Chem. C. 4 (2016) 8454–8458. https://doi.org/10.1039/C6TC02910H.

[39] D. V Talapin, J. Lee, M. V Kovalenko, E. V Shevchenko, Prospects of Colloidal Nanocrystals for Electronic and Optoelectronic Applications, (2010) 389–458.

[40] V.A. Online, L. Lai, L. Protesescu, M. V Kovalenko, M.A. Loi, Sensitized solar cells with colloidal PbS–CdS core–shell quantum dots †, (2014) 736–742. https://doi.org/10.1039/c3cp54145b.

[41] B. Chen, D. Li, F. Wang, InP Quantum Dots : Synthesis and Lighting Applications, 2002454 (2020) 1–20. https://doi.org/10.1002/smll.202002454.

[42] M.A. Ellis, G. Grandinetti, K.M. Fichter, Synthesis of Cd-free InP/ZnS Quantum Dots Suitable for Biomedical Applications, J. Vis. Exp. (2016). https://doi.org/10.3791/53684.

[43] T.-R. Kuo, S.-T. Hung, Y.-T. Lin, T.-L. Chou, M.-C. Kuo, Y.-P. Kuo, C.-C. Chen, Green Synthesis of InP/ZnS Core/Shell Quantum Dots for Application in Heavy-Metal-Free Light-Emitting Diodes, Nanoscale Res. Lett. 12 (2017) 537. https://doi.org/10.1186/s11671-017-2307-2.

[44] L.C. Lines, W. Jiang, Z. Yang, G. Lin, Cytotoxicity of InP / ZnS Quantum Dots With Different Surface Functional Groups Toward Two, 9 (2018) 1–12. https://doi.org/10.3389/fphar.2018.00763.

[45] H. Sengul, COMPARATIVE ASSESSMENT OF PHASE TRANSFER BEHAVIOUR OF INP / ZNS , Environmental Science Nano Comparative assessment of the phase transfer dots and CdSe / ZnS quantum dots under varying, (2019). https://doi.org/10.1039/C8EN01073K.

[46] V. Brunetti, I. Italiano, V. Brunetti, H. Chibli, R. Fiammengo, A. Galeone, M.A. Malvindi, G. Vecchio, R. Cingolani, J.L. Nadeau, P.P. Pompa, InP/ZnS as a safer alternative to CdSe/ZnS core/shell quantum dots: In vitro and in vivo toxicity assessment, (2012). https://doi.org/10.1039/c2nr33024e.

[47] B.J.M. Klostranec, W.C.W. Chan, Quantum Dots in Biological and Biomedical

Research : Recent Progress and Present Challenges, (n.d.). https://doi.org/10.1002/adma.200500786.

[48] H. Chibli, L. Carlini, S. Park, M. Dimitrijevic, J.L. Nadeau, Nanoscale Cytotoxicity of InP / ZnS quantum dots related to reactive oxygen species generation, (2011) 2552–2559. https://doi.org/10.1039/c1nr10131e.

[49] S. Tamang, C. Lincheneau, Y. Hermans, S. Jeong, P. Reiss, Chemistry of InP Nanocrystal Syntheses, Chem. Mater. 28 (2016) 2491–2506. https://doi.org/10.1021/acs.chemmater.5b05044.

[50] M. Green, S olution routes to III – V semiconductor quantum dots q, 6 (2002) 355–363.

[51] J. Jasinski, V.J. Leppert, S. Lam, G.A. Gibson, K. Nauka, C.C. Yang, Z. Zhou, Rapid oxidation of InP nanoparticles in air, 141 (2007) 624–627. https://doi.org/10.1016/j.ssc.2006.12.033.

[52] L. Li, P. Reiss, One-pot Synthesis of Highly Luminescent InP / ZnS Nanocrystals without, (2008) 11588–11589.

[53] G.O. Eren, S. Sadeghi, H. Bahmani Jalali, M. Ritter, M. Han, I. Baylam, R. Melikov, A. Onal, F. Oz, M. Sahin, C.W. Ow-Yang, A. Sennaroglu, R.T. Lechner, S. Nizamoglu, Cadmium-Free and Efficient Type-II InP/ZnO/ZnS Quantum Dots and Their Application for LEDs, ACS Appl. Mater. Interfaces. 13 (2021) 32022–32030. https://doi.org/10.1021/acsami.1c08118.

[54] D. V Talapin, A.L. Rogach, A. Kornowski, M. Haase, H. Weller, Highly Luminescent Monodisperse CdSe and CdSe / ZnS Nanocrystals Synthesized in a Hexadecylamine − Trioctylphosphine Oxide − Trioctylphospine Mixture, (2001).

[55] N. York, Visible Light Induced Hydrogen Production from in Situ Generated Colloidal Rhodium-Coated Cadmium Sulfide in Surfactant Vesicles Clarkson College of Technology Isolation from Pistacia Resins of a Bicyclic Triterpenoid Representing an Apparent Trapped, (2000) 2475–2476.

[56] A. Henglein, Small-Particle Research : Physicochemical Properties of Extremely Small Colloidal Metal and Semiconductor Particles, (1989).

[57] G.M. Wallraff, W.D. Hinsberg, Lithographic Imaging Techniques for the Formation of Nanoscopic Features, (1999).

[58] P.M. Petroff, A. Lorke, A. Imamoglu, E PITAXIALLY S ELF -A SSEMBLED Q UANTUM D OTS, 46 (2020). https://doi.org/10.1063/1.1381102.

[59] B.D. Ingert, M. Pileni, Limitations in Producing Nanocrystals Using Reverse Micelles as Nanoreactors **, 5 (2001) 136–139.

[60] A.P. Alivisatos, Perspectives on the Physical Chemistry of Semiconductor Nanocrystals, 3654 (1996) 13226–13239.

[61] C.B. Murray, D.J. Norris, M.G. Bawendi, Synthesis and Characterization of Nearly Monodisperse CdE (E = S , Se , Te) Semiconductor Nanocrystallites, (1993) 8706–8715.

[62] M. Bayer, E.H. Sargent, Semiconductor quantum dots: Technological progress and future challenges, 8541 (2021). https://doi.org/10.1126/science.aaz8541.

[63] L. Qu, X. Peng, Control of Photoluminescence Properties of CdSe Nanocrystals in Growth, 124 (2018) 2016–2018.

[64] S.G. Hickey, S.F. Wuister, D. Vanmaekelbergh, Single-Step Synthesis to Control the Photoluminescence Quantum Yield and Size Dispersion of CdSe Nanocrystals, (2003) 489–496.

[65] S. Lee, K. Lee, J. Jo, B. Park, Y. Kwon, S. Jang, H. Yang, emitting diode based on InP quantum dot color converters, 4 (2014) 1297–1302. https://doi.org/10.1364/OME.4.001297.

[66] L. Qu, Z.A. Peng, X. Peng, Alternative Routes toward High Quality CdSe Nanocrystals, (2001) 1–5.

[67] C.R. Bullen, P. Mulvaney, Nucleation and Growth Kinetics of CdSe Nanocrystals in Octadecene, (2004).

[68] P. Reiss, G. Quemard, S. Carayon, J. Bleuse, F. Chandezon, A. Pron, Luminescent ZnSe nanocrystals of high color purity, 84 (2004) 10–13. https://doi.org/10.1016/j.matchemphys.2003.11.002.

[69] X. Zhong, Y. Feng, W. Knoll, M. Han, Alloyed Zn x Cd 1 - x S Nanocrystals with Highly Narrow Luminescence Spectral Width, (2003) 13559–13563.

[70] D.W. Lucey, D.J. Macrae, M. Furis, Y. Sahoo, A.N. Cartwright, P.N. Prasad, Monodispersed InP Quantum Dots Prepared by Colloidal Chemistry in a Noncoordinating Solvent, (2005) 3754–3762.

[71] D. Battaglia, X. Peng, Formation of High Quality InP and InAs Nanocrystals in a Noncoordinating Solvent, (2002) 1–4.

[72] J. Jasieniak, C. Bullen, J. Van Embden, P. Mulvaney, Phosphine-Free Synthesis of CdSe Nanocrystals, (2005) 20665–20668.

[73] S. Sapra, A.L. Rogach, J. Feldmann, Phosphine-free synthesis of monodisperse CdSe nanocrystals in olive oil, (2006) 3391–3395. https://doi.org/10.1039/b607022a.

[74] G.G. Yordanov, G.D. Gicheva, B.H. Bochev, C.D. Dushkin, E. Adachi, The effects of temperature and carboxylic acid ligand on the growth of nanocrystalline CdSe in a hot paraffin matrix, 273 (2006) 10–15. https://doi.org/10.1016/j.colsurfa.2005.07.036.

[75] J. Park, J. Joo, S.G. Kwon, Y. Jang, T. Hyeon, Synthesis of Monodisperse Spherical Nanocrystals Angewandte, (2007) 4630–4660. https://doi.org/10.1002/anie.200603148.

[76] R.H. Dinegar, JOURNAL OF THE, 72 (1950).

[77] F. Wang, V.N. Richards, S.P. Shields, W.E. Buhro, Kinetics and Mechanisms of Aggregative Nanocrystal Growth, (2014). https://doi.org/10.1021/cm402139r.

[78] X. Peng, J. Wickham, A.P. Alivisatos, Kinetics of II-VI and III-V Colloidal Semiconductor Nanocrystal Growth : " Focusing " of Size Distributions, 7863 (1998) 5343–5344.

[79] O.I. Micic, C.J. Curtis, K.M. Jones, J.R. Sprague, A.J. Nozik, Synthesis and Characterization of InP Quantum Dots, (1994) 4966–4969.

[80] A.A. Guzelian, J.E.B. Katari, A. V Kadavanich, U. Banin, K. Hamad, E. Juban, A.P.

Alivisatos, R.H. Wolters, C.C. Arnold, J.R. Heath, Synthesis of Size-Selected , Surface-Passivated InP Nanocrystals, (1996) 7212–7219.

[81] O.I. Mic, Synthesis of extremely small InP quantum dots and electronic coupling in their disordered solid films, 4022 (2005). https://doi.org/10.1063/1.1379990.

[82] S. Xu, S. Kumar, T. Nann, Rapid Synthesis of High-Quality InP Nanocrystals, (2006) 1054–1055.

[83] J.A. Gerbec, D. Magana, A. Washington, G.F. Strouse, Microwave-Enhanced Reaction Rates for Nanoparticle Synthesis, (2005) 15791–15800.

[84] D.D. Lovingood, G.F. Strouse, Microwave Induced In-Situ Active Ion Etching of Growing InP Nanocrystals, (2008) 4–7.

[85] C. Li, M. Ando, N.M. Ã, Facile Preparation of Highly Luminescent InP Nanocrystals by a Solvothermal Route, 37 (2008) 856–857. https://doi.org/10.1246/cl.2008.856.

[86] W.S.H. Lee, J. Chul, Amine-derived synthetic approach to color-tunable InP / ZnS quantum dots with high fluorescent qualities, (2013). https://doi.org/10.1007/s11051-013-1750-y.

[87] W. Song, S. Lee, H. Yang, Fabrication of warm , high CRI white LED using non-cadmium quantum dots, 3 (2013) 1468–1473. https://doi.org/10.1364/OME.3.001468.

[88] O.I. Micié, J.R. Sprague, C.J. Curtis, K.M. Jones, J.L. Machol, A.J. Nozik, H. Giessen, B. Fluegel, G. Mohs, N. Peyghambarian, Synthesis and Characterization of InP , GaP , and GalnPi Quantum Dots, (1995) 7754–7759.

[89] O.B. Achorn, D. Franke, M.G. Bawendi, Seedless Continuous Injection Synthesis of Indium Phosphide Quantum Dots as a Route to Large Size and Low Size Dispersity, Chem. Mater. 32 (2020) 6532–6539. https://doi.org/10.1021/acs.chemmater.0c01906.

[90] S. Mahajan, M. Rani, R.B. Dubey, J. Mahajan, SYNTHESIS OF CdSe CRYSTAL USING HOT INJECTION METHOD, Int. J. Latest Res. Sci. Technol. 2 (2013) 518–521.

[91] J. Ministro, A study on the synthesis and the optical properties of InP-based quantum dots, University Gent, n.d.

[92] S.B. Brichkin, Synthesis and properties of colloidal indium phosphide quantum dots, Colloid J. 77 (2015) 393–403. https://doi.org/10.1134/S1061933X15040043.

[93] E.S. Cde, J. Te, A.C. Soc, Murray, C.B., Norris, D.J. & Bawendi, M.G. Synthesis and characterization of nearly monodisperse CdE (E = S, Se, Te) semiconductor nanocrystallites. J. Am. Chem. Soc. 115, 8706 − 871..., (2021). https://doi.org/10.1021/ja00072a025.

[94] X. Peng, L. Manna, W. Yang, J. Wickham, Shape control of CdSe nanocrystals, 404 (2000) 59–61.

[95] L. Manna, E.C. Scher, A.P. Alivisatos, R. V August, Synthesis of Soluble and Processable Rod- , Arrow- , Teardrop- , and Tetrapod-Shaped CdSe Nanocrystals, (2000) 12700–12706.

[96] V.F. Puntes, D. Zanchet, C.K. Erdonmez, A.P. Alivisatos, Synthesis of hcp-Co Nanodisks, (2002) 12874–12880.

[97] S. Ithurria, B. Dubertret, Quasi 2D Colloidal CdSe Platelets with Thicknesses Controlled at the Atomic Level, (2008) 16504–16505.

[98] H. Qian, L. Li, J. Ren, One-step and rapid synthesis of high quality alloyed quantum dots (CdSe – CdS) in aqueous phase by microwave irradiation with controllable temperature, 40 (2005) 1726–1736. https://doi.org/10.1016/j.materresbull.2005.05.022.

[99] P. Ramasamy, B. Kim, M.-S. Lee, J.-S. Lee, Beneficial effects of water in the colloidal synthesis of InP/ZnS core–shell quantum dots for optoelectronic applications, Nanoscale. 8 (2016) 17159–17168. https://doi.org/10.1039/C6NR04713K.

[100] W.A.C. Hen, W.E.W. Ang, L.E.I.S. Un, S.H.C. Hen, Q.U.N.Y. An, T.A.G. Uo, X.I.Z. Hou, C. Haoxing, Y.O.Z. Hang, Synthesis and characterization of InP / ZnSe / ZnS quantum dots for photo-emissive color conversion, 12 (2022) 1717–1730.

[101] A.J. Zavaraki, Q. Liu, H. Ågren, Nano-Structures & Nano-Objects Solar cell sensitized with ‘“ green ”’ InP-ZnS quantum dots : Effect of ZnS shell deposition, Nano-Structures & Nano-Objects. 22 (2020) 100461. https://doi.org/10.1016/j.nanoso.2020.100461.

[102] S.T. Quenching, Suppressed Thermal Quenching, (2021).

[103] N. Mordvinova, A. Vinokurov, T. Kuznetsova, O.I. Lebedev, S. Dorofeev, Highly luminescent core-shell InP/ZnX (X = S, Se) quantum dots prepared: Via a phosphine synthetic route, Dalt. Trans. 46 (2017) 1297–1303. https://doi.org/10.1039/c6dt03956a.

[104] M. Jiang, Y. Li, S. Li, H. Zhou, X. Cao, S. Bao, Y. Gao, H. Luo, P. Jin, Room Temperature Optical Constants and Band Gap Evolution of Phase Pure M 1 -VO 2 Thin Films Deposited at Different Oxygen Partial Pressures by Reactive Magnetron Sputtering, J. Nanomater. 2014 (2014) 1–6. https://doi.org/10.1155/2014/183954.

[105] A. Bouzidi, N. Benramdane, A. Nakrela, C. Mathieu, B. Khelifa, R. Desfeux, A. Da Costa, First synthesis of vanadium oxide thin films by spray pyrolysis technique, Mater. Sci. Eng. B. 95 (2002) 141–147. https://doi.org/10.1016/S0921-5107(02)00224-6.

[106] B. Lambert, B. Deveaud, Y. Toudic, G. Pelous, J.C. Paris, G. Grandpierre, Properties of vanadium in InP, Solid State Commun. 47 (1983) 337–340. https://doi.org/10.1016/0038-1098(83)90914-6.

[107] C. Lamsal, N.M. Ravindra, Optical properties of vanadium oxides-an analysis, J. Mater. Sci. 48 (2013) 6341–6351. https://doi.org/10.1007/s10853-013-7433-3.

[108] D. Collection, Modeling Radiation Effects on a Triple Junction Solar Cell using Silvaco ATLAS NAVAL POSTGRADUATE, (2012).

[109] P. Cedex, SPECTROSCOPIC INVESTIGATION OF VANADIUM IN lnP B. CLERJAUD, D. COTE and C. NAUD, 83 (1987) 194–197.

[110] J.C. Paris, PROPERTIES OF V A N A D I U M IN InP I +, 47 (1983) 337–340.

[111] M.A. Shafi, H. Ullah, S. Ullah, L. Khan, S. Bibi, B.M. Soucase, Numerical Simulation of Lead-Free Sn-Based Perovskite Solar Cell by Using SCAPS-1D †, (2022) 1–5.

[112] J.A. Dias, S.H. Santagneli, S.J.L. Ribeiro, Y. Messaddeq, Perovskite Quantum Dot Solar Cells : An Overview of the Current Advances and Future Perspectives, 2100205 (2021) 1–28. https://doi.org/10.1002/solr.202100205.

[113] W. Zhang, S. Ding, W. Zhuang, D. Wu, P. Liu, X. Qu, H. Liu, H. Yang, Z. Wu, K. Wang, X.W. Sun, InP / ZnS / ZnS Core / Shell Blue Quantum Dots for Efficient Light-Emitting Diodes, (n.d.). https://doi.org/10.1002/adfm.202005303.

[114] H.I. Ikeri, A.I. Onyia, P.U. Asogwa, Investigation Of Optical Characteristics Of Semiconductor Quantum Dots For Multi Junction Solar Cells Applications ., 8 (2019) 3531–3535.

[115] A.M. Smith, S. Nie, Semiconductor Nanocrystals : Structure , Properties , and Band Gap Engineering, (2010).

[116] P. Reiss, S. Carayon, J. Bleuse, A. Pron, Low polydispersity core / shell nanocrystals of CdSe / ZnSe and CdSe / ZnSe / ZnS type : preparation and optical studies, 139 (2003) 649–652. https://doi.org/10.1016/S0379-6779(03)00335-7.

[117] M. Ando, M. Horie, Y. Akazawa-ogawa, Y. Hagihara, N. Murase, Y. Shigeri, Cytotoxicity of CdSe-based quantum dots incorporated in glass nanoparticles evaluated using human keratinocyte HaCaT cells, Biosci. Biotechnol. Biochem. 8451 (2016) 1–4. https://doi.org/10.1080/09168451.2015.1069702.

[118] A. Ghicov, P. Schmuki, Self-ordering electrochemistry : a review on growth and functionality of TiO 2 nanotubes and other self-aligned MO x structures, (2009) 2791–2808. https://doi.org/10.1039/b822726h.

[119] H.E. Prakasam, K. Shankar, M. Paulose, O.K. Varghese, C.A. Grimes, ARTICLES A New Benchmark for TiO 2 Nanotube Array Growth by Anodization, (2007) 7235–7241.

[120] V. Zwilling, M. Aucouturier, E. Darque-ceretti, Anodic oxidation of titanium and TA6V alloy in chromic media . An electrochemical approach, 45 (1999) 921–929.

[121] S. Kobayashi, K. Hanabusa, Preparation of TiO 2 Hollow-Fibers Using Supramolecular Assemblies Seiji Shinkai Porous , nanostructured materials have attracted considerable attention because of their potential ap- materials is quite difficult . Nanostructured inorganic cationic charge moieties with the expectation that the, (2000) 1523–1525.

[122] J.M. Macak, H. Tsuchiya, A. Ghicov, K. Yasuda, R. Hahn, S. Bauer, P. Schmuki, TiO 2 nanotubes : Self-organized electrochemical formation , properties and applications, 11 (2007) 3–18. https://doi.org/10.1016/j.cossms.2007.08.004.

[123] C. Ruan, M. Paulose, O.K. Varghese, G.K. Mor, C.A. Grimes, Fabrication of Highly Ordered TiO 2 Nanotube Arrays Using an Organic Electrolyte, (2005) 15754–15759.

[124] K. Lee, A. Mazare, P. Schmuki, One-Dimensional Titanium Dioxide Nanomaterials : Nanotubes, (2014).

[125] V. Shrotriya, G. Li, Y. Yao, C. Chu, Y. Yang, Transition metal oxides as the buffer layer for polymer photovoltaic cells Transition metal oxides as the buffer layer for polymer photovoltaic cells, (2006) 1–4. https://doi.org/10.1063/1.2174093.

[126] O. Karatum, M.M. Aria, G.O. Eren, E. Yildiz, E.D. Glowacki, Nanoengineering InP Quantum Dot-Based Photoactive Biointerfaces for Optical Control of Neurons, 15 (2021) 1–14. https://doi.org/10.3389/fnins.2021.652608.

[127] A. Zaban, O.I. Mic, B.A. Gregg, A.J. Nozik, Photosensitization of Nanoporous TiO 2 Electrodes with InP Quantum Dots, 7463 (1998) 3153–3156.

[128] H.B. Jalali, M.M. Aria, U.M. Dikbas, S. Sadeghi, E ff ective Neural Photostimulation Using Indium-Based Type-II Quantum Dots, (2018). https://doi.org/10.1021/acsnano.8b02976.

[129] H. Zhao, X. Li, M. Cai, C. Liu, Y. You, R. Wang, A.I. Channa, F. Lin, D. Huo, G. Xu, X. Tong, Z.M. Wang, Role of Copper Doping in Heavy Metal-Free InP / ZnSe Core / Shell Quantum Dots for Highly Efficient and Stable Photoelectrochemical Cell, 2101230 (2021) 1–10. https://doi.org/10.1002/aenm.202101230.

[130] M.T. Clarke, F.N. Viscomi, T.W. Chamberlain, N. Hondow, A.M. Adawi, J. Sturge, S.C. Erwin, J.-S.G. Bouillard, S. Tamang, G.J. Stasiuk, Synthesis of super bright indium phosphide colloidal quantum dots through thermal diffusion, Commun. Chem. 2 (2019) 36. https://doi.org/10.1038/s42004-019-0138-z.

[131] T.K. Nideep, M. Ramya, M.M. Varier, M. Kailasnath, A Study of Nonlinear Optical Property of Cadmium Based Quantum Dots with Comparable Particle Size, Springer Singapore, n.d. https://doi.org/10.1007/978-981-15-9259-1.

[132] S. Kobayashi, N. Hamasaki, M. Suzuki, M. Kimura, H. Shirai, K. Hanabusa, Preparation of Helical Transition-Metal Oxide Tubes Using Organogelators as Structure-Directing Agents, 1 (2002) 6550–6551.

[133] Z. Miao, D. Xu, J. Ouyang, G. Guo, X. Zhao, Electrochemically Induced Sol − Gel Preparation of Single-Crystalline TiO 2 Nanowires, (2002).

[134] Enhancement of photocatalytic and photoelectrochemical properties of TiO2 nanotubes sensitized by SILAR - Deposited PbS nanoparticles _ Elsevier Enhanced Reader.pdf, (n.d.).

[135] J.M. Macak, S.P. Albu, P. Schmuki, Towards ideal hexagonal self-ordering of TiO 2 nanotubes pss, 183 (2007) 181–183. https://doi.org/10.1002/pssr.200701148.

[136] P. V Kamat, Quantum Dot Solar Cells . The Next Big Thing in Photovoltaics, (2013).

[137] M. Antoniadou, D.I. Kondarides, D.D. Dionysiou, P. Lianos, Quantum Dot Sensitized Titania Applicable as Photoanode in Photoactivated Fuel Cells, (2012).

[138] M.P. Genovese, I. V Lightcap, P. V Kamat, Sun-Believable Solar Paint . A Transformative One-Step Approach for Designing Nanocrystalline Solar Cells, (2012) 865–872.

[139] S. Park, T. Ikegami, K. Ebihara, Effects of substrate temperature on the properties of Ga-doped ZnO by pulsed laser deposition, 513 (2006) 90–94. https://doi.org/10.1016/j.tsf.2006.01.051.

[140] J. Verschraegen, M. Burgelman, Numerical modeling of intra-band tunneling for heterojunction solar cells in SCAPS, 515 (2007) 6276–6279. https://doi.org/10.1016/j.tsf.2006.12.049.

[141] P.E. Imoisili, T. Jen, Numerical Analysis and Performance improvement of Nanostructured Cu 2 O / TiO 2 pn heterojunction Solar Cells using SCAPS, (n.d.).

[142] M. Al-hattab, L. Moudou, M. Khenfouch, O. Bajjou, Numerical simulation of a new heterostructure CIGS / GaSe solar cell system using SCAPS-1D software, Sol. Energy. 227 (2021) 13–22. https://doi.org/10.1016/j.solener.2021.08.084.

[143] M.M.T. Al, Z.S. Yasin, Optoelectronics Simulation of CIGS - Based Solar Cells Using

a Cd - Free Nontoxic - ZrS x Se 2 − x as a Novel Buffer Layer, Brazilian J. Phys. (2022) 1–10. https://doi.org/10.1007/s13538-022-01146-z.

[144] U. Mandadapu, S.V. Vedanayakam, K. Thyagarajan, Numerical Simulation of Ch 3 Nh 3 PbI 3-X Cl x Perovskite solar cell using SCAPS-1D, (2017) 40–45.

[145] P. Ieee, P. Specialists, C. Washington, A. Niemegeers, M. Burgelman, MODELLING OF ac-CHARACTERISTICS SOLAR CELLS, (1996) 901–904.

[146] M. Burgelman, P. Nollet, S. Degrave, Modelling polycrystalline semiconductor solar cells, 362 (2000) 527–532.

[147] M. Mostefaoui, H. Mazari, S. Khelifi, A. Bouraiou, R. Dabou, Simulation of High Efficiency CIGS solar cells with SCAPS-1D software, Energy Procedia. 74 (2015) 736–744. https://doi.org/10.1016/j.egypro.2015.07.809.

[148] U. Holzwarth, N. Gibson, The Scherrer equation versus the "Debye-Scherrer equation," Nat. Nanotechnol. 6 (2011) 534–534. https://doi.org/10.1038/nnano.2011.145.

[149] O. Ehlert, A. Tiwari, T. Nann, Quantum confinement of the thermodynamic functions for the formation of electrons and holes in CdSe nanocrystals, J. Appl. Phys. 100 (2006) 1–6. https://doi.org/10.1063/1.2356607.

[150] M. Singh, M. Goyal, K. Devlal, Size and shape effects on the band gap of semiconductor compound nanomaterials, J. Taibah Univ. Sci. 12 (2018) 470–475. https://doi.org/10.1080/16583655.2018.1473946.

[151] M. Asemi, A. Suddar, M. Ghanaatshoar, Increasing the specific surface area of Cr-doped - nanoparticles by controlling the drying time for DSSC applications, J. Mater. Sci. Mater. Electron. 28 (2017) 15233–15238. https://doi.org/10.1007/s10854-017-7401-9.

[152] C. Ippen, T. Greco, A. Wedel, InP/ZnSe/ZnS: A Novel Multishell System for InP Quantum Dots for Improved Luminescence Efficiency and Its application in a Light-Emitting Device, J. Inf. Disp. 13 (2012) 91–95. https://doi.org/10.1080/15980316.2012.683537.

[153] E. Ryu, S. Kim, E. Jang, S. Jun, H. Jang, B. Kim, S. Kim, Communications, 21 (2009) 2425–2427.

[154] O.I. Mic, Synthesis of extremely small InP quantum dots and electronic coupling in their disordered solid films, 4022 (2005). https://doi.org/10.1063/1.1379990.

[155] S.J. Yang, J.H. Oh, S. Kim, H. Yang, Y.R. Do, Realization of InP / ZnS quantum dots for green , amber and red down-converted LEDs and their, (2015) 3582–3591. https://doi.org/10.1039/c5tc00028a.

[156] S. Xu, J. Ziegler, T. Nann, Rapid synthesis of highly luminescent InP and InP / ZnS nanocrystals †, (2008) 2653–2656. https://doi.org/10.1039/b803263g.

[157] K. Yong, H. Ding, I. Roy, W. Law, E.J. Bergey, A. Maitra, P.N. Prasad, Imaging Pancreatic Cancer Using Bioconjugated InP Quantum Dots, 3 (n.d.).

[158] S. Fung, B. Yang, C.K. Ng, M.K. Fung, C.C. Ling, A.B. Djuriˇ, Annealing study of titanium oxide nanotube arrays, 130 (2011) 1227–1231. https://doi.org/10.1016/j.matchemphys.2011.08.063.

[159] T.S. Bhat, A.D. Sheikh, N.L. Tarwal, S.D. Korade, C.K. Hong, J.H. Kim, ZnS passivated PbSe sensitized TiO 2 nanorod arrays to suppress photocorrosion in photoelectrochemical solar cells, Mater. Today Commun. 16 (2018) 186–193. https://doi.org/10.1016/j.mtcomm.2018.06.008.

[160] N. Simulation, P. For, Modeling Thin-film PV Devices, 153 (2004) 143–153. https://doi.org/10.1002/pip.524.

[161] S.K. M, S.P. Madhusudanan, A.R. Rajamani, M. Siaj, S.K. Batabyal, Barium Substitution in Kesterite Cu 2 ZnSnS 4 : Cu 2 Zn 1 − x Ba x SnS 4 Quinary Alloy Thin Films for E ffi cient Solar Energy Harvesting, (2020) 4–11. https://doi.org/10.1021/acs.cgd.0c00150.

[162] M. Jamil, A. Ali, K. Mahmood, M.I. Arshad, S. Tahir, M. Ajaz un Nabi, S. Ikram, N. Amin, S. Hussain, Numerical simulation of perovskite/Cu2Zn(Sn1-x Gex)S4 interface to enhance the efficiency by valence band offset engineering, J. Alloys Compd. 821 (2020) 153221. https://doi.org/10.1016/j.jallcom.2019.153221.

[163] Y. Raoui, H. Ez-Zahraouy, N. Tahiri, O. El Bounagui, S. Ahmad, S. Kazim, Performance analysis of MAPbI3 based perovskite solar cells employing diverse charge selective contacts: Simulation study, Sol. Energy. 193 (2019) 948–955. https://doi.org/10.1016/j.solener.2019.10.009.

[164] Chenming C. Hu, Modern Semiconductor Devices for Integrated Circuits, in: 2010.

[165] F. Baig, Y.H. Khattak, S. Ullah, B.M. Soucase, S. Beg, H. Ullah, Numerical analysis a guide to improve the efficiency of experimentally designed solar cell, Appl. Phys. A. 124 (2018) 471. https://doi.org/10.1007/s00339-018-1877-x.

[166] R. Toufanian, A. Piryatinski, A.H. Mahler, R. Iyer, J.A. Hollingsworth, A.M. Dennis, Bandgap Engineering of Indium Phosphide-Based Core/Shell Heterostructures Through Shell Composition and Thickness, Front. Chem. 6 (2018). https://doi.org/10.3389/fchem.2018.00567.

[167] V. Raj, F. Rougieux, L. Fu, H.H. Tan, C. Jagadish, Design of Ultrathin InP Solar Cell Using Carrier Selective Contacts, IEEE J. Photovoltaics. 10 (2020) 1657–1666. https://doi.org/10.1109/JPHOTOV.2019.2961615.

CHAPTER III

InP Quantum Dots synthesis : photoluminescence enhancement strategies

Introduction

In this chapter, we bring together the different results of analyzes and characterizations carried out on the Indium Phosphide Quantum Dots (InP) QDs prepared by hot injection method.

In the first part, we will present the first approach used to improve the photoluminescence of InP Quantum Dots described in chapter 2. It consists principally of doping InP QDs with Vanadium elements to enhance its optical properties, especially the photoluminescence properties.

In the second part, we will discuss the effect of introducing the ZnS on single-shell and double-shell as a second strategy to enhance the photoluminescence of InP QDs and decrease the surface defects effectively.

To find out more, a physical characterization is carried out through UV-visible absorbance and photoluminescence measurements. Then, to confirm the crystal structure of the synthesized Quantum Dots, XRD analysis has been used. The Transmission Electron Microscopy coupled to Energy Dispersive Spectrometry (TEM-EDS) has been used to determine the shape and the size.

The different results obtained will be presented in more detail below.

1 Effect of Vanadium doping on InP QDs

1.1 Study of structural properties: X-ray diffraction (XRD)

The crystallinity analysis of InP QDs and InP QDs doped with Vanadium (InP:V) was carried out by XRD in the 20 - 60° scan range, as shown in Figure 3-1. The XRD patterns of the InP:V with different Vanadium doping concentrations present the same spectrum, hence just one will be presented.

The X-Ray diffractograms show three strong peaks at 25.66±0.2°, 43.73±0.2° and 51.77±0°. These three strong peaks can be easily indexed to the cubic zinc blend structure of InP (in accordance with JCPDS No.73-1983).

After the doping of Vanadium, we note that the XRD patterns of InP:V QDs are analogous to XRD patterns of pure InP QDs with the presence of a high crystallinity of these nanoparticles. Moreover, there's no shift when the atom of Vanadium replaces the atom of Indium because of their similar ionic radius.

The Debye–Scherrer formula has been employed to calculate the average crystallite size D [148]:

$$D = \frac{0.9\lambda}{B\cos\theta_B}$$

Where, θ_B is referred to the maximum of Bragg diffraction peak, λ denotes the x-ray wavelength and the full width at half maximum (FWHM) of diffracted peaks is named by B.

Scherrer's formula was applied to the main peak (111), therefore, the size of the QD InP nanoparticles is approximated to be 7nm.

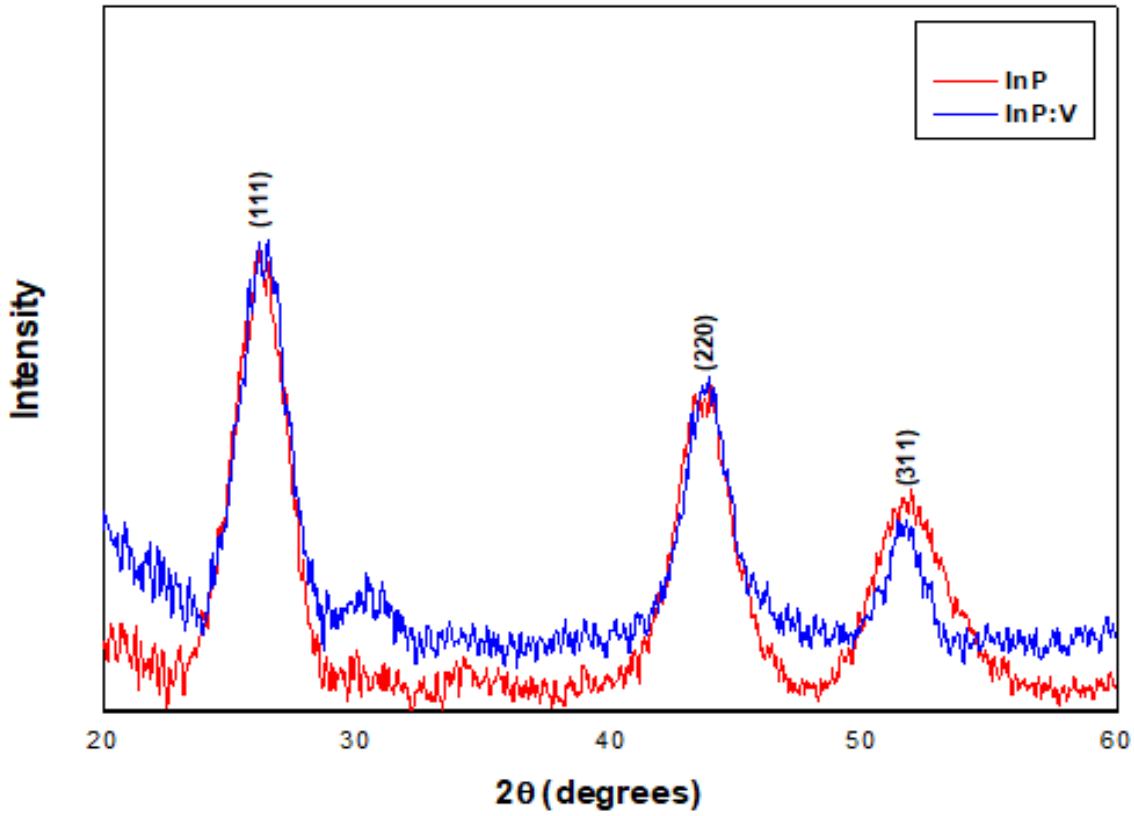

Figure 3-1: X-ray diffractogram of core InP QDs, InP doped with Vanadium synthesized by hot injection method.

1.2 Study of morphological properties

To characterize the morphology of InP QDs doped with vanadium in different concentration, we used Transmission Electron Microscopy (TEM). Figure 3-2 shows TEM images of these samples. The nanoparticle sizes of undoped InP QDs and doped InP QDs through Vanadium together with two different concentrations (5% and 10%) are decreased. The size distribution histogram which was demonstrated an average size from 10 nm to 4.50 nm and 3.6 nm. Hence, we observed that the doping element had a clear effect on the size of InP QDs. Yet, over the years, the morphological features of Vanadium doped in InP (InP:V) QDs have never been investigated. Based on this analysis, it seems that InP QDs and InP:V QDs with

spherical-shaped are very well dispersed . Moreover, the Vanadium concentration rises, while the grain size decreases.

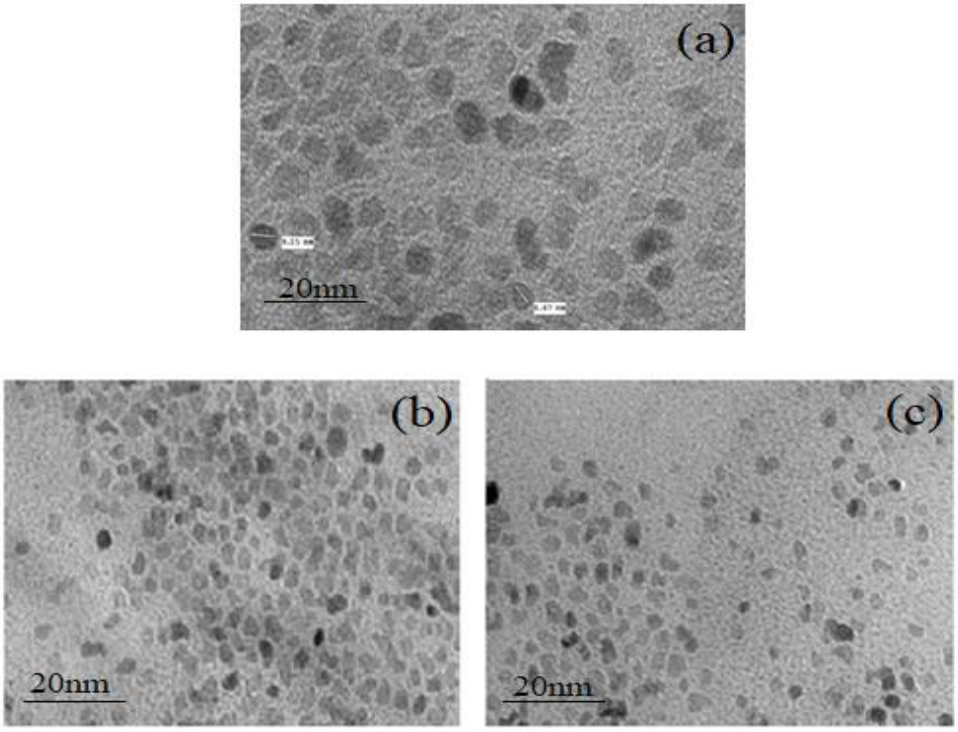

Figure 3-2: TEM image of quantum dot a) Monodisperse InP QDs. b) Monodisperse InP:V5% QDs. C) Monodisperse InP:V 10%QDs.

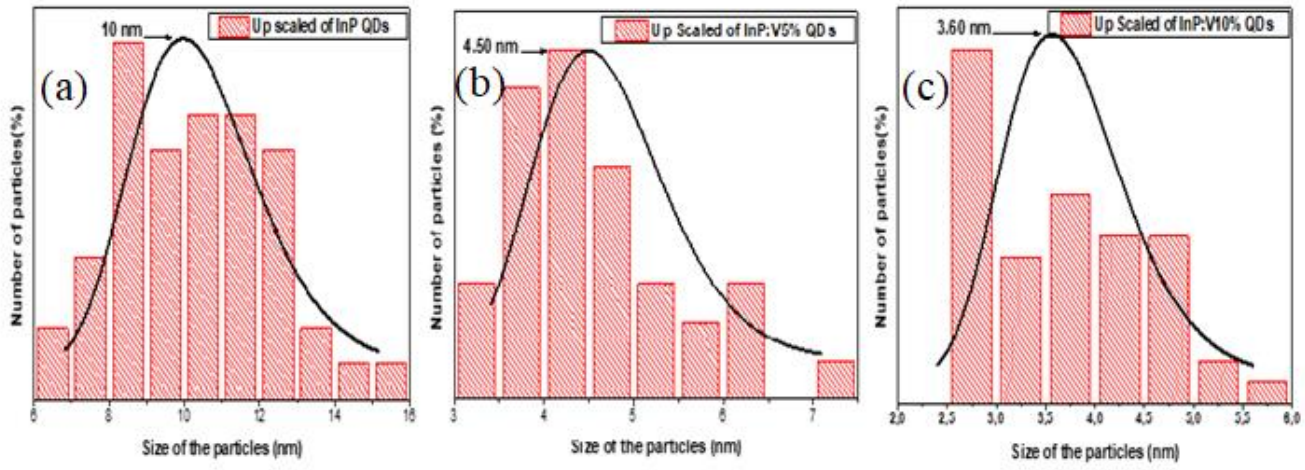

Figure 3-3: Distribution histograms of QDs. a) Size distribution of InP QDs. b) Size distribution of InP:V5% QDs. c) Size distribution of InP:V10% QDs.

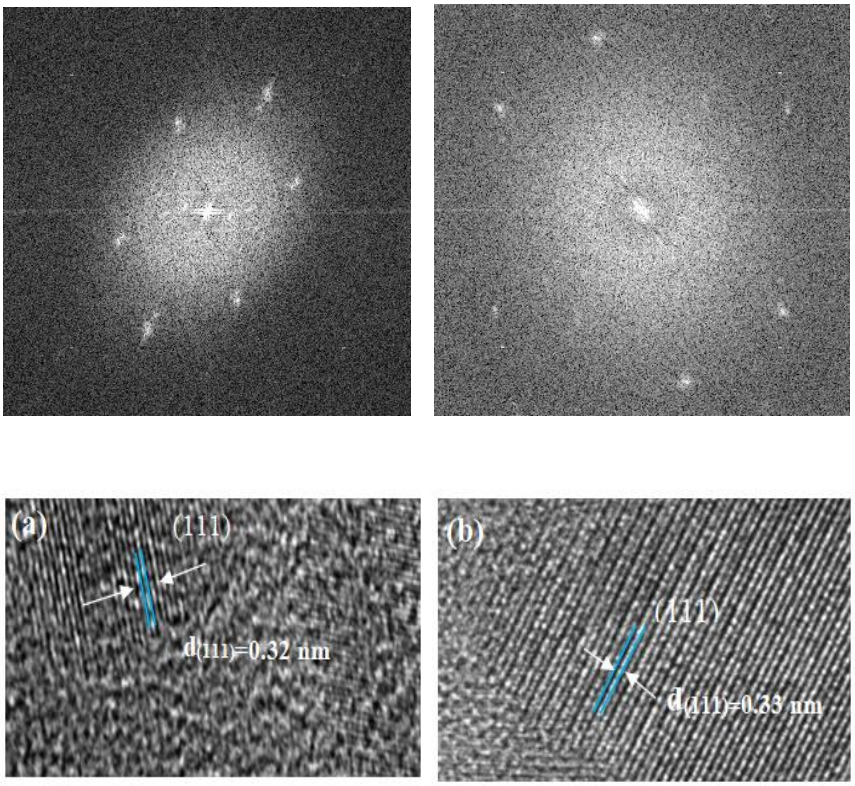

Figure 3-4: a) HRTEM micrograph showing lattice fringes of InP. b) HRTEM micrograph showing lattice fringes of InP:V QDs.

Afterward, the supplemental electron diffraction and the lattice planes can be obviously discerned in Figure 3-4 where the lattice planes of the suspension Quantum Dot obtained have an identical orientation and space with the plane (111). It means that the indices of crystallographic planes (111) are identified by using the distance between the reflection spots and the InP QDs material parameters. Moreover, Figure 3-4 confirms that the pure InP QDs and InP:V QDs each one has the same cubic and monocrystal structure. These data were deduced according to the lattice parameter and d -spacing of (111) which is corresponded to the XRD analysis results.

The distance between the planes of the InP QDs fringes has equaled to 0.32 nm, which is schematically illustrated in Figure 3-2 by the TEM image. This is associated to the (111) plane of the cubic crystals structure of InP QDs, InP:V 5% and InP:V 10% with a lattice fringe distance 0.33 nm.

1.3 Study of optical properties

1.3.1 Study of the doping vanadium effect on InP QDs photoluminescence

Photoluminescence (PL) measurement are carried out to estimate the influence of Vanadium on the optical properties of InP Quantum Dots. Figure 3-5. displays the photoluminescence (PL) spectrum of InP QDs green line and of InP:V QDs with different concentration respectively 5% (red line) and 10% (blue line). The spectra show that the InP QDs have a pronounced a strong emission bands wavelength photoluminescence peak at 630 nm with narrow emission FWHM value 63 nm at room temperature, so, this result proved the good

crystal quality of the InP QDs suspension. Hence the confinement effects of PL InP QDs green line have been detected.

On the other hand, the PL spectra of InP QDs doped by Vanadium with different doping concentrations displays two peaks. One peak located at 495 nm with an FWHM values 82 nm corresponds to the InP:V 5% and the other peak of InP:V 10% appeared at 498 nm with narrow emission and an FWHM values 82 nm. This line corresponds band-to-band radiative transitions. This size-reliance is a result of the quantum size effect active on the InP QDs. So, it was clearly that the photoluminescence decreases with the increase of the concentration of doping element. Therefore, these result presents the poor effect of Vanadium doping on InP photoluminescence.

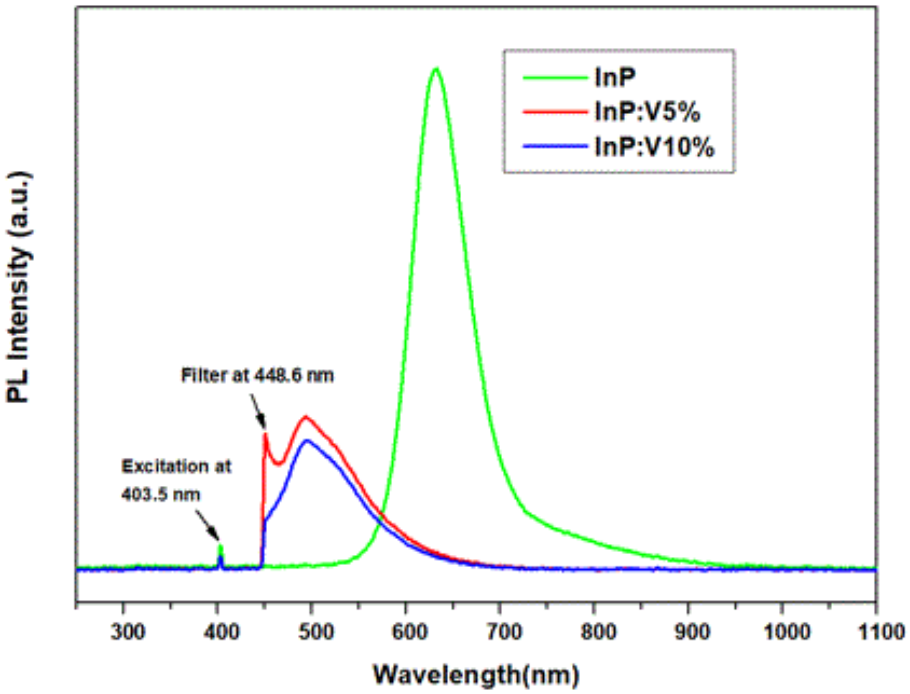

Figure 3-5: PL spectra of InP QDs and InP:V QDs .

The formation of InP:V QDs was identified from a gradual dark coloration in the reaction mixture and also in a decrease of absorbance in the UV-Vis. The comparison was exemplified

between the InP QDs and InP:V QDs in the position peak with the increase of the concentration of the dopant element. Therefore, the blue shift in the measured spectrum is due to the increased band gap. Usually, the band gap and the particle size were allied owing to the quantum confinement effect.

Hence, a substantially broader and weaker emission bands wavelength is observed. Noting that the band-tailing (Urbach tails) gives rise to this shift. However, the structures need more improvements to have good optical properties in the future research. We conclude the highest concentration of InP QDs doped with Vanadium was the lower the PL intensity (green line), so we speak in this doping the poor photoluminescence efficiency.

1.3.2 Study of redispersion method on InP QDs photoluminescence

To study the effect of the redispersion of nanoparticles on the photoluminescence; three cycles of washing and redispersion with Dichloromethane solvent via centrifuge using different speed respectively at 2000 rpm at10 min, 1000 rpm at 10 min and 3000 rpm at 5 min redispersion the InP Quantum Dots us shown in Figure 3-6.

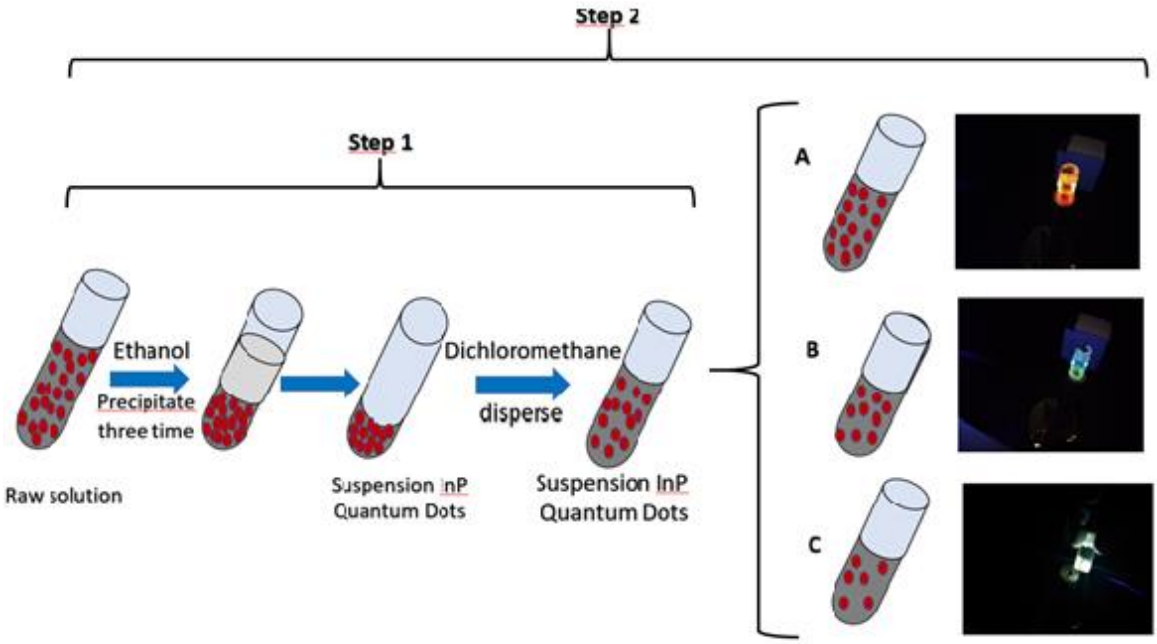

Figure 3-6: scheme of purification and redispersion process for InP QDs.

So, a clear dispersion of InP QDs was observed in Figure 3-6 by Transmission Electron Microscopy (TEM) image. Therefore, as seen in figure 3-7, a blue shift of photoluminescence spectrum as demonstrated in Table 3-1 caused by the resuspension procedure between the solution A, B and C with reference to the result in TEM as shown in Figure 3.8. Hence, during the process of redispersion of Quantum Dot we observed the solubility of agglomerated nanoparticles. As seen in Figure 3-9, the nanoparticle sizes of InP QDs are decreased with an average diameter from 10 nm to 7.71 nm, 5.62 nm and 4.75 nm in the dispersion solution A, B and C respectively.

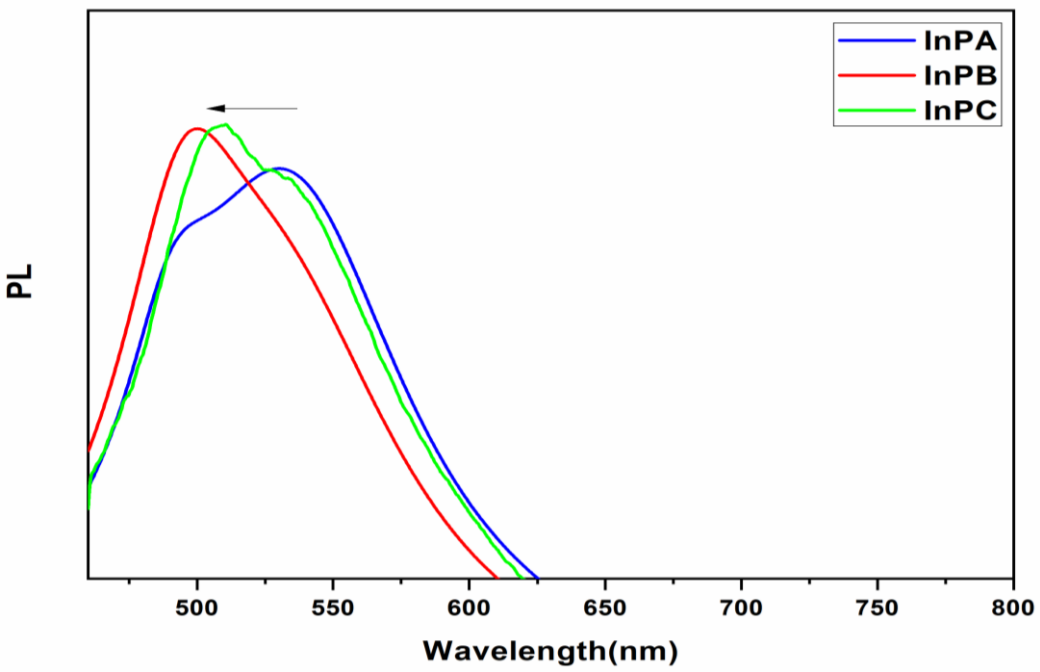

Figure 3-7: PL fit spectra of InP QDs after the redispersion.

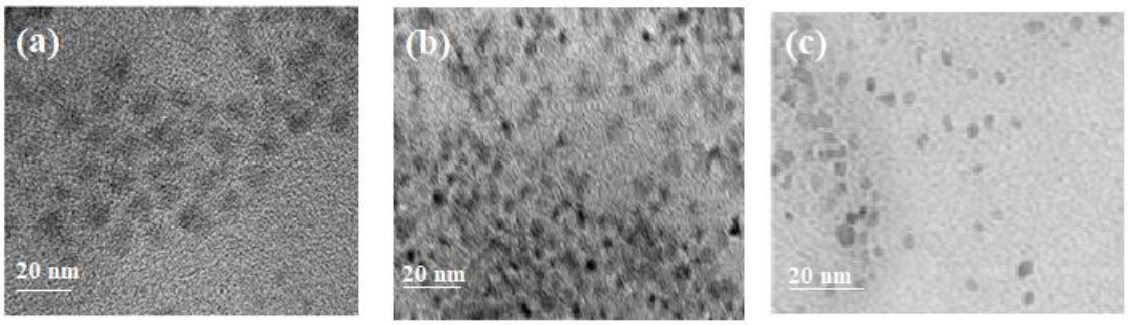

Figure 3-8: TEM image of InP QDs with redispersion process.

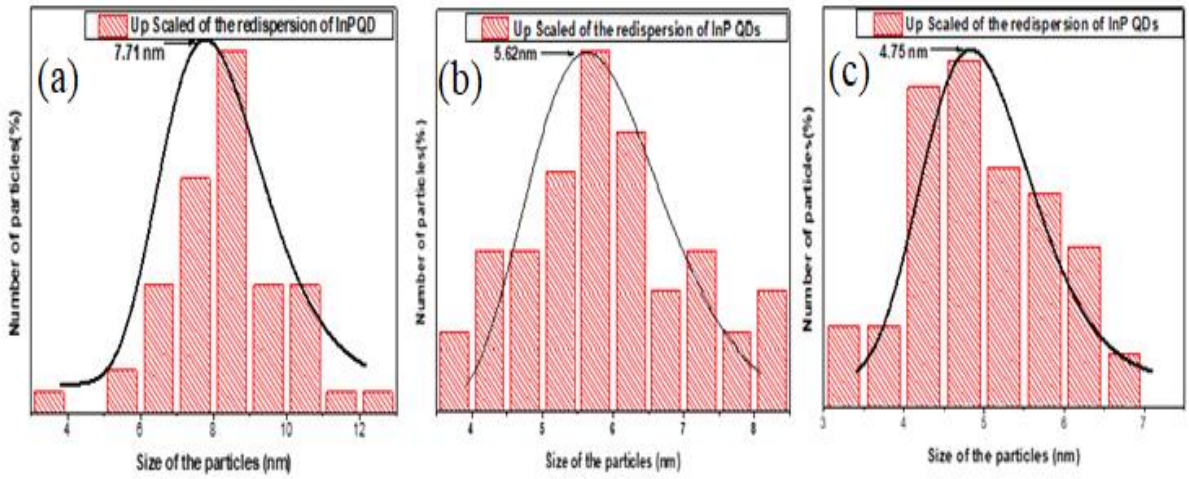

Figure 3-9: The size distribution histograms of QDs. a) Size distribution of the redispersion of InP QDs (solution A). b) Size distribution of the redispersion of InP QDs (solution B). c) Size distribution of the redispersion of InP QDs (solution C).

Table 3-1:Result of PL Fit of InP QD and InP doped with Vanadium varying from 5% to 10%.

	Peak 1 Position (nm)	Peak 2 Position (nm)	FWHM		I1	I2	I1/I2
InP	630		63		10310	2800	0.98
InP A	490	533	Peak 1 40	Peak 2 109	2754		
InP B	491	528	55	113	5935	7099	0.83
InP C	502	525	27	100	1486	6478	0.22
InP:V 5%	495	-	82		2661	-	-
InP:V10%	498	-	82		2661	-	-

1.3.3 Study of the doping vanadium effect on InP QDs absorption properties

Figure 3-10 presents the absorption peak of InP QDs (blue line) which was situated at 868 *nm* at room temperature. On other side to investigate the effects of dopant element and to compare it with the result of the optical properties of InP QDs, so one absorption peak was located at 585 *nm* of InP:V 5% QDs (red line) and for the other InP:V 10% QDs was sited at 666 *nm* (green line).We observed that the impact of vanadium on pure InP QDs has been

detected, which the absorption spectrum has been blue shifted to weaker wavelengths from 868 to 585 *nm*. This result showing the presence of the particles in the quantum regime. Previous various researchers have demonstrated that the absorption spectra dependent on the particle size distribution[149]. Hence, in this study the remarkable decrease in absorbance is proved by the quantum confinement effect.

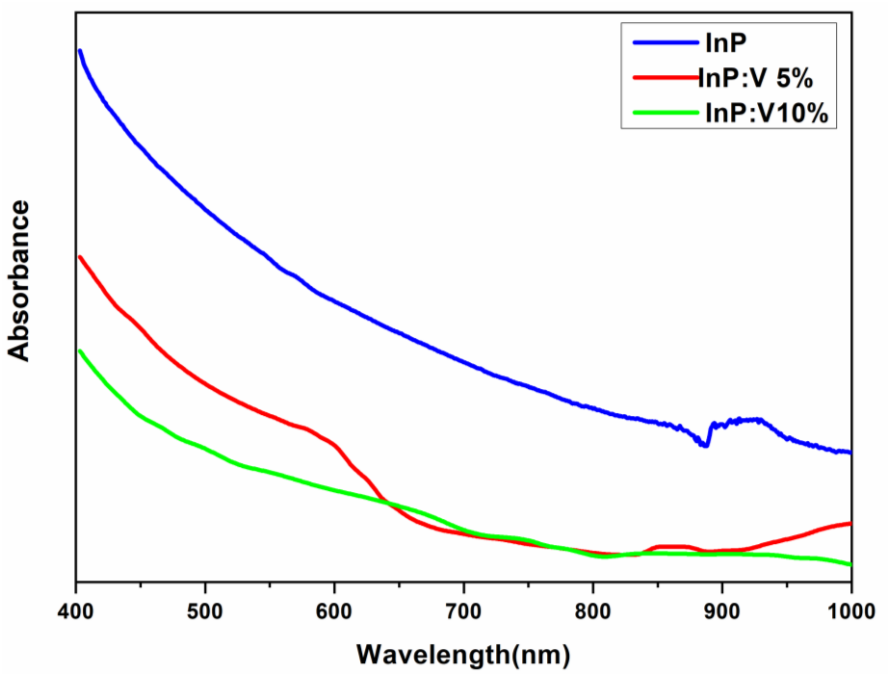

Figure 3-10: UV−vis spectra of InP QDs and InP: VQDs with different concentration.

In order to prove these results, Figure 3-11 and 3-12 present the optical gaps of InP QDs and InP:V QDs which were predicted by Tauc's relation under different concentration 5% and 10% respectively. According to Figure 3-11 and 3-12, the quantum dots exhibit a direct band gap energy values of the suspension solution are: 1.88 eV, 2.73 eV, and 3.05 eV. It can note that a shift was founded in the band gap of vanadium doped suspension solution respect to pure InP QDs.

This phenomenon indicates that the gap energies of our solutions increase with the increase in the vanadium content, which confirm the result obtained with TEM, due to the confinement of

the electrons and holes at nanoscale that can be called "quantum size effect" according to the studies of Madan Singh et Al [150].

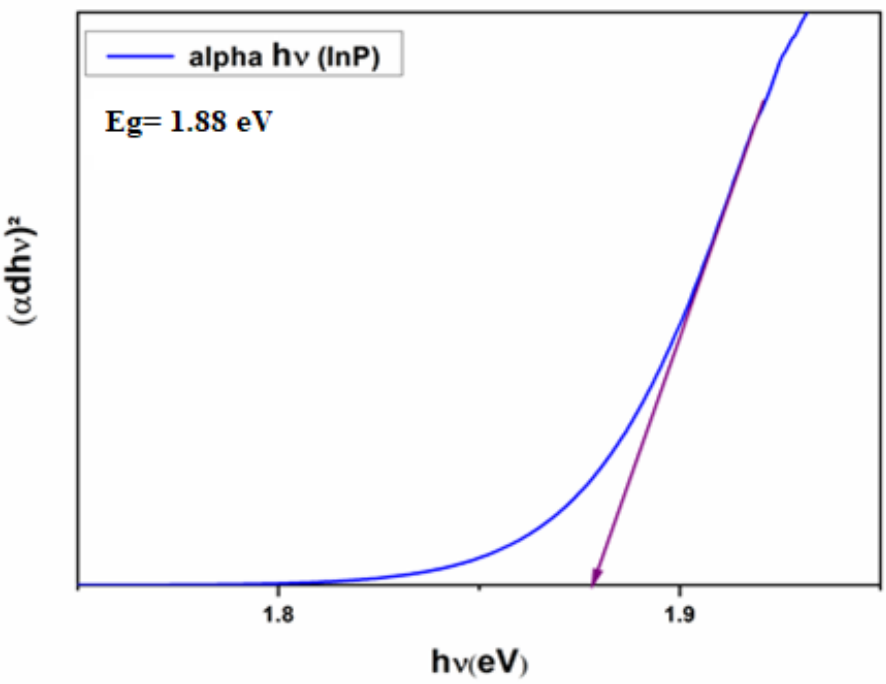

Figure 3-11: The band gap energy of InP QDs.

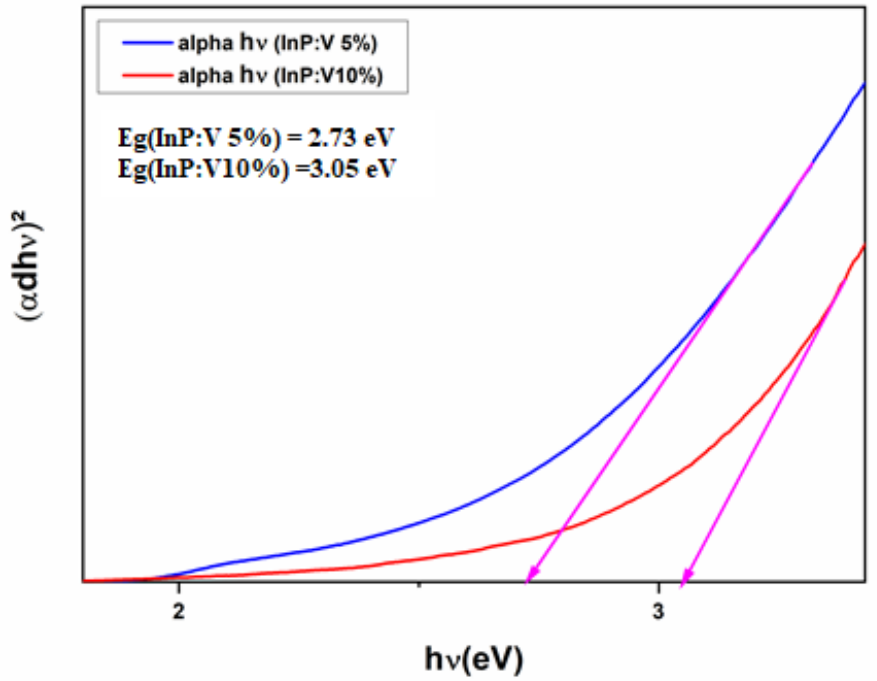

Figure 3-12: The band gap energy of InP:V QDs.

We saw that we are trying to improve the photoluminescence of InP QDs doping with Vanadium. However, no enhancement is happening. That's why we choose another strategy by passivating the InP QDS by introducing the ZnS as a shell.

2 Effect growth of InP/ZnS and InP/ZnS/ZnS Quantum Dots

2.1 X-ray diffraction (XRD)

To study the impact of shell growth on the crystal structure of the InP QDs, we have used the XRD. The X-Ray diffractograms in Figure 3-13 show three strong peaks in all samples, which can be easily indexed to the cubic zinc blend structure of InP. After the growth of ZnS (ICDD: 04-003-6940), we note a shift of the diffraction peaks towards the wide angles. Hence, this shift of the diffraction peaks of the core/shell QDs and core/shell/shell QDs explained by the presence of crystalline ZnS, which the latter has a lattice parameters smaller than those of InP (5.4Å against 5.9Å or 7.7% difference in lattice parameters in zinc blende structure) [151,152]. On the other side, the narrowing of the peaks during the growth of the shells in the main peak (111) indicates that the particles become larger during shell synthesis. In this way, the Debye–Scherrer formula has been employed to calculate the average crystallite size D:

$$D = \frac{0.9\lambda}{B\cos\theta_B}$$

Where,θ_B is referred to the maximum of Bragg diffraction peak, λ denotes the x-ray wavelength and the full width at half maximum (FWHM) of diffracted peaks is named by Scherrer's formula was applied to the main peak (111), therefore, the size of the QD nanoparticle is reported in Table 3-2.

Table 3-2: The average crystallite size D estimated using Scherrer's formula.

Particles	2θ	FWHM	Size determined by Scherrer (nm)
Core InP QDs	26.55	5.074	1.60
Core/Shell InP/QDs	27.20	2.79	2.92
Core/Shell/Shell InP/ZnS/ZnS QDs	27.69	1.85	4.42

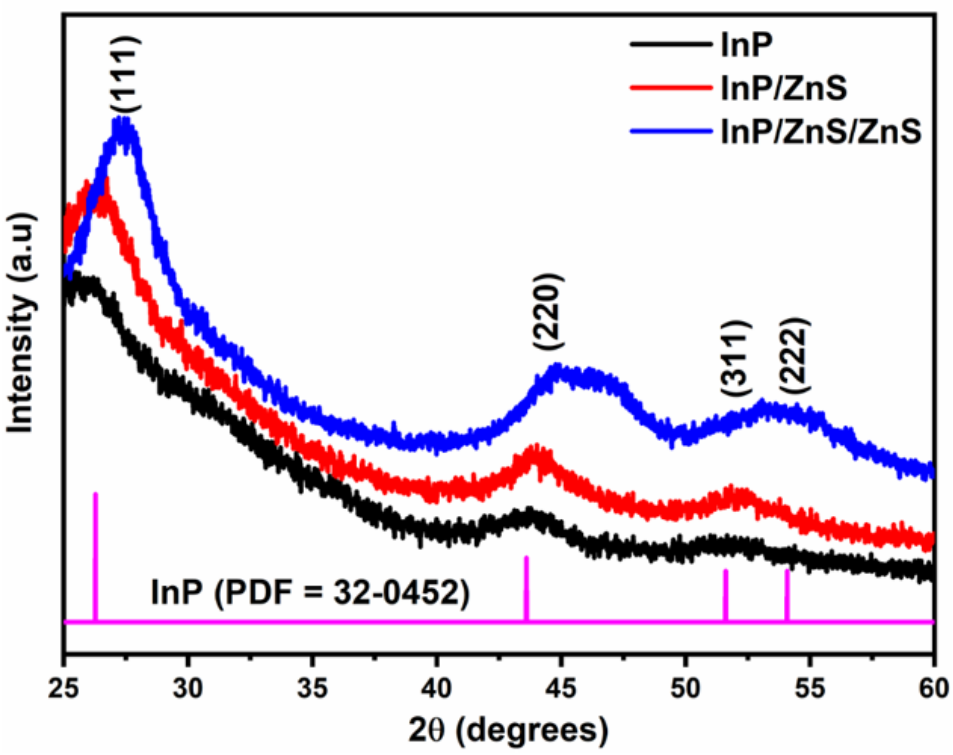

Figure 3- 13: X-ray diffractogram of core InP QDs, InP/ZnS QDs and InP/ZnS/ZnS QDs synthesized by Schlenk method.

2.2 Morphological properties of the particles by TEM

To confirm this increase in size after shell synthesis, Transmission Electron Microscopy (TEM) imaging was performed on the core QDs. In this regard, shell growth is carried out

directly following the growth of *InP* QDs, and this step includes annealing with $Zn(St)_2$ for 2h/3h; after that, a solution of DDT was injected into the solution it was left to react for 1 hour at 230°C [42,153]. During this growth, the alignment of the band gaps, the lattice parameters, and the structures of the materials of the core and shell materials of the heterostructure are to be considered. By following this procedure, we obtained an increase in size after shell growth. The electron microscopy in transmission (TEM) images in Figure 3-14 reveals an increase in nanocrystal size from 2.52nm for the InP-only core to 4.25nm for InP/ZnS QDs (with one-time shelling) and 5.48nm for InP/ZnS/ZnS QDs (with two times shelling).

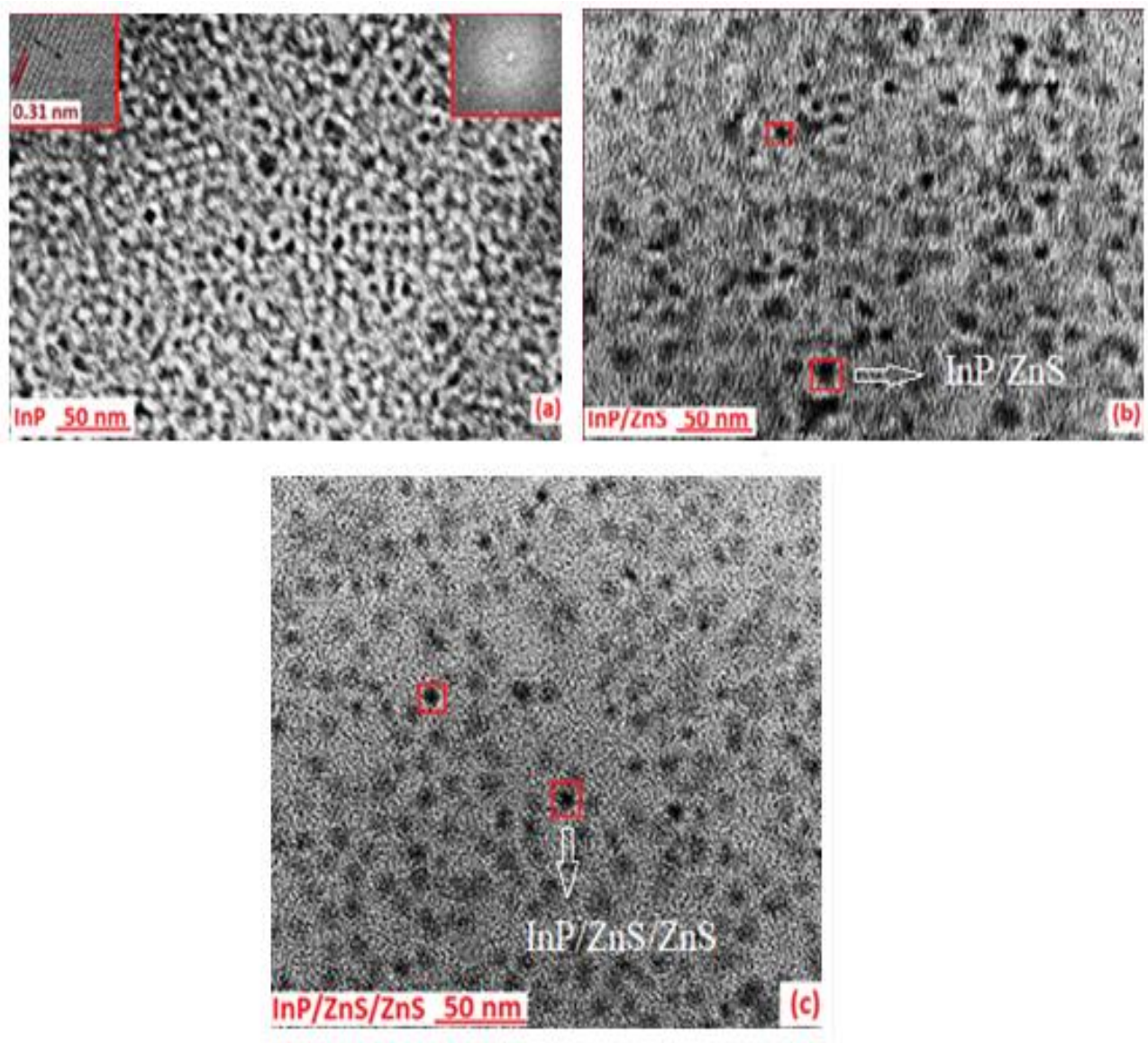

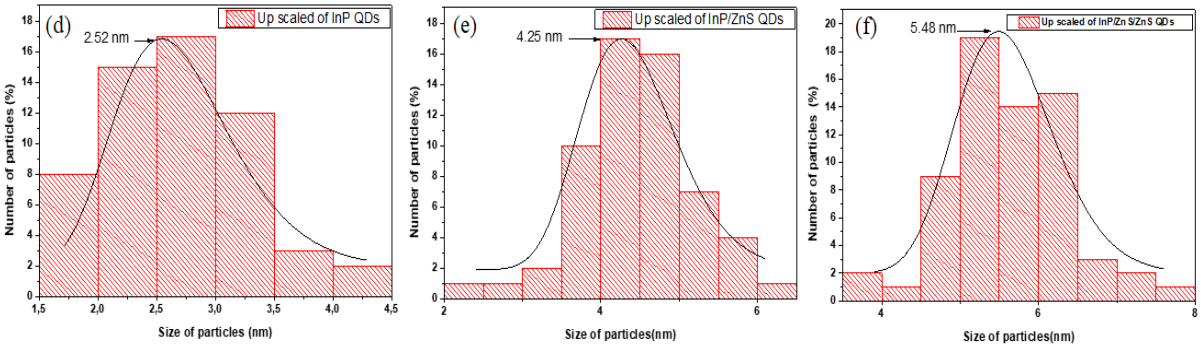

Figure 3-14: (a) TEM image of InP QDs. Inset 1 presents lattice fringes of InP QDs and Inset 2 shows its corresponding to selected area electron diffraction pattern SAED image, (b) TEM image of InP/ZnS QDs, (c) InP/ZnS/ZnS QDs, (d) distribution histogram of the particle of size InP QDs, (e) distribution histogram of the particle size InP/ZnS QDs and (f) distribution histogram of the particle size InP/ZnS/ZnS QDs QDs.

This result is confirmed by the particle size distribution histogram in Figure 3-14 (d,e,f). Therefore, the TEM images show that the crystals remain spherical during the reaction. Moreover, the selected area electron diffraction (SAED) (insert 1.) and the interplanar distance (insert 2.) have been presented in Figure 3-14 (a) where the lattice planes of the InP QDs obtained have an interplanar distance of d = 0.31 nm corresponding to the plane (111).

On the other side, the estimation of the crystal size from the main peak (111) using Scherrer equation agree with the quantities determined by TEM.

2.3 Analyse par spectroscopie UV-V visible

The analysis of the optical properties of QDs classically includes the measurement of absorbance and photoluminescence. The evolution of the absorption and PL spectra during the growth of the ZnS shell and ZnS /ZnS Shell/Shell is shown in Figure 3-15 and 3-17. This

growth was accompanied by an emission peak with a shoulder that appears at ~600 nm to ~680 nm in the absorption spectra. The excitonic peak is shifted to longer wavelengths. This phenomenon explains by a decrease in the energy levels of the nanoparticles due to the delocalization of electrons in the disordered arrangement of the nanoparticle.[154] Also, the broadening of this excitonic peak is related to intra-gap defects that mask the excitonic absorption, and its appearance depends on the number of intra-gap energy levels.

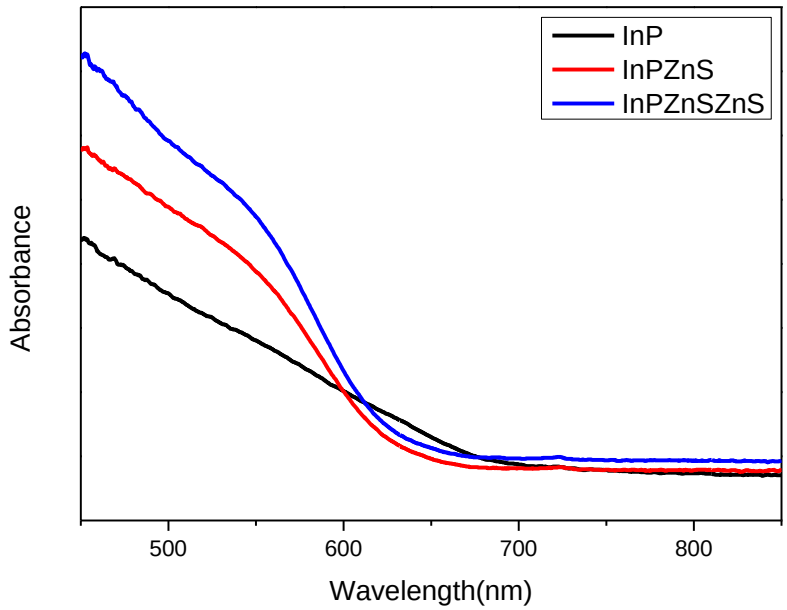

Figure 3-15: The absorption spectra.

Furthermore, Figure 3-16 displays a Tauc-plot based on the absorption curve to estimate the InP, InP/ZnS and InP/ZnS/ZnS band gap, which is around 3.63 eV, which is similar to the published value[113,155]. The bandgap energy of InP passivated by ZnS and ZnS/ZnS shows a down-shift in bandgap energy, resulting in broader absorption [101]. This phenomenon indicates that the gap energies of the shell core decrease when the quantum dot size increases, which confirms the result obtained with TEM, due to the confinement of the electrons and

holes at the nanoscale which can be called the "quantum size effect" according to the studies of Madan Singh et al [150].

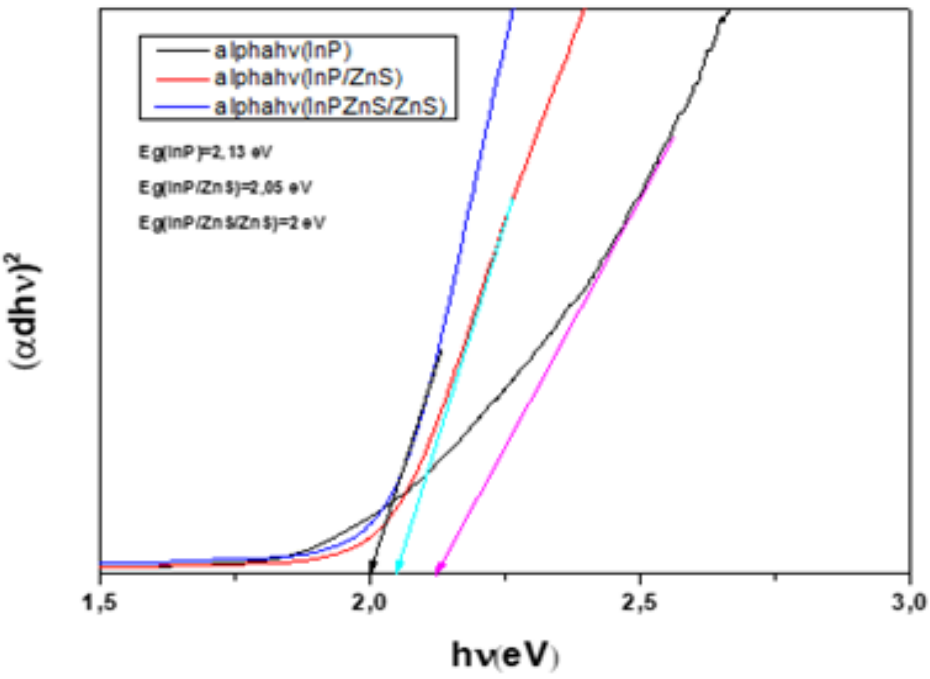

Figure 3-16: corresponding calculated bandgap.

The PL spectrum acquired at excitation wavelength λex = 450nm shifts from 580nm to 640nm with the passivation of ZnS as shown in Figure 3-17. The shift of the shoulder in the absorption spectra, as well as that of λem, towards wavelengths, is an indication of the decrease in the gap of QDs when they are enriched in ZnS. At the same time, the peak widened a little, its width at half height increasing from 27.98nm to 32.12nm. This indicates a slightly wider size distribution of the core/shell/shell system than for the core/shell. On the other side, surface defects can also widen the peak. Stokes shift and broad PL spectra of InP QDs and InP/ZnS tend to confirm the presence of emissive defects in these QDs.

We continued with the growth of a thin ZnS shell on the core/shell InP/ZnS. An increase in the intensity of PL is observed with a shift of λem towards the redshift. This implies that the surface defects have been passivated and that the ZnS is deposited in a heteroepitaxial on the

surface of the heart without diffusion of Zn^{2+}inside the heart [156]. The intensity of PL is higher in the case of InP/ZnS QDs and InP/ZnS/ZnS QDs emitting at 580 nm than at 640 nm. Therefore, the role of the intermediate shell is to bind more easily to the core (thanks to the lower crystal lattice parameters) and allow good cohesion of the second shell (ZnS) on the QD. These elements in the shells allow better photochemical stability of the nanocrystals while improving the optical properties since they increase the intensity of photoluminescence intensity. Hence, the intensity of the peak is a function of the passivation of the surface of the QDs. Therefore, the growth of ZnS according to the curves passes the surface defects, and it is a gain in PL. The valence and conduction bands of InP are in the gap of ZnS, the resulting InP/ZnS core /shell structure is Type I with exciton confinement in InP.

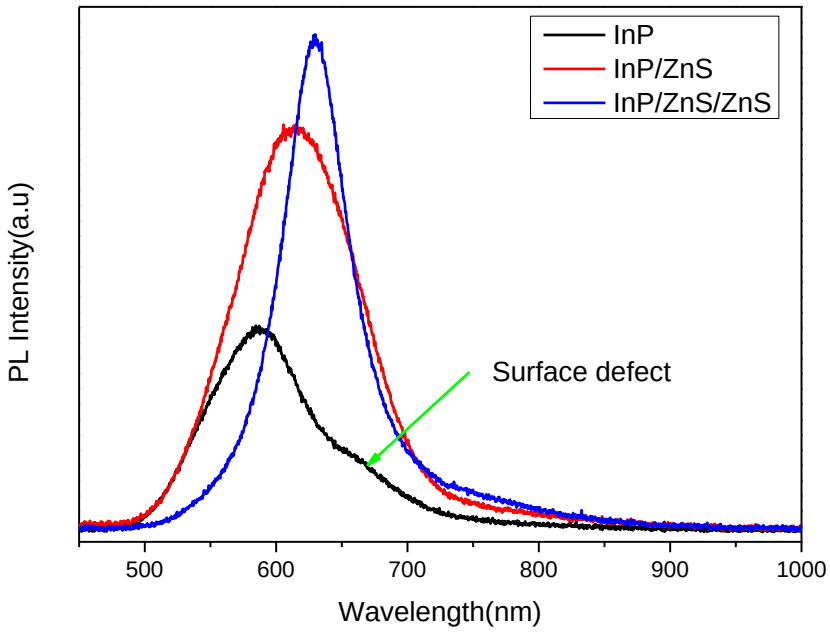

Figure 3-17: PL spectra of InP, InP/ZnS and InP/ZnS/ZnS QDs

After having characterized and studied the optical properties of InP, InP/ZnS and InP/ZnS/ZnS Quantum Dots. We analyzed the fluorescence spectra.

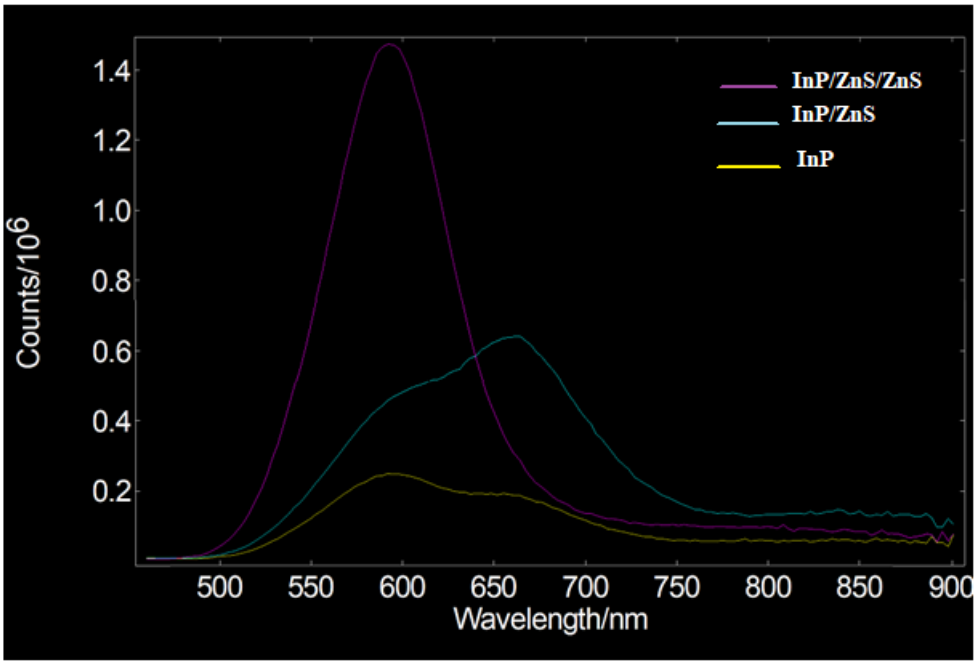

Figure 3-18: Evolution of the emission spectra of InP,InP/ZnSand InP/ZnS/ZnS Quantum Dots synthesized by hot injection method.

We followed the evolution of the fluorescence spectra of InP Quantum Dots during the synthesis of the ZnS shell and double shell ZnS/ZnS with an excitation 450 nm. The emission spectra are shifted towards shorter wavelengths as shown in in Figure 3-18. The shift is all the greater the more the larger the amount of ZnS precursors added and the larger the initial size of the InP/ZnS core/shell. Indeed, for InP/ZnS and InP/ZnS/ZnS the average emission wavelength is between about 500 nm and 545 nm for core initially emitting between 500 and 620 nm. We interpreted this loss in wavelength as the result of the diffusion of zinc atoms in the Quantum Dots particles.

On the other side, we wanted to study the evolution of the lifetime of InP nanocrystals with and without ZnS shells as demonstrated in Figure 3-19.

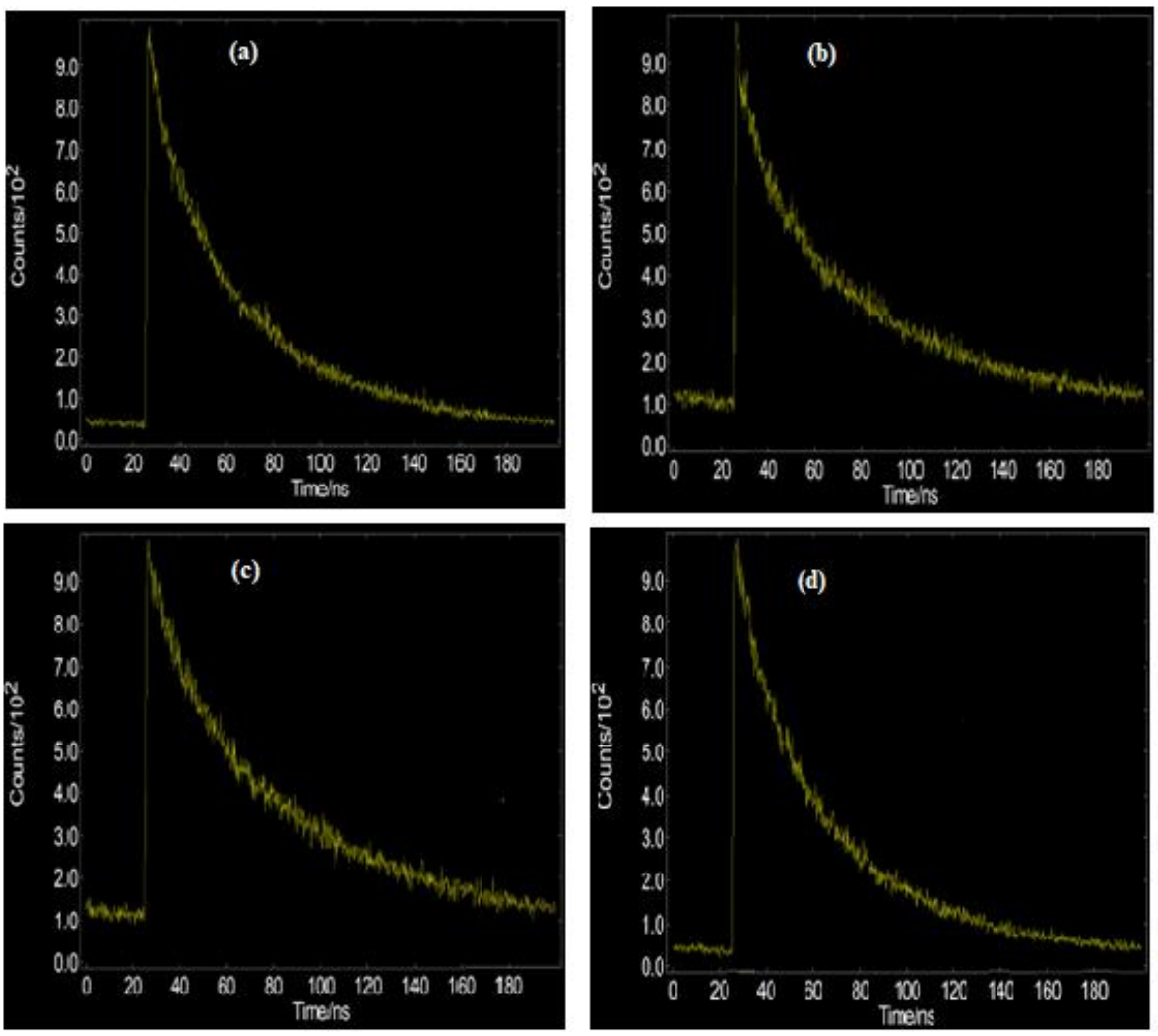

Figure 3-19: a) Lifetimes measured of InP QDs at 590 nm. (b) Lifetimes measured of InP QDs at 670 nm. (c) Lifetimes measured of InP/ZnS QDs at 670. (d) Lifetimes measured of InP/ZnS/ZnS QDs at 590 nm.

By taking advantage of the shell growth that allows for good crystalline Quantum Dots with precise size control, a lifetime extension was summarized in the table 3-4.

Table 3-3: The lifetime measured of the emissions of the Quantum Dots.

	Exc. λ, nm	Emission maxima, nm	Lifetimes determined	The best fit	The second lifetime	ns (%)
InP	405	590	(11 ns (68%),47 ns (32%))	670	8 ns (86%)	60 ns (14%)
InP/ZnS	405	590	(13 ns (60 %), 54 ns (40 %))	670	15ns (58%)	73 ns (42%)
InP/ZnS/ZnS	405	590	(14 ns (46%), 50 ns (36%)	……	Only one maximum	Only one maximum

The values at 590 nm are very similar, but the intensity of this emission increases when we are covering the QD. Two and three lifetimes are usual in this type of emissions (we detect the two slower lifetimes, the faster is usually less than 1 ns, and we don't see it).

Conclusion

The morphological, structural, and optical properties of InP QDS, Vanadium doped InP QDs, core/shell InP/ZnS QDs and core/shell/shell InP/ZnS/ZnS QDs as a function of the synthesis conditions have been studied in this chapter. TEM observation has indeed confirmed the morphology expected for each synthesis. The nanoparticles from hot injection synthesis are of zinc blend structure. According to the first strategy, the doping result showed no improvement in the optical properties especially in the photoluminescence despite growth QDs revealed by electron microscopy. The use of Vanadium as a dopant element does not allow to perform the synthesis at higher temperature to improve the properties of QDs.

Hence, a new process of InP QDs was set up by introducing the ZnS on single-shell and double-shell. The results obtained by introducing a ZnS shell are satisfactory, related to the mesh agreement with the core material. Therefore, the growth of a ZnS shell considerably increases the intensity of PL and leads to a greater dispersion in size and the reduction of surface defects. Moreover, it influences the fluorescence emitting properties. The evolution of the fluorescence lifetime and intensity gave us information on the type of exchange between the molecules and the particle. This study allowed us to understand how energy distribution in such a system.

So, shell growth by introducing the ZnS is proving to be a good method to enhance the photoluminescence

References

[1] S. Mahajan, M. Rani, R. Dubey, J. Mahajan, H. Ece, International Journal of Latest Research in Science and Technology, Int. J. Latest Res. Sci. Technol. 2 (2013) 518–521.

[2] C. Burda, X. Chen, R. Narayanan, M.A. El-sayed, Chemistry and Properties of Nanocrystals of Different Shapes, 2005.

[3] R. Koole, E. Groeneveld, D. Vanmaekelbergh, Size Effects on Semiconductor Nanoparticles, n.d. https://doi.org/10.1007/978-3-662-44823-6.

[4] F. Schulz, G.T. Dahl, S. Besztejan, M.A. Schroer, F. Lehmku, G. Gru, T. Vossmeyer, H. Lange, Ligand Layer Engineering To Control Stability and Interfacial Properties of Nanoparticles, (2016). https://doi.org/10.1021/acs.langmuir.6b01704.

[5] O. Yarema, M. Yarema, D. Bozyigit, W.M.M. Lin, V. Wood, Independent Composition and Size Control for Highly Luminescent Indium-Rich Silver Indium Selenide, (2015) 11134–11142. https://doi.org/10.1021/acsnano.5b04636.

[6] K.D. Wegner, F. Dussert, D. Truffier-boutry, A. Benayad, Influence of the Core / Shell Structure of Indium Phosphide Based Quantum Dots on Their Photostability and Cytotoxicity, 7 (2019) 1–12. https://doi.org/10.3389/fchem.2019.00466.

[7] C.A.S. No, Agents Classified by the IARC Monographs , Volumes 1 – 132, (2012).

[8] J.O. Uif, T. Rvbouvn, D. Sfhjnf, 1BTU QSFTFOU BOE GVUVSF PG JOEJVN QIPTQIJEF RVBOUVN EPUT, 15 (2022) 4468–4489.

[9] P. Ramasamy, K. Ko, J. Kang, J. Lee, Two-Step " Seed-Mediated " Synthetic Approach to Colloidal Indium Phosphide Quantum Dots with High-Purity Photo- and Electroluminescence, (2018). https://doi.org/10.1021/acs.chemmater.8b02049.

[10] V. Brunetti, H. Chibli, R. Fiammengo, A. Galeone, M.A. Malvindi, G. Vecchio, R. Cingolani, L. Nadeau, P. Paolo, quantum dots : in vitro and in vivo toxicity assessment, (2013) 307–317. https://doi.org/10.1039/c2nr33024e.

[11] D.A.G. Ramirez, J.S.A. Cerón, M.L.G. Herrera, J.P.L. Arias, M.P. González, Effect of the indium myristate precursor concentration on the structural , optical , chemical surface , and electronic properties of InP quantum dots passivated with ZnS, J. Mater. Sci. Mater. Electron. 30 (2019) 4885–4894. https://doi.org/10.1007/s10854-019-00783-6.

[12] Q. Zhou, J. Zhou, M. Zeng, G. Wang, Y. Chen, S. Lin, Photoelectrochemical Performance of Quantum dot-Sensitized TiO 2 Nanotube Arrays : a Study of Surface Modification by Atomic Layer Deposition Coating, (2017). https://doi.org/10.1186/s11671-017-2036-6.

[13] M. Ni, M.K.H.L. Ã, D.Y.C. Leung, K. Sumathy, A Review and Recent Developments in Photocatalytic Water-Splitting Using TiO2 for Hydrogen Production A review and recent developments in photocatalytic water-splitting using TiO 2 for hydrogen production, (2007). https://doi.org/10.1016/j.rser.2005.01.009.

[14] L.B. Hoch, P. Szymanski, K. Kaur, L. He, K. Liao, Q. Qiao, L.M. Reyes, Carrier dynamics and the role of surface defects : Designing a photocatalyst for gas-phase CO 2 reduction, (2016) 8011–8020. https://doi.org/10.1073/pnas.1609374113.

[15] Black Anatase TiO 2 Nanotubes with Tunable Orientation for High Performance Supercapacitors, (2019). https://doi.org/10.1021/acs.jpcc.9b05070.

[16] N. Cross, D.J. Woodsworth, Investigating the Electronic Properties of a Carbon, (2008).

[17] A.E. Commission, P. Reiss, A.E. Commission, J. Villain, Dans un laboratoire de nanosciences, (2011).

[18] U. Resch-genger, M. Grabolle, S. Cavaliere-jaricot, R. Nitschke, T. Nann, Quantum dots versus organic dyes as fluorescent labels, 5 (2008) 763–775. https://doi.org/10.1038/NMETH.1248.

[19] P. Reiss, M. Carrie, C. Lincheneau, L. Vaure, S. Tamang, Synthesis of Semiconductor Nanocrystals , Focusing on Nontoxic and Earth-Abundant Materials, (2016). https://doi.org/10.1021/acs.chemrev.6b00116.

[20] R. Saran, R.J. Curry, technologies, Nat. Publ. Gr. 10 (2016). https://doi.org/10.1038/nphoton.2015.280.

[21] M.A. Reed, R.J. Aggarwal, R.J. Matyi, T.M. Moore, A.E. Wetsel, Physical review, 60 (1988).

[22] C. Cea, Les nanocristaux semi-conducteurs fluorescents font leur gamme, (2005).

[23] M.T. Clarke, F.N. Viscomi, T.W. Chamberlain, N. Hondow, A.M. Adawi, J. Sturge, S.C. Erwin, J.G. Bouillard, S. Tamang, G.J. Stasiuk, colloidal quantum dots through thermal diffusion, Commun. Chem. (n.d.). https://doi.org/10.1038/s42004-019-0138-z.

[24] F.O.R.T.W. Orth, T. Exas, Q. Aprimer, QuantumDots: APrimer, (n.d.).

[25] Y. Wan, J. Norman, J. Bowers, Quantum dot microcavity lasers on silicon substrates, 1st ed., Elsevier Inc., 2019. https://doi.org/10.1016/bs.semsem.2019.05.002.

[26] Z.I. Alferov, The history and future of semiconductor heterostructures, (1998) 1–14.

[27] V. Biju, T. Itoh, A. Anas, Semiconductor quantum dots and metal nanoparticles : syntheses , optical properties , and biological applications, (2008) 2469–2495. https://doi.org/10.1007/s00216-008-2185-7.

[28] A. Physics, Optical Properties of Semiconductor Nanocrystals Cambridge Studies in Modern Optics, n.d.

[29] N. Fernández-delgado, M. Herrera, A.H. Tavabi, M. Luysberg, R.E. Dunin-borkowski, Applied Surface Science Structural and chemical characterization of CdSe-ZnS core-shell quantum dots, Appl. Surf. Sci. 457 (2018) 93–97. https://doi.org/10.1016/j.apsusc.2018.06.149.

[30] Q. Zhao, P.A. Graf, W.B. Jones, A. Franceschetti, J. Li, L. Wang, K. Kim, Shape Dependence of Band-Edge Exciton Fine Structure in CdSe Nanocrystals, (2007).

[31] I. Review, " 5 = 5;„ +, 75 (1995) 3728–3731.

[32] A.L. Rogach, No Title, n.d.

[33] M. Rosen, M. Kuno, M. Nirmal, D.J. Norris, M. Bawendi, Band-edge exciton in quantum dots of semiconductors with a degenerate valence band: Dark and bright exciton states, 54 (1996) 4843–4856.

[34] O. Stier, M. Grundmann, D. Bimberg, Electronic and optical properties of strained quantum dots modeled by 8-band k – p theory, 59 (1999) 5688–5701.

[35] A. Franceschetti, A. Zunger, Pseudopotential calculations of electron and hole addition spectra of InAs , InP , and Si quantum dots, 62 (2000) 2614–2623.

[36] E. Alkhazraji, A.M. Ragheb, M.A. Esmail, Q. Tareq, H. Fathallah, Electro-absorption and Electro-optic Characterization of L-Band InAs / InP Quantum-dash Waveguide, (2020). https://doi.org/10.1109/JPHOT.2020.2988584.

[37] M.D. Tessier, D. Dupont, K. De Nolf, J. De Roo, Z. Hens, Economic and Size-Tunable Synthesis of InP/ZnE (E = S, Se) Colloidal Quantum Dots., Chem. Mater. 27 (2015) 4893–4898. https://doi.org/10.1021/acs.chemmater.5b02138.

[38] A.M. Nightingale, J.C. DeMello, Improving the ensemble optical properties of InP quantum dots by indium precursor modification, J. Mater. Chem. C. 4 (2016) 8454–8458. https://doi.org/10.1039/C6TC02910H.

[39] D. V Talapin, J. Lee, M. V Kovalenko, E. V Shevchenko, Prospects of Colloidal Nanocrystals for Electronic and Optoelectronic Applications, (2010) 389–458.

[40] V.A. Online, L. Lai, L. Protesescu, M. V Kovalenko, M.A. Loi, Sensitized solar cells with colloidal PbS–CdS core–shell quantum dots †, (2014) 736–742. https://doi.org/10.1039/c3cp54145b.

[41] B. Chen, D. Li, F. Wang, InP Quantum Dots : Synthesis and Lighting Applications, 2002454 (2020) 1–20. https://doi.org/10.1002/smll.202002454.

[42] M.A. Ellis, G. Grandinetti, K.M. Fichter, Synthesis of Cd-free InP/ZnS Quantum Dots Suitable for Biomedical Applications, J. Vis. Exp. (2016). https://doi.org/10.3791/53684.

[43] T.-R. Kuo, S.-T. Hung, Y.-T. Lin, T.-L. Chou, M.-C. Kuo, Y.-P. Kuo, C.-C. Chen, Green Synthesis of InP/ZnS Core/Shell Quantum Dots for Application in Heavy-Metal-Free Light-Emitting Diodes, Nanoscale Res. Lett. 12 (2017) 537. https://doi.org/10.1186/s11671-017-2307-2.

[44] L.C. Lines, W. Jiang, Z. Yang, G. Lin, Cytotoxicity of InP / ZnS Quantum Dots With Different Surface Functional Groups Toward Two, 9 (2018) 1–12. https://doi.org/10.3389/fphar.2018.00763.

[45] H. Sengul, COMPARATIVE ASSESSMENT OF PHASE TRANSFER BEHAVIOUR OF INP / ZNS , Environmental Science Nano Comparative assessment of the phase transfer dots and CdSe / ZnS quantum dots under varying, (2019). https://doi.org/10.1039/C8EN01073K.

[46] V. Brunetti, I. Italiano, V. Brunetti, H. Chibli, R. Fiammengo, A. Galeone, M.A. Malvindi, G. Vecchio, R. Cingolani, J.L. Nadeau, P.P. Pompa, InP/ZnS as a safer alternative to CdSe/ZnS core/shell quantum dots: In vitro and in vivo toxicity assessment, (2012). https://doi.org/10.1039/c2nr33024e.

[47] B.J.M. Klostranec, W.C.W. Chan, Quantum Dots in Biological and Biomedical

Research : Recent Progress and Present Challenges, (n.d.). https://doi.org/10.1002/adma.200500786.

[48] H. Chibli, L. Carlini, S. Park, M. Dimitrijevic, J.L. Nadeau, Nanoscale Cytotoxicity of InP / ZnS quantum dots related to reactive oxygen species generation, (2011) 2552–2559. https://doi.org/10.1039/c1nr10131e.

[49] S. Tamang, C. Lincheneau, Y. Hermans, S. Jeong, P. Reiss, Chemistry of InP Nanocrystal Syntheses, Chem. Mater. 28 (2016) 2491–2506. https://doi.org/10.1021/acs.chemmater.5b05044.

[50] M. Green, S olution routes to III – V semiconductor quantum dots q, 6 (2002) 355–363.

[51] J. Jasinski, V.J. Leppert, S. Lam, G.A. Gibson, K. Nauka, C.C. Yang, Z. Zhou, Rapid oxidation of InP nanoparticles in air, 141 (2007) 624–627. https://doi.org/10.1016/j.ssc.2006.12.033.

[52] L. Li, P. Reiss, One-pot Synthesis of Highly Luminescent InP / ZnS Nanocrystals without, (2008) 11588–11589.

[53] G.O. Eren, S. Sadeghi, H. Bahmani Jalali, M. Ritter, M. Han, I. Baylam, R. Melikov, A. Onal, F. Oz, M. Sahin, C.W. Ow-Yang, A. Sennaroglu, R.T. Lechner, S. Nizamoglu, Cadmium-Free and Efficient Type-II InP/ZnO/ZnS Quantum Dots and Their Application for LEDs, ACS Appl. Mater. Interfaces. 13 (2021) 32022–32030. https://doi.org/10.1021/acsami.1c08118.

[54] D. V Talapin, A.L. Rogach, A. Kornowski, M. Haase, H. Weller, Highly Luminescent Monodisperse CdSe and CdSe / ZnS Nanocrystals Synthesized in a Hexadecylamine − Trioctylphosphine Oxide − Trioctylphospine Mixture, (2001).

[55] N. York, Visible Light Induced Hydrogen Production from in Situ Generated Colloidal Rhodium-Coated Cadmium Sulfide in Surfactant Vesicles Clarkson College of Technology Isolation from Pistacia Resins of a Bicyclic Triterpenoid Representing an Apparent Trapped, (2000) 2475–2476.

[56] A. Henglein, Small-Particle Research : Physicochemical Properties of Extremely Small Colloidal Metal and Semiconductor Particles, (1989).

[57] G.M. Wallraff, W.D. Hinsberg, Lithographic Imaging Techniques for the Formation of Nanoscopic Features, (1999).

[58] P.M. Petroff, A. Lorke, A. Imamoglu, E PITAXIALLY S ELF -A SSEMBLED Q UANTUM D OTS, 46 (2020). https://doi.org/10.1063/1.1381102.

[59] B.D. Ingert, M. Pileni, Limitations in Producing Nanocrystals Using Reverse Micelles as Nanoreactors **, 5 (2001) 136–139.

[60] A.P. Alivisatos, Perspectives on the Physical Chemistry of Semiconductor Nanocrystals, 3654 (1996) 13226–13239.

[61] C.B. Murray, D.J. Norris, M.G. Bawendi, Synthesis and Characterization of Nearly Monodisperse CdE (E = S , Se , Te) Semiconductor Nanocrystallites, (1993) 8706–8715.

[62] M. Bayer, E.H. Sargent, Semiconductor quantum dots: Technological progress and future challenges, 8541 (2021). https://doi.org/10.1126/science.aaz8541.

[63] L. Qu, X. Peng, Control of Photoluminescence Properties of CdSe Nanocrystals in Growth, 124 (2018) 2016–2018.

[64] S.G. Hickey, S.F. Wuister, D. Vanmaekelbergh, Single-Step Synthesis to Control the Photoluminescence Quantum Yield and Size Dispersion of CdSe Nanocrystals, (2003) 489–496.

[65] S. Lee, K. Lee, J. Jo, B. Park, Y. Kwon, S. Jang, H. Yang, emitting diode based on InP quantum dot color converters, 4 (2014) 1297–1302. https://doi.org/10.1364/OME.4.001297.

[66] L. Qu, Z.A. Peng, X. Peng, Alternative Routes toward High Quality CdSe Nanocrystals, (2001) 1–5.

[67] C.R. Bullen, P. Mulvaney, Nucleation and Growth Kinetics of CdSe Nanocrystals in Octadecene, (2004).

[68] P. Reiss, G. Quemard, S. Carayon, J. Bleuse, F. Chandezon, A. Pron, Luminescent ZnSe nanocrystals of high color purity, 84 (2004) 10–13. https://doi.org/10.1016/j.matchemphys.2003.11.002.

[69] X. Zhong, Y. Feng, W. Knoll, M. Han, Alloyed Zn x Cd 1 - x S Nanocrystals with Highly Narrow Luminescence Spectral Width, (2003) 13559–13563.

[70] D.W. Lucey, D.J. Macrae, M. Furis, Y. Sahoo, A.N. Cartwright, P.N. Prasad, Monodispersed InP Quantum Dots Prepared by Colloidal Chemistry in a Noncoordinating Solvent, (2005) 3754–3762.

[71] D. Battaglia, X. Peng, Formation of High Quality InP and InAs Nanocrystals in a Noncoordinating Solvent, (2002) 1–4.

[72] J. Jasieniak, C. Bullen, J. Van Embden, P. Mulvaney, Phosphine-Free Synthesis of CdSe Nanocrystals, (2005) 20665–20668.

[73] S. Sapra, A.L. Rogach, J. Feldmann, Phosphine-free synthesis of monodisperse CdSe nanocrystals in olive oil, (2006) 3391–3395. https://doi.org/10.1039/b607022a.

[74] G.G. Yordanov, G.D. Gicheva, B.H. Bochev, C.D. Dushkin, E. Adachi, The effects of temperature and carboxylic acid ligand on the growth of nanocrystalline CdSe in a hot paraffin matrix, 273 (2006) 10–15. https://doi.org/10.1016/j.colsurfa.2005.07.036.

[75] J. Park, J. Joo, S.G. Kwon, Y. Jang, T. Hyeon, Synthesis of Monodisperse Spherical Nanocrystals Angewandte, (2007) 4630–4660. https://doi.org/10.1002/anie.200603148.

[76] R.H. Dinegar, JOURNAL OF THE, 72 (1950).

[77] F. Wang, V.N. Richards, S.P. Shields, W.E. Buhro, Kinetics and Mechanisms of Aggregative Nanocrystal Growth, (2014). https://doi.org/10.1021/cm402139r.

[78] X. Peng, J. Wickham, A.P. Alivisatos, Kinetics of II-VI and III-V Colloidal Semiconductor Nanocrystal Growth : " Focusing " of Size Distributions, 7863 (1998) 5343–5344.

[79] O.I. Micic, C.J. Curtis, K.M. Jones, J.R. Sprague, A.J. Nozik, Synthesis and Characterization of InP Quantum Dots, (1994) 4966–4969.

[80] A.A. Guzelian, J.E.B. Katari, A. V Kadavanich, U. Banin, K. Hamad, E. Juban, A.P.

Alivisatos, R.H. Wolters, C.C. Arnold, J.R. Heath, Synthesis of Size-Selected , Surface-Passivated InP Nanocrystals, (1996) 7212–7219.

[81] O.I. Mic, Synthesis of extremely small InP quantum dots and electronic coupling in their disordered solid films, 4022 (2005). https://doi.org/10.1063/1.1379990.

[82] S. Xu, S. Kumar, T. Nann, Rapid Synthesis of High-Quality InP Nanocrystals, (2006) 1054–1055.

[83] J.A. Gerbec, D. Magana, A. Washington, G.F. Strouse, Microwave-Enhanced Reaction Rates for Nanoparticle Synthesis, (2005) 15791–15800.

[84] D.D. Lovingood, G.F. Strouse, Microwave Induced In-Situ Active Ion Etching of Growing InP Nanocrystals, (2008) 4–7.

[85] C. Li, M. Ando, N.M. Ã, Facile Preparation of Highly Luminescent InP Nanocrystals by a Solvothermal Route, 37 (2008) 856–857. https://doi.org/10.1246/cl.2008.856.

[86] W.S.H. Lee, J. Chul, Amine-derived synthetic approach to color-tunable InP / ZnS quantum dots with high fluorescent qualities, (2013). https://doi.org/10.1007/s11051-013-1750-y.

[87] W. Song, S. Lee, H. Yang, Fabrication of warm , high CRI white LED using non-cadmium quantum dots, 3 (2013) 1468–1473. https://doi.org/10.1364/OME.3.001468.

[88] O.I. Micié, J.R. Sprague, C.J. Curtis, K.M. Jones, J.L. Machol, A.J. Nozik, H. Giessen, B. Fluegel, G. Mohs, N. Peyghambarian, Synthesis and Characterization of InP , GaP , and GalnPi Quantum Dots, (1995) 7754–7759.

[89] O.B. Achorn, D. Franke, M.G. Bawendi, Seedless Continuous Injection Synthesis of Indium Phosphide Quantum Dots as a Route to Large Size and Low Size Dispersity, Chem. Mater. 32 (2020) 6532–6539. https://doi.org/10.1021/acs.chemmater.0c01906.

[90] S. Mahajan, M. Rani, R.B. Dubey, J. Mahajan, SYNTHESIS OF CdSe CRYSTAL USING HOT INJECTION METHOD, Int. J. Latest Res. Sci. Technol. 2 (2013) 518–521.

[91] J. Ministro, A study on the synthesis and the optical properties of InP-based quantum dots, University Gent, n.d.

[92] S.B. Brichkin, Synthesis and properties of colloidal indium phosphide quantum dots, Colloid J. 77 (2015) 393–403. https://doi.org/10.1134/S1061933X15040043.

[93] E.S. Cde, J. Te, A.C. Soc, Murray, C.B., Norris, D.J. & Bawendi, M.G. Synthesis and characterization of nearly monodisperse CdE (E = S, Se, Te) semiconductor nanocrystallites. J. Am. Chem. Soc. 115, 8706 − 871..., (2021). https://doi.org/10.1021/ja00072a025.

[94] X. Peng, L. Manna, W. Yang, J. Wickham, Shape control of CdSe nanocrystals, 404 (2000) 59–61.

[95] L. Manna, E.C. Scher, A.P. Alivisatos, R. V August, Synthesis of Soluble and Processable Rod- , Arrow- , Teardrop- , and Tetrapod-Shaped CdSe Nanocrystals, (2000) 12700–12706.

[96] V.F. Puntes, D. Zanchet, C.K. Erdonmez, A.P. Alivisatos, Synthesis of hcp-Co Nanodisks, (2002) 12874–12880.

[97] S. Ithurria, B. Dubertret, Quasi 2D Colloidal CdSe Platelets with Thicknesses Controlled at the Atomic Level, (2008) 16504–16505.

[98] H. Qian, L. Li, J. Ren, One-step and rapid synthesis of high quality alloyed quantum dots (CdSe – CdS) in aqueous phase by microwave irradiation with controllable temperature, 40 (2005) 1726–1736. https://doi.org/10.1016/j.materresbull.2005.05.022.

[99] P. Ramasamy, B. Kim, M.-S. Lee, J.-S. Lee, Beneficial effects of water in the colloidal synthesis of InP/ZnS core–shell quantum dots for optoelectronic applications, Nanoscale. 8 (2016) 17159–17168. https://doi.org/10.1039/C6NR04713K.

[100] W.A.C. Hen, W.E.W. Ang, L.E.I.S. Un, S.H.C. Hen, Q.U.N.Y. An, T.A.G. Uo, X.I.Z. Hou, C. Haoxing, Y.O.Z. Hang, Synthesis and characterization of InP / ZnSe / ZnS quantum dots for photo-emissive color conversion, 12 (2022) 1717–1730.

[101] A.J. Zavaraki, Q. Liu, H. Ågren, Nano-Structures & Nano-Objects Solar cell sensitized with ‘“ green ”’ InP-ZnS quantum dots : Effect of ZnS shell deposition, Nano-Structures & Nano-Objects. 22 (2020) 100461. https://doi.org/10.1016/j.nanoso.2020.100461.

[102] S.T. Quenching, Suppressed Thermal Quenching, (2021).

[103] N. Mordvinova, A. Vinokurov, T. Kuznetsova, O.I. Lebedev, S. Dorofeev, Highly luminescent core-shell InP/ZnX (X = S, Se) quantum dots prepared: Via a phosphine synthetic route, Dalt. Trans. 46 (2017) 1297–1303. https://doi.org/10.1039/c6dt03956a.

[104] M. Jiang, Y. Li, S. Li, H. Zhou, X. Cao, S. Bao, Y. Gao, H. Luo, P. Jin, Room Temperature Optical Constants and Band Gap Evolution of Phase Pure M 1 -VO 2 Thin Films Deposited at Different Oxygen Partial Pressures by Reactive Magnetron Sputtering, J. Nanomater. 2014 (2014) 1–6. https://doi.org/10.1155/2014/183954.

[105] A. Bouzidi, N. Benramdane, A. Nakrela, C. Mathieu, B. Khelifa, R. Desfeux, A. Da Costa, First synthesis of vanadium oxide thin films by spray pyrolysis technique, Mater. Sci. Eng. B. 95 (2002) 141–147. https://doi.org/10.1016/S0921-5107(02)00224-6.

[106] B. Lambert, B. Deveaud, Y. Toudic, G. Pelous, J.C. Paris, G. Grandpierre, Properties of vanadium in InP, Solid State Commun. 47 (1983) 337–340. https://doi.org/10.1016/0038-1098(83)90914-6.

[107] C. Lamsal, N.M. Ravindra, Optical properties of vanadium oxides-an analysis, J. Mater. Sci. 48 (2013) 6341–6351. https://doi.org/10.1007/s10853-013-7433-3.

[108] D. Collection, Modeling Radiation Effects on a Triple Junction Solar Cell using Silvaco ATLAS NAVAL POSTGRADUATE, (2012).

[109] P. Cedex, SPECTROSCOPIC INVESTIGATION OF VANADIUM IN lnP B. CLERJAUD, D. COTE and C. NAUD, 83 (1987) 194–197.

[110] J.C. Paris, PROPERTIES OF V A N A D I U M IN InP I +, 47 (1983) 337–340.

[111] M.A. Shafi, H. Ullah, S. Ullah, L. Khan, S. Bibi, B.M. Soucase, Numerical Simulation of Lead-Free Sn-Based Perovskite Solar Cell by Using SCAPS-1D †, (2022) 1–5.

[112] J.A. Dias, S.H. Santagneli, S.J.L. Ribeiro, Y. Messaddeq, Perovskite Quantum Dot Solar Cells : An Overview of the Current Advances and Future Perspectives, 2100205 (2021) 1–28. https://doi.org/10.1002/solr.202100205.

[113] W. Zhang, S. Ding, W. Zhuang, D. Wu, P. Liu, X. Qu, H. Liu, H. Yang, Z. Wu, K. Wang, X.W. Sun, InP / ZnS / ZnS Core / Shell Blue Quantum Dots for Efficient Light-Emitting Diodes, (n.d.). https://doi.org/10.1002/adfm.202005303.

[114] H.I. Ikeri, A.I. Onyia, P.U. Asogwa, Investigation Of Optical Characteristics Of Semiconductor Quantum Dots For Multi Junction Solar Cells Applications ., 8 (2019) 3531–3535.

[115] A.M. Smith, S. Nie, Semiconductor Nanocrystals : Structure , Properties , and Band Gap Engineering, (2010).

[116] P. Reiss, S. Carayon, J. Bleuse, A. Pron, Low polydispersity core / shell nanocrystals of CdSe / ZnSe and CdSe / ZnSe / ZnS type : preparation and optical studies, 139 (2003) 649–652. https://doi.org/10.1016/S0379-6779(03)00335-7.

[117] M. Ando, M. Horie, Y. Akazawa-ogawa, Y. Hagihara, N. Murase, Y. Shigeri, Cytotoxicity of CdSe-based quantum dots incorporated in glass nanoparticles evaluated using human keratinocyte HaCaT cells, Biosci. Biotechnol. Biochem. 8451 (2016) 1–4. https://doi.org/10.1080/09168451.2015.1069702.

[118] A. Ghicov, P. Schmuki, Self-ordering electrochemistry : a review on growth and functionality of TiO 2 nanotubes and other self-aligned MO x structures, (2009) 2791–2808. https://doi.org/10.1039/b822726h.

[119] H.E. Prakasam, K. Shankar, M. Paulose, O.K. Varghese, C.A. Grimes, ARTICLES A New Benchmark for TiO 2 Nanotube Array Growth by Anodization, (2007) 7235–7241.

[120] V. Zwilling, M. Aucouturier, E. Darque-ceretti, Anodic oxidation of titanium and TA6V alloy in chromic media . An electrochemical approach, 45 (1999) 921–929.

[121] S. Kobayashi, K. Hanabusa, Preparation of TiO 2 Hollow-Fibers Using Supramolecular Assemblies Seiji Shinkai Porous , nanostructured materials have attracted considerable attention because of their potential ap- materials is quite difficult . Nanostructured inorganic cationic charge moieties with the expectation that the, (2000) 1523–1525.

[122] J.M. Macak, H. Tsuchiya, A. Ghicov, K. Yasuda, R. Hahn, S. Bauer, P. Schmuki, TiO 2 nanotubes : Self-organized electrochemical formation , properties and applications, 11 (2007) 3–18. https://doi.org/10.1016/j.cossms.2007.08.004.

[123] C. Ruan, M. Paulose, O.K. Varghese, G.K. Mor, C.A. Grimes, Fabrication of Highly Ordered TiO 2 Nanotube Arrays Using an Organic Electrolyte, (2005) 15754–15759.

[124] K. Lee, A. Mazare, P. Schmuki, One-Dimensional Titanium Dioxide Nanomaterials : Nanotubes, (2014).

[125] V. Shrotriya, G. Li, Y. Yao, C. Chu, Y. Yang, Transition metal oxides as the buffer layer for polymer photovoltaic cells Transition metal oxides as the buffer layer for polymer photovoltaic cells, (2006) 1–4. https://doi.org/10.1063/1.2174093.

[126] O. Karatum, M.M. Aria, G.O. Eren, E. Yildiz, E.D. Glowacki, Nanoengineering InP Quantum Dot-Based Photoactive Biointerfaces for Optical Control of Neurons, 15 (2021) 1–14. https://doi.org/10.3389/fnins.2021.652608.

[127] A. Zaban, O.I. Mic, B.A. Gregg, A.J. Nozik, Photosensitization of Nanoporous TiO 2 Electrodes with InP Quantum Dots, 7463 (1998) 3153–3156.

[128] H.B. Jalali, M.M. Aria, U.M. Dikbas, S. Sadeghi, E ff ective Neural Photostimulation Using Indium-Based Type-II Quantum Dots, (2018). https://doi.org/10.1021/acsnano.8b02976.

[129] H. Zhao, X. Li, M. Cai, C. Liu, Y. You, R. Wang, A.I. Channa, F. Lin, D. Huo, G. Xu, X. Tong, Z.M. Wang, Role of Copper Doping in Heavy Metal-Free InP / ZnSe Core / Shell Quantum Dots for Highly Efficient and Stable Photoelectrochemical Cell, 2101230 (2021) 1–10. https://doi.org/10.1002/aenm.202101230.

[130] M.T. Clarke, F.N. Viscomi, T.W. Chamberlain, N. Hondow, A.M. Adawi, J. Sturge, S.C. Erwin, J.-S.G. Bouillard, S. Tamang, G.J. Stasiuk, Synthesis of super bright indium phosphide colloidal quantum dots through thermal diffusion, Commun. Chem. 2 (2019) 36. https://doi.org/10.1038/s42004-019-0138-z.

[131] T.K. Nideep, M. Ramya, M.M. Varier, M. Kailasnath, A Study of Nonlinear Optical Property of Cadmium Based Quantum Dots with Comparable Particle Size, Springer Singapore, n.d. https://doi.org/10.1007/978-981-15-9259-1.

[132] S. Kobayashi, N. Hamasaki, M. Suzuki, M. Kimura, H. Shirai, K. Hanabusa, Preparation of Helical Transition-Metal Oxide Tubes Using Organogelators as Structure-Directing Agents, 1 (2002) 6550–6551.

[133] Z. Miao, D. Xu, J. Ouyang, G. Guo, X. Zhao, Electrochemically Induced Sol − Gel Preparation of Single-Crystalline TiO 2 Nanowires, (2002).

[134] Enhancement of photocatalytic and photoelectrochemical properties of TiO2 nanotubes sensitized by SILAR - Deposited PbS nanoparticles _ Elsevier Enhanced Reader.pdf, (n.d.).

[135] J.M. Macak, S.P. Albu, P. Schmuki, Towards ideal hexagonal self-ordering of TiO 2 nanotubes pss, 183 (2007) 181–183. https://doi.org/10.1002/pssr.200701148.

[136] P. V Kamat, Quantum Dot Solar Cells . The Next Big Thing in Photovoltaics, (2013).

[137] M. Antoniadou, D.I. Kondarides, D.D. Dionysiou, P. Lianos, Quantum Dot Sensitized Titania Applicable as Photoanode in Photoactivated Fuel Cells, (2012).

[138] M.P. Genovese, I. V Lightcap, P. V Kamat, Sun-Believable Solar Paint . A Transformative One-Step Approach for Designing Nanocrystalline Solar Cells, (2012) 865–872.

[139] S. Park, T. Ikegami, K. Ebihara, Effects of substrate temperature on the properties of Ga-doped ZnO by pulsed laser deposition, 513 (2006) 90–94. https://doi.org/10.1016/j.tsf.2006.01.051.

[140] J. Verschraegen, M. Burgelman, Numerical modeling of intra-band tunneling for heterojunction solar cells in SCAPS, 515 (2007) 6276–6279. https://doi.org/10.1016/j.tsf.2006.12.049.

[141] P.E. Imoisili, T. Jen, Numerical Analysis and Performance improvement of Nanostructured Cu 2 O / TiO 2 pn heterojunction Solar Cells using SCAPS, (n.d.).

[142] M. Al-hattab, L. Moudou, M. Khenfouch, O. Bajjou, Numerical simulation of a new heterostructure CIGS / GaSe solar cell system using SCAPS-1D software, Sol. Energy. 227 (2021) 13–22. https://doi.org/10.1016/j.solener.2021.08.084.

[143] M.M.T. Al, Z.S. Yasin, Optoelectronics Simulation of CIGS - Based Solar Cells Using

a Cd - Free Nontoxic - ZrS x Se 2 − x as a Novel Buffer Layer, Brazilian J. Phys. (2022) 1–10. https://doi.org/10.1007/s13538-022-01146-z.

[144] U. Mandadapu, S.V. Vedanayakam, K. Thyagarajan, Numerical Simulation of Ch 3 Nh 3 PbI 3-X Cl x Perovskite solar cell using SCAPS-1D, (2017) 40–45.

[145] P. Ieee, P. Specialists, C. Washington, A. Niemegeers, M. Burgelman, MODELLING OF ac-CHARACTERISTICS SOLAR CELLS, (1996) 901–904.

[146] M. Burgelman, P. Nollet, S. Degrave, Modelling polycrystalline semiconductor solar cells, 362 (2000) 527–532.

[147] M. Mostefaoui, H. Mazari, S. Khelifi, A. Bouraiou, R. Dabou, Simulation of High Efficiency CIGS solar cells with SCAPS-1D software, Energy Procedia. 74 (2015) 736–744. https://doi.org/10.1016/j.egypro.2015.07.809.

[148] U. Holzwarth, N. Gibson, The Scherrer equation versus the "Debye-Scherrer equation," Nat. Nanotechnol. 6 (2011) 534–534. https://doi.org/10.1038/nnano.2011.145.

[149] O. Ehlert, A. Tiwari, T. Nann, Quantum confinement of the thermodynamic functions for the formation of electrons and holes in CdSe nanocrystals, J. Appl. Phys. 100 (2006) 1–6. https://doi.org/10.1063/1.2356607.

[150] M. Singh, M. Goyal, K. Devlal, Size and shape effects on the band gap of semiconductor compound nanomaterials, J. Taibah Univ. Sci. 12 (2018) 470–475. https://doi.org/10.1080/16583655.2018.1473946.

[151] M. Asemi, A. Suddar, M. Ghanaatshoar, Increasing the specific surface area of Cr-doped - nanoparticles by controlling the drying time for DSSC applications, J. Mater. Sci. Mater. Electron. 28 (2017) 15233–15238. https://doi.org/10.1007/s10854-017-7401-9.

[152] C. Ippen, T. Greco, A. Wedel, InP/ZnSe/ZnS: A Novel Multishell System for InP Quantum Dots for Improved Luminescence Efficiency and Its application in a Light-Emitting Device, J. Inf. Disp. 13 (2012) 91–95. https://doi.org/10.1080/15980316.2012.683537.

[153] E. Ryu, S. Kim, E. Jang, S. Jun, H. Jang, B. Kim, S. Kim, Communications, 21 (2009) 2425–2427.

[154] O.I. Mic, Synthesis of extremely small InP quantum dots and electronic coupling in their disordered solid films, 4022 (2005). https://doi.org/10.1063/1.1379990.

[155] S.J. Yang, J.H. Oh, S. Kim, H. Yang, Y.R. Do, Realization of InP / ZnS quantum dots for green , amber and red down-converted LEDs and their, (2015) 3582–3591. https://doi.org/10.1039/c5tc00028a.

[156] S. Xu, J. Ziegler, T. Nann, Rapid synthesis of highly luminescent InP and InP / ZnS nanocrystals †, (2008) 2653–2656. https://doi.org/10.1039/b803263g.

[157] K. Yong, H. Ding, I. Roy, W. Law, E.J. Bergey, A. Maitra, P.N. Prasad, Imaging Pancreatic Cancer Using Bioconjugated InP Quantum Dots, 3 (n.d.).

[158] S. Fung, B. Yang, C.K. Ng, M.K. Fung, C.C. Ling, A.B. Djuriˇ, Annealing study of titanium oxide nanotube arrays, 130 (2011) 1227–1231. https://doi.org/10.1016/j.matchemphys.2011.08.063.

[159] T.S. Bhat, A.D. Sheikh, N.L. Tarwal, S.D. Korade, C.K. Hong, J.H. Kim, ZnS passivated PbSe sensitized TiO 2 nanorod arrays to suppress photocorrosion in photoelectrochemical solar cells, Mater. Today Commun. 16 (2018) 186–193. https://doi.org/10.1016/j.mtcomm.2018.06.008.

[160] N. Simulation, P. For, Modeling Thin-film PV Devices, 153 (2004) 143–153. https://doi.org/10.1002/pip.524.

[161] S.K. M, S.P. Madhusudanan, A.R. Rajamani, M. Siaj, S.K. Batabyal, Barium Substitution in Kesterite Cu 2 ZnSnS 4 : Cu 2 Zn 1 − x Ba x SnS 4 Quinary Alloy Thin Films for E ffi cient Solar Energy Harvesting, (2020) 4–11. https://doi.org/10.1021/acs.cgd.0c00150.

[162] M. Jamil, A. Ali, K. Mahmood, M.I. Arshad, S. Tahir, M. Ajaz un Nabi, S. Ikram, N. Amin, S. Hussain, Numerical simulation of perovskite/Cu2Zn(Sn1-x Gex)S4 interface to enhance the efficiency by valence band offset engineering, J. Alloys Compd. 821 (2020) 153221. https://doi.org/10.1016/j.jallcom.2019.153221.

[163] Y. Raoui, H. Ez-Zahraouy, N. Tahiri, O. El Bounagui, S. Ahmad, S. Kazim, Performance analysis of MAPbI3 based perovskite solar cells employing diverse charge selective contacts: Simulation study, Sol. Energy. 193 (2019) 948–955. https://doi.org/10.1016/j.solener.2019.10.009.

[164] Chenming C. Hu, Modern Semiconductor Devices for Integrated Circuits, in: 2010.

[165] F. Baig, Y.H. Khattak, S. Ullah, B.M. Soucase, S. Beg, H. Ullah, Numerical analysis a guide to improve the efficiency of experimentally designed solar cell, Appl. Phys. A. 124 (2018) 471. https://doi.org/10.1007/s00339-018-1877-x.

[166] R. Toufanian, A. Piryatinski, A.H. Mahler, R. Iyer, J.A. Hollingsworth, A.M. Dennis, Bandgap Engineering of Indium Phosphide-Based Core/Shell Heterostructures Through Shell Composition and Thickness, Front. Chem. 6 (2018). https://doi.org/10.3389/fchem.2018.00567.

[167] V. Raj, F. Rougieux, L. Fu, H.H. Tan, C. Jagadish, Design of Ultrathin InP Solar Cell Using Carrier Selective Contacts, IEEE J. Photovoltaics. 10 (2020) 1657–1666. https://doi.org/10.1109/JPHOTOV.2019.2961615.

CHAPTER IV

TiO2/QDs for photoelectrochemical measurement: experimental and simulation study

Introduction

This chapter presents the physic-chemical characterization of the materials synthesized in this work. It is devoted to the structural and morphological properties of nanostructured titanium dioxide deposited on titanium metal plates decorated with core InP QDs, core/shell InP/ZnS QDs and core/shell/shell InP/ZnS/ZnS QDs. This part focuses more particularly on the morphology of Quantum Dots deposited by spin coating into TiO_2 with the aim to obtain good efficiency in the photocurrent response.

In the second part, we will see the numerical simulation which must include the different parameters concerning the photovoltaic cells. This step is very important, because it allows us to enhance the performance of our solar cells. This last part is therefore based on the simulation and results obtained for the core/shell InP/ZnS quantum dots structure.

1 Characterization of TiO_2, TiO_2/InP, TiO_2/InP/ZnS and TiO_2/InP/ZnS/ZnS Quantum Dots nanostructures

1.1 Structural characterization

The crystallographic behavior of pure TiO_2 NTAs layers deposited on titanium metal plates unmodified and modified with Core $InP\ QDs$ and $Shell/Core\ InP/ZnS\ QDs$ and $Core/Shell/Shell\ InP/ZnS/ZnS$ QDs is characterized by X-ray diffraction (XRD) measurements as shown in Figure 4-1. Therefore, we can easily identify the group of peaks characteristic of the pure TiO_2 NTAs well crystalized in anatase phase at 2θ equal to 25.07° (101), 37.51° (103), 38.12° (004), 39.8° (112), 47.71° (200), 53.56° (105),54.79° (211),62.43° (204) ,68.46° (116) according to (JCPDS 21-1272) [15,134]. The peaks relating to the zinc blende $InP\ QDs$ crystal positioned at 2θ equal to 26.8°(111), 43.73°(220) and 51.7°(311) corresponding to

InP (JCPDS 32-0452) and ZnS (JCPDS 05-0566), respectively [100,126,157]. We notice well that, the intensity peaks of core/shell (1) and core /shell (2) are particularly increased compared to the core InP peak, suggesting the formation of Quantum Dots nanoparticles decorated on the surface of TiO_2 NTAs.

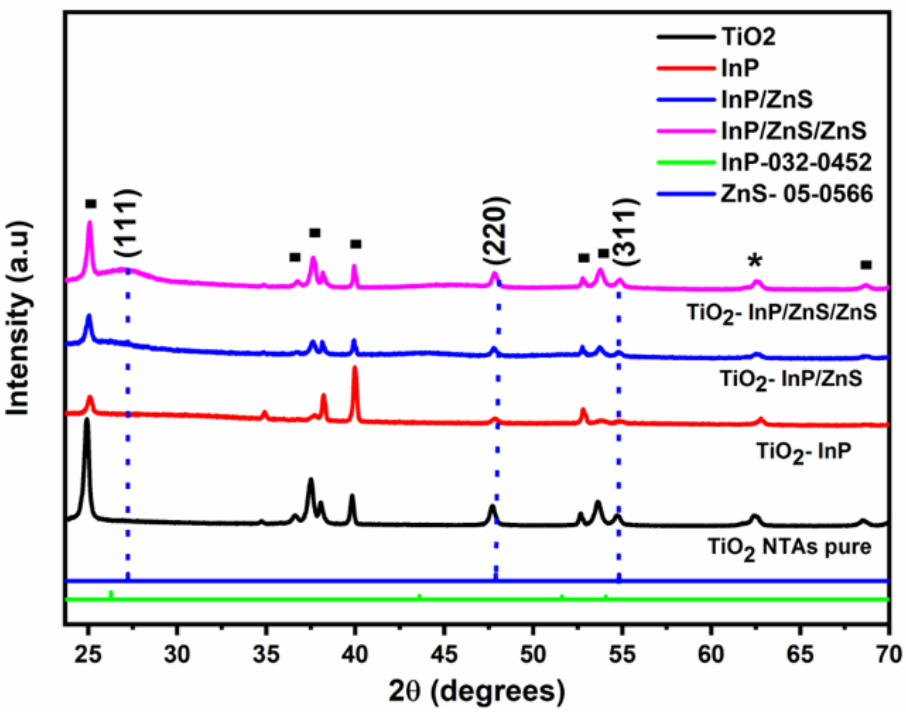

Figure 4-1: X-ray diffraction patterns of pure TiO_2 NTAs decorated with InP QDs, InP/ZnS QDs, and InP/ZnS/ZnS QDs.

1.2 Morphological characterization

To improve the performance of titanium oxide, it is necessary to control the morphology and nature of the crystalline layers developed in the material. Therefore, the morphology of the specific surface developed TiO_2-InP, TiO_2-InP/ZnS and TiO_2-InP/ZnS/ZnS were characterized by transmission electron microscopy (TEM) and by (FESM).

In Figure 4-2 (a) shows the HRFESM image of TiO_2 NTAs before and after surface modifications by core InP and $shell\ /core\ InP/ZnS\ QDs$ and $InP/ZnS/ZnS$ nanoparticles deposited by spin coating method. HRFSEM observation shows that the morphology of the

pure TiO_2 NTAs films has a better alignment and a highly ordered structure. Therefore a morphology similar to that described in the bibliography [118,134,158].

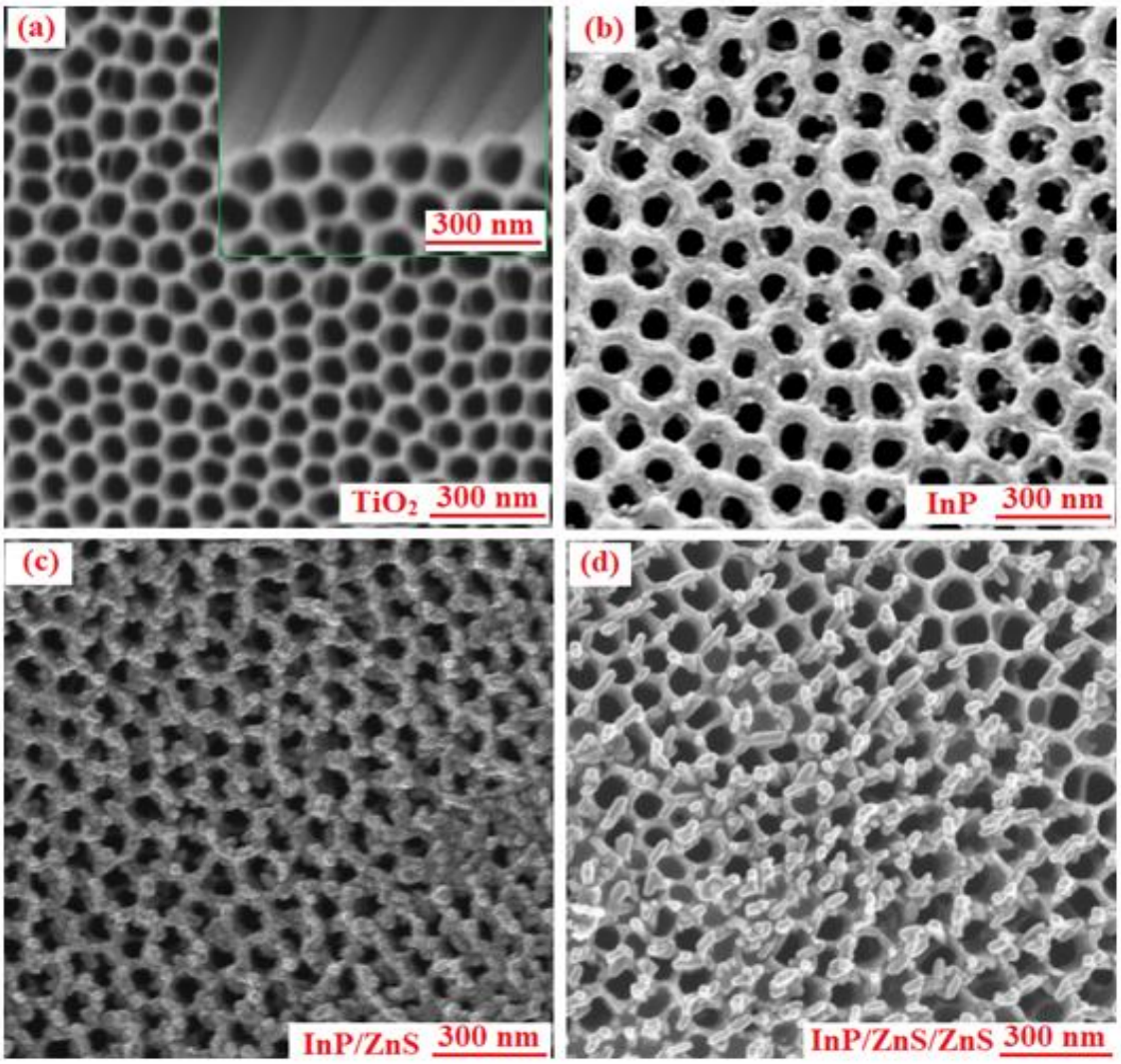

Figure 4-2: FSEM images showing top views of: (a) pure TiO_2 and (b,c,d) of InP QDs, InP/ZnS QDs, and InP/ZnS/ZnS QDs decorated TiO_2 NTAs.

Moreover, Figure 4-2 (b, c, d) shows the top of the nanotubes after decoration of Quantum Dots above the TiO_2 NTAs by spin coating method. For all the samples considered, nanoparticles are observed at the top of the nanotubes. It appears spherical nanoparticles with

a good dispersion of the Quantum Dots. This difference in morphology due to a shell growth of quantum dots.

These nanoparticles tend to agglomerate. It is difficult to estimate their size from these images, due to their agglomeration, but also because of the resolution of these images, limiting the possibility of precisely determine their diameter. It can nevertheless be estimated that these nanoparticles have an overall size of less than 20 nm. On other way, the characteristic peaks of the Quantum Dots are indeed present in the EDS spectra in Figure 4-3, confirming the presence of Ti, O, C, In, P, Zn, S.

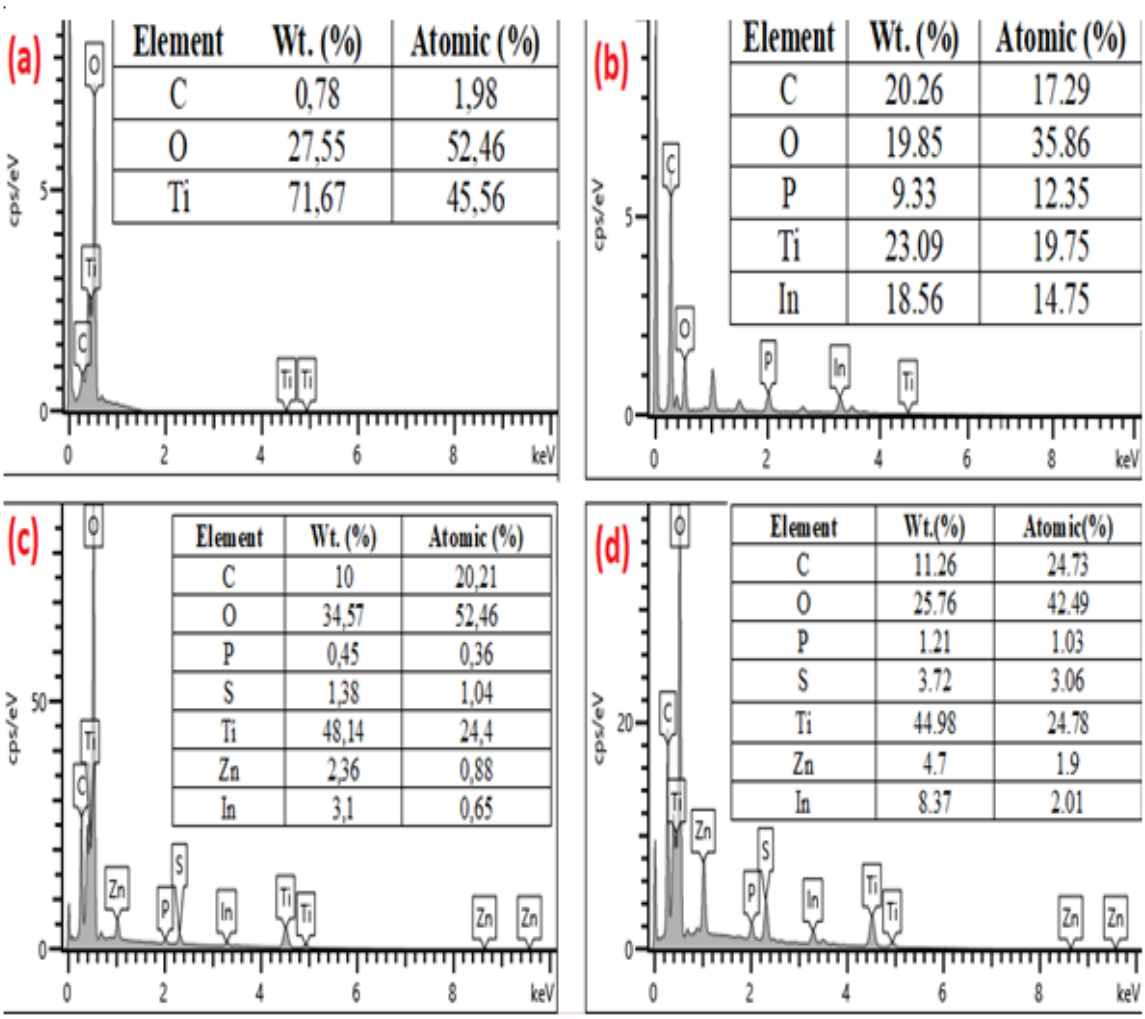

Figure 4-3: EDX analyses of EDS spectrum of (a) TiO_2 NTAs, (b) TiO_2/InP (c) TiO_2/InP/ZnS and (d) TiO_2/InP/ZnS/ZnS.

Additionally, we had use of transmission electron microscopy TEM to obtain further information on the morphology and distribution of the deposited nanoparticles. Figure 4-4 shows well deposited QDs on the oxide of titanium nanotubes presented us very small dark spot on the surface of nanotubes (red circles around the nanoparticles). Moreover, in Figures 4-4 provide further information on the crystallinity of the nanoparticles. We observe the inter-atomic distances of several zones. These interplanar distances are rather in good agreement with the plane of TiO_2 NTAS.

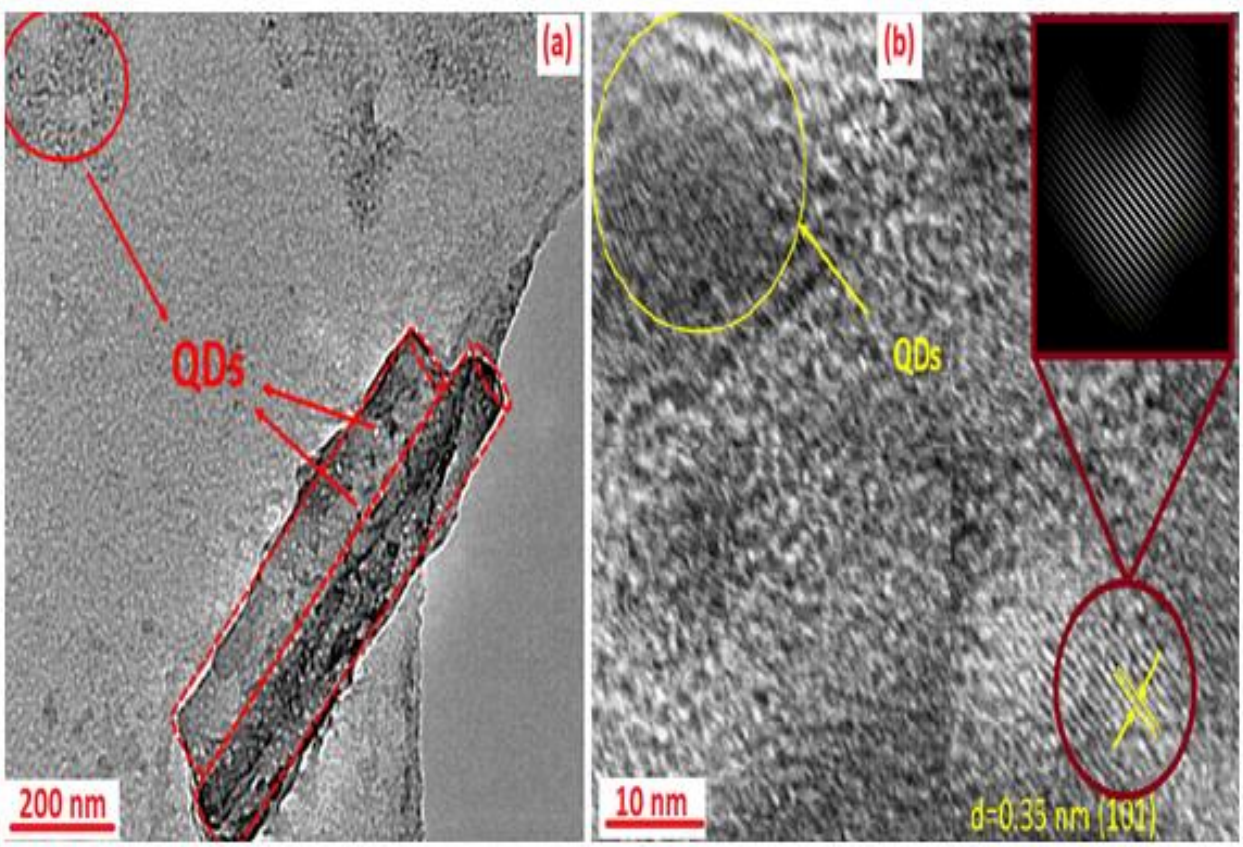

Figure 4-4: (a) TEM image of Quantum dots decorated TiO_2NTAs and (b) HR-TEM image showing lattice fringes of TiO_2 and Quantum Dots decorated TiO_2 NTAs.

1.3 Photoelectrochemical Performance

To investigate the photocurrent response of Quantum Dots decorated TiO_2 NTAs, the photoelectrochemical properties of TiO_2/InP QDs, TiO_2/InP/ZnS QDs and TiO_2/InP/ZnS films were recorded using a standard three-electrode PEC cell as shown in chapter 2. Both photoanodes were occasionally illuminated at a given potential (0.1976V) for several cycles to check the reproducibility of their photo responses using a Na2S 0.5M electrolyte. In the Figure 4-5(a), it was observed an immediate change in the current upon illumination. The photocurrent is instantly retracted to original values once the sample is illuminated or the light is switched off. This trend was repeated at each on-off cycle for 0.1976 V relative to the reference electrode (CE). It is understandably that InP/ZnS QDs are particularly useful to sensitize TiO_2 NTAs nanotubes (we used TiO_2 NTAs like a support), since we perceive a significant improvement in the photoelectrochemical properties of TiO_2/InP/ZnS QDs, TiO_2/InP/ZnS/ZnS QDs following the deposition by spin coating compared to TiO_2/InP QDs. The difference has been seen in the case of the sample TiO_2/InP/ZnS QDs with the value 2.14×10^{-6} mA/cm² and TiO_2/InP/ZnS/ZnS QDs with the value 3.10×10^{-6} mA/cm², and TiO_2/InP/ZnS/ZnS QDs, almost 4 and 6 times higher than TiO_2/InP/ZnS QDs, respectively. Hence, this measurement aims to observe the dynamic behavior of the material and to assess whether the charges recombine rapidly into the TiO_2 NTAs Nanotubes from the quantum dots. Therefore, the core/shell QDs and core/shell/shell QDs have good efficiency in the photocurrent response compared to core QDs due to the successful passivation of non-radiative recombination sites such as surface trap states as shown reported Onuralp Karatum and his collaborators [126][159]. Furthermore, to precisely estimate the rise and decay times, which are defined as the times it takes for a photodetector to reach 90% and fall to 10% of steady state values respectively in Figure 4-5(b). The device shows that TiO_2/InP, periodically illuminated, has a fast rise time (1s) and a fast fall time (1s). In contrast, TiO_2/InP/ZnS has a

slower rise time (2.8 s) and a slower fall time (2.8 s). TiO_2/InP showed a fast rise time (2.2 s) and a decay time (2.2 s) than TiO_2/InP/ZnS/ZnS. Trapped carriers in localized states limit the rise time and the decay time.

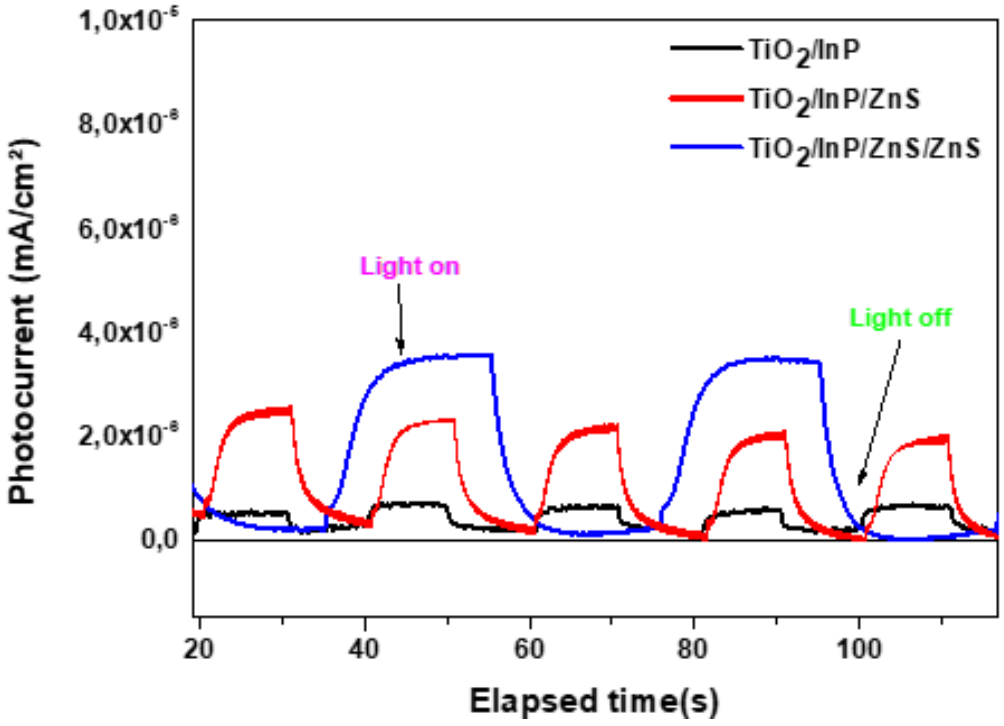

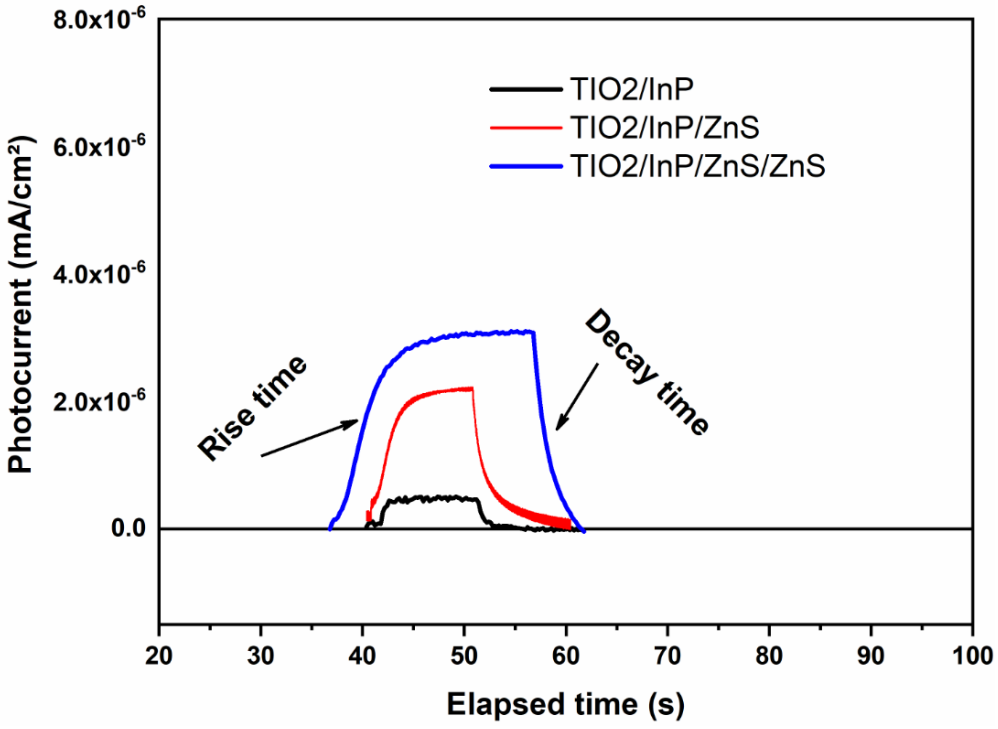

Figure 4-5: (a) Photocurrent response of TiO_2/InP, TiO_2/InP/ZnS and TiO_2/InP/ZnS/ZnS under applied potential of -0.1976 V dark and under illumination. (b) Time resolved photocurrent response of the device.

2 Numerical Analysis

2.1 Definition of simulation

Simulation is a tool used by the researcher to study the results of an action on an element without carrying out the experiment on the real element. By varying the parameters one by one and starting again with the same initial conditions. When the simulation tool uses a computer, it is called digital simulation. There have also been analogical simulators and it was envisaged in the 1970s to build stochastic ones. [160] It allows a more accurate assessment of the behavior of structures and materials with greater precision, thus enabling manufacturers to save costs for industry. However, calculation costs remain a limitation to the systematic industrial use of codes. Therefore, numerical techniques are continuously being improved. Numerical simulation is commonly used for solar cell optimization. Indeed, it has the following advantages:

- It avoids the need to manufacture several prototype cells with different parameters.

- It is independent of the technology used (the parameters can therefore be varied widely).

- The influence of each zone of the cell can be separated in the case of parameters (means mobility, diffusion length and lifetime).

Whatever the structure of a solar cell, an optimization of its parameters is necessary to predict its best performance before moving on to the technological phase.

Typically, the parameters to be optimized are cell thickness, doping levels and profiles, contact configuration and optical confinement.

2.2 Fundamental equations

The numerical simulation of photovoltaic structures consists of solving a set of equations that govern the electrostatic potential and the densities of the charge carriers in a specific simulation domain. This system of equations is solved using commercial software for the simulation of semiconductor devices. These equations which describe the physical phenomena within the photovoltaic cell are derived from Maxwell's equations.

They are mainly, Poisson's equation, continuity, and transport equations. The Poisson equation expresses the variation of the electrostatic field at local densities of local charge densities. [109][161]

2.3 Basic modeling equations

The basic equations are the Poisson equation, the two current equations and the two continuity equations. The Poisson equation relates the variations of the electrostatic potential to local charge densities. The continuity and transport equations describe how the electron and hole densities change as a function of transport, generation and transport, and recombination mechanisms. [12,13] The solution of these basic equations allows to find simultaneously the distributions of electrons, holes, potential and space charge. The numerical simulation is based on solving these three fundamentals equations which govern the charge transport in the semiconductors: Poisson equation and continuity equations for electrons and holes.

The detailed equation used is expressed in [162,163].

$$\frac{d^2\psi}{dx^2} = \frac{\partial E}{\partial x} = -\frac{\rho}{\varepsilon} = \frac{q}{\varepsilon}[p - n + N_D^+ - N_A^-] \qquad (4.1)$$

$$\frac{\partial J_n}{\partial x} + G_n - U_n(n,p) = 0 \tag{4.2}$$

$$-\frac{\partial J_p}{\partial x} + G_p - U_p(n,p) = 0 \tag{4.3}$$

Where $\varepsilon = \varepsilon_0 k_s$ is dielectric constant, (N_A^-, N_D^-) are doping densities, (n, p) are electron and holes densities, ψ is electrostatic potential, q is the electron charge, (J_n, J_p) are electron density and holes, G is the generation rate.

Charge carriers drift-diffusion equations are [164].

$$J_n = qn\mu_n\epsilon + qD_n\frac{\partial n}{\partial \chi} \tag{4.4}$$

$$J_p = qp\mu_p\epsilon - qD_p\frac{\partial p}{\partial \chi} \tag{4.5}$$

The Einstein diffusion equation describes that diffusion coefficient depends upon the carrier lifetime and mobility [165].

$$D_{(n,p)} = \sqrt{\mu_{(n,p)}\frac{kT}{q}\tau_{(n,p)}} \tag{4.6}$$

Where, (μ_p, μ_n) are carrier mobility, $\mu_{(n,p)}$ is the net recombination rate and $D_n \; and \; D_p$ are electron-hole diffusion coefficient.

2.4 Description and structure of device

The developed structure in this thesis was TiO_2/InP/ZnS. The taken structure comprised of n-type electrode TiO_2, slightly p-type photoactive methylammonium lead iodide InP layer, n-type electron transport layer ZnS [166,167]. The device was originally fabricated to analysis its effect on photocatalysis but to better understand the device physics we replicated the same structure in SCAPS-1d environment. In our work we used simulation at room temperature

with incidence light power density of 100mW/cm^2. The material physical input parameters are shown in Table 4.1

Table 4-1: Device physical parameters.

Parameters	InP (Absorber)	ZnS (ETM)
W (μm)	0.8	0.06
E_g (eV)	1.4	2.4
χ (eV)	4.170	4.5
or	12.5	9
$N_c(cm^{-3})$	2.2×1018	1.8×1019
N_v (cm^{-3})	1.8×1019	2.4×1018
n, p (cm^{-3})	1×1015 /1×1015	1×1017
μ_e (cm^2/Vs)	1000	100
μ_p (cm^2/Vs)	400	25

Now to analyze the effect of device parameters on solar cell performance we simulated the structure in SCAPS-1D. There were three different structure that were simulated in SCAPS-1D based on assumption taken from photocatalysis setup. The first structure consists of TiO_2/InP and in this TiO_2 was considered as a back electrode/substrate on which InP was deposited. The second structure TiO_2/InP/ZnS was used for simulation. In this setup of the device structure ZnS was considered as electron transport layer whereas InP was taken as absorber layer/active layer for solar cell with an assumption that while depositing a layer of ZnS on top of InP, we also doped InP with Zn ions at surface thus changing the conductivity of InP from intrinsic to a p-type material as given in the literature. The third structure of solar

cell is TiO_2/InP/ZnS/ZnS and results for JV characteristic along with quantum efficiency of solar cells are given in figure 4.6 and figure 4.7 below.

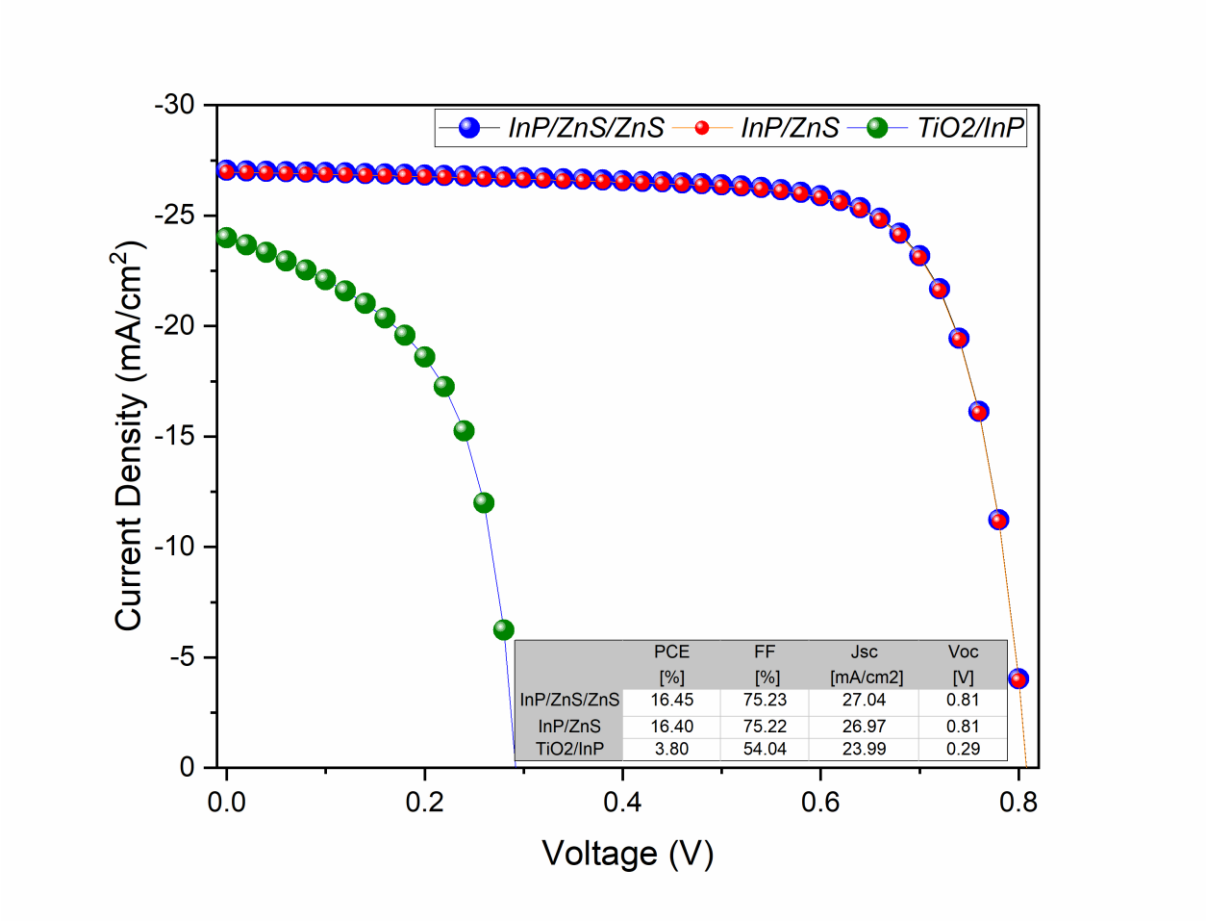

Figure 4-6: JV Characteristic curve for InP solar cell.

The results for JV characteristic curve of all three structure shows that performance of the device was enhanced by introducing a layer of ZnS on top of InP absorber layer as if effectively convert the absorb light in to charge carriers which are collected at the terminal. These results are also verified from the quantum efficiency (QE%) graph given in figure 4.7 below. The InP was able to successfully utilize the full spectrum of light when coated with ZnS layer on top. And adding an extra layer of ZnS on top of already deposited ZnS layer only introduces small changes in QE graph.

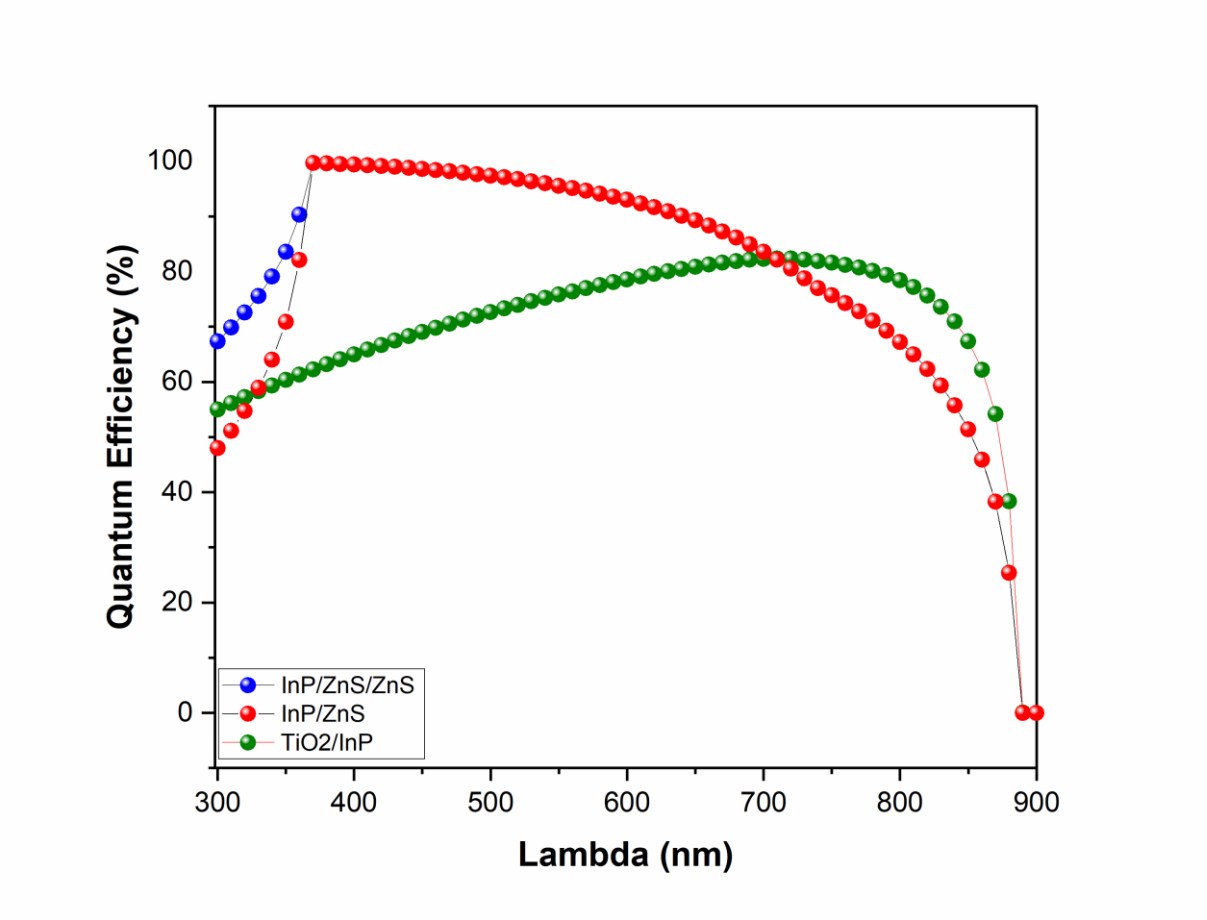

Figure 4-7: Quantum Efficiency of InP solar cell.

Conclusion

This chapter gathers the Physic-chemical characterizations of the nanostructured TiO_2/InP, TiO_2/InP/ZnS and TiO_2/InP/ZnS/ZnS films. XRD analysis of nanostructured TiO_2, deposited on metallic titanium plates, revealed the presence of the anatase phase in all samples. We also studied the influence on the structure and morphology of TiO_2 decorated with Quantum Dots. In this chapter, we presented the photoelectrochemical tests carried out on the TiO_2 nanotubes decorated by InP QDs, InP/ZnS QDs and InP/ZnS/ZnS QDs. The photoelectrochemical properties of prepared nanostructures were measured using a simple cell with a potentiostat and three electrodes. An improvement in photocurrent was observed after deposition of core/shell and core/shell/shell into TiO2 NATs. The increase in photocurrent is almost 4 and 6 times higher than TiO_2/InP QDs.

In a second step, we studied the effect of introducing ZnS layers on the layer of TiO_2/ InP by simulation method. During this process we used the TiO_2 as a back electrode/substrate. The simulation result showed that the addition of ZnS layer on top of InP absorber layer had a direct influence especially in JV characteristic curve. In addition, the adding of the second layer of ZnS on top of already deposited ZnS layer only introduced small changes in Quantum Efficiency result. Finally, based on the results, the ZnS layer increases the performance of InP/ TiO_2 QDS solar cells.

References

[1] S. Mahajan, M. Rani, R. Dubey, J. Mahajan, H. Ece, International Journal of Latest Research in Science and Technology, Int. J. Latest Res. Sci. Technol. 2 (2013) 518–521.

[2] C. Burda, X. Chen, R. Narayanan, M.A. El-sayed, Chemistry and Properties of Nanocrystals of Different Shapes, 2005.

[3] R. Koole, E. Groeneveld, D. Vanmaekelbergh, Size Effects on Semiconductor Nanoparticles, n.d. https://doi.org/10.1007/978-3-662-44823-6.

[4] F. Schulz, G.T. Dahl, S. Besztejan, M.A. Schroer, F. Lehmku, G. Gru, T. Vossmeyer, H. Lange, Ligand Layer Engineering To Control Stability and Interfacial Properties of Nanoparticles, (2016). https://doi.org/10.1021/acs.langmuir.6b01704.

[5] O. Yarema, M. Yarema, D. Bozyigit, W.M.M. Lin, V. Wood, Independent Composition and Size Control for Highly Luminescent Indium-Rich Silver Indium Selenide, (2015) 11134–11142. https://doi.org/10.1021/acsnano.5b04636.

[6] K.D. Wegner, F. Dussert, D. Truffier-boutry, A. Benayad, Influence of the Core / Shell Structure of Indium Phosphide Based Quantum Dots on Their Photostability and Cytotoxicity, 7 (2019) 1–12. https://doi.org/10.3389/fchem.2019.00466.

[7] C.A.S. No, Agents Classified by the IARC Monographs , Volumes 1 – 132, (2012).

[8] J.O. Uif, T. Rvbouvn, D. Sfhjnf, 1BTU QSFTFOU BOE GVUVSF PG JOEJVN QIPTQIJEF RVBOUVN EPUT, 15 (2022) 4468–4489.

[9] P. Ramasamy, K. Ko, J. Kang, J. Lee, Two-Step " Seed-Mediated " Synthetic Approach to Colloidal Indium Phosphide Quantum Dots with High-Purity Photo- and Electroluminescence, (2018). https://doi.org/10.1021/acs.chemmater.8b02049.

[10] V. Brunetti, H. Chibli, R. Fiammengo, A. Galeone, M.A. Malvindi, G. Vecchio, R. Cingolani, L. Nadeau, P. Paolo, quantum dots : in vitro and in vivo toxicity assessment, (2013) 307–317. https://doi.org/10.1039/c2nr33024e.

[11] D.A.G. Ramirez, J.S.A. Cerón, M.L.G. Herrera, J.P.L. Arias, M.P. González, Effect of the indium myristate precursor concentration on the structural , optical , chemical surface , and electronic properties of InP quantum dots passivated with ZnS, J. Mater. Sci. Mater. Electron. 30 (2019) 4885–4894. https://doi.org/10.1007/s10854-019-00783-6.

[12] Q. Zhou, J. Zhou, M. Zeng, G. Wang, Y. Chen, S. Lin, Photoelectrochemical Performance of Quantum dot-Sensitized TiO 2 Nanotube Arrays : a Study of Surface Modification by Atomic Layer Deposition Coating, (2017). https://doi.org/10.1186/s11671-017-2036-6.

[13] M. Ni, M.K.H.L. Ã, D.Y.C. Leung, K. Sumathy, A Review and Recent Developments in Photocatalytic Water-Splitting Using TiO2 for Hydrogen Production A review and recent developments in photocatalytic water-splitting using TiO 2 for hydrogen production, (2007). https://doi.org/10.1016/j.rser.2005.01.009.

[14] L.B. Hoch, P. Szymanski, K. Kaur, L. He, K. Liao, Q. Qiao, L.M. Reyes, Carrier dynamics and the role of surface defects : Designing a photocatalyst for gas-phase CO 2 reduction, (2016) 8011–8020. https://doi.org/10.1073/pnas.1609374113.

[15] Black Anatase TiO 2 Nanotubes with Tunable Orientation for High Performance Supercapacitors, (2019). https://doi.org/10.1021/acs.jpcc.9b05070.

[16] N. Cross, D.J. Woodsworth, Investigating the Electronic Properties of a Carbon, (2008).

[17] A.E. Commission, P. Reiss, A.E. Commission, J. Villain, Dans un laboratoire de nanosciences, (2011).

[18] U. Resch-genger, M. Grabolle, S. Cavaliere-jaricot, R. Nitschke, T. Nann, Quantum dots versus organic dyes as fluorescent labels, 5 (2008) 763–775. https://doi.org/10.1038/NMETH.1248.

[19] P. Reiss, M. Carrie, C. Lincheneau, L. Vaure, S. Tamang, Synthesis of Semiconductor Nanocrystals , Focusing on Nontoxic and Earth-Abundant Materials, (2016). https://doi.org/10.1021/acs.chemrev.6b00116.

[20] R. Saran, R.J. Curry, technologies, Nat. Publ. Gr. 10 (2016). https://doi.org/10.1038/nphoton.2015.280.

[21] M.A. Reed, R.J. Aggarwal, R.J. Matyi, T.M. Moore, A.E. Wetsel, Physical review, 60 (1988).

[22] C. Cea, Les nanocristaux semi-conducteurs fluorescents font leur gamme, (2005).

[23] M.T. Clarke, F.N. Viscomi, T.W. Chamberlain, N. Hondow, A.M. Adawi, J. Sturge, S.C. Erwin, J.G. Bouillard, S. Tamang, G.J. Stasiuk, colloidal quantum dots through thermal diffusion, Commun. Chem. (n.d.). https://doi.org/10.1038/s42004-019-0138-z.

[24] F.O.R.T.W. Orth, T. Exas, Q. Aprimer, QuantumDots: APrimer, (n.d.).

[25] Y. Wan, J. Norman, J. Bowers, Quantum dot microcavity lasers on silicon substrates, 1st ed., Elsevier Inc., 2019. https://doi.org/10.1016/bs.semsem.2019.05.002.

[26] Z.I. Alferov, The history and future of semiconductor heterostructures, (1998) 1–14.

[27] V. Biju, T. Itoh, A. Anas, Semiconductor quantum dots and metal nanoparticles : syntheses , optical properties , and biological applications, (2008) 2469–2495. https://doi.org/10.1007/s00216-008-2185-7.

[28] A. Physics, Optical Properties of Semiconductor Nanocrystals Cambridge Studies in Modern Optics, n.d.

[29] N. Fernández-delgado, M. Herrera, A.H. Tavabi, M. Luysberg, R.E. Dunin-borkowski, Applied Surface Science Structural and chemical characterization of CdSe-ZnS core-shell quantum dots, Appl. Surf. Sci. 457 (2018) 93–97. https://doi.org/10.1016/j.apsusc.2018.06.149.

[30] Q. Zhao, P.A. Graf, W.B. Jones, A. Franceschetti, J. Li, L. Wang, K. Kim, Shape Dependence of Band-Edge Exciton Fine Structure in CdSe Nanocrystals, (2007).

[31] I. Review, " 5 = 5;„ +, 75 (1995) 3728–3731.

[32] A.L. Rogach, No Title, n.d.

[33] M. Rosen, M. Kuno, M. Nirmal, D.J. Norris, M. Bawendi, Band-edge exciton in quantum dots of semiconductors with a degenerate valence band: Dark and bright exciton states, 54 (1996) 4843–4856.

[34] O. Stier, M. Grundmann, D. Bimberg, Electronic and optical properties of strained quantum dots modeled by 8-band k – p theory, 59 (1999) 5688–5701.

[35] A. Franceschetti, A. Zunger, Pseudopotential calculations of electron and hole addition spectra of InAs , InP , and Si quantum dots, 62 (2000) 2614–2623.

[36] E. Alkhazraji, A.M. Ragheb, M.A. Esmail, Q. Tareq, H. Fathallah, Electro-absorption and Electro-optic Characterization of L-Band InAs / InP Quantum-dash Waveguide, (2020). https://doi.org/10.1109/JPHOT.2020.2988584.

[37] M.D. Tessier, D. Dupont, K. De Nolf, J. De Roo, Z. Hens, Economic and Size-Tunable Synthesis of InP/ZnE (E = S, Se) Colloidal Quantum Dots., Chem. Mater. 27 (2015) 4893–4898. https://doi.org/10.1021/acs.chemmater.5b02138.

[38] A.M. Nightingale, J.C. DeMello, Improving the ensemble optical properties of InP quantum dots by indium precursor modification, J. Mater. Chem. C. 4 (2016) 8454–8458. https://doi.org/10.1039/C6TC02910H.

[39] D. V Talapin, J. Lee, M. V Kovalenko, E. V Shevchenko, Prospects of Colloidal Nanocrystals for Electronic and Optoelectronic Applications, (2010) 389–458.

[40] V.A. Online, L. Lai, L. Protesescu, M. V Kovalenko, M.A. Loi, Sensitized solar cells with colloidal PbS–CdS core–shell quantum dots †, (2014) 736–742. https://doi.org/10.1039/c3cp54145b.

[41] B. Chen, D. Li, F. Wang, InP Quantum Dots : Synthesis and Lighting Applications, 2002454 (2020) 1–20. https://doi.org/10.1002/smll.202002454.

[42] M.A. Ellis, G. Grandinetti, K.M. Fichter, Synthesis of Cd-free InP/ZnS Quantum Dots Suitable for Biomedical Applications, J. Vis. Exp. (2016). https://doi.org/10.3791/53684.

[43] T.-R. Kuo, S.-T. Hung, Y.-T. Lin, T.-L. Chou, M.-C. Kuo, Y.-P. Kuo, C.-C. Chen, Green Synthesis of InP/ZnS Core/Shell Quantum Dots for Application in Heavy-Metal-Free Light-Emitting Diodes, Nanoscale Res. Lett. 12 (2017) 537. https://doi.org/10.1186/s11671-017-2307-2.

[44] L.C. Lines, W. Jiang, Z. Yang, G. Lin, Cytotoxicity of InP / ZnS Quantum Dots With Different Surface Functional Groups Toward Two, 9 (2018) 1–12. https://doi.org/10.3389/fphar.2018.00763.

[45] H. Sengul, COMPARATIVE ASSESSMENT OF PHASE TRANSFER BEHAVIOUR OF INP / ZNS , Environmental Science Nano Comparative assessment of the phase transfer dots and CdSe / ZnS quantum dots under varying, (2019). https://doi.org/10.1039/C8EN01073K.

[46] V. Brunetti, I. Italiano, V. Brunetti, H. Chibli, R. Fiammengo, A. Galeone, M.A. Malvindi, G. Vecchio, R. Cingolani, J.L. Nadeau, P.P. Pompa, InP/ZnS as a safer alternative to CdSe/ZnS core/shell quantum dots: In vitro and in vivo toxicity assessment, (2012). https://doi.org/10.1039/c2nr33024e.

[47] B.J.M. Klostranec, W.C.W. Chan, Quantum Dots in Biological and Biomedical

Research : Recent Progress and Present Challenges, (n.d.). https://doi.org/10.1002/adma.200500786.

[48] H. Chibli, L. Carlini, S. Park, M. Dimitrijevic, J.L. Nadeau, Nanoscale Cytotoxicity of InP / ZnS quantum dots related to reactive oxygen species generation, (2011) 2552–2559. https://doi.org/10.1039/c1nr10131e.

[49] S. Tamang, C. Lincheneau, Y. Hermans, S. Jeong, P. Reiss, Chemistry of InP Nanocrystal Syntheses, Chem. Mater. 28 (2016) 2491–2506. https://doi.org/10.1021/acs.chemmater.5b05044.

[50] M. Green, S olution routes to III – V semiconductor quantum dots q, 6 (2002) 355–363.

[51] J. Jasinski, V.J. Leppert, S. Lam, G.A. Gibson, K. Nauka, C.C. Yang, Z. Zhou, Rapid oxidation of InP nanoparticles in air, 141 (2007) 624–627. https://doi.org/10.1016/j.ssc.2006.12.033.

[52] L. Li, P. Reiss, One-pot Synthesis of Highly Luminescent InP / ZnS Nanocrystals without, (2008) 11588–11589.

[53] G.O. Eren, S. Sadeghi, H. Bahmani Jalali, M. Ritter, M. Han, I. Baylam, R. Melikov, A. Onal, F. Oz, M. Sahin, C.W. Ow-Yang, A. Sennaroglu, R.T. Lechner, S. Nizamoglu, Cadmium-Free and Efficient Type-II InP/ZnO/ZnS Quantum Dots and Their Application for LEDs, ACS Appl. Mater. Interfaces. 13 (2021) 32022–32030. https://doi.org/10.1021/acsami.1c08118.

[54] D. V Talapin, A.L. Rogach, A. Kornowski, M. Haase, H. Weller, Highly Luminescent Monodisperse CdSe and CdSe / ZnS Nanocrystals Synthesized in a Hexadecylamine − Trioctylphosphine Oxide − Trioctylphospine Mixture, (2001).

[55] N. York, Visible Light Induced Hydrogen Production from in Situ Generated Colloidal Rhodium-Coated Cadmium Sulfide in Surfactant Vesicles Clarkson College of Technology Isolation from Pistacia Resins of a Bicyclic Triterpenoid Representing an Apparent Trapped, (2000) 2475–2476.

[56] A. Henglein, Small-Particle Research : Physicochemical Properties of Extremely Small Colloidal Metal and Semiconductor Particles, (1989).

[57] G.M. Wallraff, W.D. Hinsberg, Lithographic Imaging Techniques for the Formation of Nanoscopic Features, (1999).

[58] P.M. Petroff, A. Lorke, A. Imamoglu, E PITAXIALLY S ELF -A SSEMBLED Q UANTUM D OTS, 46 (2020). https://doi.org/10.1063/1.1381102.

[59] B.D. Ingert, M. Pileni, Limitations in Producing Nanocrystals Using Reverse Micelles as Nanoreactors **, 5 (2001) 136–139.

[60] A.P. Alivisatos, Perspectives on the Physical Chemistry of Semiconductor Nanocrystals, 3654 (1996) 13226–13239.

[61] C.B. Murray, D.J. Norris, M.G. Bawendi, Synthesis and Characterization of Nearly Monodisperse CdE (E = S , Se , Te) Semiconductor Nanocrystallites, (1993) 8706–8715.

[62] M. Bayer, E.H. Sargent, Semiconductor quantum dots: Technological progress and future challenges, 8541 (2021). https://doi.org/10.1126/science.aaz8541.

[63] L. Qu, X. Peng, Control of Photoluminescence Properties of CdSe Nanocrystals in Growth, 124 (2018) 2016–2018.

[64] S.G. Hickey, S.F. Wuister, D. Vanmaekelbergh, Single-Step Synthesis to Control the Photoluminescence Quantum Yield and Size Dispersion of CdSe Nanocrystals, (2003) 489–496.

[65] S. Lee, K. Lee, J. Jo, B. Park, Y. Kwon, S. Jang, H. Yang, emitting diode based on InP quantum dot color converters, 4 (2014) 1297–1302. https://doi.org/10.1364/OME.4.001297.

[66] L. Qu, Z.A. Peng, X. Peng, Alternative Routes toward High Quality CdSe Nanocrystals, (2001) 1–5.

[67] C.R. Bullen, P. Mulvaney, Nucleation and Growth Kinetics of CdSe Nanocrystals in Octadecene, (2004).

[68] P. Reiss, G. Quemard, S. Carayon, J. Bleuse, F. Chandezon, A. Pron, Luminescent ZnSe nanocrystals of high color purity, 84 (2004) 10–13. https://doi.org/10.1016/j.matchemphys.2003.11.002.

[69] X. Zhong, Y. Feng, W. Knoll, M. Han, Alloyed Zn x Cd 1 - x S Nanocrystals with Highly Narrow Luminescence Spectral Width, (2003) 13559–13563.

[70] D.W. Lucey, D.J. Macrae, M. Furis, Y. Sahoo, A.N. Cartwright, P.N. Prasad, Monodispersed InP Quantum Dots Prepared by Colloidal Chemistry in a Noncoordinating Solvent, (2005) 3754–3762.

[71] D. Battaglia, X. Peng, Formation of High Quality InP and InAs Nanocrystals in a Noncoordinating Solvent, (2002) 1–4.

[72] J. Jasieniak, C. Bullen, J. Van Embden, P. Mulvaney, Phosphine-Free Synthesis of CdSe Nanocrystals, (2005) 20665–20668.

[73] S. Sapra, A.L. Rogach, J. Feldmann, Phosphine-free synthesis of monodisperse CdSe nanocrystals in olive oil, (2006) 3391–3395. https://doi.org/10.1039/b607022a.

[74] G.G. Yordanov, G.D. Gicheva, B.H. Bochev, C.D. Dushkin, E. Adachi, The effects of temperature and carboxylic acid ligand on the growth of nanocrystalline CdSe in a hot paraffin matrix, 273 (2006) 10–15. https://doi.org/10.1016/j.colsurfa.2005.07.036.

[75] J. Park, J. Joo, S.G. Kwon, Y. Jang, T. Hyeon, Synthesis of Monodisperse Spherical Nanocrystals Angewandte, (2007) 4630–4660. https://doi.org/10.1002/anie.200603148.

[76] R.H. Dinegar, JOURNAL OF THE, 72 (1950).

[77] F. Wang, V.N. Richards, S.P. Shields, W.E. Buhro, Kinetics and Mechanisms of Aggregative Nanocrystal Growth, (2014). https://doi.org/10.1021/cm402139r.

[78] X. Peng, J. Wickham, A.P. Alivisatos, Kinetics of II-VI and III-V Colloidal Semiconductor Nanocrystal Growth : " Focusing " of Size Distributions, 7863 (1998) 5343–5344.

[79] O.I. Micic, C.J. Curtis, K.M. Jones, J.R. Sprague, A.J. Nozik, Synthesis and Characterization of InP Quantum Dots, (1994) 4966–4969.

[80] A.A. Guzelian, J.E.B. Katari, A. V Kadavanich, U. Banin, K. Hamad, E. Juban, A.P.

Alivisatos, R.H. Wolters, C.C. Arnold, J.R. Heath, Synthesis of Size-Selected , Surface-Passivated InP Nanocrystals, (1996) 7212–7219.

[81] O.I. Mic, Synthesis of extremely small InP quantum dots and electronic coupling in their disordered solid films, 4022 (2005). https://doi.org/10.1063/1.1379990.

[82] S. Xu, S. Kumar, T. Nann, Rapid Synthesis of High-Quality InP Nanocrystals, (2006) 1054–1055.

[83] J.A. Gerbec, D. Magana, A. Washington, G.F. Strouse, Microwave-Enhanced Reaction Rates for Nanoparticle Synthesis, (2005) 15791–15800.

[84] D.D. Lovingood, G.F. Strouse, Microwave Induced In-Situ Active Ion Etching of Growing InP Nanocrystals, (2008) 4–7.

[85] C. Li, M. Ando, N.M. Ã, Facile Preparation of Highly Luminescent InP Nanocrystals by a Solvothermal Route, 37 (2008) 856–857. https://doi.org/10.1246/cl.2008.856.

[86] W.S.H. Lee, J. Chul, Amine-derived synthetic approach to color-tunable InP / ZnS quantum dots with high fluorescent qualities, (2013). https://doi.org/10.1007/s11051-013-1750-y.

[87] W. Song, S. Lee, H. Yang, Fabrication of warm , high CRI white LED using non-cadmium quantum dots, 3 (2013) 1468–1473. https://doi.org/10.1364/OME.3.001468.

[88] O.I. Micié, J.R. Sprague, C.J. Curtis, K.M. Jones, J.L. Machol, A.J. Nozik, H. Giessen, B. Fluegel, G. Mohs, N. Peyghambarian, Synthesis and Characterization of InP , GaP , and GalnPi Quantum Dots, (1995) 7754–7759.

[89] O.B. Achorn, D. Franke, M.G. Bawendi, Seedless Continuous Injection Synthesis of Indium Phosphide Quantum Dots as a Route to Large Size and Low Size Dispersity, Chem. Mater. 32 (2020) 6532–6539. https://doi.org/10.1021/acs.chemmater.0c01906.

[90] S. Mahajan, M. Rani, R.B. Dubey, J. Mahajan, SYNTHESIS OF CdSe CRYSTAL USING HOT INJECTION METHOD, Int. J. Latest Res. Sci. Technol. 2 (2013) 518–521.

[91] J. Ministro, A study on the synthesis and the optical properties of InP-based quantum dots, University Gent, n.d.

[92] S.B. Brichkin, Synthesis and properties of colloidal indium phosphide quantum dots, Colloid J. 77 (2015) 393–403. https://doi.org/10.1134/S1061933X15040043.

[93] E.S. Cde, J. Te, A.C. Soc, Murray, C.B., Norris, D.J. & Bawendi, M.G. Synthesis and characterization of nearly monodisperse CdE (E = S, Se, Te) semiconductor nanocrystallites. J. Am. Chem. Soc. 115, 8706 − 871..., (2021). https://doi.org/10.1021/ja00072a025.

[94] X. Peng, L. Manna, W. Yang, J. Wickham, Shape control of CdSe nanocrystals, 404 (2000) 59–61.

[95] L. Manna, E.C. Scher, A.P. Alivisatos, R. V August, Synthesis of Soluble and Processable Rod- , Arrow- , Teardrop- , and Tetrapod-Shaped CdSe Nanocrystals, (2000) 12700–12706.

[96] V.F. Puntes, D. Zanchet, C.K. Erdonmez, A.P. Alivisatos, Synthesis of hcp-Co Nanodisks, (2002) 12874–12880.

[97] S. Ithurria, B. Dubertret, Quasi 2D Colloidal CdSe Platelets with Thicknesses Controlled at the Atomic Level, (2008) 16504–16505.

[98] H. Qian, L. Li, J. Ren, One-step and rapid synthesis of high quality alloyed quantum dots (CdSe – CdS) in aqueous phase by microwave irradiation with controllable temperature, 40 (2005) 1726–1736. https://doi.org/10.1016/j.materresbull.2005.05.022.

[99] P. Ramasamy, B. Kim, M.-S. Lee, J.-S. Lee, Beneficial effects of water in the colloidal synthesis of InP/ZnS core–shell quantum dots for optoelectronic applications, Nanoscale. 8 (2016) 17159–17168. https://doi.org/10.1039/C6NR04713K.

[100] W.A.C. Hen, W.E.W. Ang, L.E.I.S. Un, S.H.C. Hen, Q.U.N.Y. An, T.A.G. Uo, X.I.Z. Hou, C. Haoxing, Y.O.Z. Hang, Synthesis and characterization of InP / ZnSe / ZnS quantum dots for photo-emissive color conversion, 12 (2022) 1717–1730.

[101] A.J. Zavaraki, Q. Liu, H. Ågren, Nano-Structures & Nano-Objects Solar cell sensitized with ‘“ green ”’ InP-ZnS quantum dots : Effect of ZnS shell deposition, Nano-Structures & Nano-Objects. 22 (2020) 100461. https://doi.org/10.1016/j.nanoso.2020.100461.

[102] S.T. Quenching, Suppressed Thermal Quenching, (2021).

[103] N. Mordvinova, A. Vinokurov, T. Kuznetsova, O.I. Lebedev, S. Dorofeev, Highly luminescent core-shell InP/ZnX (X = S, Se) quantum dots prepared: Via a phosphine synthetic route, Dalt. Trans. 46 (2017) 1297–1303. https://doi.org/10.1039/c6dt03956a.

[104] M. Jiang, Y. Li, S. Li, H. Zhou, X. Cao, S. Bao, Y. Gao, H. Luo, P. Jin, Room Temperature Optical Constants and Band Gap Evolution of Phase Pure M 1 -VO 2 Thin Films Deposited at Different Oxygen Partial Pressures by Reactive Magnetron Sputtering, J. Nanomater. 2014 (2014) 1–6. https://doi.org/10.1155/2014/183954.

[105] A. Bouzidi, N. Benramdane, A. Nakrela, C. Mathieu, B. Khelifa, R. Desfeux, A. Da Costa, First synthesis of vanadium oxide thin films by spray pyrolysis technique, Mater. Sci. Eng. B. 95 (2002) 141–147. https://doi.org/10.1016/S0921-5107(02)00224-6.

[106] B. Lambert, B. Deveaud, Y. Toudic, G. Pelous, J.C. Paris, G. Grandpierre, Properties of vanadium in InP, Solid State Commun. 47 (1983) 337–340. https://doi.org/10.1016/0038-1098(83)90914-6.

[107] C. Lamsal, N.M. Ravindra, Optical properties of vanadium oxides-an analysis, J. Mater. Sci. 48 (2013) 6341–6351. https://doi.org/10.1007/s10853-013-7433-3.

[108] D. Collection, Modeling Radiation Effects on a Triple Junction Solar Cell using Silvaco ATLAS NAVAL POSTGRADUATE, (2012).

[109] P. Cedex, SPECTROSCOPIC INVESTIGATION OF VANADIUM IN lnP B. CLERJAUD, D. COTE and C. NAUD, 83 (1987) 194–197.

[110] J.C. Paris, PROPERTIES OF V A N A D I U M IN InP I +, 47 (1983) 337–340.

[111] M.A. Shafi, H. Ullah, S. Ullah, L. Khan, S. Bibi, B.M. Soucase, Numerical Simulation of Lead-Free Sn-Based Perovskite Solar Cell by Using SCAPS-1D †, (2022) 1–5.

[112] J.A. Dias, S.H. Santagneli, S.J.L. Ribeiro, Y. Messaddeq, Perovskite Quantum Dot Solar Cells : An Overview of the Current Advances and Future Perspectives, 2100205 (2021) 1–28. https://doi.org/10.1002/solr.202100205.

[113] W. Zhang, S. Ding, W. Zhuang, D. Wu, P. Liu, X. Qu, H. Liu, H. Yang, Z. Wu, K. Wang, X.W. Sun, InP / ZnS / ZnS Core / Shell Blue Quantum Dots for Efficient Light-Emitting Diodes, (n.d.). https://doi.org/10.1002/adfm.202005303.

[114] H.I. Ikeri, A.I. Onyia, P.U. Asogwa, Investigation Of Optical Characteristics Of Semiconductor Quantum Dots For Multi Junction Solar Cells Applications ., 8 (2019) 3531–3535.

[115] A.M. Smith, S. Nie, Semiconductor Nanocrystals : Structure , Properties , and Band Gap Engineering, (2010).

[116] P. Reiss, S. Carayon, J. Bleuse, A. Pron, Low polydispersity core / shell nanocrystals of CdSe / ZnSe and CdSe / ZnSe / ZnS type : preparation and optical studies, 139 (2003) 649–652. https://doi.org/10.1016/S0379-6779(03)00335-7.

[117] M. Ando, M. Horie, Y. Akazawa-ogawa, Y. Hagihara, N. Murase, Y. Shigeri, Cytotoxicity of CdSe-based quantum dots incorporated in glass nanoparticles evaluated using human keratinocyte HaCaT cells, Biosci. Biotechnol. Biochem. 8451 (2016) 1–4. https://doi.org/10.1080/09168451.2015.1069702.

[118] A. Ghicov, P. Schmuki, Self-ordering electrochemistry : a review on growth and functionality of TiO 2 nanotubes and other self-aligned MO x structures, (2009) 2791–2808. https://doi.org/10.1039/b822726h.

[119] H.E. Prakasam, K. Shankar, M. Paulose, O.K. Varghese, C.A. Grimes, ARTICLES A New Benchmark for TiO 2 Nanotube Array Growth by Anodization, (2007) 7235–7241.

[120] V. Zwilling, M. Aucouturier, E. Darque-ceretti, Anodic oxidation of titanium and TA6V alloy in chromic media . An electrochemical approach, 45 (1999) 921–929.

[121] S. Kobayashi, K. Hanabusa, Preparation of TiO 2 Hollow-Fibers Using Supramolecular Assemblies Seiji Shinkai Porous , nanostructured materials have attracted considerable attention because of their potential ap- materials is quite difficult . Nanostructured inorganic cationic charge moieties with the expectation that the, (2000) 1523–1525.

[122] J.M. Macak, H. Tsuchiya, A. Ghicov, K. Yasuda, R. Hahn, S. Bauer, P. Schmuki, TiO 2 nanotubes : Self-organized electrochemical formation , properties and applications, 11 (2007) 3–18. https://doi.org/10.1016/j.cossms.2007.08.004.

[123] C. Ruan, M. Paulose, O.K. Varghese, G.K. Mor, C.A. Grimes, Fabrication of Highly Ordered TiO 2 Nanotube Arrays Using an Organic Electrolyte, (2005) 15754–15759.

[124] K. Lee, A. Mazare, P. Schmuki, One-Dimensional Titanium Dioxide Nanomaterials : Nanotubes, (2014).

[125] V. Shrotriya, G. Li, Y. Yao, C. Chu, Y. Yang, Transition metal oxides as the buffer layer for polymer photovoltaic cells Transition metal oxides as the buffer layer for polymer photovoltaic cells, (2006) 1–4. https://doi.org/10.1063/1.2174093.

[126] O. Karatum, M.M. Aria, G.O. Eren, E. Yildiz, E.D. Glowacki, Nanoengineering InP Quantum Dot-Based Photoactive Biointerfaces for Optical Control of Neurons, 15 (2021) 1–14. https://doi.org/10.3389/fnins.2021.652608.

[127] A. Zaban, O.I. Mic, B.A. Gregg, A.J. Nozik, Photosensitization of Nanoporous TiO 2 Electrodes with InP Quantum Dots, 7463 (1998) 3153–3156.

[128] H.B. Jalali, M.M. Aria, U.M. Dikbas, S. Sadeghi, E ff ective Neural Photostimulation Using Indium-Based Type-II Quantum Dots, (2018). https://doi.org/10.1021/acsnano.8b02976.

[129] H. Zhao, X. Li, M. Cai, C. Liu, Y. You, R. Wang, A.I. Channa, F. Lin, D. Huo, G. Xu, X. Tong, Z.M. Wang, Role of Copper Doping in Heavy Metal-Free InP / ZnSe Core / Shell Quantum Dots for Highly Efficient and Stable Photoelectrochemical Cell, 2101230 (2021) 1–10. https://doi.org/10.1002/aenm.202101230.

[130] M.T. Clarke, F.N. Viscomi, T.W. Chamberlain, N. Hondow, A.M. Adawi, J. Sturge, S.C. Erwin, J.-S.G. Bouillard, S. Tamang, G.J. Stasiuk, Synthesis of super bright indium phosphide colloidal quantum dots through thermal diffusion, Commun. Chem. 2 (2019) 36. https://doi.org/10.1038/s42004-019-0138-z.

[131] T.K. Nideep, M. Ramya, M.M. Varier, M. Kailasnath, A Study of Nonlinear Optical Property of Cadmium Based Quantum Dots with Comparable Particle Size, Springer Singapore, n.d. https://doi.org/10.1007/978-981-15-9259-1.

[132] S. Kobayashi, N. Hamasaki, M. Suzuki, M. Kimura, H. Shirai, K. Hanabusa, Preparation of Helical Transition-Metal Oxide Tubes Using Organogelators as Structure-Directing Agents, 1 (2002) 6550–6551.

[133] Z. Miao, D. Xu, J. Ouyang, G. Guo, X. Zhao, Electrochemically Induced Sol − Gel Preparation of Single-Crystalline TiO 2 Nanowires, (2002).

[134] Enhancement of photocatalytic and photoelectrochemical properties of TiO2 nanotubes sensitized by SILAR - Deposited PbS nanoparticles _ Elsevier Enhanced Reader.pdf, (n.d.).

[135] J.M. Macak, S.P. Albu, P. Schmuki, Towards ideal hexagonal self-ordering of TiO 2 nanotubes pss, 183 (2007) 181–183. https://doi.org/10.1002/pssr.200701148.

[136] P. V Kamat, Quantum Dot Solar Cells . The Next Big Thing in Photovoltaics, (2013).

[137] M. Antoniadou, D.I. Kondarides, D.D. Dionysiou, P. Lianos, Quantum Dot Sensitized Titania Applicable as Photoanode in Photoactivated Fuel Cells, (2012).

[138] M.P. Genovese, I. V Lightcap, P. V Kamat, Sun-Believable Solar Paint . A Transformative One-Step Approach for Designing Nanocrystalline Solar Cells, (2012) 865–872.

[139] S. Park, T. Ikegami, K. Ebihara, Effects of substrate temperature on the properties of Ga-doped ZnO by pulsed laser deposition, 513 (2006) 90–94. https://doi.org/10.1016/j.tsf.2006.01.051.

[140] J. Verschraegen, M. Burgelman, Numerical modeling of intra-band tunneling for heterojunction solar cells in SCAPS, 515 (2007) 6276–6279. https://doi.org/10.1016/j.tsf.2006.12.049.

[141] P.E. Imoisili, T. Jen, Numerical Analysis and Performance improvement of Nanostructured Cu 2 O / TiO 2 pn heterojunction Solar Cells using SCAPS, (n.d.).

[142] M. Al-hattab, L. Moudou, M. Khenfouch, O. Bajjou, Numerical simulation of a new heterostructure CIGS / GaSe solar cell system using SCAPS-1D software, Sol. Energy. 227 (2021) 13–22. https://doi.org/10.1016/j.solener.2021.08.084.

[143] M.M.T. Al, Z.S. Yasin, Optoelectronics Simulation of CIGS - Based Solar Cells Using

a Cd - Free Nontoxic - ZrS x Se 2 − x as a Novel Buffer Layer, Brazilian J. Phys. (2022) 1–10. https://doi.org/10.1007/s13538-022-01146-z.

[144] U. Mandadapu, S.V. Vedanayakam, K. Thyagarajan, Numerical Simulation of Ch 3 Nh 3 PbI 3-X Cl x Perovskite solar cell using SCAPS-1D, (2017) 40–45.

[145] P. Ieee, P. Specialists, C. Washington, A. Niemegeers, M. Burgelman, MODELLING OF ac-CHARACTERISTICS SOLAR CELLS, (1996) 901–904.

[146] M. Burgelman, P. Nollet, S. Degrave, Modelling polycrystalline semiconductor solar cells, 362 (2000) 527–532.

[147] M. Mostefaoui, H. Mazari, S. Khelifi, A. Bouraiou, R. Dabou, Simulation of High Efficiency CIGS solar cells with SCAPS-1D software, Energy Procedia. 74 (2015) 736–744. https://doi.org/10.1016/j.egypro.2015.07.809.

[148] U. Holzwarth, N. Gibson, The Scherrer equation versus the "Debye-Scherrer equation," Nat. Nanotechnol. 6 (2011) 534–534. https://doi.org/10.1038/nnano.2011.145.

[149] O. Ehlert, A. Tiwari, T. Nann, Quantum confinement of the thermodynamic functions for the formation of electrons and holes in CdSe nanocrystals, J. Appl. Phys. 100 (2006) 1–6. https://doi.org/10.1063/1.2356607.

[150] M. Singh, M. Goyal, K. Devlal, Size and shape effects on the band gap of semiconductor compound nanomaterials, J. Taibah Univ. Sci. 12 (2018) 470–475. https://doi.org/10.1080/16583655.2018.1473946.

[151] M. Asemi, A. Suddar, M. Ghanaatshoar, Increasing the specific surface area of Cr-doped - nanoparticles by controlling the drying time for DSSC applications, J. Mater. Sci. Mater. Electron. 28 (2017) 15233–15238. https://doi.org/10.1007/s10854-017-7401-9.

[152] C. Ippen, T. Greco, A. Wedel, InP/ZnSe/ZnS: A Novel Multishell System for InP Quantum Dots for Improved Luminescence Efficiency and Its application in a Light-Emitting Device, J. Inf. Disp. 13 (2012) 91–95. https://doi.org/10.1080/15980316.2012.683537.

[153] E. Ryu, S. Kim, E. Jang, S. Jun, H. Jang, B. Kim, S. Kim, Communications, 21 (2009) 2425–2427.

[154] O.I. Mic, Synthesis of extremely small InP quantum dots and electronic coupling in their disordered solid films, 4022 (2005). https://doi.org/10.1063/1.1379990.

[155] S.J. Yang, J.H. Oh, S. Kim, H. Yang, Y.R. Do, Realization of InP / ZnS quantum dots for green , amber and red down-converted LEDs and their, (2015) 3582–3591. https://doi.org/10.1039/c5tc00028a.

[156] S. Xu, J. Ziegler, T. Nann, Rapid synthesis of highly luminescent InP and InP / ZnS nanocrystals †, (2008) 2653–2656. https://doi.org/10.1039/b803263g.

[157] K. Yong, H. Ding, I. Roy, W. Law, E.J. Bergey, A. Maitra, P.N. Prasad, Imaging Pancreatic Cancer Using Bioconjugated InP Quantum Dots, 3 (n.d.).

[158] S. Fung, B. Yang, C.K. Ng, M.K. Fung, C.C. Ling, A.B. Djuriˇ, Annealing study of titanium oxide nanotube arrays, 130 (2011) 1227–1231. https://doi.org/10.1016/j.matchemphys.2011.08.063.

[159] T.S. Bhat, A.D. Sheikh, N.L. Tarwal, S.D. Korade, C.K. Hong, J.H. Kim, ZnS passivated PbSe sensitized TiO 2 nanorod arrays to suppress photocorrosion in photoelectrochemical solar cells, Mater. Today Commun. 16 (2018) 186–193. https://doi.org/10.1016/j.mtcomm.2018.06.008.

[160] N. Simulation, P. For, Modeling Thin-film PV Devices, 153 (2004) 143–153. https://doi.org/10.1002/pip.524.

[161] S.K. M, S.P. Madhusudanan, A.R. Rajamani, M. Siaj, S.K. Batabyal, Barium Substitution in Kesterite Cu 2 ZnSnS 4 : Cu 2 Zn 1 − x Ba x SnS 4 Quinary Alloy Thin Films for E ffi cient Solar Energy Harvesting, (2020) 4–11. https://doi.org/10.1021/acs.cgd.0c00150.

[162] M. Jamil, A. Ali, K. Mahmood, M.I. Arshad, S. Tahir, M. Ajaz un Nabi, S. Ikram, N. Amin, S. Hussain, Numerical simulation of perovskite/Cu2Zn(Sn1-x Gex)S4 interface to enhance the efficiency by valence band offset engineering, J. Alloys Compd. 821 (2020) 153221. https://doi.org/10.1016/j.jallcom.2019.153221.

[163] Y. Raoui, H. Ez-Zahraouy, N. Tahiri, O. El Bounagui, S. Ahmad, S. Kazim, Performance analysis of MAPbI3 based perovskite solar cells employing diverse charge selective contacts: Simulation study, Sol. Energy. 193 (2019) 948–955. https://doi.org/10.1016/j.solener.2019.10.009.

[164] Chenming C. Hu, Modern Semiconductor Devices for Integrated Circuits, in: 2010.

[165] F. Baig, Y.H. Khattak, S. Ullah, B.M. Soucase, S. Beg, H. Ullah, Numerical analysis a guide to improve the efficiency of experimentally designed solar cell, Appl. Phys. A. 124 (2018) 471. https://doi.org/10.1007/s00339-018-1877-x.

[166] R. Toufanian, A. Piryatinski, A.H. Mahler, R. Iyer, J.A. Hollingsworth, A.M. Dennis, Bandgap Engineering of Indium Phosphide-Based Core/Shell Heterostructures Through Shell Composition and Thickness, Front. Chem. 6 (2018). https://doi.org/10.3389/fchem.2018.00567.

[167] V. Raj, F. Rougieux, L. Fu, H.H. Tan, C. Jagadish, Design of Ultrathin InP Solar Cell Using Carrier Selective Contacts, IEEE J. Photovoltaics. 10 (2020) 1657–1666. https://doi.org/10.1109/JPHOTOV.2019.2961615.

CHAPTER V

General conclusion and outlook

Conclusion

In the first chapter, we presented the different properties and the main methods of synthesis of semiconductor particles of InP QDs, InP doped with vanadium, core /shell InP/ZnS and TiO2 NATs. We have focused on the effect of combining InP QDs, InP/ZnS CDs and InP/ZnS/ZnS QDs with TiO2 NATs to improve the photoelectrochemical performance in several application areas and more specifically in solar cell.

In the second chapter, we presented the different synthesis methods and devices used for the formation of Quantum Dots and the synthesise of TiO2 NATs. Also, we have described the numerical analysis used in this work.

In the third chapter, we exhibited the synthesis of InP nanoparticles from InP Quantum Dots by acting on the experimental parameters of the hot injection method to improve optical properties in particular the photoluminescence. A study systematic has shown that the doping of InP by Vanadium, does not allow to obtain good results in the photoluminescence properties while there's a decrease on the size of the nanoparticle. In contrast, the results obtained by introducing a ZnS shell are satisfactory, related to the lattice agreement with the core material. Therefore, the growth of a ZnS shell considerably increases the intensity of PL and leads to a greater dispersion in size and the reduction of surface defects resulting on the enhancement of the InP QDs photoluminescence and it influences the fluorescence emitting properties. Also, the surface morphology of these QDs has a more regular spherical form and is well dispersed.

In the fourth chapter, we studied and compared the photoelectrochemical efficiency of the decoration of TiO2 NATs by Quantum Dots nanoparticles of InP, InP/ZnS and InP/ZnS/ZnS. We have demonstrated an increase in the photocurrent almost 4 and 6 times higher than TiO_2/InP QDs. Therefore, this measurement aims to observe the dynamic behavior of the

material and to assess whether the charges recombine rapidly into the TiO_2 NTAs Nanotubes from the quantum dots. So, a good efficiency in the photocurrent response was obtained following the growth core/shell/shell system due to the successful passivation of non-radiative recombination sites such as surface trap states.

Moreover, in this fourth chapter, we also studied to illustrate the simulation and results of different characteristic parameters of the InP/TiO2, InP/ZnS/TiO2and InP/ZnS/Tio2 based Quantum Dots photovoltaic cell. Therefore, according to the results obtained, we notice that for the three structures, the improvement in the JV result was due to the introduction of ZnS layer on top of InP absorber layer. Moreover that, a small change was done in Quantum Efficiency when we added of the second layer of ZnS. Finally, based on the results, the InP was able to successfully utilize the full spectrum of light when coated with ZnS layer on top. Finally, based on the results, we proposed that the introducing of ZnS layer is a strategy to increase the performance of InP/TiO2 QDs based solar cells.

In the future, it would be interesting:

- ✓ Synthesise InP Quantum Dots and perovskite Quantum Dots with a higher aspect ratio, using other ligands and phosphor precursors.
- ✓ To study the influence of perovskite Quantum Dots on the morphology and optical properties.
- ✓ To determine other electronic properties from photoelectrochemical measurements.
- ✓ To define the optimal conditions of synthesis allowing the improvement of the photoluminescence properties.
- ✓ Determine the influence of Vanadium and other material doping on the perovskite Quantum Dot to compare with these results.

Annexes

Published articles:

Imen Harabi, Yousaf Hameed Khattak, Safa Jemai, Shafi Ullah, Hanae Toura, Bernabe Mari Soucase, InP/ZnS/ZnS Core/Shell Quantum Dots for InP Luminescence and photoelectrochemical improvement, Journal Physica B: Physics of Condensed Matter,414634.

Khattak, Y. H., Baig, F., Toura, H., **Harabi, Imen**., Beg, S., & Soucase, B. M. (2019). Single step electrochemical deposition for the fabrication of CZTS kesterite thin films for solar cells. Applied Surface Science, 497, 143794.

Safa Jemai, Anouar Hajjaji, Faisal Baig, **Imen Harabi**, Bernabe Mari Soucase, Brahim Bessais (2021). Crystal growth and design of various shapes of PbS micro and nanocrystals from a hydrothermal process. Materials characterization 175, 111036

Afrah Atri, Mosaab Echabaane, Amel Bouzidi, **Imen Harabi**, Bernabe Mari Soucase, Rafik Ben Chaâbane (2023).Green synthesis of copper oxide nanoparticles using Ephedra Alata plant extract and a study of their antifun, antibacterial activity and photocatalytic performance inder sunlight. Helyion, Volume 9, ISSUE2, E13484.

Scientific communications:

Imen Harabi**,** Bernabe Mari Soucase, Safa Jemai, "Quantum Dots, optical and morphological properties", Poster presentation, 5th Online International Conference on Nanomaterials and Nanotechnology,29- May-2022- Online conference.

Imen Harabi, Bernabe Mari Soucase, Safa Jemai, "InP injection Synthesis of Indium Phosphide Quantum Dots, Optical and Morphological Properties", Oral presentation, 4th International Conference on Material Science & Nanotechnology (ICMSN 2022),25-26 March 2022- Online conference.

Imen Harabi**,** Bernabe Mari Soucase, Safa Jemai, Miguel Mollar "Indium Phosphide Based Colloidal Quantum Dot using Hot Injection Method for Photovoltaic Applications", Poster presentation, 9th International Colloids Conference,19-23 june-2019- Online conference.